#349 SEPTEMBER 2019
SPECIAL ISSUE

ICES REPORT ON OCEAN CLIMATE 2018

Prepared by the Working Group on Oceanic Hydrgraphy

ICES COOPERATIVE RESEARCH REPORT

RAPPORT DES RECHERCHES COLLECTIVES

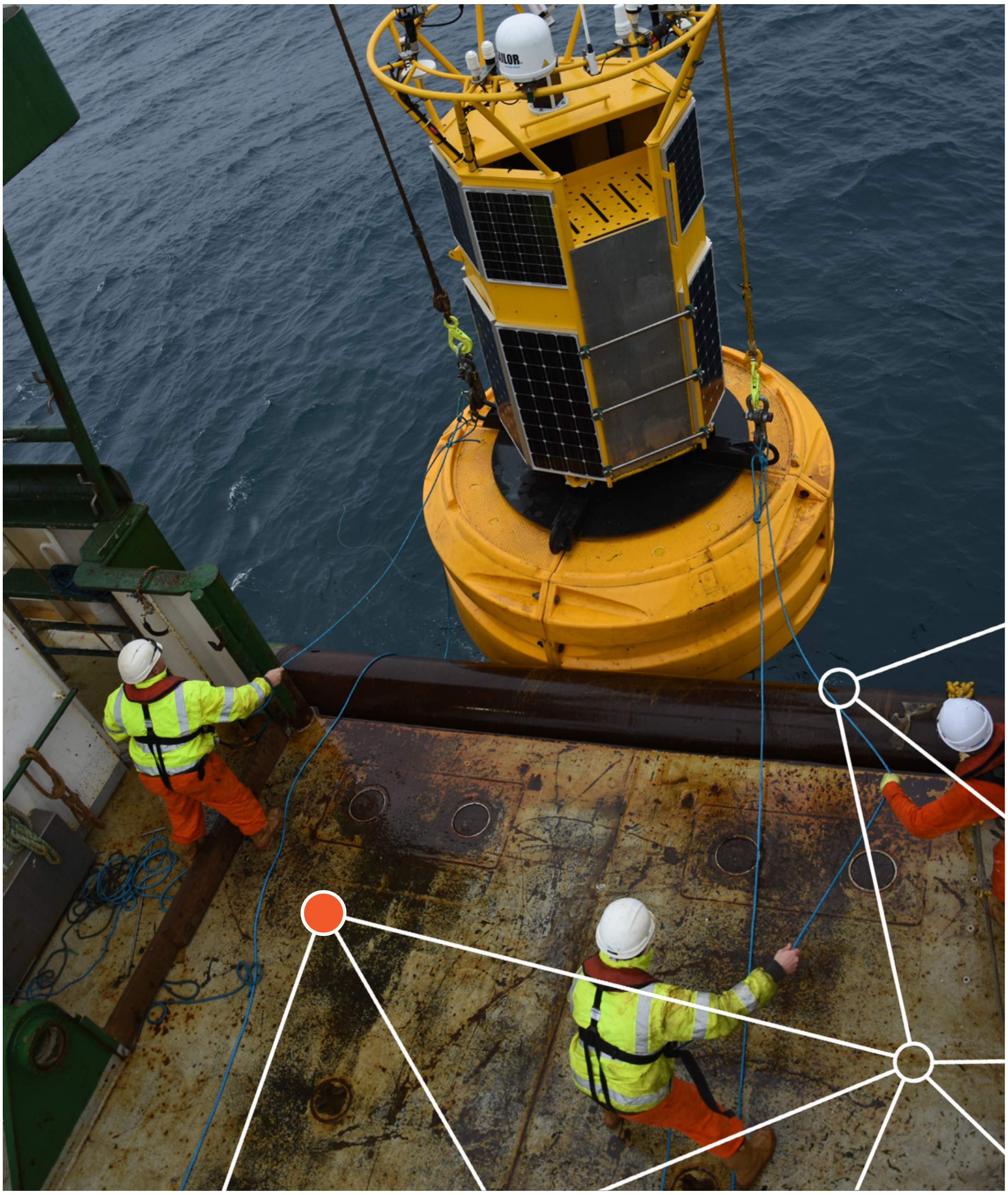

ICES INTERNATIONAL COUNCIL FOR THE EXPLORATION OF THE SEA
CIEM CONSEIL INTERNATIONAL POUR L'EXPLORATION DE LA MER

Members of ICES Working Group on Oceanic Hydrography (WGOH), Bergen, Norway, March 2019.

International Council for the Exploration of the Sea
Conseil International pour l'Exploration de la Mer

H. C. Andersens Boulevard 44–46
DK-1553 Copenhagen V
Denmark
Telephone (+45) 33 38 67 00
Telefax (+45) 33 93 42 15
www.ices.dk
info@ices.dk

Recommended format for purposes of citation:
González-Pola, C., Larsen, K. M. H., Fratantoni, P., and Beszczynska-Möller, A. (Eds.) 2019. ICES Report on Ocean Climate 2018. ICES Cooperative Research Report No. 349. 122 pp. https://doi.org/10.17895/ices.pub.5461

Series Editor: Emory D. Anderson

Cover image: The M6 weather buoy being deployed on the Marine Institute's annual ocean climate survey.
Photo: Tomasz Szmuski, Marine Institute, Galway, Ireland
DOI: https://doi.org/10.17895/ices.pub.5461
ISBN 978-87-7482-234-9
ISSN 2707-7144

ICES COOPERATIVE RESEARCH REPORT
RAPPORT DES RECHERCHES COLLECTIVES

ICES REPORT ON OCEAN CLIMATE 2018

#349 SEPTEMBER 2019
SPECIAL ISSUE

Prepared by the Working Group on Oceanic Hydrography

FOREWORD

The ICES Report on Ocean Climate (IROC) was written by the following members of ICES Working Group on Oceanic Hydrography (WGOH) and collaborators (in alphabetical order by surname): Wilken-Jon von Appen (AWI, Bremerhaven); Barbara Berx (MSS, Aberdeen); Agnieszka Beszczynska-Möller (IOPAN, Sopot); Gereon Budeus (AWI, Bremerhaven); Léon Chafik (MISU, Stockholm); Hjálmar Hátún (FAMRI, Tórshavn); Boris Cisewski (TI-SF, Bremerhaven); Eugene Colbourne (DFO, St. John's); Caroline Cusack (Marine Institute, Galway); Frédéric Cyr (DFO, St. John's); Damien Desbruyères (IFREMER/LOPS, Brest); Stephen Dye (CEFAS, Lowestoft); Almudena Fontán (AZTI, San Sebastián); Paula Fratantoni (NOAA, Woods Hole); César González-Pola (IEO, Gijón); David Hebert (DFO, Dartmouth); Jenny Hindson (MSS, Aberdeen); N. Penny Holliday (NOC, Southampton); Randi Ingvaldsen (IMR, Bergen); Sam Jones (SAMS, Oban); M. Femke de Jong (NIOZ & Utrecht University, Texel); Holger Klein (BSH, Hamburg); Nicolas Kolodziejczyk (UBO, Brest); Karin Margretha H. Larsen (FAMRI, Tórshavn); Peter Loewe (BSH, Hamburg); Kieran Lyons (Marine Institute, Galway); Manuela Köllner (BSH, Hamburg); John Mortensen (GINR, Nuuk); Kjell-Arne Mork (IMR, Bergen); Roger Pettipas (BIO, Dartmouth); Gilles Reverdin (LOCEAN, Paris); Ricardo Sánchez-Leal (IEO, Cadiz); Achim Schulz (BSH, Hamburg); Tim Smyth (PML, Plymouth); Alexander Trofimov (PINRO, Murmansk); Héðinn Valdimarsson (MFRI, Reykjavik); Victor Valencia (AZTI, San Sebastián); Pedro Vélez-Belchí (IEO, Tenerife); Karin Wesslander (SMHI, Göteborg); Tycjan Wodzinowski (MIR-PIB, Gdynia); Igor Yashayaev (DFO, Dartmouth); and Svein Østerhus (NORCE, Bergen).

For a list of authors by section, including full affiliation and contact details, see Section 8. For a complete list of data providers, see Section 9.

Technical assistance during the assembly of this report was provided by Rocío Graña (IEO, Gijón).

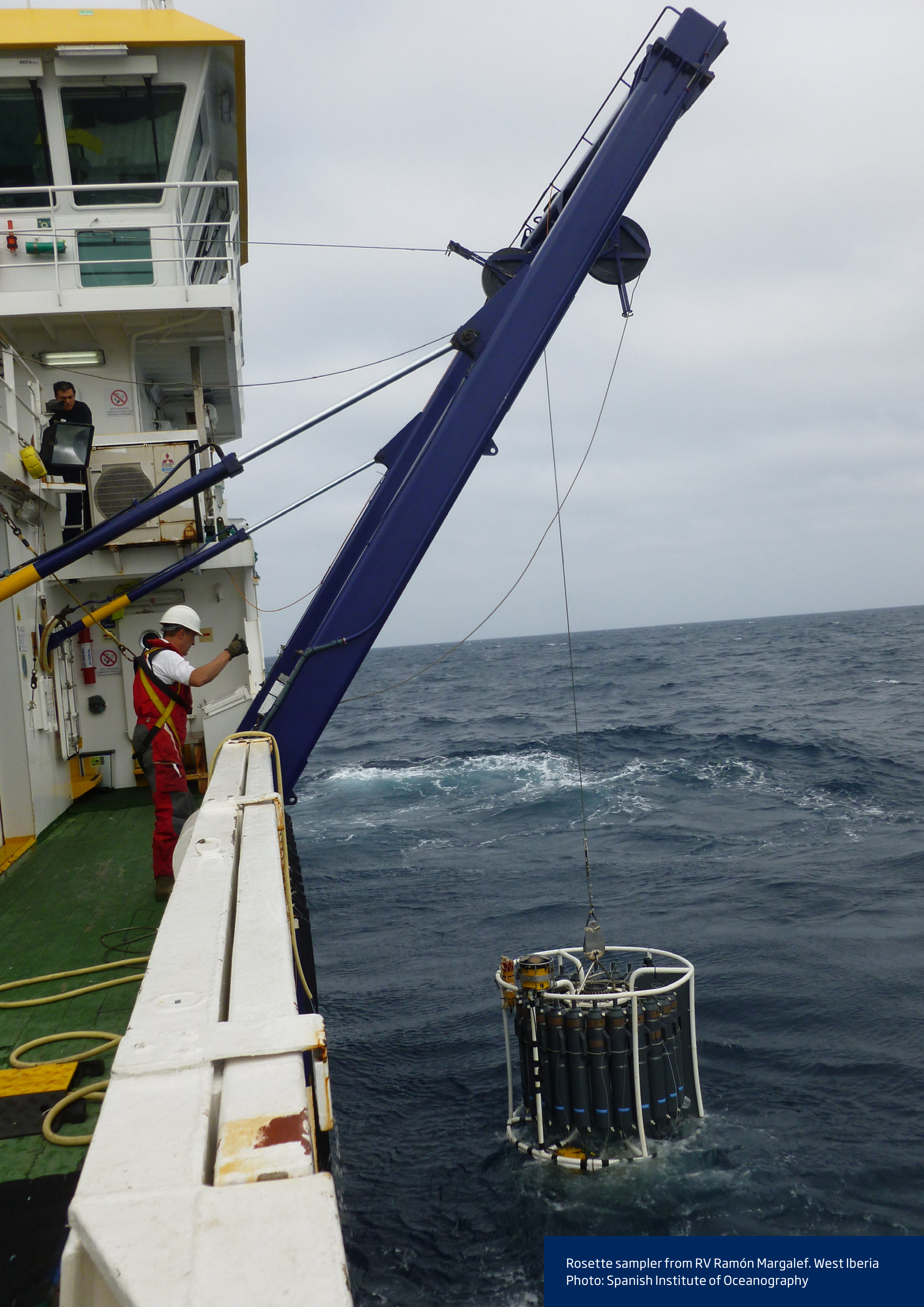

Rosette sampler from RV Ramón Margalef. West Iberia
Photo: Spanish Institute of Oceanography

1. INTRODUCTION

Long time-series on ocean properties are rare for the surface ocean and even more uncommon for the deep ocean. The North Atlantic region is unique in having a relatively large number of locations where oceanographic data have been collected repeatedly for multiple years or decades; the longest records extend back more than a century.

The IROC combines decades of ocean observations across the North Atlantic ICES region to describe the current status of sea temperature and salinity, and atmospheric conditions, as well as observed trends and recent variability. The IROC production focuses the main efforts from ICES WGOH (González-Pola et.al. 2019)

Section 1 synthesizes information from the longest time-series into an overview of changes across the ICES Area. The main focus of this report is the observed variability in the upper ocean (upper 1000 m), and a summary of upper ocean conditions is provided in Section 2. Section 2.3 provides gridded fields constructed by optimal analysis of the Argo float data, distributed by the Coriolis data centre in France, whereas Section 2.4 provides, for the first time, an overview of surface sampling along two shipping routes crossing the Subpolar Gyre. Finally, section 2.5 continues to provide an estimate of the Subpolar Gyre Index.

The next two sections consist of short regional summaries on the variability of North Atlantic upper (Section 4), inter-mediate and deep waters (Section 5). Although the focus of the report is on temperature and salinity measurements, additional complementary datasets are included through-out the report, such as sea level pressure (SLP), air temperature, and ice cover.

The data presented here represent the accumulated knowledge obtained by many individuals and institutions over decades of observations. A list of contacts for each dataset is provided in Section 9, including e-mail addresses for the individuals who provided information, and the data centres at which full archives are maintained. Much of the data included in this report, and additional data, are available to download via a web tool at http://ocean.ices.dk/iroc. A more detailed overview of a particular region, and a full description of some of the datasets used to develop the time-series presented in this report, can be found in the annual meeting reports of the ICES WGOH at http://www.ices.dk/community/groups/Pages/WGOH.aspx.

The ICES WGOH met 19–21 March 2019 in Bergen, Norway, to review oceanographic conditions in the North Atlantic in 2018. The joint analysis of the existing hydrographical time-series provided the following highlights.

1.1 HIGHLIGHTS FOR THE NORTH ATLANTIC

The accelerated freshening in the upper ocean, first observed in the eastern subpolar North Atlantic in 2016, has expanded northward into the Nordic seas influencing the Greenland Sea, the northern Norwegian Sea to Fram Strait, and the southern reaches of the Barents Sea. Freshening is also observed spreading westward into the Irminger Sea and eastward into the North Sea.

Throughout the subpolar region, freshening is accompanied by moderate cooling at just a few sites, indicating that the large changes in salinity are decoupled from changes in temperature.

Freshening of central waters in the northeast Subtropical Gyre and intergyre region (Bay of Biscay, West Iberia, Gulf of Cadiz, and Canaries) was enhanced and extended deeper into the water column. In contrast to northern regions, temperature decreased in concert with freshening, thereby conserving water mass properties.

- Coupled with atmospheric conditions, sea surface temperatures (SST) exhibited a tripole pattern, with warm conditions in both the subtropical and Nordic seas regions and cooler conditions in the subpolar region. A cold anomaly observed in the surface and upper ocean of the central subpolar North Atlantic intensified and expanded after weakening in 2017.

- Scotian and Northeast US shelves were warmer than normal, accompanied by notable freshening at several sites.

- Extremely warm temperatures were observed near the surface in spring-summer across the Baltic Sea and the North Sea (>1.5°C higher than normal), with less pronounced warming observed from Biscay to Ireland (+0.5–1.0°C).

1.2 HIGHLIGHTS FOR THE NORTH ATLANTIC ATMOSPHERE IN THE WINTER OF 2017/2018

- The winter North Atlantic Oscillation (NAO) index was near neutral, ending a run of four consecutive winters with a strong positive index.

- The anomaly in sea level pressure (SLP) did not resemble a typical NAO pattern. Instead, a low-pressure anomaly was centred over northern France, and a large-scale, high-pressure anomaly was split to the northeast and southwest of Iceland, across the Nordic seas, the northwestern Atlantic, and the Labrador Sea.

- Northwesterly wind anomalies between Cape Farewell and Iberia and north-easterly wind anomalies from northern Norway to Rockall contributed to cold conditions across Europe's Atlantic coast from Gibraltar to Tromsø.

- Air temperatures were cold over the Subpolar Gyre, including over the Irminger Sea and Iceland Basin. Warmer-than-average conditions were evident in the Greenland Sea, Barents Sea, and west of the Azores towards Nova Scotia, spreading northward into the western Labrador Sea.

- The Barents Sea experienced notably stronger winds than average across the remainder of 2018, part of a pattern of strong winds stretching from the western Subpolar Gyre through the Norwegian Sea. This affected a number of scientific cruises in the region.

1.3 BEYOND 2018: INITIAL ASSESSMENT OF THE NORTH ATLANTIC ATMOSPHERE IN WINTER 2018/2019

- The SLP pattern for December 2018–March 2019 suggests a second consecutive, weakly positive, near-neutral NAO index winter. In contrast to the previous winter, high pressure across western Europe through to Iceland led to warm conditions in Europe and cold air temperatures south of Newfoundland. Wind speeds were generally lower than average in winter 2018/2019, particularly east of Newfoundland, south of Cape Farewell, and in a band stretching across the Nordic seas from Scoresby Sund in Greenland to the North Cape of Norway.

- Experimental forecasts from the US (over seasonal periods) and the UK (over 1–5 years) suggest a warmer outlook for the Subpolar Gyre region more typical of the long term average (1981–2010).

Passive acoustic mooring deployed on Scotian Shelf.
Photo: David Herbert, Fisheries and Oceans Canada, Dartmouth, Nova Scotia.

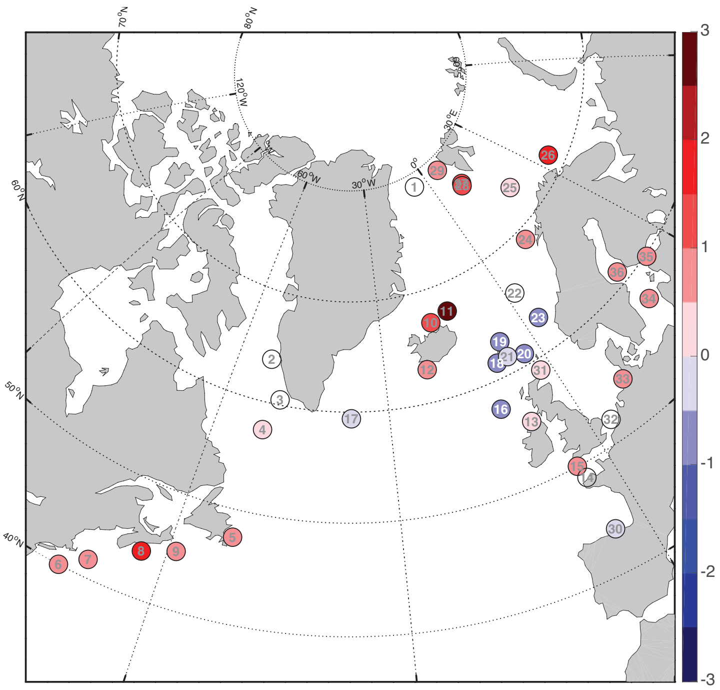

FIGURE 1.1.
Upper ocean temperature anomalies at selected locations across the North Atlantic. The anomalies are normalized with respect to the standard deviation (s.d.; e.g. a value of +2 indicates 2 s.d. above normal). Upper panel: map of conditions in 2018. Lower panels: time-series of normalized anomalies at each of the selected stations. Colour intervals 0.5 s.d.; reds: positive/warm; blues: negative/cool. More details can be found in Section 4.

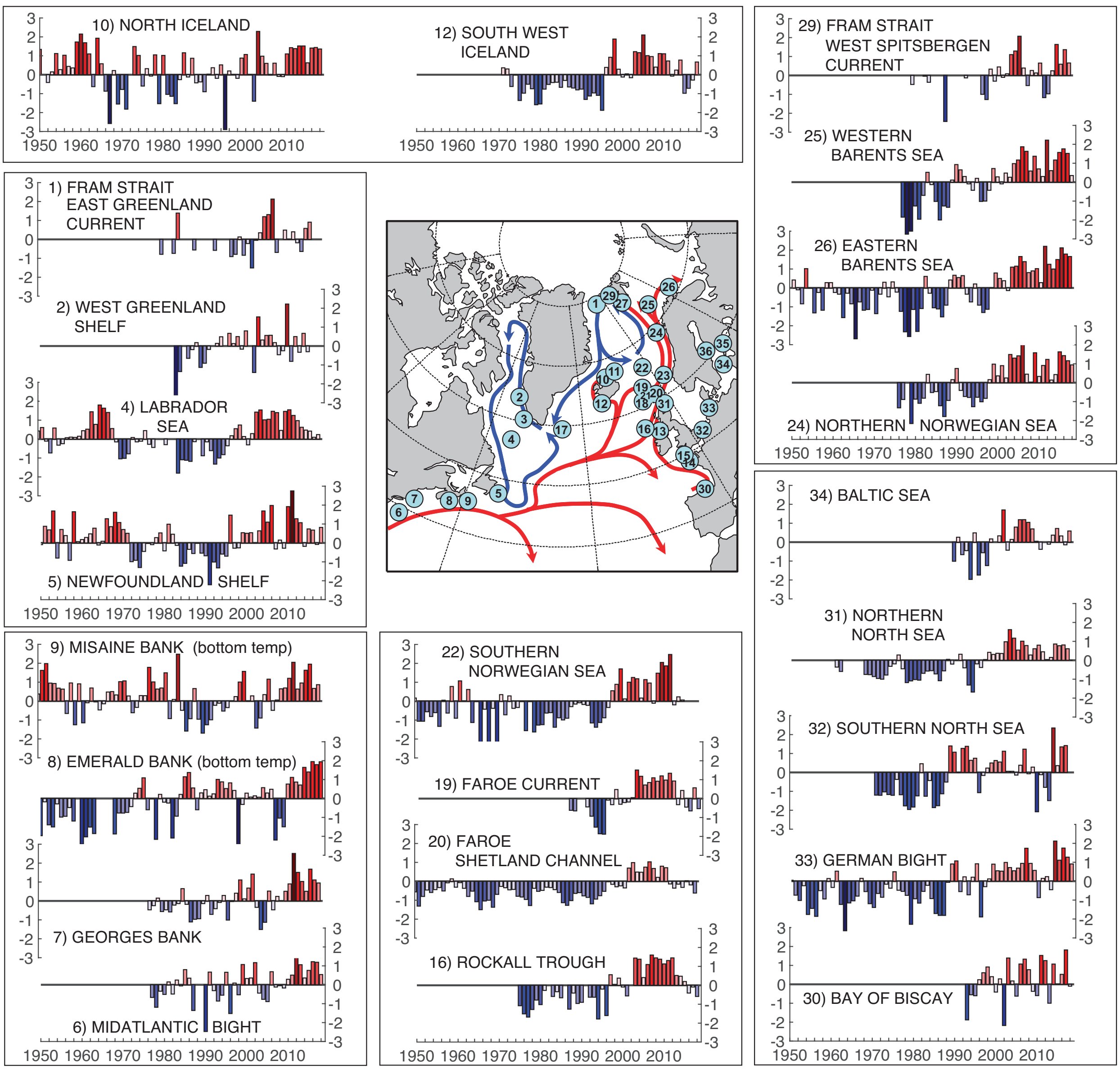

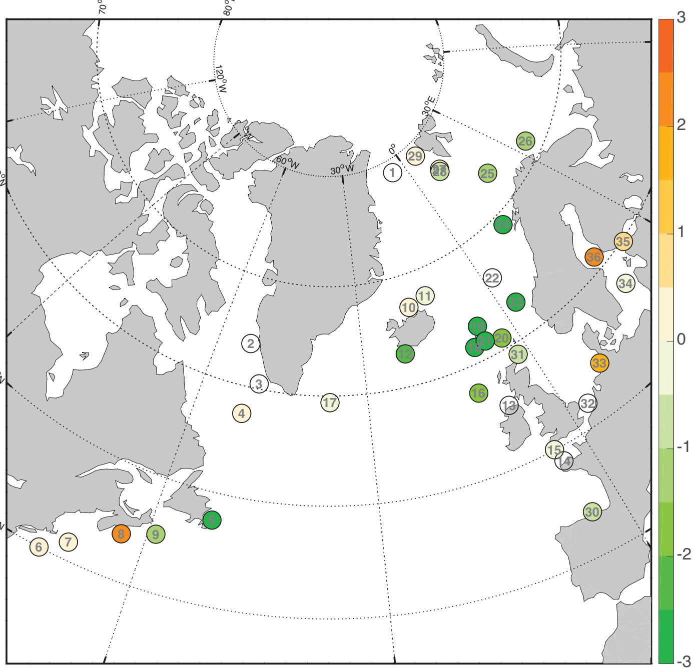

FIGURE 1.2.
Upper ocean salinity anomalies at selected locations across the North Atlantic. The anomalies are calculated relative to a long-term mean and normalized with respect to the s.d. (e.g. a value of +2 indicates 2 s.d. above normal). Upper panel: map of conditions in 2018. Lower panels: time-series of normalized anomalies at each of the selected stations. Colour intervals 0.5 s.d.; oranges = positive/saline; greens = negative/fresh. More details can be found in Section 4.

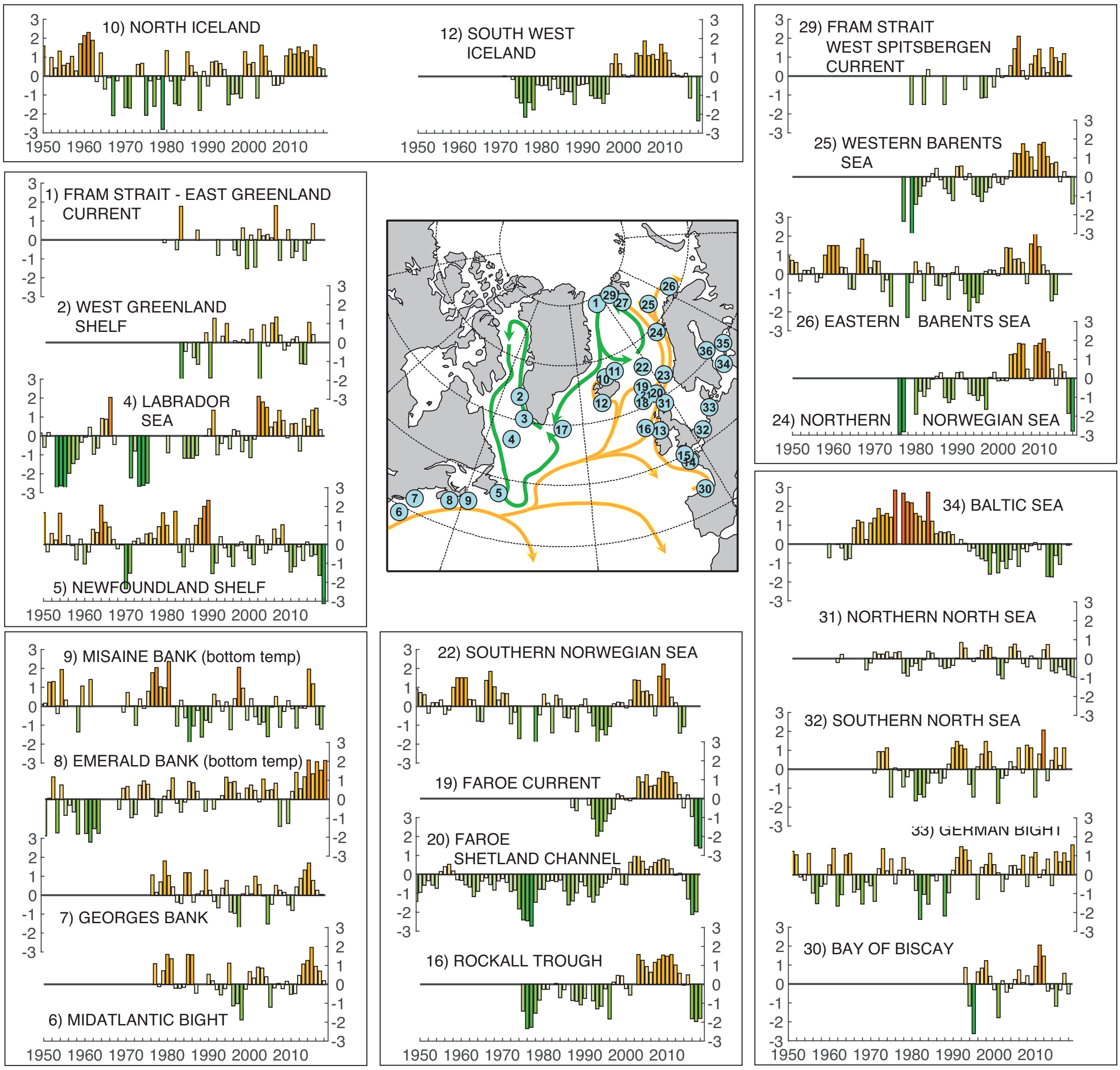

Dissolved Oxygen sample analysis on board the RV Celtic Explorer.
Photo: Tomasz Szmuski, Marine Institute, Galway, Ireland

2. SUMMARY OF UPPER OCEAN CONDITIONS IN 2018

This section summarizes conditions in the upper layers of the North Atlantic during 2018 using data from (i) a selected set of sustained observations, (ii) gridded sea surface temperature (SST) data, and (iii) gridded vertical profiles of temperature and salinity from Argo floats.

2.1 *IN SITU* STATIONS AND SECTIONS

Where *in situ* section and station data are presented in the summary tables and figures, normalized anomalies have been provided to allow a better comparison of trends across regions (Figures 1.1, 1.2, and 2.1; Tables 2.1 and 2.2). The anomalies have been normalized by dividing the values by the s.d. of the data during 1981–2010 (or the closest time-period available). A value of +2 thus represents data (temperature or salinity) measuring 2 s.d. higher than normal.

"Sustained observations" or "time-series" are regular measurements of ocean temperature and salinity made over a long period (10–100 years). Most measurements are made 1–4 times a year, but some are made more frequently.

"Anomalies" are the mathematical differences between each individual measurement and the average value of temperature, salinity, or other variables at each location. Positive anomalies in temperature and salinity imply warm or saline conditions; negative anomalies imply cool or fresh conditions.

"Seasonal cycle" describes the short-term changes at the surface of the ocean brought about by the passing of the seasons; the ocean surface is cold in winter and warms through spring and summer. Temperature and salinity changes caused by the seasonal cycle are usually much greater than the prolonged year-to-year changes we describe here.

	2009	2010	2011	2012	2013	2014	2015	2016	2017	2018
1		0.49	0.01	0.40	-0.18	-0.64	0.58	0.91		
2	-0.25	2.22	-0.81	0.50	-0.33	0.67	-0.30			
3	0.70	1.15	0.57	1.28	0.18	0.83	-0.47	-0.41		
4	0.46	1.46	1.55	1.25	0.98	0.62	0.48	0.42	0.10	0.24
5	-0.28	1.92	2.75	1.28	1.07	-0.18	0.74	0.68	-0.08	0.82
6	-0.17	0.29	0.51	2.15	1.06	0.36	0.76	1.22	1.19	0.54
7	0.00	0.51	0.90	2.51	1.51	1.03	0.51	1.68	1.11	0.95
8	-1.50	0.76	1.12	0.87	0.71	1.64	1.40	1.95	1.79	1.94
9	0.65	0.69	1.20	2.05	0.64	0.96	1.63	1.95	0.67	0.87
10	-0.10	1.10	1.43	1.38	1.52	1.52	0.63	1.41	1.44	1.36
11	0.46	0.30	1.03	0.64	0.79	1.89	0.89	1.15	2.62	2.78
12	1.12	1.11	0.73	-0.07	0.24	0.77	-0.98	-0.72	-0.28	0.67
13	1.45	0.40	1.04	0.62	0.42	1.72	0.73	1.59	1.96	0.42
14	-0.80	-1.95	0.06	0.38	-0.83	1.58	1.04	0.61		
15	-0.66	0.02	0.05	0.59	-0.26	0.70	0.25	0.19	0.63	0.56
16	1.38	1.13	1.31	1.45	0.52	0.48	0.20	-0.41	-0.09	-0.59
17	-0.73	0.55	0.69	-0.29		-0.01	-0.43	-0.75		-0.43
18	1.41	0.73	1.28	-0.03	0.04	0.55	0.13	-0.04	0.21	-0.62
19	1.20	0.98	1.34	0.93	-0.32	0.43	-0.45	-0.65	0.57	-0.53
20	0.21	0.80	0.72	-0.14	-0.36	-0.15	-0.32	0.03	-0.19	-0.62
21	0.84	1.23	0.83	0.31	0.41	0.50	0.15	-0.12	0.13	-0.07
22	1.48	2.05	1.87	2.47	-0.19	0.23	0.06			
23	1.71	0.86	1.12	0.44	0.55	0.33	0.52	0.38	0.76	-0.55
24	1.58	0.33	0.91	1.23	0.14	0.43	1.63	1.43	1.16	0.94
25	1.37	0.70	0.30	2.22	0.61	1.17	1.57	1.76	1.52	0.35
26	0.90	1.02	0.28	2.20	1.25	1.00	1.50	2.12	1.79	1.66
27	0.55	0.40	1.02	0.90	0.03	1.12	0.95	1.42	1.50	1.46
28	0.53	-0.01		0.60	-0.23	1.17		0.88	2.35	1.10
29	0.26	0.13	0.65	-1.17	-0.97	0.25	1.64	0.59	1.36	0.66
30	-0.37	-0.60	1.53	1.25	-1.00	1.07	0.02	0.53	1.82	-0.10
31	0.61	0.80	0.45	0.04	0.15	0.86	0.77	0.81	0.61	0.00
32	0.28	-2.08	-0.12	-0.79	-1.49	2.35	0.36	1.35	1.42	
33	0.57	-0.87	0.15	0.24	-0.45	2.12	1.11	1.75	1.27	0.91
34	0.70	0.05	-0.38		-0.11	0.37	0.72	0.33	-0.14	0.59
35	1.48	0.38	-0.36	0.74	1.08	0.07	0.29	1.07	0.99	0.97
36	1.36	-0.53	-1.16	-0.17	0.02	1.46	1.42	1.60	1.16	0.54

	2009	2010	2011	2012	2013	2014	2015	2016	2017	2018
1		0.54	-0.93	-0.60		-1.08	-0.17	0.86		
2	-0.18	0.17	0.31	-1.12	-1.15	1.07	0.42			
3	1.24	0.07	1.20	-0.14	0.80	-0.47	0.15	-1.28		
4	0.82	-0.10	0.64	0.66	-0.80	0.91	0.51	1.36	1.47	0.33
5	-0.37	-1.46	-1.17	-0.13	-0.85	0.13	-0.62	-0.54	-1.64	-3.07
6	0.16	-0.53	-0.49	0.47	1.07	1.26	1.95	0.95	0.70	0.19
7	0.15	-0.52	-0.81	0.44	0.89	1.33	1.70	0.78	0.26	0.04
8	-1.28	0.42	1.42	0.56	1.19	2.07	1.35	1.99	1.54	2.05
9	-0.27	0.29	-0.13	-1.16	-0.09	-0.11	1.96	1.18	-0.98	-1.21
10	1.07	1.43	1.16	1.54	1.24	1.34	1.01	1.65	0.44	0.38
11	0.66	0.99	1.13	1.55	1.22	-0.04	0.90	1.06	1.01	-0.10
12	1.69	1.24	0.85	0.17	0.06	-0.04	0.17	-1.14	-3.22	-2.35
13										
14	-0.02	-0.11	0.87	1.17	0.11	-0.54	0.46	0.36		
15	0.75	0.46	1.31	0.76	0.79	0.46	1.43	0.85	1.37	-0.23
16	1.54	1.49	1.57	1.02	0.58	-0.05	0.50	-1.82	-1.97	-1.80
17	0.13	1.39	0.85	0.46		0.35	0.71	0.49		-0.08
18	1.61	1.53	1.41	0.31	0.46	-0.08	0.32	-1.53	-2.28	-2.77
19	1.43	1.39	1.17	0.83	0.22	-0.49	0.20	-0.95	-2.49	-2.61
20	0.76	0.83	0.76	0.30	-0.04	0.06	-0.34	-1.30	-2.12	-1.98
21	1.32	1.43	0.91	0.79	0.20	-0.42	-0.45	-1.43	-2.35	-2.76
22	1.59	2.23	1.45	0.48	0.18	-1.42	-1.08			
23	2.01	1.82	1.53	0.69	0.30	-0.63	0.17	-0.97	-2.57	-3.07
24	1.73	1.85	2.07	1.40	0.49	-0.36	0.71	0.34	-1.86	-2.79
25	0.35	1.73	1.82	1.07	0.70	0.78	-0.25	0.28	0.03	-1.43
26	0.52	0.88	1.60	0.34	-0.02	0.16	-0.74	-1.28	-0.56	-1.46
27	0.64	0.95	1.74	1.71	0.98	1.57	0.67	1.02	1.02	0.26
28	0.71	0.82		1.45	1.00	1.74		1.21	0.95	-0.74
29	0.63	1.08	1.42	0.45	0.18	1.50	0.97	0.76	1.18	0.05
30	-0.04	0.93	2.05	1.47	-0.38	-0.26	-1.18	-0.32	0.56	-0.52
31	0.03	-0.53	0.47	0.74	-0.65	-0.76	-0.43	-0.58	-0.86	-0.95
32	1.13	-1.47	0.80	2.07	-0.60	0.47	1.13	0.20	1.13	
33	1.17	-0.15	0.25	0.82	-0.58	1.21	0.67	1.15	0.70	1.57
34	-0.08	0.08	-0.29	0.03	-1.71	-1.74	-0.61	-1.08		-0.06
35	0.87	0.78	-0.85	-1.12	0.57	0.20	-0.27	-0.04	0.76	0.93
36	0.64	2.17	2.18	1.03	0.40	1.01	-0.65	-0.20	1.33	2.40

TABLES 2.1 AND 2.2.

Changes in temperature (Table 2.1, top) and salinity (Table 2.2, bottom) at selected stations in the North Atlantic region during the past decade, 2009–2018. The index numbers on the left can be used to cross-reference each point with information in Figures 1.1 and 1.2 and in Table 2.3. Unless specified, these are upper-layer anomalies. The anomalies are normalized with respect to the s.d. (e.g. a value of +2 indicates that the data observation of temperature or salinity for that year was 2 s.d. above normal). Blank boxes indicate that data were unavailable for a particular year at the time of publication. Note that no salinity data are available for Station 13. Colour intervals 0.5 s.d.; red = warm; blue = cold; orange = saline; green = fresh.

Index	Description	Section	Measurement depth	Reference period	Lat	Lon	Mean T	S.D.	Mean S	S.D.
1	Fram Strait - East Greenland Current	4.21	50-500 m	1983-2010	78.83	-6.00	0.69	0.57	34.650	0.135
2	Fylla section - Station 4 - Greenland Shelf	4.1	0-50 m	1983-2010	63.88	-53.37	2.64	1.10	33.162	0.392
3	Cape Desolation section - Station 3 - Greenland Shelf	4.1	75-200 m	1983-2010	60.47	-50.00	5.72	0.66	34.923	0.062
4	Central Labrador Sea	4.2	15 - 50 m	1981-2010	57.07	-50.92	4.68	0.69	34.635	0.176
5	Station 27 - Newfoundland Shelf temperature - Canada	4.3	0-175 m	1981-2010	47.55	-52.59	0.33	0.39	31.946	0.166
6	NE US continental shelf - Northern Mid Atlantic Bight	4.5	1-30 m	1981-2010	40.00	-71.00	11.36	0.94	32.710	0.430
7	NE US continental shelf - Northwest Georges Bank	4.5	1-30 m	1981-2010	41.50	-68.30	10.00	0.79	32.580	0.270
8	Emerald Basin - Central Scotian Shelf - Canada	4.4	250 m (Near Bottom)	1981-2010	44.00	-63.00		0.83		0.151
9	Misaine Bank - Northeast Scotian Shelf - Canada	4.4	100 m (Near Bottom)	1981-2010	45.00	-59.00		0.63		0.134
10	Siglunes Station 2-4 - North Iceland - North Icelandic Irminger Current - spring	4.6	50-150 m	1981-2010	67.00	-18.00	3.41	0.98	34.859	0.108
11	Langanes Station 2-6 - Northeast Iceland - East Icelandic Current - spring	4.6	0-50 m	1981-2010	67.50	-13.50	1.22	0.61	34.729	0.067
12	Selvogsbanki Station 5 - Southwest Iceland - Irminger Current - spring	4.6	0-200 m	1981-2010	63.00	-21.47	7.88	0.47	35.187	0.049
13	Point 33 - Astan	4.10	5 m	1998-2010	48.78	-3.94	12.79	0.34	35.206	0.112
14	Western Channel Observatory (WCO) -E1 - UK	4.10	0-40 m	1981-2010	50.03	-4.37	12.43	0.93	35.200	0.100
15	Malin Head Weather Station	4.11	Surface	1981-2010	55.37	-7.34	10.25	0.57		
16	Ellett Line - Rockall Trough - UK (section average)	4.12	30-800 m	1981-2010	56.75	-11.00	9.35	0.28	35.351	0.036
17	Central Irminger Sea subpolar-mode water	4.15	200-400 m	1991-2010	59.40	-36.80	4.35	0.53	34.900	0.031
18	Faroe Bank Channel - West Faroe Islands	4.16	Upper Layer High Salinity Core	1988-2010	61.40	-8.30	8.80	0.36	35.302	0.043
19	Faroe Current - North Faroe Islands (modified North Atlantic water)	4.16	Upper Layer High Salinity Core	1987-2010	63.00	-6.00	8.11	0.39	35.249	0.043
20	Faroe Shetland Channel - Shetland Shelf (North Atlantic water)	4.16	Upper Layer High Salinity Core	1981-2010	61.00	-3.00	9.95	0.47	35.398	0.051
21	Faroe Shetland Channel - Faroe Shelf (modified North Atlantic water)	4.16	Upper Layer High Salinity Core	1981-2010	61.50	-6.00	8.32	0.54	35.256	0.055
22	Ocean Weather Station Mike	4.19	50 m	1981-2010	66.00	2.00	7.71	0.44	35.176	0.036
23	Southern Norwegian Sea - Svinøy section - Atlantic water	4.19	50-200 m	1981-2010	63.00	3.00	8.04	0.39	35.234	0.039
24	Central Norwegian Sea - Gimsøy section - Atlantic water	4.19	50-200 m	1981-2010	69.00	12.00	6.89	0.34	35.154	0.031
25	Fugløya - Bear Island section - Western Barents Sea - Atlantic inflow	4.19	50-200 m	1981-2010	73.00	20.00	5.55	0.46	35.078	0.035
26	Kola section - Eastern Barents Sea	4.20	0-200 m	1981-2010	71.50	33.50	4.22	0.52	34.771	0.056
27	Greenland Sea section - West of Spitsbergen 76.5°N	4.19	200 m	1996-2010	76.50	10.50	3.19	0.61	35.058	0.043
28	Northern Norwegian Sea - Sørkapp section - Atlantic water	4.19	50-200 m	1981-2010	76.33	10.00	4.08	0.60	35.073	0.038
29	Fram Strait - West Spitsbergen Current	4.21	50-500 m	1983-2010	78.83	7.00	3.11	0.69	35.027	0.038
30	Santander Station 6 (shelf break) - Bay of Biscay - Spain	4.7	0-30 m	1993-2010	43.71	-3.78	15.74	0.32	35.460	0.160
31	Fair Isle Current water (waters entering North Sea from Atlantic)	4.17	0-100 m	1981-2010	59.00	-2.00	9.93	0.61	34.874	0.132
32	Section average - Felixstowe - Rotterdam - 52°N	4.17	Surface	1981-2010	52.00	3.00		0.72		0.212
33	North Sea - Helgoland Roads	4.17	Surface	1981-2010	54.18	7.90	10.26	0.75	32.096	0.568
34	Baltic Proper - east of Gotland - Baltic Sea	4.18	Surface T Surface S	1990-2010 1987-2010	57.50	19.50	9.27	1.03	7.172	0.196
35	Baltic - LL7 - Baltic Sea	4.18	70 m	1991-2010	59.51	24.50	3.97	0.73	7.961	0.666
36	Baltic - SR5 - Baltic Sea	4.18	110 m	1991-2010	61.05	19.35	3.27	0.58	6.428	0.141

TABLE 2.3.

Details of the datasets included in Figures 1.1 and 1.2 and in Tables 2.1 and 2.2. Blank boxes indicate that no information was available for the area at the time of publication. T = temperature, S = salinity. Some data are calculated from an average of more than one station; in such cases, the latitudes and longitudes presented here represent a nominal midpoint along that section.

2.2 SEA SURFACE TEMPERATURE

Satellites have been measuring SST for approximately 40 years, which has led to the creation of gridded data-sets. Figure 2.1 shows seasonal SST anomalies for 2018 extracted from the Optimum Interpolation SST dataset version 2 (OISST.v2) provided by the NOAA-CIRES Climate Diagnostics Center, USA. The data may be less reliable at high latitudes, where *in situ* data are sparse and satellite data are hindered by cloud cover. Regions with ice cover for > 50% of the averaging period appear blank.

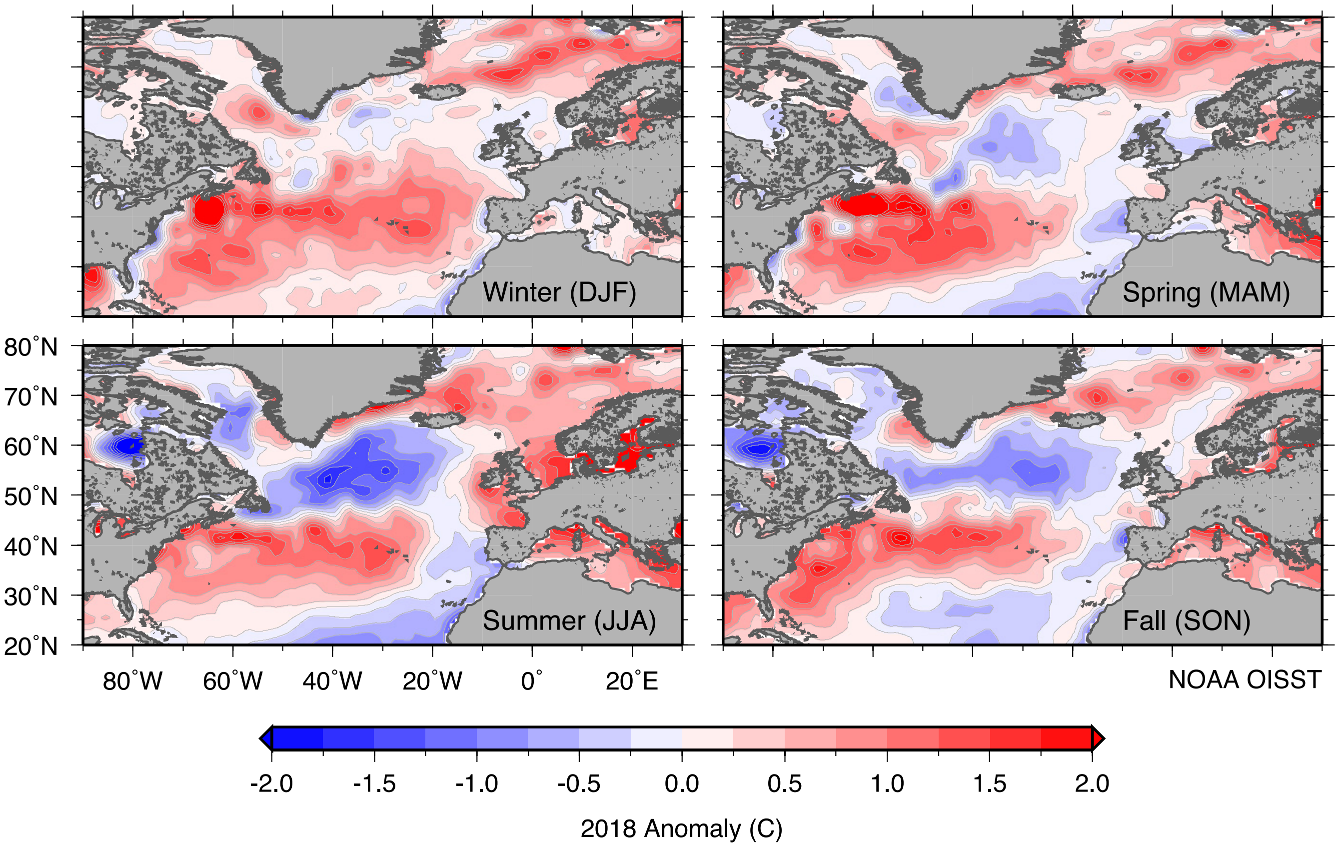

FIGURE 2.1.
Maps of seasonal SST anomalies (°C) over the North Atlantic for 2018 from the NOAA OISST.v2 dataset provided by the NOAA-CIRES Climate Diagnostics Center, USA. The data are produced on a 1° grid from a combination of satellite and *in situ* temperature data. The colour-coded temperature scale is the same in all panels, and the anomaly is calculated with respect to mean conditions for 1981–2010. Regions with ice cover for > 50% of the averaging period appear blank.

2.3 ARGO GRIDDED TEMPERATURE AND SALINITY FIELDS

N. Kolodziejczyk, and D. Desbruyères

The Argo[1] network of profiling floats has been set up to monitor the large-scale global ocean variability. Argo data are transmitted in real time and made available by the two Global Data Assembly Centres (Argo-GDAC). Delayed-mode data undergo expert calibration processes and are delivered later. In the North Atlantic, temperature and salinity conditions of the upper 2000 m have been adequately described since 2002. This dataset is thus suitable for an overview of oceanographic conditions in this basin and provides the general context for the data collected at stations and sections, mostly located at the periphery of the basin, by WGOH partners.

2.3.1 ISAS: Gridded temperature and salinity fields

Temperature and salinity gridded fields are estimated on a regular half-degree grid using the *In Situ* Analysis System (ISAS; Gaillard *et al*., 2016). The dataset used for generating ISAS gridded fields is available to download from the Coriolis Argo GDAC[2]. Coriolis assembles many types of data transmitted in real time, merging the Argo dataset with data collected by the Global Telecommunications Systems (GTS), such as mooring data, marine animals, and CTDs. However, the Argo dataset remains the main contributor in the open ocean.

For the optimal interpolation procedure, the *in situ* temperature and salinity profiles are vertically interpolated on 152 standard levels between the surface and 2000 m depth. The horizontal mapping to produce gridded fields is performed at each standard level independently. The mapping method is based on an optimal estimation algorithm and includes a horizontal smoothing through specified covariance scales. The results presented here were produced with the last version of ISAS. The reference state was computed as the mean of a 2005–2012 analysis (using ISAS13; Gaillard *et al*., 2016), and the *a priori* variances were computed from the same dataset. Two ISAS gridded temperature and salinity products have been used:

- Over the period 2002–2015, the ISAS15 product was used (Kolodziejczyk *et al*., 2017). The ISAS15 product is the highest quality product in delayed mode, since only delayed mode *in situ* data are used. Data are preprocessed, and an extra quality control is applied to *in situ* profiles before they are included in the analysis.

- During the last years of the analysed series (2016–2018), the near real time (NRT) dataset has been used, which is prepared by Coriolis at the end of each month from real time data. Data are interpolated using ISAS v6, including only real time mode data (i.e. only from automatic QC processing). Delayed-mode data are being progressively taken into account for the previous years, replacing the NRT data.

ISAS interpolated fields are used to compute seasonal to interannual maps of temperature and salinity anomalies at surface (10 m depth) and within intermediate layers, i.e. temperature and salinity averaged between 800 and 1200 m depth. Note that the temperature and salinity anomalies are computed using the World Ocean Atlas-2005 climatology as climatological reference (WOA05[3]). WOA05 mainly reflects the climatological oceanic conditions of the pre-Argo period (before the 2000s). Thus, temperature and salinity anomalies reflect changes compared with this period. In order to compute temperature and salinity anomalies, the climatological monthly temperature and salinity from WOA5 are removed from each month of the ISAS fields over the period 2013–2018. Note that the temperature and salinity fields are blanked in regions where the Argo coverage is either too sparse or unavailable. To discard undersampled grid points, which are mostly found within shallow shelf regions, a criterion was chosen of > 80% of explained variance provided by the objective analysis.

The mixed-layer depth is an indicator of winter convection intensity in the North Atlantic and Nordic seas. Winter heat and freshwater fluxes control the buoyancy loss (increase in density) of the ocean surface layers and trigger deep convection. In order to compare all areas over the decade, the mixed-layer depth is defined as the depth at which density changes by > 0.03 kg m^{-3} with respect to the ten-meter depth value. This is a common criterion used for the global ocean (de Boyer Montégut *et al*., 2004). Given the stratification in the North Atlantic and Nordic seas, it is probably not the optimal criterion to define the mixed layer in this region. However, this criterion allows the comparison of the relative winter mixed-layer depth across multiple years. March is commonly selected as the period for maximum mixed-layer

1) http://www.argo.ucsd.edu
2) http://www.coriolis.eu.org/
3) https://www.nodc.noaa.gov/OC5/SELECT/woaselect/woaselect.html

depth, at the end of the winter season, and before spring restratification. However, this is not completely accurate, because the time of the deepest mixed layer may vary from year-to-year at a single location and may not occur at the same time of year across the whole basin (between February and March in the North Atlantic).

2.3.2 Surface layers

Seasonal cycle

During winter 2018 in the middle of the Subpolar Gyre (north of 45°N, and between 50°W and 10°W) and in the Labrador Sea, the near-surface waters (10 m depth) were anomalously colder and fresher than the WOA05 pre-Argo (before 2002) climatological winter (Figure 2.2). South of 50°N, near-surface waters were extremely warm and salty in the western basin, indicating a northward shift of the Gulf Stream compared with the pre-Argo 1990s conditions. South of 45°N, a warmer-than-normal Subtropical Gyre was also observed. The Subpolar Gyre cold anomaly persisted throughout 2018 (Figure 2.2). However, during summer 2018, the Greenland basins were anomalously warm relative to pre-Argo climatological conditions. Fresh salinity anomalies (Figure 2.2, lower panel) were reported around the southern tip of Greenland throughout the entire year, whereas a salty anomaly progressively emerged in the Greenland and Labrador seas. The subtropical front associated with the Gulf Stream exhibited positive salinity anomalies, with patterns comparable to those exhibited by seasonal temperatures. This confirms a northward shift in the Subtropical Front.

In the Irminger Sea, winter 2018 was one of coldest winters over the 2002–2018 period (thick red line; Figure 2.3, Irminger Sea). Near-surface temperatures were well below the pre-Argo seasonal climatology (thick black line), in line with the colder-than-usual 2015–2017 winters. Near-surface temperatures in the Labrador Sea were anomalously cold (Figure 2.3, Labrador Sea). The 2018 cold conditions continue the cooling trend that began in 2014 after more than a decade of warming. Summer near-surface temperatures were also the coldest measured since 2002.

In contrast, the seasonal cycle of near-surface temperature in the Gulf Stream region (Figure 2.3, Gulf Stream) continued the warm shift observed over the last few years. Both winter and summer temperatures exhibited maximum values > 1°C above the pre-Argo period. Off the European coast in the Eastern Atlantic (Figure 2.3, Eastern Atlantic), seasonal near-surface temperatures were within the 2002–2018 range and did not significantly differ from the climatological seasonal cycle of the pre-Argo period.

Mixed-layer depth

During winter 2018, mixed layers in the Labrador and Irminger seas were shallower than 1000 m depth (Figure 2.5), whereas mixed layers in the Greenland Sea exceeded 1000 m depth. These conditions differed from the deep mixed layers observed during winters 2015–2017 in both the Subpolar Gyre and the Greenland Sea (deeper than 1000 m depth; Figure 2.5). The 2018 conditions are similar to those observed during winter 2013, whereas they are the opposite of winter 2014 conditions (deep mixed layer in the Subpolar Gyre and shallow mixed layer in the Greenland Sea). The 2018 shallow layers in both the Labrador and Irminger basins may reflect shallower winter convection, although a relatively deep convection persisted in the Greenland Sea.

Interannual variability

In 2018, the persistence of a coherent cold anomaly over the central Subpolar Gyre was the most salient feature observed for the North Atlantic annual near-surface temperature anomaly (using WOA05 as reference climatology; Figure 2.6, upper panel). This Subpolar cold anomaly increased in size during 2013–2015, with minimum temperature anomalies exceeding 2°C. During 2016-2017, the cold anomaly appeared to have diminished in intensity (–1°C). However, in 2018, the Subpolar cold anomaly again increased in intensity (>–2°C) and shifted farther north, past 50°N.

In contrast, since 2012, the Nordic seas north of 65°N have exhibited persistent warm anomalies (> 2°C) near the surface, notably in the Greenland Sea and along the eastern Greenland coast (Figure 2.6, upper panel). In the Subtropical Gyre, surface waters remained warmer in 2018, especially in the Gulf Stream region where a northward shift of the Subtropical Front may explain the extreme warm anomalies (> 3°C).

During the 2013–2018 period, the persistent subpolar near-surface cold anomaly also coincided with a near-surface fresh anomaly (about 0.4 pss). More precisely, in 2013, a fresh anomaly (0.4 pss) appeared in the western Atlantic basin around 45°N and subsequently moved across the Subpolar Gyre towards the eastern North Atlantic. This fresh anomaly entered the Irminger Basin in 2016 (Figure 2.6, lower panel). Around the Greenland coast, a strong negative near-surface salinity anomaly was observed during 2014–2018 in both the Labrador and Irminger basins. In this region, the fresher near-surface water may be explained by an increase in freshwater flux from the atmosphere, the ocean, or the Greenland ice sheet melt.

2.3.3 Deep layers

Within the intermediate layer (800–1200 m depth; Figure 2.7, upper panel), the Labrador and the Irminger seas were warmer than pre-Argo conditions (0.4°C) until 2014. However, the warming anomaly has not been seen since 2015 (0°C anomaly), reflecting a return to oceanic conditions similar to the pre-Argo period. The time-series of temperature averaged between 800 and 1000 m depth in both the Labrador (Figure 2.8, Labrador Sea) and Irminger seas (Figure 2.8, Irminger Sea) confirm this trend. The deep temperature in the Labrador and Irminger basins increased during 2002–2014, peaking in 2011 (+0.4°C) and 2013 (+0.3°C), respectively. From 2015 to 2018, temperatures have been rapidly decreasing (Figure 2.8, Labrador and Irminger seas). Note that in the eastern Atlantic region between Iceland and Ireland, persistent cold conditions (colder than pre-Argo conditions) have been observed since 2002.

In contrast, the deep waters of the Greenland Sea have unabatedly warmed since 2002, reaching an amplitude of 0.3°C (Figure 2.7, upper panel; and Figure 2.8, Greenland Sea). The Mediterranean Outflow Water (MOW) at 1000 m depth was warmer and saltier south of 40°N and off the Strait of Gibraltar. Since 2013, the salty (> 0.04 pss) and warm anomaly appears to be gradually expanding westward into the Subtropical Basin (Figure 2.7; lower panel). In contrast, a cold and fresh anomaly persists south of Iceland to Rockall Trough and has intensified in 2016 and 2018 (Figure 2.7, lower panel).

Celtic Explorer, transit.
Photo: Holger Klein, Federal Maritime and Hydrographic Agency, Hamburg, Germany

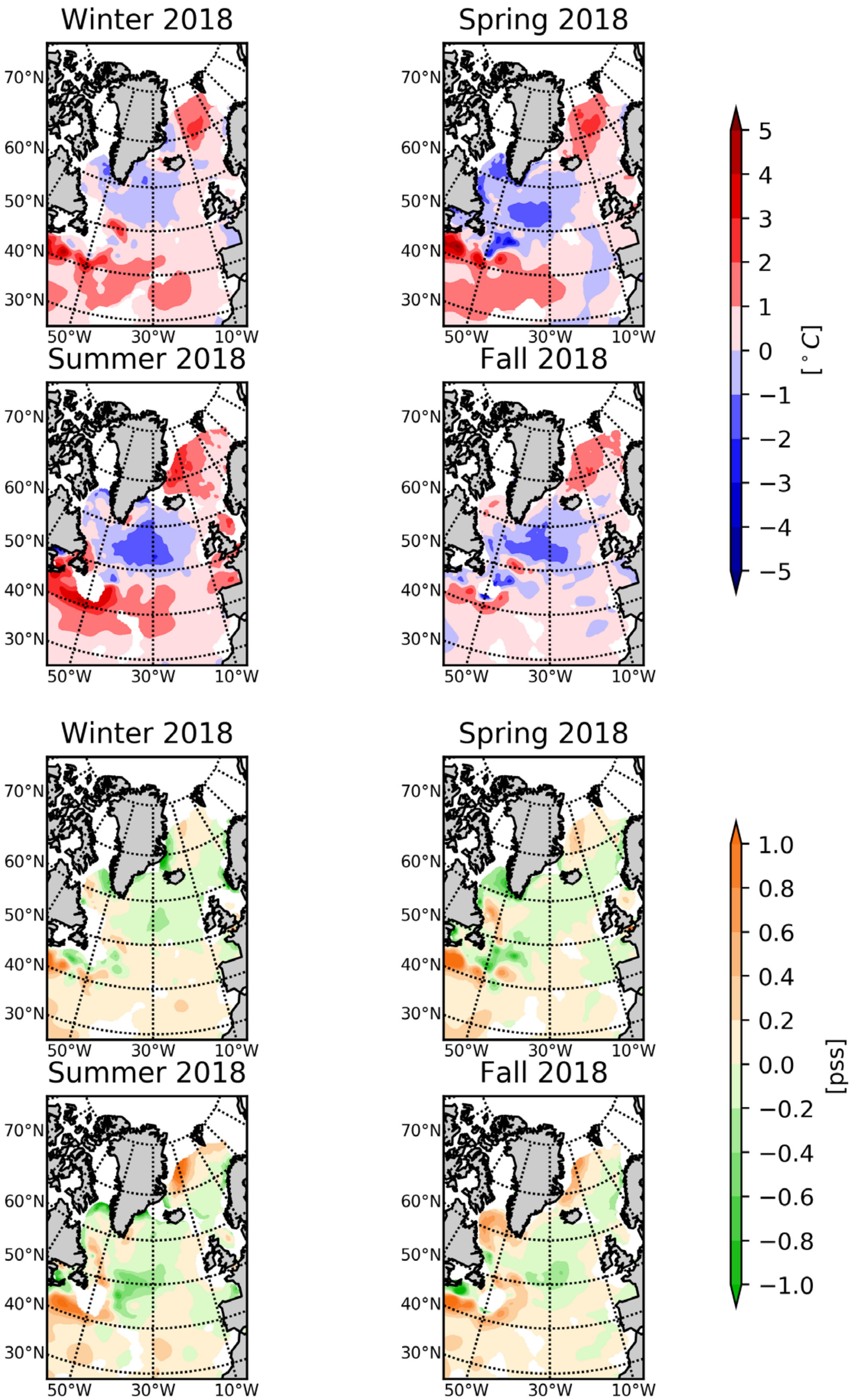

FIGURE 2.2.
Maps of 2018 seasonal temperature (upper) and salinity (lower) anomalies at 10 m depth in the North Atlantic. Anomalies are the differences between the ISAS monthly mean values and the reference climatology, World Ocean Atlas 05 (WOA05). The colour-coded scale is the same in all panels. Data prepared from the Coriolis, ISAS monthly analysis of Argo data.

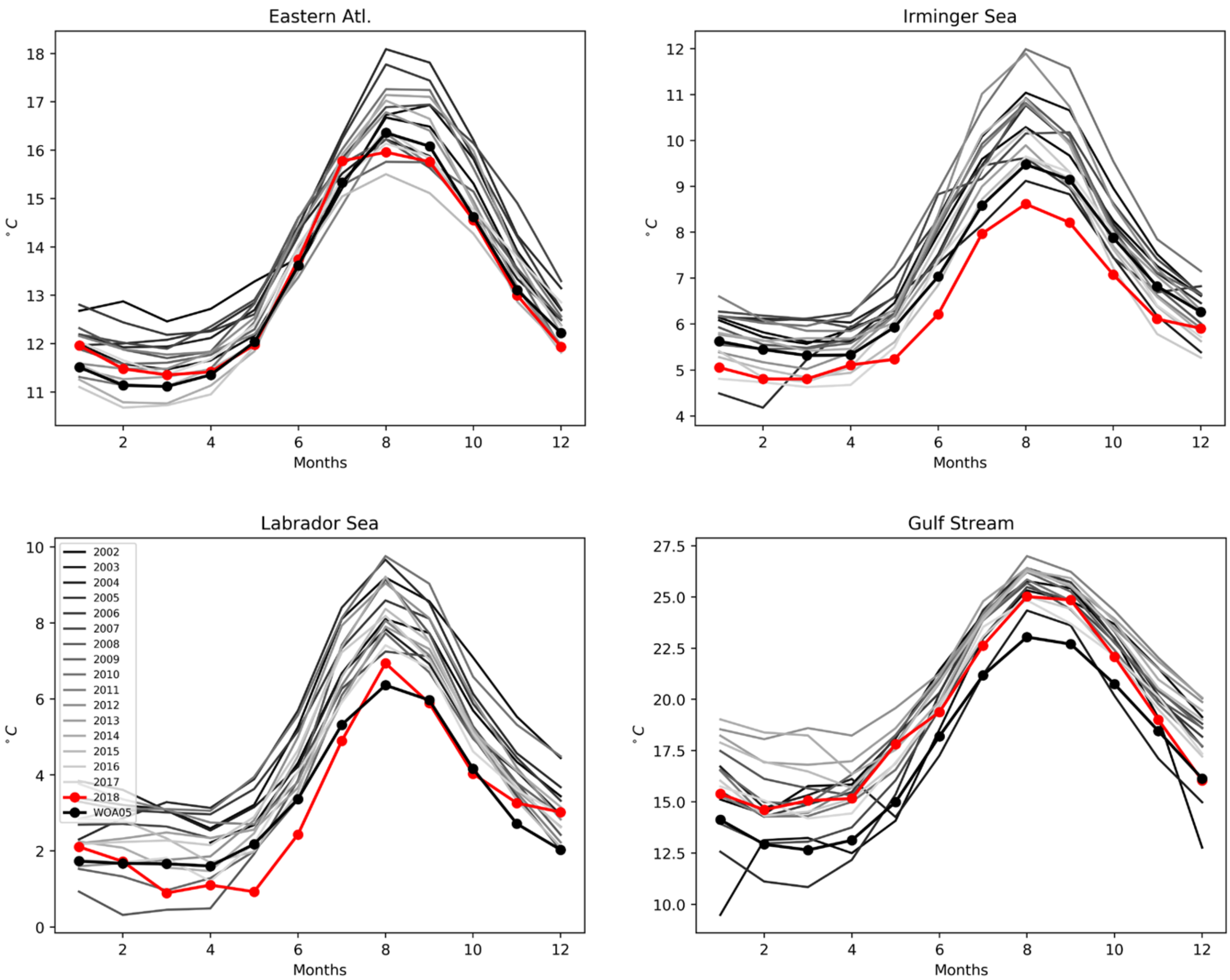

FIGURE 2.3.
Seasonal cycle for near-surface temperature (10 m depth) at four points in the North Atlantic basin (see stations in Figure 2.4). (a) Eastern Atlantic (station 1 in Figure 2.4); (b) Irminger Sea (station 2 in Figure 2.4); (c) Labrador Sea (station 3 in Figure 2.4), and (d) Gulf Stream region (station 4 in Figure 2.4). In thick red, the year 2018; in thick black, the WOA05 climatology; other curves show the years 2002–2017.

Oil rig in the North Sea.
Photo: Holger Klein, Federal Maritime and Hydrographic Agency, Hamburg, Germany

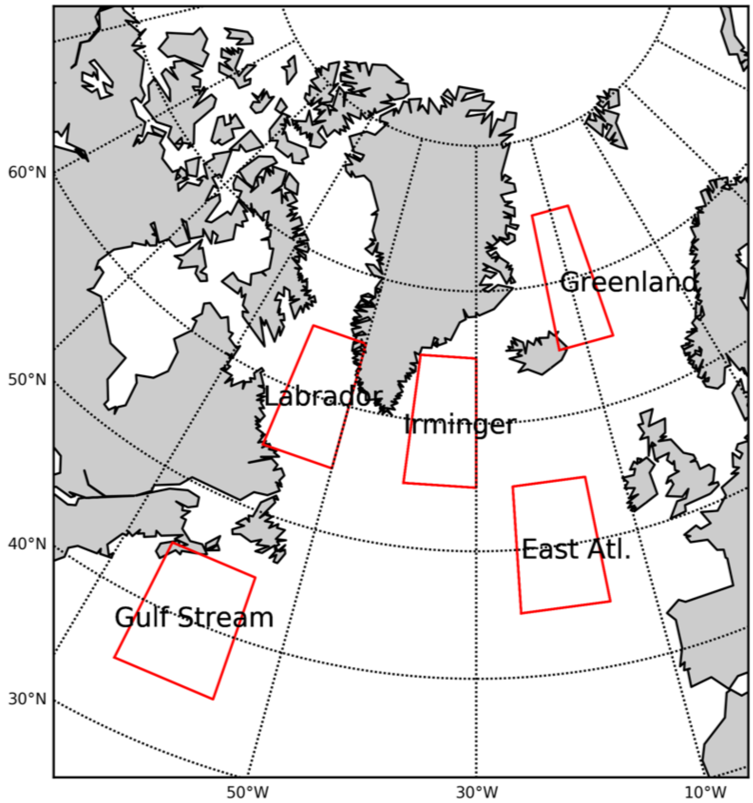

FIGURE 2.4.
Positions of five points (Argo stations) in the North Atlantic basin: Eastern Atlantic (East Atl.), Irminger Sea, Labrador Sea, Gulf Stream region, and Greenland Sea.

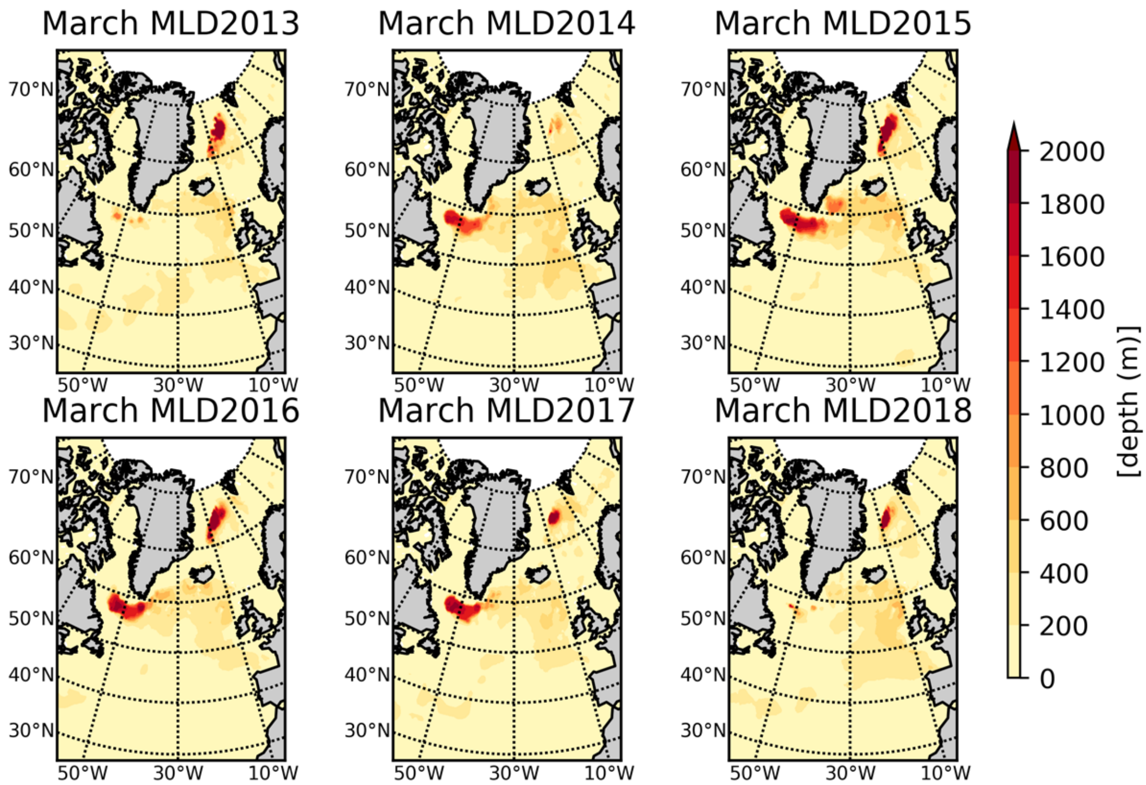

FIGURE 2.5.
Maps of North Atlantic winter (March) MLD for 2013–2018. From the ISAS monthly analysis of Argo data. Note that from 2018, the mixed-layer depth is defined as the depth at which the density has increased by > 0.03 kg m^{-3} from the density at 10 m depth. This criterion is able to represent MLD in areas affected by both temperature and salinity (ice melting).

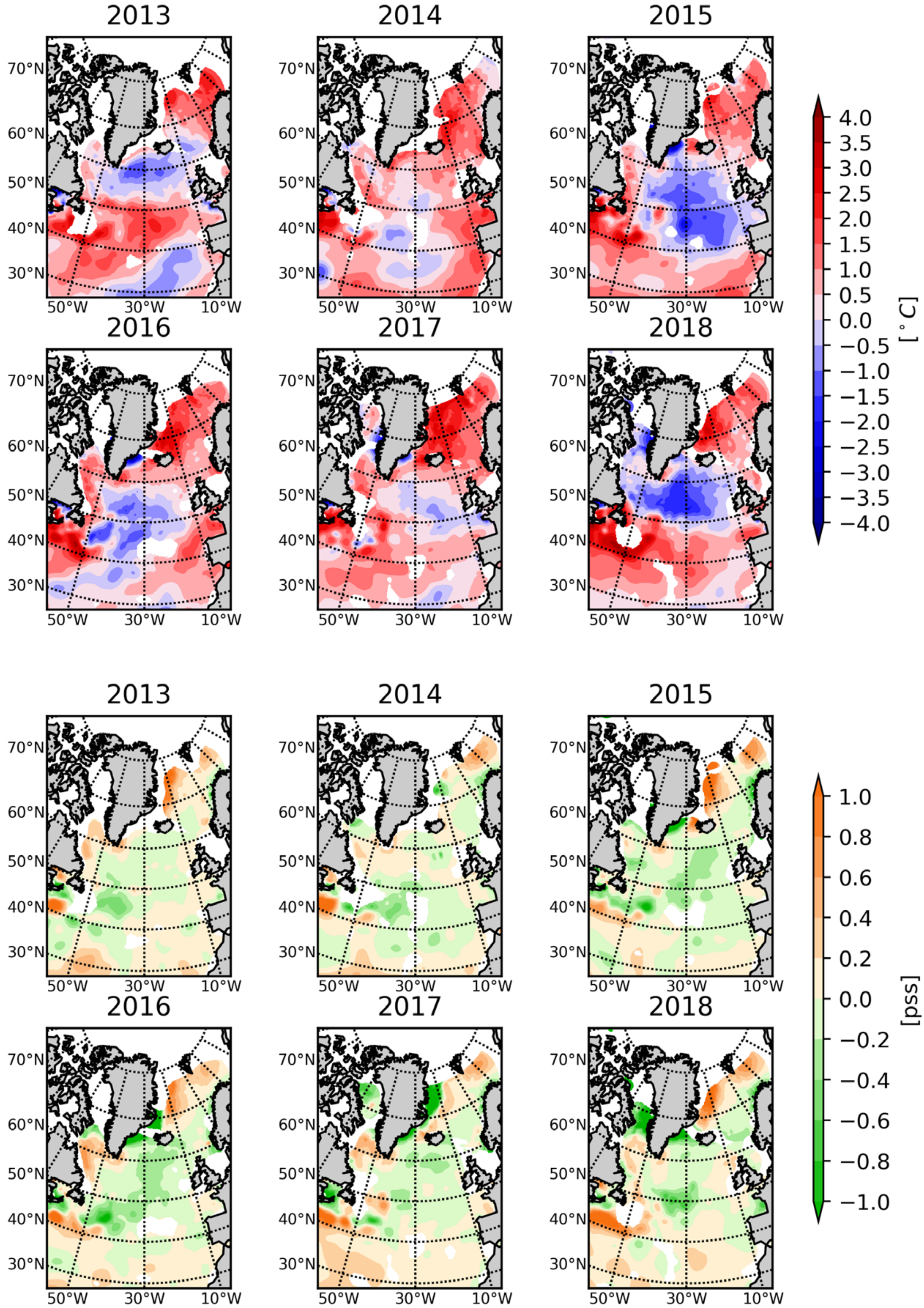

FIGURE 2.6.
Maps of annual temperature (upper) and salinity (lower) anomalies at 10 m depth in the North Atlantic for the period 2013–2018. Anomalies are the differences between the ISAS monthly mean values and the reference climatology, WOA05. The colour-coded scale is the same in all panels. Data prepared from the Coriolis, ISAS monthly analysis of Argo data.

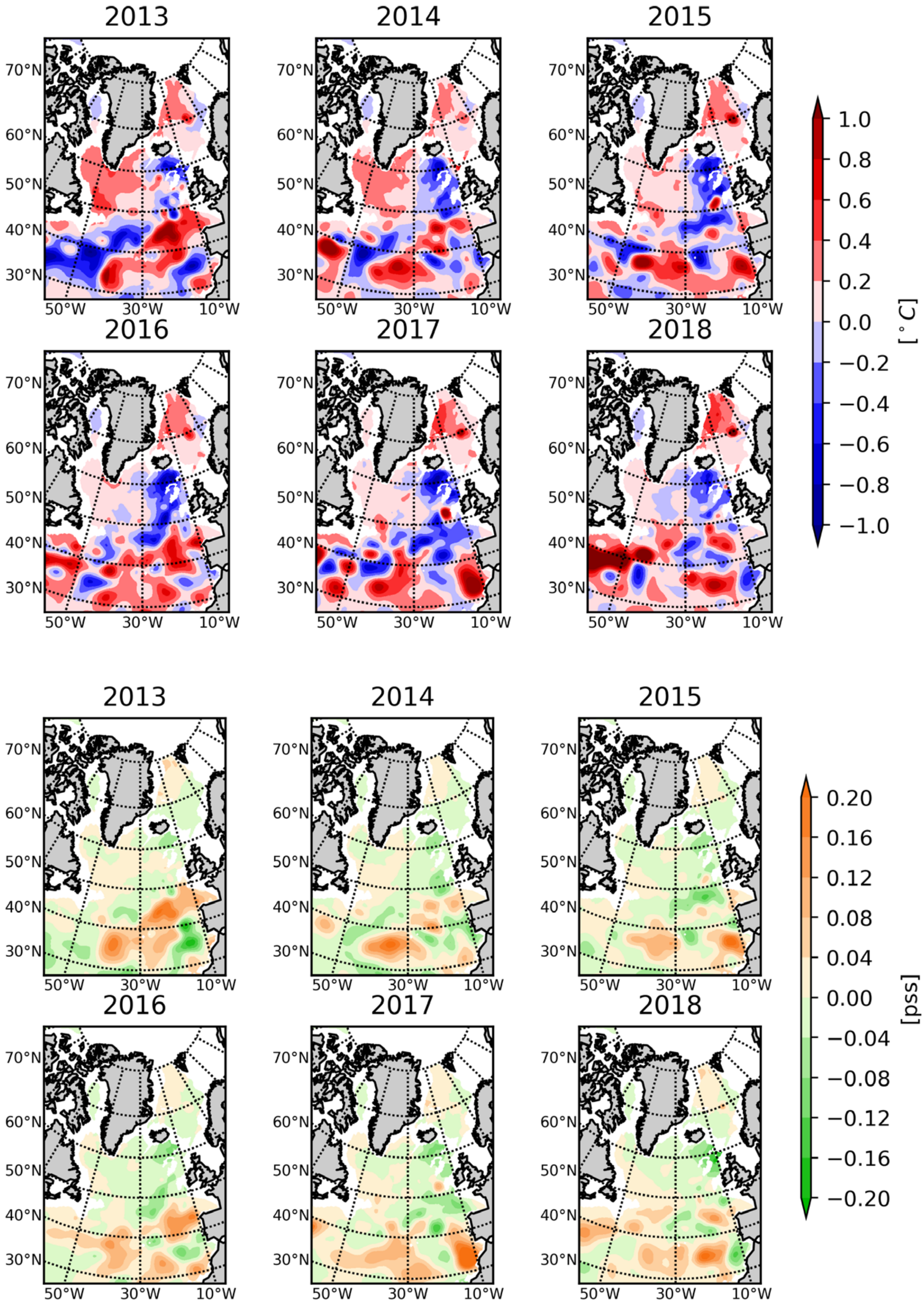

FIGURE 2.7.
Maps of annual temperature (upper) and salinity (lower) anomalies at 1000 m depth in the North Atlantic for the period 2013–2018. Anomalies are the differences between the ISAS monthly mean values and the reference climatology, WOA05. The colour-coded scale is the same in all panels. Data prepared from the Coriolis, ISAS monthly analysis of Argo data.

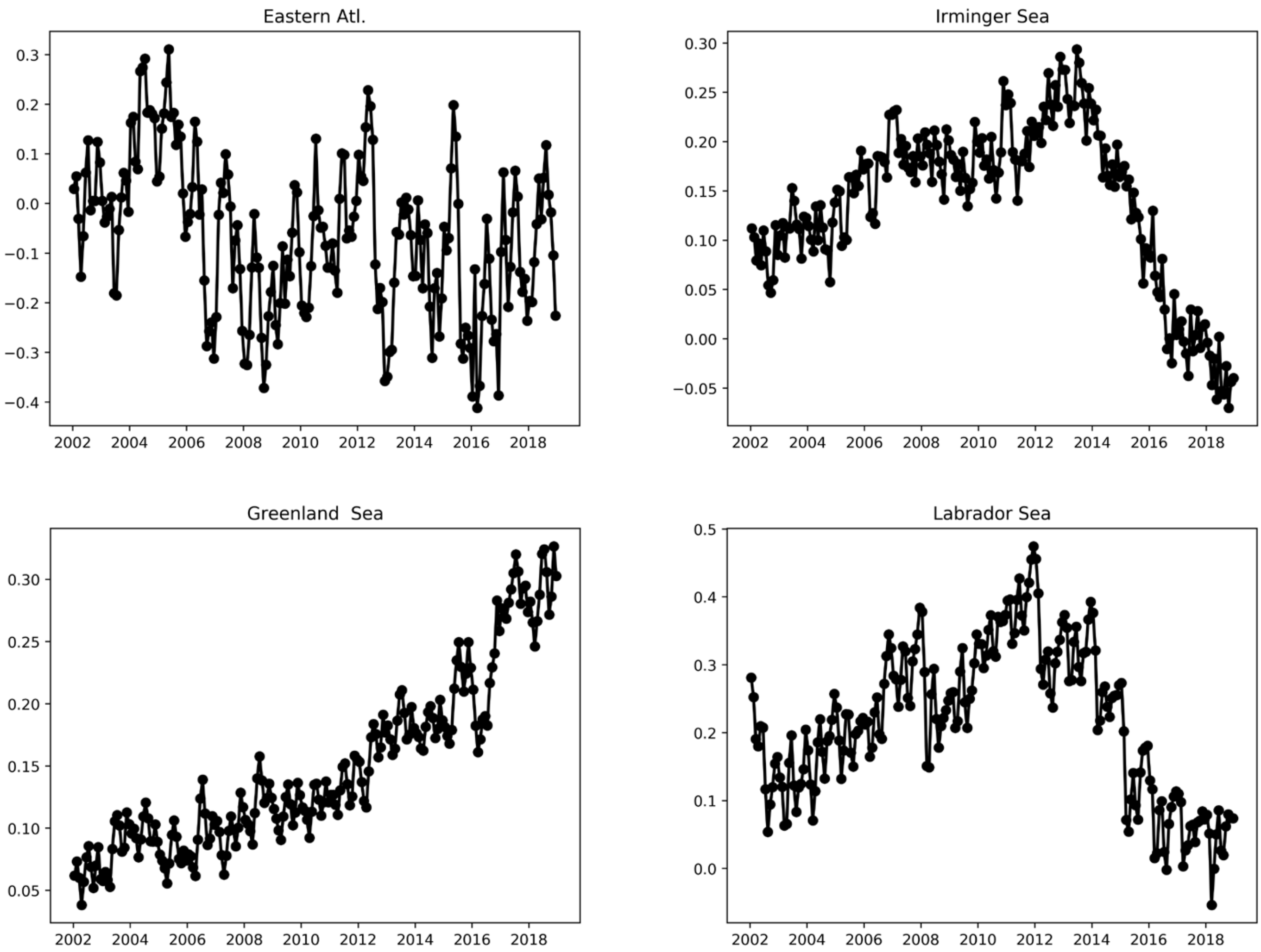

FIGURE 2.8.
Time-series of temperature anomalies (using WOA05 as reference) averaged over the period 2002–2018 and over the 800–1200 m layer in (a) Eastern Atlantic region (25°W, 15°W, 45°N, 55°N); (b) Labrador Sea (60°W, 50°W, 55°N, 65°N) ; (c) Greenland Sea (15°W, 5°W, 65°N, 75°N), and (d) Irminger Sea (40°W, 30°W, 55°N, 65°N).

North of Faroes.
Photo: Karin M. H. Larsen, Faroe Marine Research Institute, Tórshavn, Faroe Islands.

2.4 SURFACE SAMPLING ALONG AX01 AND AX02 (NORTH ATLANTIC SUBPOLAR GYRE)

G. Reverdin

Surface sampling was conducted along two shipping routes (Figure 2.9): line AX02 between southern Newfoundland and Reykjavik (since mid-1993 until June 2016), and line AX01 between Denmark and west Greenland (since mid-1997; MV "Nuka Arctica"). The sampling campaigns are part of a concerted multidisciplinary effort, which includes the measurement of currents with a shipboard ADCP on-board the MV "Nuka Arctica" (University of Bergen, Norway) and fCO2 measurements on-board the RV "Skogafoss" (NOAA/AOML) and the "Nuka Arctica". Both ships were equipped with a thermosalinograph (TSG) and XBT launchers.

In winter and early spring of 2015 and 2016, the nominal AX01 route was not often followed because of the large extent of sea ice and numerous winter storms. In June 2016, the TSG on AX01 was discontinued, but seasonal sampling has continued with a shiprider (four times in 2018). A TSG was installed in November 2018 on MV "Selfoss", but the ship was unfortunately moved by the company (EIMSKIP) soon after to a route in northern Europe.

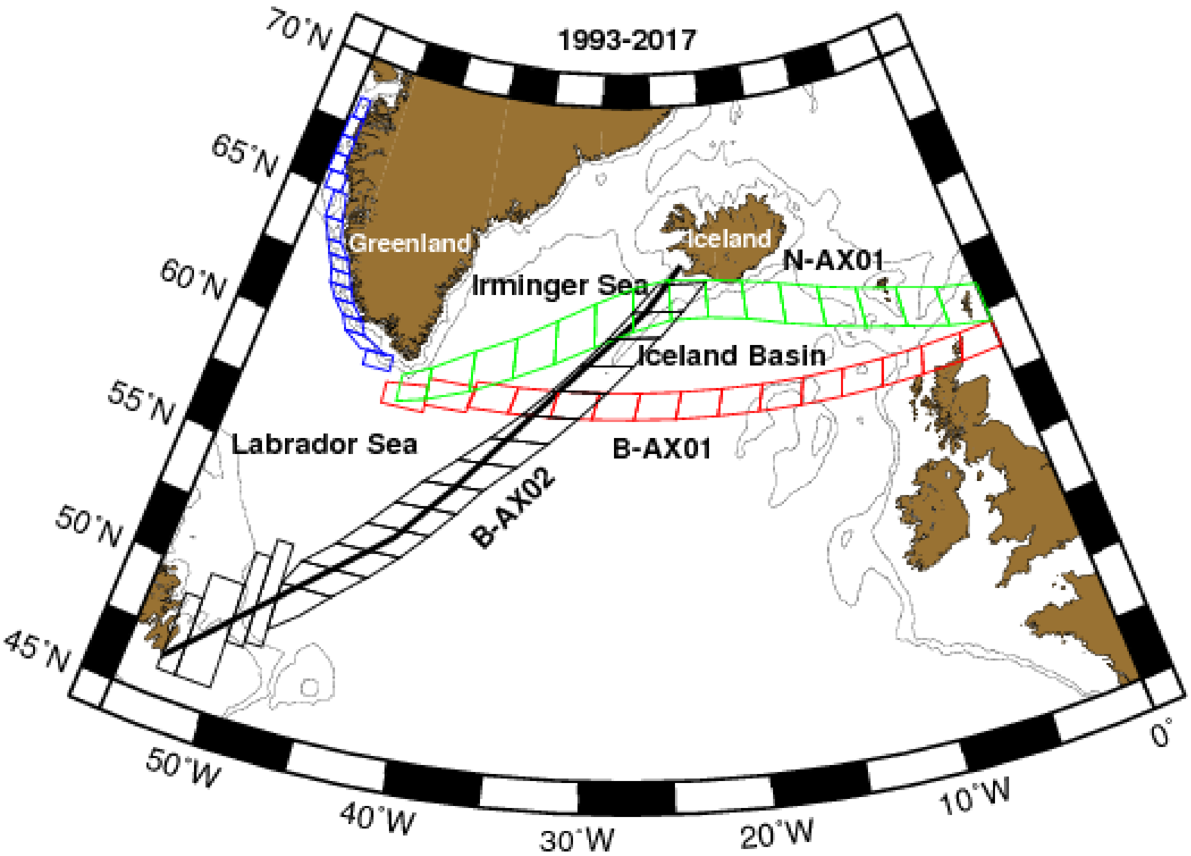

FIGURE 2.9.
Map of the bins along B-AX02 (black), B-AX01 (red), G-AX02 (blue), and N-AX01 (green). A typical example of ship track is shown along B-AX02.

Hovmöller diagrams are presented for SST and SSS as a function of latitude (B-AX02; Figure 2.10, left panels) and longitude (B-AX01; Figure 2.10, right panels) along nominal lines (Figure 2.9). For B-AX01, the information presented is limited to the part of the section between the shelf break off Cape Farewell and northeast of Scotland (Figure 2.9). The diagrams in Figure 2.10 show deviations from the average seasonal cycle during the period 1993–2018. To complement the TSG measurements, nearby Argo 5 m depth data were also used.

Along B-AX02 (Figure 2.10, left panels) there are usually large changes in the anomalies, particularly for salinity, near 53°N at the northern reach of the northwest corner region, at the latitude of the Charlie-Gibbs fracture zone. In 2018, fresh anomalies were present in the northern part of the section, but at a lower intensity than those observed from mid-2016 to early 2018. The year 2018 was also colder than average, particularly in its second half, except on the Newfoundland shelves and near Iceland.

Along B-AX01 (Figure 2.10, right panels), the very fresh anomalies observed near 59°N since mid-2015 in the Iceland Basin, east of the Reykjanes Ridge, and until 15°W, were still present, but had decreased strongly relative to 2016–2017. Temperature anomalies were negative across the section, as has been the trend for the past four years. In contrast to BAX01, for the time-series along N-AX01 (Figure 2.9, conducted since 1996), large negative anomalies were still present in 2018 east of Iceland, particularly near the Faroes.

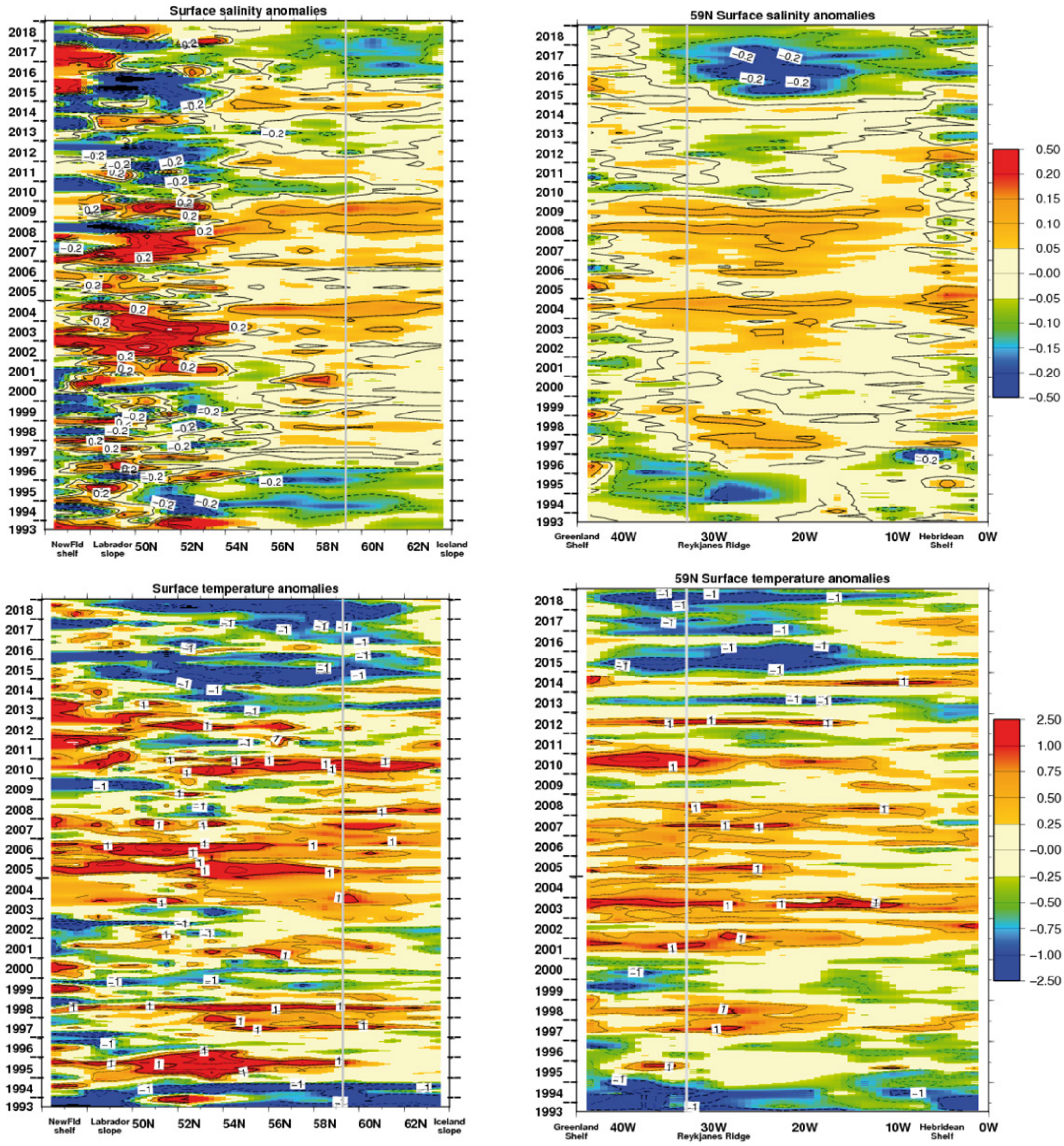

FIGURE 2.10.
B-AX02 (left) and B-AX01 (right) Hovmöller diagrams of deviations from an average sea-sonal cycle. Salinity (top with vertical lines indicative of the crossing of the two lines), and temperature (lower panel). See Figure 2.9 for the positions of the lines.

2.5 SUBPOLAR GYRE INDEX

L. Chafik, H. Hátún, and B. Berx

The surface circulation of the North Atlantic is dominated by two gyres, one that circulates warmer water in a clockwise direction, known as the Subtropical Gyre, and another that circulates cooler waters in the opposite direction, known as the Subpolar Gyre. The Subpolar Gyre encompasses a host of currents, of which the main ones are: the North Atlantic, East Greenland, and Labrador currents. Both the Subtropical and Subpolar gyres are driven by a combination of processes, the most important for the Subpolar Gyre being the strength and direction of surface winds, the exchange of heat between atmosphere and ocean, and the large-scale circulation known as the overturning circulation (Berx and Payne, 2017).

The principal dynamics of the North Atlantic Subpolar Gyre are revealed through sea surface height variability over the Subpolar and Subtropical gyres. Satellite altimetry measurements are available since 1993 (Pujol *et al.*, 2016). An updated version of the gyre index has been produced by applying the method of Häkkinen and Rhines (2004) to this 24-yeardataset (1993–2016). The Subpolar Gyre index now appears as the second principal component and not as the first principal component, as previously reported (Hátún and Chafik, 2018). The new Subpolar Gyre index does not include the trend associated with the first mode, but it is still adept in capturing the main dynamics and intensity of the cyclonic Subpolar Gyre circulation, and is recognized to have significant implications for a wide range of climatic (Hátún *et al.*, 2005; Buckley and Marshall, 2016; Moffa-Sánchez and Hall, 2017) and ecological (Hátún *et al.*, 2009, 2016, 2017) aspects in the North Atlantic.

The Subpolar Gyre is strongly affected by the atmospheric circulation of the North Atlantic, as often summarized by the NAO Index. However, the advantage of using the Subpolar Gyre index for ocean research, instead of the NAO index, is that it integrates the oceanic imprint of the various atmospheric drivers and, thus, has more direct implications for the marine climate and ecosystems in the subpolar North Atlantic.

The Subpolar Gyre index was negative in the early 1990s, reflecting a period of strong gyre circulation (anomalously low sea surface heights, Figure 2.11) intensified by the anomalously strong atmospheric forcing which, in turn, was represented by a very high NAO index during the late 1980s to early 1990s (Delworth *et al.*, 2016).

A rapid reversal of the westerly winds that occurred during winter 1995/1996 switched the NAO index to negative in 1996. This was followed by a period with average or negative NAO values. As a result, the Subpolar Gyre index transitioned to a positive phase, indicating a weaker and contracted gyre circulation (anomalously high sea surface heights, Figure 2.11). This modified gyre shape, most notably in the eastern North Atlantic, permitted a larger contribution of warm, saline, and nutrient-poor subtropical waters to Atlantic inflows towards the Arctic, which ultimately accessed the central Subpolar Gyre, further weakening its strength.

Since 2014, strong atmospheric forcing and winter convection, associated with a positive NAO index (e.g. Yashayaev and Loder, 2017), have resulted in a return of the Subpolar Gyre to a very strong and expanded circulation, similar to that in the early 1990s. This is clearly illustrated by a switch to negative Subpolar Gyre index values in the past few years (Figure 2.11).

The Subpolar Gyre index in 2018 remained negative, with larger values than 2017 but not as strong as the observed values in 2015/2016.

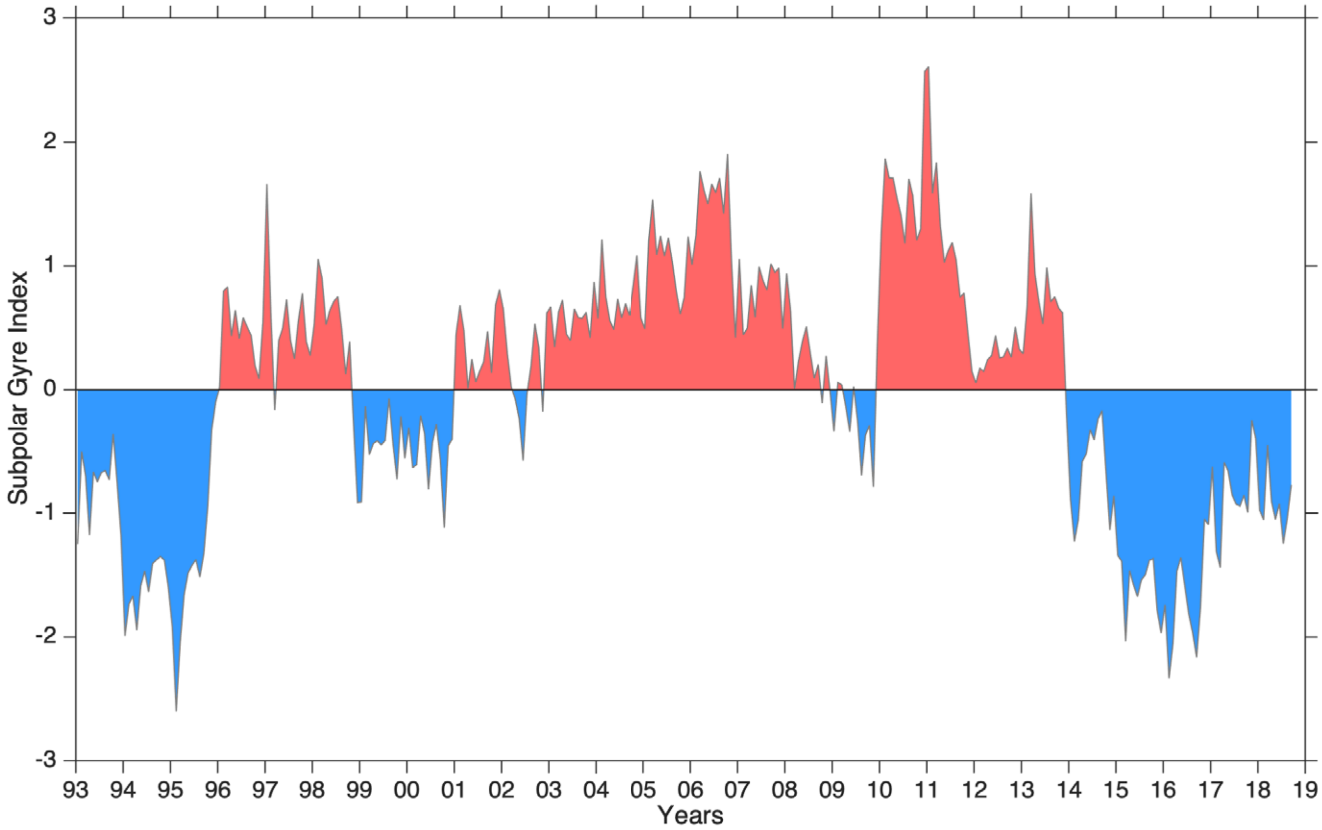

FIGURE 2.11.
The monthly gyre index (second principal component) from January 1993 until September 2018. Data source: altimetry data were obtained through the Copernicus Marine Environment Monitoring Service (http://marine.copernicus.eu). Index source: https://bolin.su.se/data/chafik-2019-2

Ocean sunset in the Atlantic
Photo: Tomasz Szumski,
Marine Institute, Galway, Ireland

Dissolved Oxygen sample fixation.
Photo: Tomasz Szumski, Marine Institute, Galway, Ireland

3. NORTH ATLANTIC ATMOSPHERE

S. Dye

The North Atlantic Oscillation (NAO) is a pattern of atmospheric variability that has a significant impact on oceanic conditions. It affects windspeed, precipitation, evaporation, and the exchange of heat between ocean and atmosphere, and its effects are most strongly felt in winter. The NAO index is a simple device used to describe the state of the NAO. It is a measure of the strength of the sea level air pressure gradient between Iceland and Lisbon, Portugal. When the NAO index is positive, there is a strengthening of the Icelandic low-pressure system and the Azores high-pressure system. This produces stronger mid-latitude westerly winds, with colder and drier conditions over the western North Atlantic, and warmer, wetter conditions in the eastern North Atlantic. When the NAO index is negative, there is a reduced pressure gradient, and the effects tend to be reversed.

There are several slightly different versions of the NAO index calculated by climate scientists. The Hurrell winter (December/January/February/March, or DJFM) NAO index (Hurrell et al., 2003) is the most commonly used and is particularly relevant to the eastern North Atlantic. Note that although we may think of winter as coming at the end of the year, here the "winter season" spans an annual boundary and precedes the year of interest; thus, winter December 2017–March 2018 sets up conditions for summer 2018.

The NAO is the dominant pattern of atmospheric pressure variability in the North Atlantic. However, when the NAO itself is weak (i.e. the dominant atmospheric pattern is not a NAO-type pattern), this may be because a different pattern is occurring. Two other dominant atmospheric regimes have been identified as useful descriptors: (i) the Atlantic Ridge mode, when a strong anticyclonic ridge develops off western Europe (similar to the East Atlantic pattern); and (ii) the Blocking regime, when an anticyclonic ridge develops over Scandinavia. The four regimes (positive NAO, negative NAO, Atlantic Ridge, and Blocking) have all been occurring at around the same frequency (20–30% of all winter days) since 1950 (Hurrell and Deser, 2010). For this reason, we also include maps of SLP, windspeed, and air temperature, as this offers a more detailed understanding of the North Atlantic atmospheric variability than the NAO Index.

3.1 THE NORTH ATLANTIC OSCILLATION NAO INDEX

Following a long period of increase from an extreme and persistent negative phase in the 1960s to a most extreme and persistent positive phase during the late 1980s and early 1990s, the Hurrell NAO index underwent a large and rapid decrease during winter 1995/1996. For many of the years between 1996 and 2009, the Hurrell winter NAO index was fairly weak and a less useful descriptor of atmospheric conditions, mainly because the sea-level pressure patterns were not typical for the NAO. In winter 2009/2010, the index was strongly negative (Figure 3.1) and its anomaly pattern exerted a dominant influence on atmospheric conditions. This was the strongest negative anomaly since 1969 and the second strongest negative value for the Hurrell winter NAO index on record (starting in 1864). Winter 2014/2015 saw the strongest NAO index since 1995 and the fourth-most positive NAO index in the last 110 years (Hurrell and National Center for Atmospheric Research Staff, 2017). In winter 2016/2017, the NAO index was strong and positive (+1.47) for the fourth consecutive winter, the first such positive run since 1992–1995. This run was brought to an end in winter 2017/2018, with an index that was near neutral (+0.30).

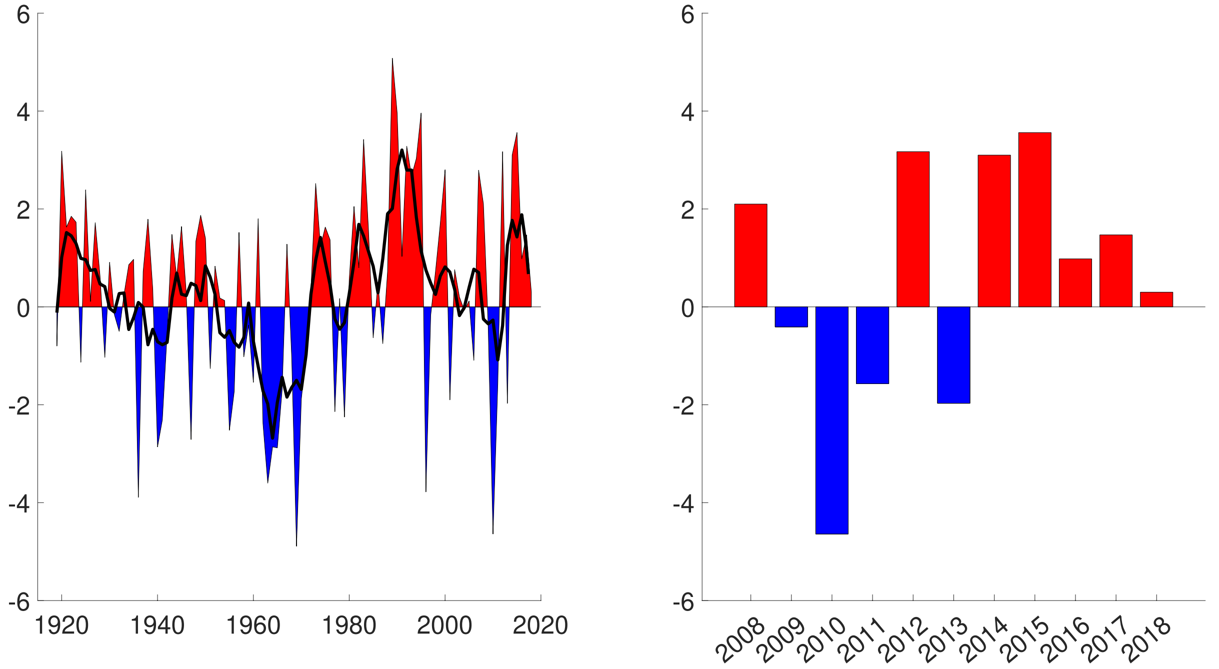

FIGURE 3.1.
The Hurrell winter (DJFM) NAO index for the past 100 years with a two-year running mean applied (left panel) and for the current decade (right panel). Data source: NAO Index Data provided by the Climate Analysis Section, NCAR, Boulder, USA, (Hurrell and National Center for Atmospheric Research Staff, 2018).

3.2 SEA LEVEL PRESSURE AND WIND SPEED

The spatial pattern of atmospheric conditions indicated by a particular NAO index value is more understandable when the anomaly fields are mapped. Impacts on ocean properties are particularly dominated by winter conditions. Therefore, SLP and windspeed maps are included here for the winter period (Figures 3.2 and 3.3).

The top panel of Figure 3.2 shows winter SLP averaged over 30 years (1981–2010). The dominant features ("action centres") are the Iceland Low, situated southwest of Iceland, and the Azores High, west of Gibraltar. The middle panel of Figure 3.2 shows the mean SLP for winter 2017/2018 (December 2017 through March 2018). The bottom panel shows the 2017/2018 winter SLP anomaly (i.e. the difference between the top and middle panels).

SLP patterns are closely related to wind patterns. The geostrophic (or "gradient") wind blows parallel with the isobars, with lower pressure to the left; the closer the isobars, the stronger the wind. The strength of winter-mean-surface-wind averaged over the 30-year period (1981–2010) is shown in the upper panel of Figure 3.3. The middle panel shows the mean surface wind for winter 2017/2018 and the lower panel the anomaly in winter 2017/2018.

The SLP anomaly for winter 2017/2018 (Figure 3.2) did not resemble a typical NAO pattern. Instead, a strong low-pressure (cyclonic) anomaly was centred over northern France and extended across most of Europe south of Scandinavia. A large-scale high-pressure anomaly was split to the northeast and southwest of Iceland, with extended anticyclonic ridges across the Nordic seas, Northwest Atlantic, and the Labrador Sea. The influence of this was seen in mixed wind patterns (Figure 3.3). A northwesterly wind anomaly, with stronger winds than usual, occurred in a narrow band between Cape Farewell and Iberia and the surrounding area. Weaker-than-average winds were evident over the northern North Sea and in a band that extended from west of Scotland, along the Norwegian coast, and into the Barents Sea. The location of the SLP cyclonic anomaly brought winds from a northeasterly direction across the Norwegian Sea and Iceland Basin west of the Faroes. Later in the year, the Barents Sea experienced notably stronger winds than average. This was part of a pattern of strong winds stretching from the western Subpolar Gyre to the Norwegian Sea, which affected a number of scientific cruises in the region.

CTD deployed with pilot whales around. Photo: David Herbert, Fisheries and Oceans Canada, Dartmouth, Nova Scotia

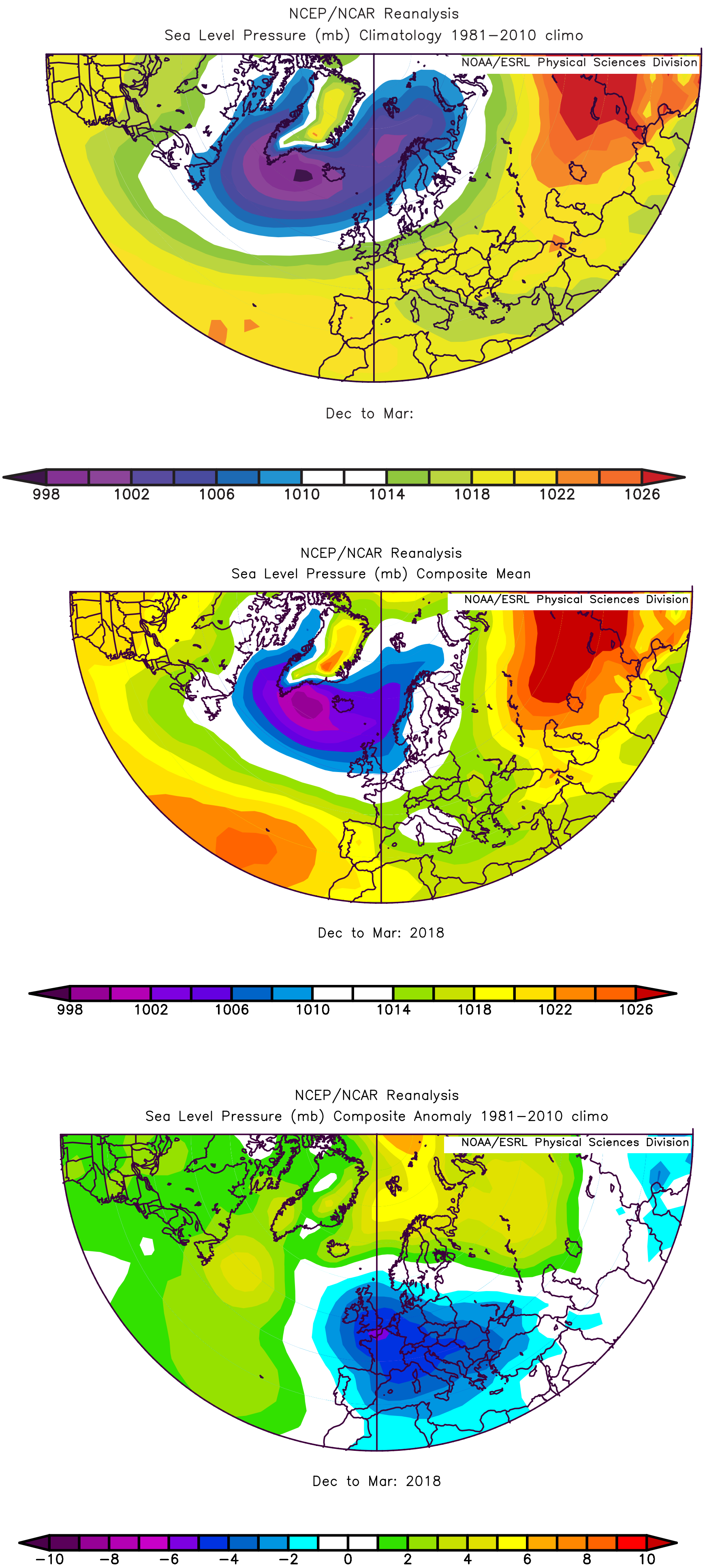

FIGURE 3.2.
Winter (DJFM) SLP fields. Top panel: SLP averaged over 30 years (1981–2010). Middle panel: SLP in winter 2017/2018. Bottom panel: winter 2017/2018 SLP anomaly, calculated as the difference between the top and middle panels. Images provided by the NOAA/ESRL Physical Sciences Division, Boulder, CO, USA.

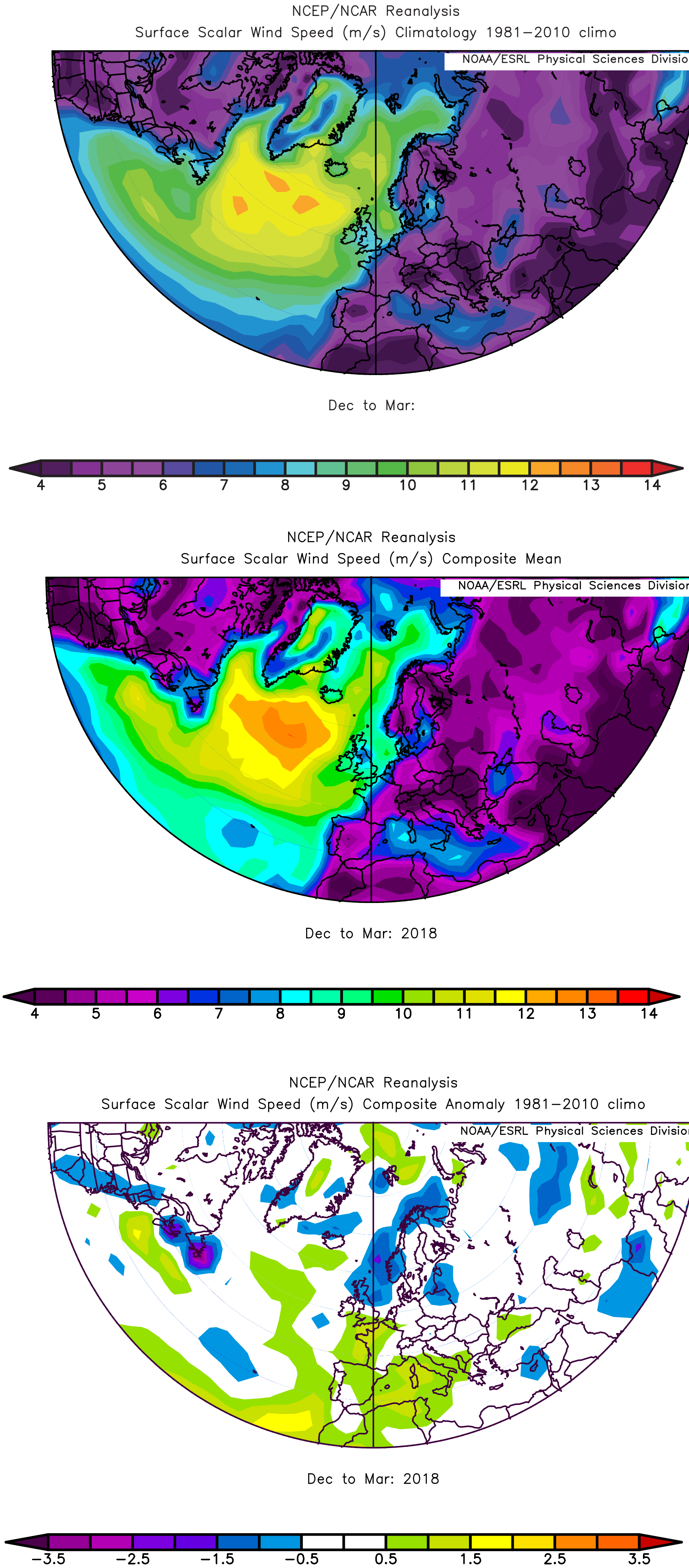

FIGURE 3.3.
Winter (DJFM) windspeed fields. Top panel: scalar windspeed averaged over 30 years (1981–2010). Middle panel: scalar windspeed in winter 2017/2018. Bottom panel: winter 2017/2018 scalar windspeed anomaly, calculated as the difference between the top and middle panels. Images provided by the NOAA/ESRL Physical Sciences Division, Boulder, CO, USA.

3.3 SURFACE AIR TEMPERATURE

North Atlantic winter mean surface air temperatures are shown in Figure 3.4 (Kalnay *et al*., 1996). The 1981–2010 mean conditions (Figure 3.4, top panel) show warm temperatures penetrating far to the north on the eastern side of the North Atlantic and the Nordic seas, caused by the northward movement of warm oceanic water. The middle panel of Figure 3.4 shows the conditions in winter 2017/2018, and the bottom panel shows the difference between the two.

Winter 2017/2018 air temperatures were colder than average (1981–2010) over the Subpolar Gyre, the Irminger Sea, and the eastern North Atlantic, consistent with the relatively cool SST anomalies observed in the Subpolar Gyre in recent years. Around the eastern margin of the North Atlantic, air temperatures were particularly cold in the south, over Morocco and Iberia, and in the north over Norway. Warmer conditions were evident southwest of the Subpolar Gyre, particularly over the northern Barents Sea, the northern Labrador Sea, the East Greenland coast north of the Denmark Strait and extending to the Fram Strait and the Arctic Ocean.

3.4 OUTLOOK BEYOND 2017

An initial assessment of the North Atlantic atmosphere at the end of the IROC year is included. Atmospheric conditions during winter are a determining factor of oceanic conditions for the following year; therefore, this outlook offers some predictive capability for spring–autumn 2019.

The SLP pattern for December 2018–February 2019 suggests a second consecutive weakly positive, near-neutral NAO index winter. In contrast to winter 2016/2017, SLP pattern, anticyclonic anomalies lay across western Europe through to Iceland, although a cyclonic anomaly sat south of Cape Farewell in the middle of the North Atlantic. This may mean that upper ocean conditions in the western part of the region resembled those that would be expected in response to a negative NAO winter, although conditions in the east were closer to those expected in response to a NAO positive winter. Air temperatures were relatively warm across Europe, the Nordic seas, and the Labrador Sea. Colder-than-normal air temperatures were limited to the south of Newfoundland. Wind speeds across the region were generally lower than average in December 2018—February 2019 (DJF), particularly east of Newfoundland, south of Cape Farewell, and in a band stretching across the Nordic seas from Scoresby Sund in Greenland to the North Cape of Norway.

Recent advances in understanding the predictability of the NAO are showing significant skill in seasonal predictions for the European winter through predictability of winter NAO (Scaife *et al*., 2014), Arctic Oscillation (AO), and Sudden Stratospheric Warming (SSW) events (Scaife *et al*., 2015). Results published by the Met Office suggest that there is even significant skill in predicting the winter NAO index one year ahead (Dunstone *et al*., 2016), with a correlation coefficient (r) between observed and predicted NAO of about 0.4 for the second winter, comparing well with that of about 0.6 for the first winter (Scaife *et al*.,2014).

Experimental forecasts from the US (over seasonal periods[4]) and UK (over 1–5 years; Met Office Decadal forecast January 2019[5]) suggest a warmer outlook for the Subpolar Gyre region, more closely resembling the long-term average (1981–2010) than the last few cold anomaly years. Experimental forecasts are at an early stage and these examples are noted here so that we can track their performance and gauge their utility as they develop. The seasonal forecast made early last year for warmer conditions in summer and autumn did not predict the re-emergence of cool conditions in the surface Subpolar Gyre.

.

4) www.cpc.ncep.noaa.gov/products/NMME/
5) https://www.metoffice.gov.uk/research/climate/seasonal-to-decadal/long-range/decadal-fc/index

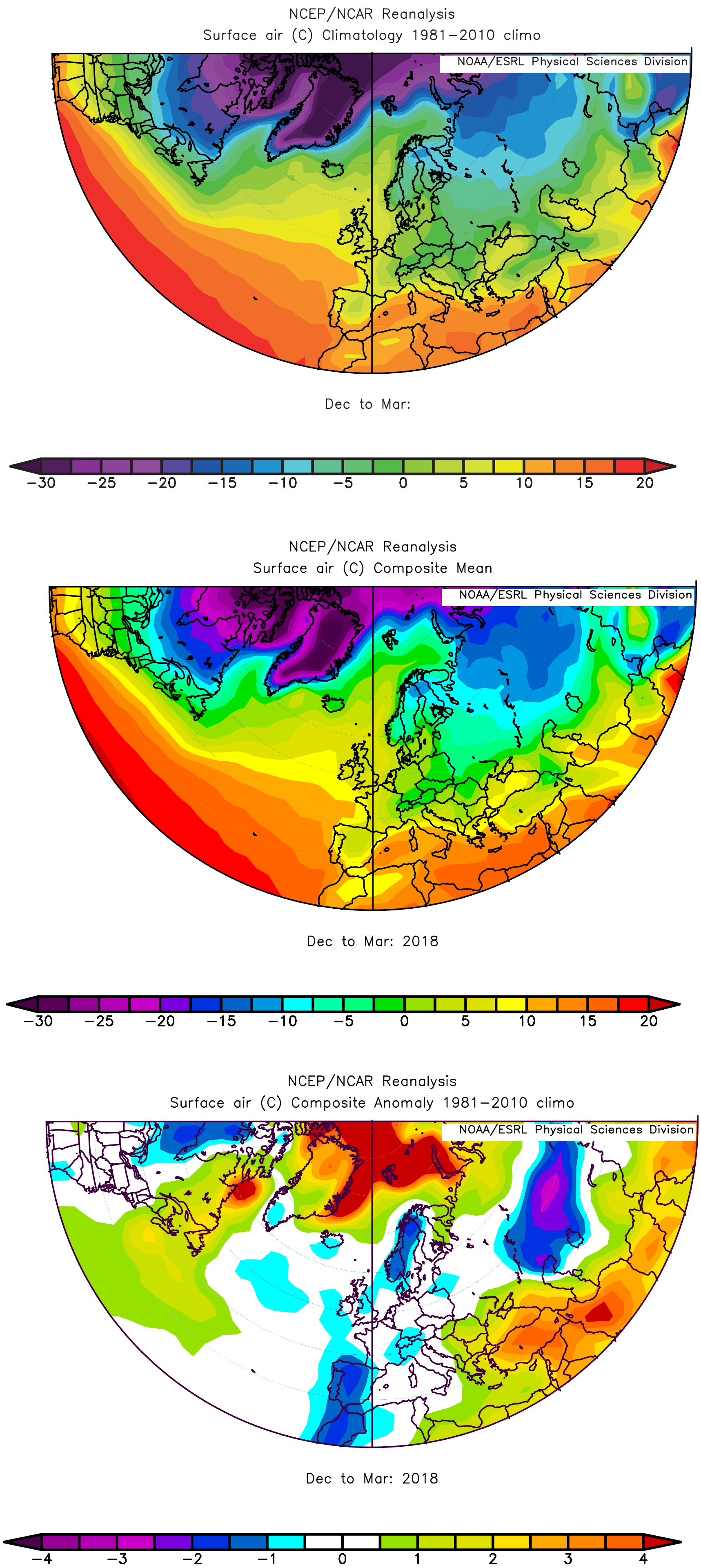

FIGURE 3.4.
Winter (DJFM) surface air temperature fields. Top panel: surface air temperature averaged over 30 years (1981–2010). Middle panel: surface air temperatures in winter 2017/2018. Bottom panel: winter 2017/2018 surface air temperature anomaly, calculated as the difference between the top and middle panels. Images provided by the NOAA/ESRL Physical Sciences Division, Boulder, CO, USA (available online at [http://www.cdc.noaa.gov/)](http://www.cdc.noaa.gov/)

The Marine Institute deploys an Argo Float on the annual ocean climate survey.
Photo: Tomasz Szumski, Marine Institute, Galway, Ireland

4. DETAILED AREA DESCRIPTIONS, PART I: THE UPPER OCEAN

INTRODUCTION

This section presents time-series from sustained observations in each of the ICES Areas shown in Figure 4.1. The general pattern of oceanic circulation in the upper layers of the North Atlantic in relation to the areas described here is shown in Figure 4.2. In addition to temperature and salinity, other indices are presented where available, such as air temperature and sea ice extent. The regional context of the sections and stations are summarized, noting any significant changes.

Most standard sections or stations are sampled annually or more frequently. Many of the time-series presented here have been extracted from larger datasets and have been chosen as indicators of the conditions in a particular area. Where appropriate, data are presented as anomalies to demonstrate how the values compare with the average or "normal" conditions (usually the long-term mean of each parameter during 1981–2010). For datasets that do not extend as far back as 1981, the average conditions have been calculated from the start of the dataset through to 2010.

In places, the seasonal cycle has been removed from a dataset either by calculating the average seasonal cycle during 1981–2010 or by drawing on other sources, such as regional climatology datasets. Smoothed versions of most time-series are included using a "Loess smoother", a locally weighted regression with a two- or five-year window (chosen depending on which was the most appropriate for each time-series).

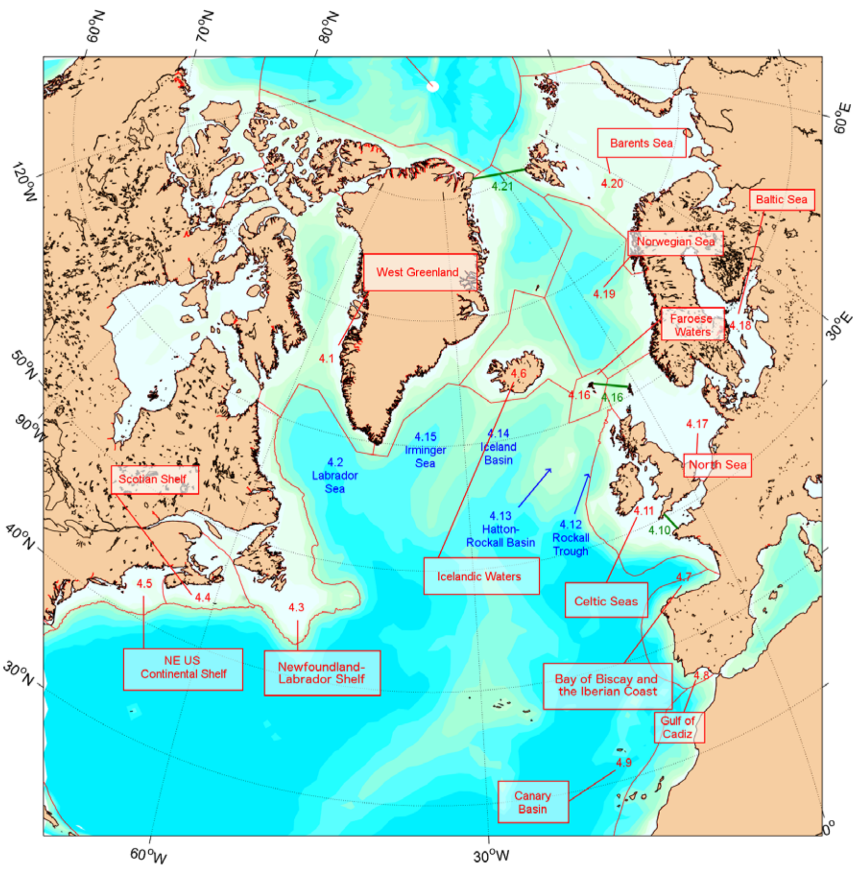

FIGURE 4.1.
Schematic of marine areas used to organize data presented in this section. Numbers refer to the subsection number. Regions are labelled in red, ocean basins are labelled in blue, and straits are labelled in green. NOAA LME boundaries[6] are shown as background reference, but hydrograpic regions are loosely defined so they do not perfectly overlap.

6) http://lme.edc.uri.edu/index.php

In some areas, data are sampled regularly enough to allow a good description of the seasonal cycle. Where possible, monthly data from 2018 are presented and compared with the average seasonal conditions and statistics.

Although there are no real boundaries in the ocean, it is intended that the data presented represent conditions in a particular area. This section groups datasets into areas based on existing definitions. The NOAA Large Marine Ecosystems (LMEs)[6] serve as an overall reference as they cover all regions. However, ICES Marine Ecoregions[7], the bathymetry of ocean basins[8], and the general pattern of ocean circulation, are also taken into account (Figure 4.2).

While the data presented offer the best available indicative time-series within a region, it should be noted that, in large areas with complex circulation patterns, consideration should be given to how representative these data are of the whole ecoregion.

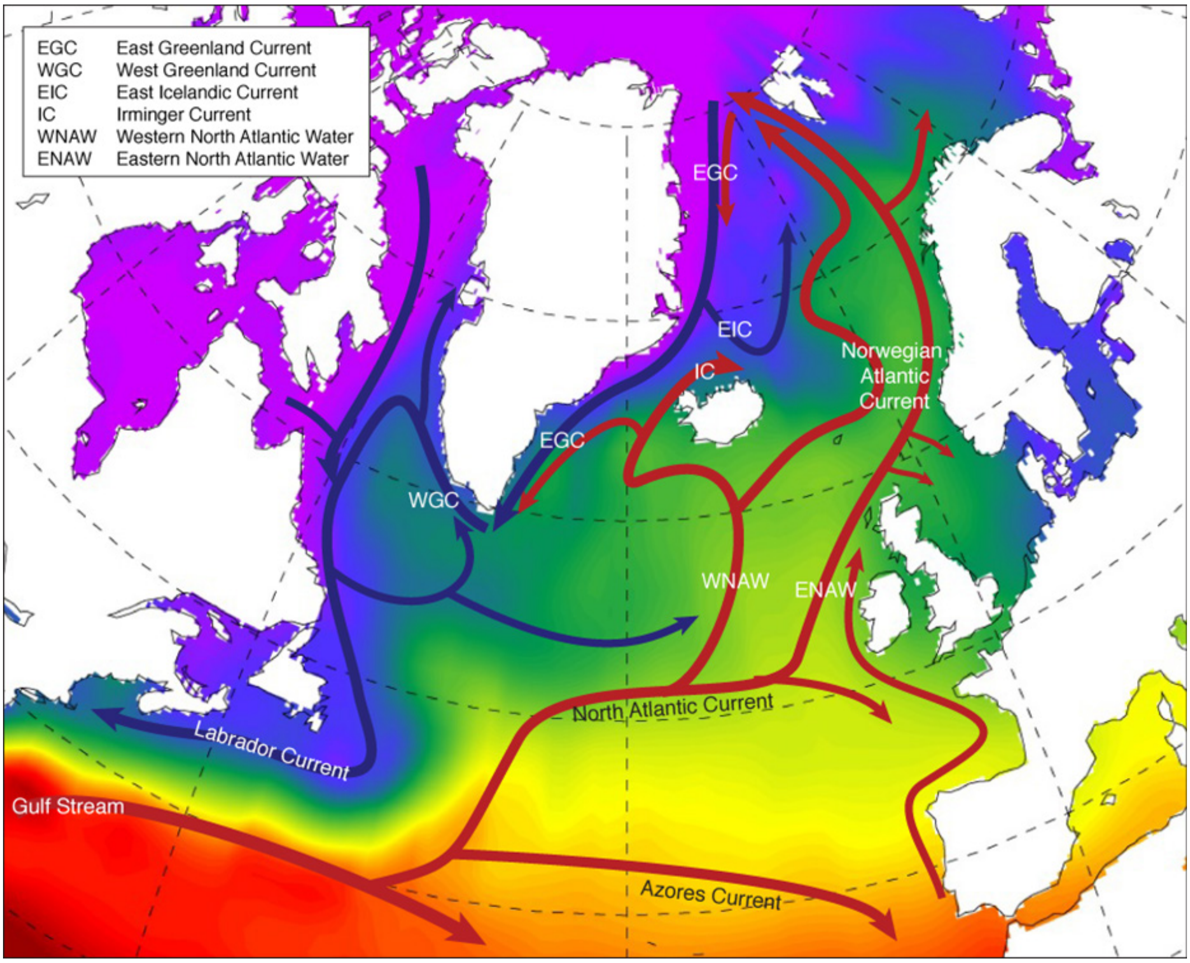

FIGURE 4.2.
Schematic of the general circulation of the upper ocean (0–1000 m) in the North Atlantic. Blue arrows: movement of cooler waters of the Subpolar Gyre; red arrows: movement of warmer waters of the Subtropical Gyre.

6) http://lme.edc.uri.edu/index.php
7) http://www.ices.dk/community/advisory-process/Pages/ICES-ecosystems-and-advisory-areas.aspx
8) http://www.gebco.net/data_and_products/undersea_feature_names/

4.1 WEST GREENLAND

B. Cisewski and J. Mortensen

The NOAA LME project identifies the ecosystem of the Canadian Eastern Arctic–Western Greenland as a single LME. Here, only conditions in the Western Greenland portion of the region are examined. The hydrographic conditions presented are monitored at two oceanographic sections across the continental slope of West Greenland, located in the southwestern part of the ecoregion at a position that is influenced by the West Greenland Current (WGC; Figure 4.3).

The WGC carries water northward along the west coast of Greenland, and consists of two components: (i) a cold, fresh inshore component, which is a mixture of Polar Water and melt water; and (ii) a warmer, saltier offshore component, which is called Irminger Sea Water. Being part of the cyclonic Subpolar Gyre, the WGC is subject to hydrographic variations on the time-scale range associated with variability in the gyre.

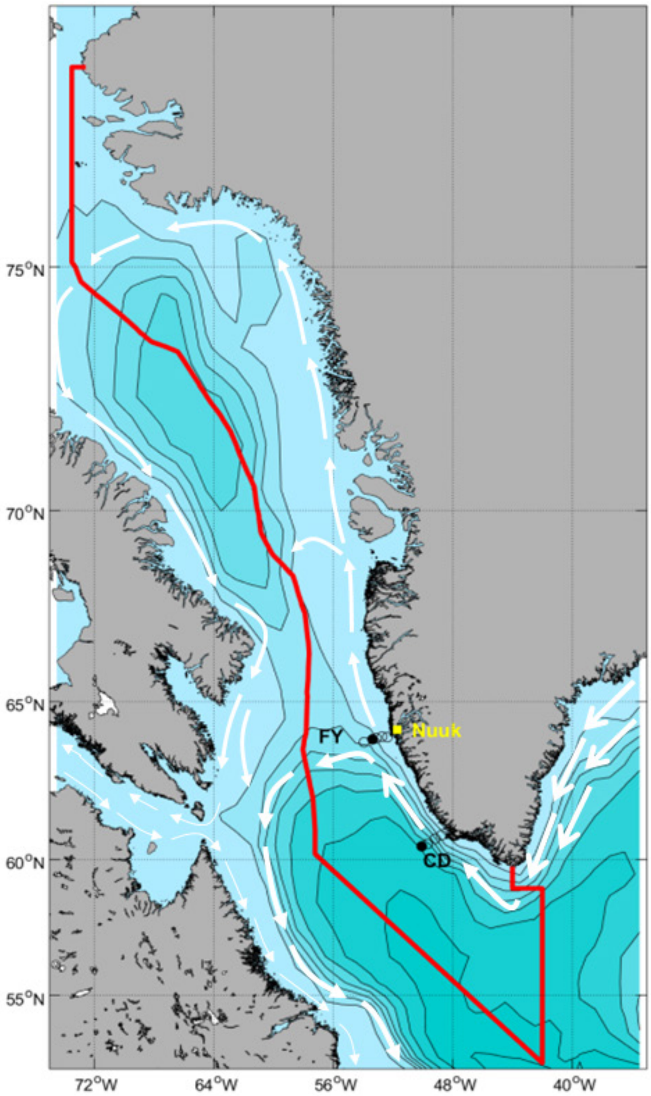

FIGURE 4.3.
Circulation schematic for the Labrador Sea and Davis Strait. The location of Nuuk is marked in yellow. White arrows show the path of the surface circulation. The thick arrows are the WGC. The red lines show the extent of NAFO Area 1a, Western Greenland. The circles labelled “FY” are the stations of the Fyllas Bank hydrographic section stations. Station 4 is marked as a black circle. The circles labelled “CD” are the Cape Desolation hydrographic section stations. Station 3 is marked as a black circle.

The West Greenland shelf and adjacent seas are delineated in the north by the NOAA LME boundaries and in the south by ICES ecoregion boundaries. The conditions presented here are from two hydrographic sections across the southwest Greenland continental shelf sampled twice annually (in June/July by the Greenland Institute of Natural Resources and in autumn by the Thünen Institute of Sea Fisheries, Germany). The time-series shown are from the continental slope influenced by the WGC. In autumn 2018, the Cape Desolation and Fyllas Bank sections were not occupied owing to mechanical problems with the survey vessel.

The WGC carries warm and saline Subpolar Mode Water (SPMW) northward along the West Greenland continental slope. The WGC is overlaid by a colder, fresher surface water mass derived from a variety of sources.

In winter 2017/2018, the NAO index was positive (0.3) for the fifth consecutive winter. The annual mean air temperature at Nuuk Weather Station in West Greenland was −1.7°C in 2018, which was 0.3°C below the long-term mean (1981–2010; Cappelen, 2019).

The water properties between 0 and 50 m depth at Fyllas Bank Station 4 are used to monitor variability in the fresh surface water component of the WGC in June/July. In 2018, the temperature of this water mass was 1.36°C, 0.33°C below its long-term mean (1981–2010, T_{mean} = 1.69°C). Salinity decreased in 2018, being 0.11 above its long-term mean (1981–2010, S_{mean} = 33.27).

The temperature and salinity of the SPMW component of the WGC started to increase towards the end of the 1990s. This coincided with changes in the Subpolar Gyre caused by the entry of warm and saline water from the Subtropical Gyre. By mid-July 2018, water temperatures in the 75–200 m layer at Cape Desolation Station 3 (KD3) was 4.41°C and salinity was 34.83, i.e. 0.24°C and 0.05 below the long-term means, respectively (1992–2010, T_{mean} = 4.65°C and S_{mean} = 34.88).

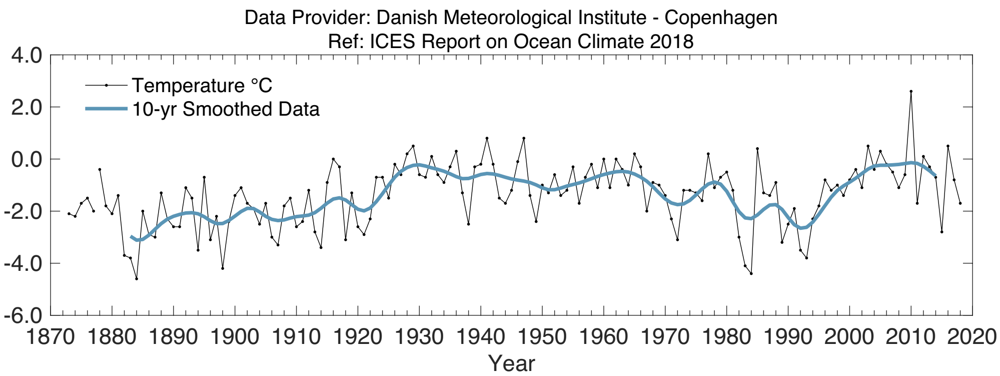

FIGURE 4.4. West Greenland. Annual mean air temperature at Nuuk station (64.16°N 51.75°W). Data source: Cappelen (2019).

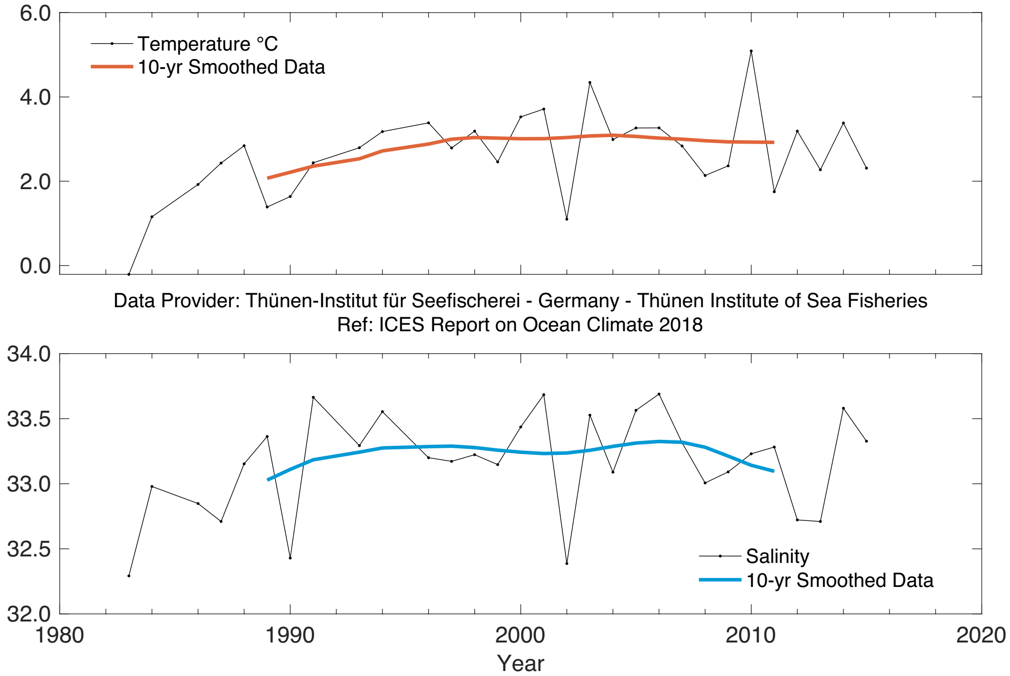

FIGURE 4.5. West Greenland. Mean temperature (upper panel) and salinity (lower panel) in the 0–50 m water layer at Fyllas Bank Station 4 (63.88°N 53.37°W). Data until 2015.

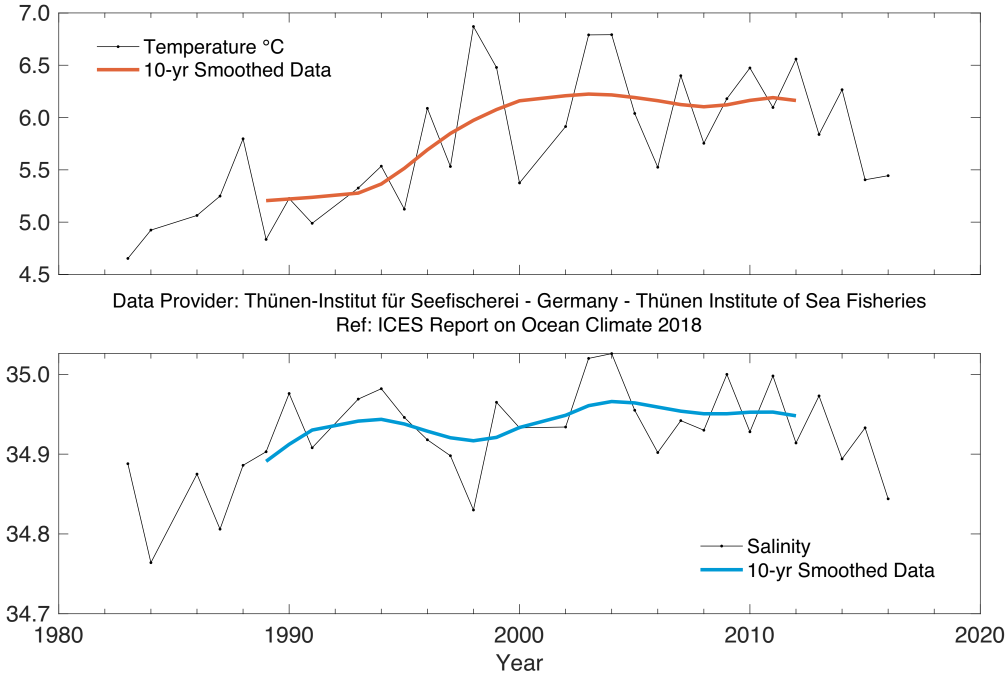

FIGURE 4.6. West Greenland. Temperature (upper panel) and salinity (lower panel) in 75–200 m water layer at Cape Desolation Station 3 (60.47°N 50°W). Data until 2016.

4.2 LABRADOR SEA

I. Yashayaev

The Labrador Sea is located between Greenland and the Labrador coast of eastern Canada. Its deep semi-enclosed basin is bound by the West Greenland and the Newfoundland–Labrador shelves. Cold, low-salinity waters of polar origin circle the Labrador Sea in an anticlockwise current system that includes both the north-flowing WGC on the eastern side and the south-flowing Labrador Current on the western side. Patches of warmer and saltier Atlantic water (AW), typically found under the offshore extension of the WGC, can be traced to their origin in the low latitudes of the North Atlantic by following the North Atlantic Current and Gulf Stream. The AW mixes with other water masses and progressively becomes colder and fresher as it flows north into the Labrador Sea, following its eastern boundary, and eventually circuits the sea's northern and western peripheries.

Interannual changes in the hydrographic conditions of the Labrador Sea are controlled by a number of factors, including the annual heat loss to the atmosphere, heat and salt gain from the AW, and freshwater gain from the Arctic outflow, sea ice melt, precipitation, and continental run-off. In addition, instantaneous conditions and process development depend on the cumulative effect of past heat, salt, and freshwater gains and their respective temperature, salinity, and density changes, also termed ocean preconditioning (Yashayaev and Loder, 2017).

In the Labrador Sea, surface heat losses in winter result in the formation of dense intermediate-depth waters (200–2500 m). This process makes the Labrador Sea the primary region in the northern hemisphere for the atmospheric ventilation of the Atlantic Ocean's intermediate-depth waters. Through winter cooling of surface and subsurface waters and their subsequent mixing and sinking to depths of 500–2500 m (depending on winter severity), a relatively dense and deep intermediate water mass, known as Labrador Sea Water (LSW), is formed. This water spreads over the Atlantic Ocean ventilating its deep layers and feeding and driving the global ocean's overturning circulation or ocean conveyor belt.

2018 – The fifth consecutive year adding to deepening of winter convection and intermediate water mass production in the Labrador Sea during winter 2017/2018.

Oceanographic monitoring of the Labrador Sea

The Atlantic Zone Off-Shelf Monitoring Program (AZOMP), conducted by Fisheries and Oceans Canada, provides observations on ocean climate and plankton variability in the North Atlantic, affecting climate and ecosystems at regional to global scales. An annual survey of the Atlantic Repeat 7-West (AR7W) line in the Labrador Sea has been conducted by the Bedford Institute of Oceanography since 1990, usually in May. This survey was initially part of the World Ocean Circulation Experiment and is currently the core component of AZOMP. This key Atlantic transect has been occupied and sampled at least yearly for a 30-year period (1990–2019), with only one interruption in 2017. The ship-based sampling of the Labrador Sea was resumed during the 2018 AZOMP mission carried out on-board the CCGS Hudson (Figure 4.7).

The International Argo Program has provided the oceanographic community with unprecedented year-round monitoring of key oceanographic variables from the sea surface to 2000 m. The central Labrador Sea ship survey and Argo float observations have been used to construct time-series of temperature, salinity, and density absolute values and anomalies averaged annually revealing interannual-to-multidecadal changes in regional conditions over nearly eight decades. Examples of these series for the upper (50–200 m) and deep intermediate (1000–1800 m) layers are presented in figures 4.8 and 5.11 (see Section 5.2.5), respectively. Key factors causing these properties to change are (i) advection of freshwater from the Arctic, continental run-off and precipitation, and heat and salt from other Atlantic basins; and (ii) local atmospheric forcing, mainly, but not exclusively, projected onto the deep Labrador Sea through winter convection. In order to better understand the appearance and causes of interannual-to-multidecadal changes in the region, the progressive developments of deep convection alternated with periods of ocean “relaxation” over the past thirty years are described in more detail.

Deep convection, water ventilation, and hydrographic trends

A sequence of severe winters in the early 1990s led to deep convection, with the maximum depth reached in 1993/1994. This process filled the upper 2500 m of the water column with cold, fresh and dense water. Conditions have generally become milder since the mid-1990s. During 1995–2011, the upper and deep layers of the Labrador Sea became warmer and more saline as heat losses to the atmosphere decreased and AW became increasingly dominant (Figures 4.8 and 5.11; see Section 5.2.5). However, over the past eight years (2011–2018), the upper and intermediate layers have shown a cooling and freshening trend.

A short spike of cooling and freshening in the deep intermediate series (Figure 5.11, Section 5.2.5) was associated with the deep convection event of 2007/2008 (Yashayaev and Loder, 2009). The 2009/2010 and 2010/2011 winter heat losses were low in magnitude and were matched by record-weak convection, with the MLD typically not exceeding 800 m. The situation changed abruptly the following year, starting a new and important trend in LSW production and regional hydrographic properties. In winter 2011/2012, convection reached, and

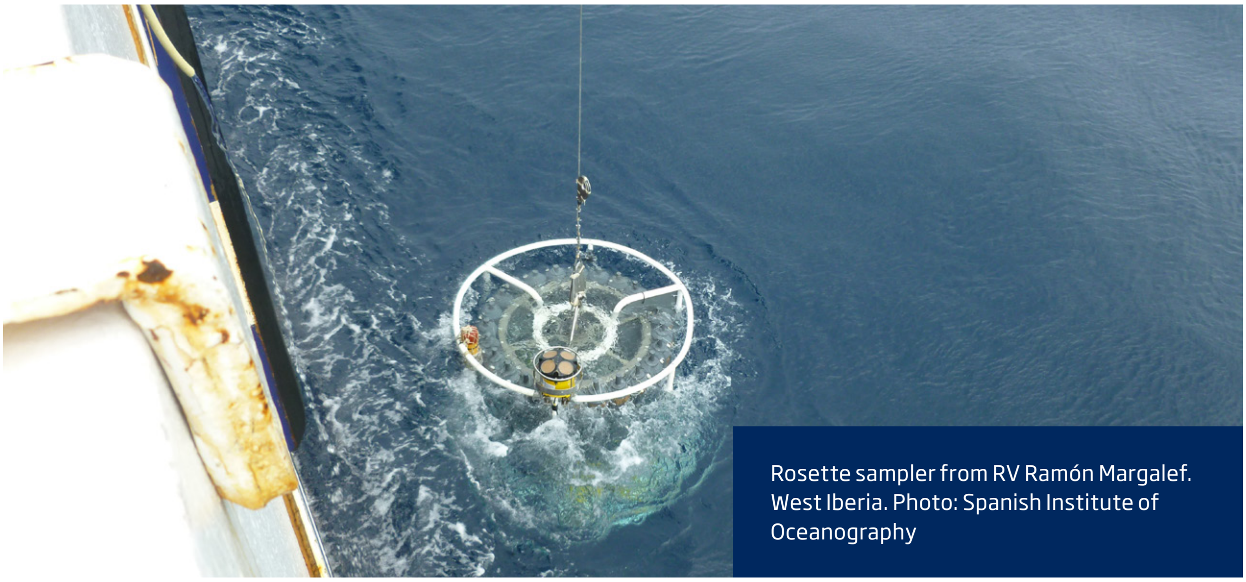

Rosette sampler from RV Ramón Margalef. West Iberia. Photo: Spanish Institute of Oceanography possibly exceeded, 1400 m in depth, evident from both Argo float and ship survey temperature and salinity profile data. Interestingly, 2012 salinity in the top 50 m was the lowest since 2003, possibly influencing the strength of convection in winter 2012/2013, which was not as deep as in the previous year. The situation reversed once again in 2014, when a strong winter cooling triggered convective mixing in the Labrador Sea reaching deeper than 1600 m. Convection continued to deepen over the following four winters reaching, and probably exceeding, 2000 m depth at the end of the period. The mixed part of the water column became colder and denser with each cooling cycle.

The observed multiyear development in convection is the result of recurring, relatively strong, surface winter cooling (often, but not always, coinciding with high NAO), which causes deep mixing and results in the preconditioning of the water column. This may, in turn, facilitate a deeper convection the next year under a weaker winter cooling. The water column preconditioning can also be viewed as the ocean's own "memory" or ability to carry forward some information from past winter cooling events. This suggests that certain properties imposed on the water column by a stronger-than-usual convective mixing in previous years, such as low temperature, weak vertical stability, and weak overall stratification, may result in the kind of preconditioning that facilitated the strengthening and deepening of convection observed in winter 2017/2018.

In winter 2017/2018, as in the previous two winters (Yashayaev and Loder, 2017), the mid-high latitude North Atlantic experienced a more moderate cumulative loss of oceanic heat to the atmosphere than the two-decade record-high observed in winter 2014/2015. Winter 2017/2018 heat losses in the Labrador Sea were the lowest since winter 2013/2014. Despite the reduction in cumulative winter heat losses, the depth of winter convection has been steadily increasing since 2014/2015, forming the most significant class of LSW since 1994, in terms of volume, depth, and density. This persistence in LSW development is the result of water column preconditioning at intermediate depths.

Temperature and salinity profiles obtained by the ship survey and Argo floats show that the winter mixed layer, and hence convection in the central Labrador Sea, reached and exceeded 2000 m in 2018 (the deepest since the beginning of the century). This continues the 7-year trend of winter mixed-layer deepening. A reservoir filled with this newly ventilated, record deep, cold and fairly fresh LSW is evident in seawater property sections (not shown). LSW formed in 2018 is characterized by low temperature (< 3.3°C) and salinity (< 34.86) between 1000 and 2000 m. The winter convection during 2015–2018, especially winter 2017/2018, is arguably the deepest since the record-deep cooling down to 2400 m in 1994. The current LSW year class is one of the largest ever observed outside of the early 1990s.

Hydrographic changes in the Labrador Sea over the past eighty years

The long-term changes observed in the Labrador Sea until 2016 have been extensively discussed in a series of publications (Yashayaev, 2007; Yashayaev and Loder, 2009, 2016, 2017). Here, the series is updated (Figures 4.8 and 5.11; see Section 5.2.5) and major points concerning long-term variability in temperature and salinity are revisited.

The deep intense winter mixing during the five consecutive winters from 2013/2014 to 2017/2018 and the associated progressive cooling of the top 2000 m have interrupted the general warming and stratification-building trend that has persisted in the intermediate waters of the Labrador Sea since the mid-1990s. Despite the decrease in surface heat losses in the two last winters with respect to winter 2014/2015, the water column cooling has continued after 2015 as the result of multiyear convective preconditioning.

As a result of the discussed processes, winter cooling enhanced by convective preconditioning, both the upper (50–200 m) and deeper (1000–1800 m) layers have been cooling since 2011 (Figures 4.8 and 5.11; see Section 5.2.5). However, the freshening trend seen between 2011 and 2016 in the newly-formed or newly-ventilated LSW has reversed since 2016. This recent increase in subsurface salinity made the LSW formed in winter 2017/2018, and the top 2000 m layer as a whole, the densest since the mid-1990s.

In 2013, 2015, and 2018, relatively short freshwater events spread across the upper layer of the central basin (Figure 4.8).

With respect to multidecadal changes in the subpolar North Atlantic, the progressively deepening convective mixing that reoccurred in the Labrador Sea during at least six out of seven recent winters (the exception is winter 2012/2013, which had a convective event comparable to or weaker than the one in winter 2011/2012) has reversed the general warming trend observed in the intermediate waters during 1994–2011. As a result of this intermittent recurrence of intensified LSW formation, the annual average temperature and density in the region's upper 2000 m have predominantly varied on a bi-decadal time-scale rather than having a long-term trend, as might be expected from anthropogenic climate change.

The above-average regional winter cooling during 2012–2018, enhanced by convective preconditioning, has increased the depth to which cooled gas-saturated waters sink to below 2000 m. The strong winter convection in winter 2017/2018 further added to increased gas uptakes (dissolved oxygen, anthropogenic gases, and carbon dioxide) and consequently increased gas concentrations in the lower part of the Labrador Sea 0-2000 m layer.

Conclusion

Winter convection in the Labrador Sea is one of the main factors controlling interannual–to–multidecadal variability in the intermediate layer throughout the North Atlantic, and a key process driving or strongly influencing the Atlantic Meridional Overturning Circulation. This makes the Labrador Sea one of the few locations globally where surface waters are exchanged with those residing at much greater depths. In addition, this process also has an important role in biogeochemical cycling in the Labrador Sea, and strong convection enhances the entrainment of gases, such as oxygen and carbon dioxide, into the deep water from the atmosphere and upper-layer freshwater.

Interannual variability in Labrador Sea ocean heat content and cumulative surface heat loss during the cooling season indicate that anomalously strong winter atmospheric cooling, associated with the NAO, is continuing to drive the recurrent convection. In turn, recurrent deep convection is contributing to decadal-scale variability in deep-water properties and in the transport across and from the subpolar North Atlantic (by the ocean's western boundary and interior pathways) and potentially the Atlantic Meridional Overturning Circulation.

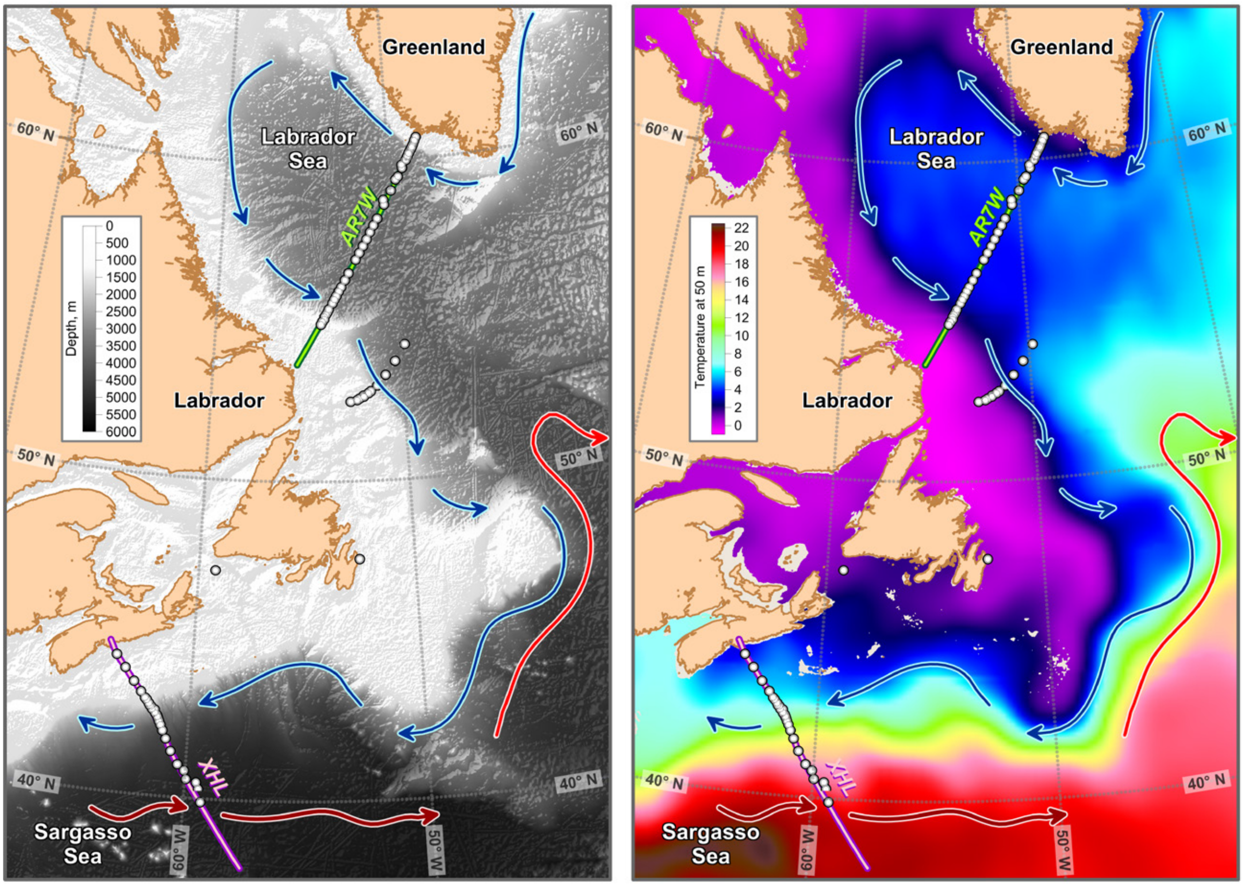

FIGURE 4.7.
Labrador Sea. Topography, surface currents, and temperature at 50 m in the Atlantic Zone Offshore Monitoring Program (AZOMP) domain. The CTD stations, AR7W, and Extended Halifax lines occupied in the 2018 AZOMP mission, HUD2018-008, April 28 to May 24, are shown in both panels.

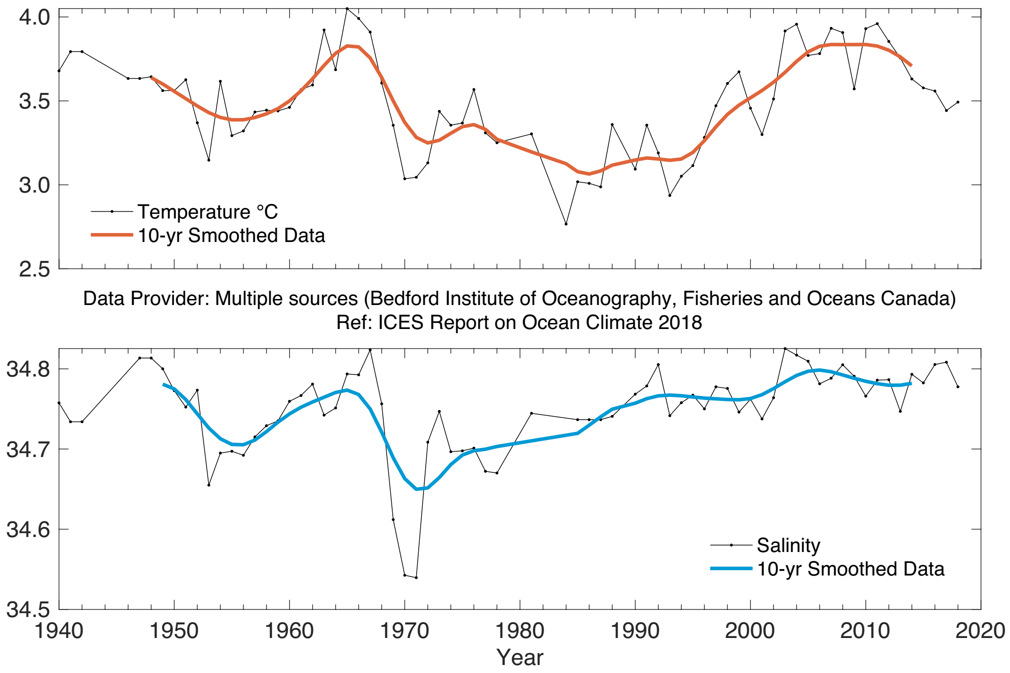

FIGURE 4.8.
Labrador Sea. Potential temperature (upper panel) and salinity (lower panel) anomalies at 50-200 m, from CTD and Argo data in the west-central Labrador Sea (centred at 56.7°N 52.5°W). Estimates of seasonal cycle (derived from all data in the time-series) have been removed from the observations.

4.3 NEWFOUNDLAND-LABRADOR SHELF

F. Cyr and E. Colbourne

The Newfoundland–Labrador Shelf region is situated on the western side of the Labrador Sea, stretching from the Hudson Strait to the tail of the Grand Banks. It is dominated by shallow banks separated by deeper channels or saddles. The circulation is dominated by the south-flowing Labrador Current, which brings cold and freshwater from the north as well as sea ice and icebergs to southern areas of the Grand Banks.

Hydrographic conditions are determined in part by the strength of winter atmospheric circulation over the Northwest Atlantic (e.g. winter NAO index), advection by the Labrador Current, cross-shelf exchange with warmer continental slope water, and bottom topography. Superimposed are large seasonal and interannual variations in solar heat input, sea ice cover, and storm-forced mixing. The resulting water mass on the shelf exhibits large annual cycles with strong horizontal and vertical temperature and salinity gradients.

The 2017/2018 winter NAO index (average monthly values between December and February[9]) is a key indicator of climate conditions in the Northwest Atlantic. While it decreased from the record high in 2015, it remained relatively high in 2018 at +1.3 (sixth highest since 1950). This high winter NAO caused winter air temperature to be generally colder than normal over the Labrador Shelf. However, the westward shift of SLP patterns relative to their long-term position resulted in warmer-than-normal air temperature over the Newfoundland Shelf. In March, a reversal in the position of the low and high SLP patterns above the Northwest Atlantic caused warmer-than-normal temperatures above Labrador, with the air temperature at Cartwright being 6°C (2.1 s.d.) above average. This anomalous SLP pattern explains why the winter NAO

> Ocean temperatures off Newfoundland and Labrador were near normal or slightly below normal in 2018.

9) https://www.ncdc.noaa.gov/teleconnections/nao

index as defined in Section 1 (December/January/February/March), is much lower than the one used here. Over the course of 2018, the air temperature at Cartwright was near normal at –0.2 s.d. (Figure 4.10). The sea ice extent on the Newfoundland-Labrador Shelf was slightly above the long-term average in 2018, at +0.7 s.d., despite being characterized by a negative anomaly in the middle of the season caused by the warm temperature in March (Figure 4.9).

At the standard monitoring site off eastern Newfoundland (Station 27), the depth-averaged annual water temperature has experienced a cooling trend during the past several years from a record high of +1.4°C (2.8 s.d.) above normal in 2011 (Figure 4.11). In 2018, the depth-averaged temperature at Station 27 was slightly above normal by 0.3°C (0.8 s.d.), whereas salinity exhibited the freshest anomaly since 1948 at –3.1 s.d. below normal.

A robust index of ocean climate conditions in eastern Canadian waters is the extent of the cold intermediate layer (CIL), which is defined as the continental shelf waters with temperature below 0°C (Figure 4.12). This winter-cooled water remains isolated throughout summer and early autumn between the seasonally heated upper layer and warmer shelf-slope water. During the 1960s, when the NAO was at the most negative phase recorded for the 20th century, the volume of CIL water was at a minimum (warmer-than-normal conditions), and during the high NAO years of the early 1990s, the CIL volume reached near-record high values (colder-than-normal conditions). From the early 1990s until 2011, the CIL area experienced a shrinking trend as ocean temperatures increased, reaching a record low CIL area on the Newfoundland Shelf in 2011. After this record low, the CIL rapidly re-expanded as the result of a succession of positive winter NAO phases and prevailing cold winter conditions (e.g. the CIL area in 2014 was at its highest level since the early 1990s). In recent years, the CIL has been shrinking again and its area in summer 2018 was below normal off southern Labrador (–1.9 s.d.) and slightly below normal (–0.6 s.d.) off eastern Newfoundland.

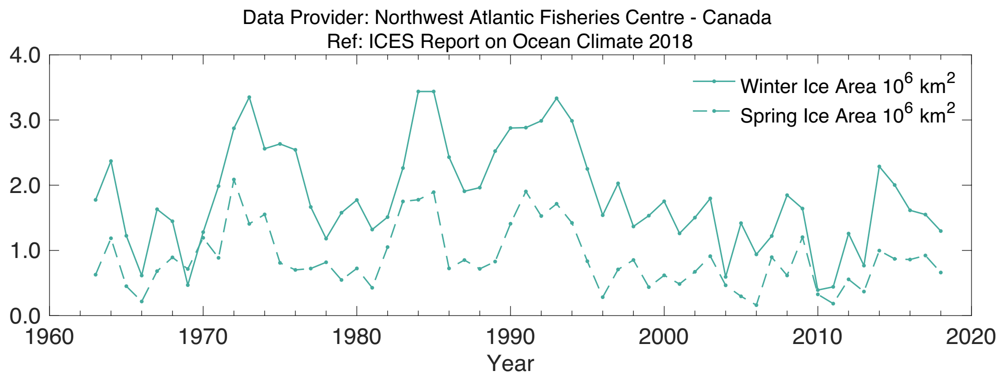

FIGURE 4.9.
Northwest Atlantic: Newfoundland-Labrador Shelf. Winter and spring sea ice areas off Newfoundland-Labrador between 45°N and 55°N.

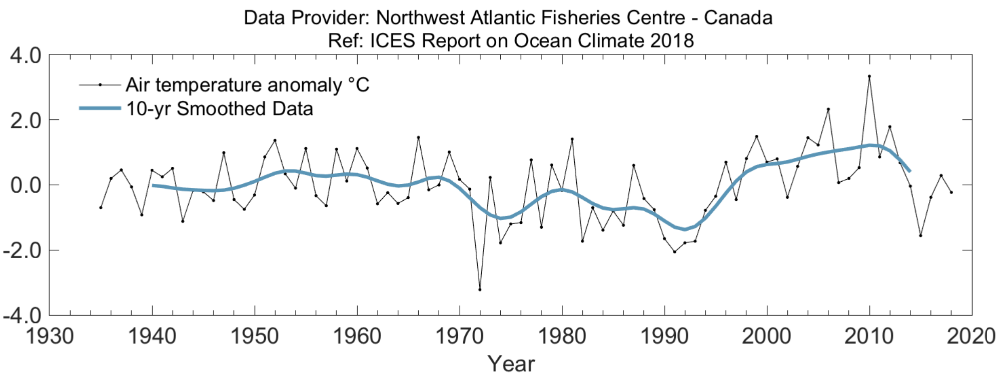

FIGURE 4.10.
Northwest Atlantic: Newfoundland-Labrador Shelf. Annual air temperature anomalies at Cartwright on the Labrador coast.

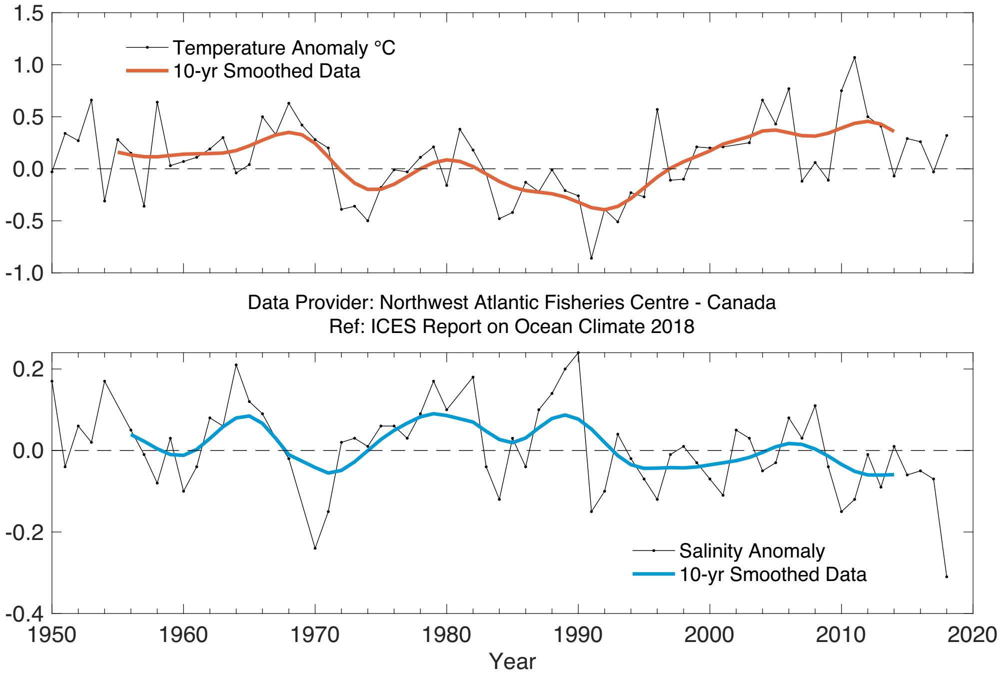

FIGURE 4.11. Northwest Atlantic: Newfoundland-Labrador Shelf. Annual depth-averaged Newfoundland Shelf temperature (top panel) and salinity (bottom panel) anomalies at Station 27 (47.55°N 52.59°W).

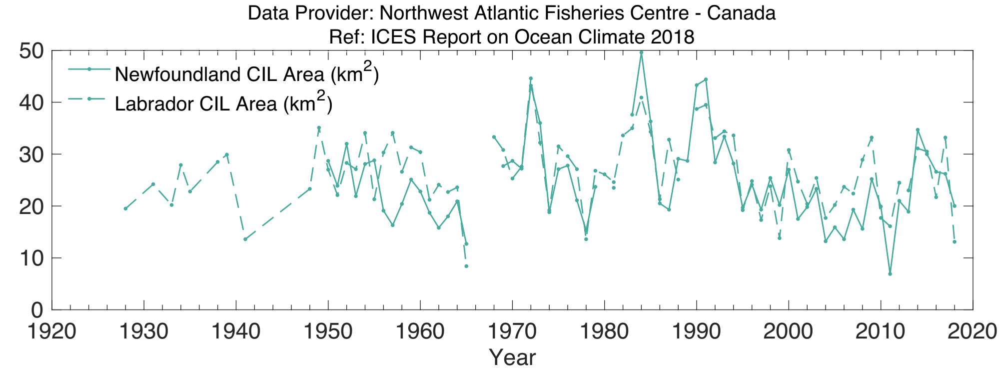

FIGURE 4.12. Northwest Atlantic: Newfoundland-Labrador Shelf. Spatial extent of CIL.

Mooring deployment in the Bay of Biscay.
Photo: Spanish Institute of Oceanography

4.4 SCOTIAN SHELF

D. Hebert and R. Pettipas

The Scotian Shelf is the continental shelf off the coast of Nova Scotia and is identified as a NOAA LME. It is characterized by complex topography consisting of many offshore shallow banks and deep mid-shelf basins. It is separated from the Newfoundland Shelf to the northeast by the Laurentian Channel, and borders the Gulf of Maine to the southwest. Surface circulation is dominated by a general flow towards the southwest that is interrupted by clockwise circulation around the banks and anticlockwise circulation around the basins, both of which vary seasonally in strength.

Hydrographic conditions on the Scotian Shelf are determined by heat transfer between the ocean and the atmosphere, inflow from the Gulf of St Lawrence and the Newfoundland Shelf, and exchange with offshore slope waters. Water properties have large seasonal cycles and are modified by freshwater run-off, precipitation, and melting of sea ice. Temperature and salinity exhibit strong horizontal and vertical gradients that are modified by diffusion, mixing, currents, and shelf topography.

In 2018, annual mean air temperature over the Scotian Shelf (Figure 4.13, represented by Sable Island observations) was +0.5°C (+0.8 s.d.) above the long-term mean (1981–2010). The amount of sea ice on the Scotian Shelf in 2018, as measured by the total area of ice seaward of Cabot Strait, between Nova Scotia and Newfoundland, from January to April, was 10 800 km^{2,} well below the long-term mean coverage of 32 000 km^2 (Figure 4.14). After an above-average year in 2015, conditions returned to those similar to the 2010–2013 period, which had extremely low coverage.

Topography separates the northeastern Scotian Shelf from the rest of the shelf. In the northeast, the bottom tends to be covered by relatively cold water (2–5°C), whereas the basins in the central and southwestern regions typically have bottom temperatures of 6–10°C. The origin of the latter is the offshore slope waters, whereas water in the northeast comes principally from the Gulf of St Lawrence. The interannual variability of the two water masses differs.

Measurements of temperatures at 100 m at the Misaine Bank Station capture the changes in the northeast (Figure 4.15). They revealed well above-average temperatures in 2018, +0.5°C (+0.8 s.d.), and below-average salinity, –0.16 (–1.2 s.d.). The deep Emerald Basin anomalies represent the slope-water intrusions onto the shelf that are subsequently trapped in the inner basins. In 2018, the 250 m temperature and salinity anomalies were well above normal, +1.6°C (+1.9 s.d.) and +0.31 (+2.0 s.d.), respectively, slightly below the record in 2016 (Figure 4.16). Model simulations of the region showed a large flux of warm salty water from the slope region. Ocean temperatures and salinity in the deep basins of the Scotian Shelf were well above normal in 2018, reflective of warm salty conditions in the slope region offshore.

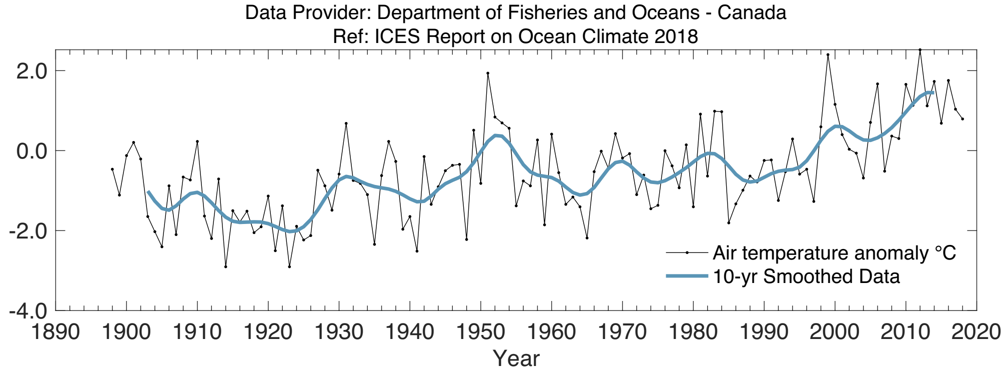

FIGURE 4.13.
Northwest Atlantic: Scotian Shelf. Air temperature anomalies at Sable Island on the Scotian Shelf.

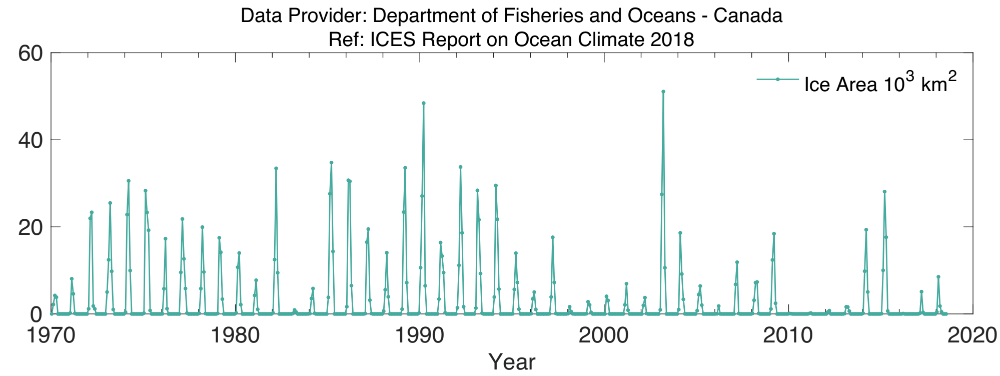

FIGURE 4.14. Northwest Atlantic: Scotian Shelf. Monthly means of ice area seaward of Cabot Strait.

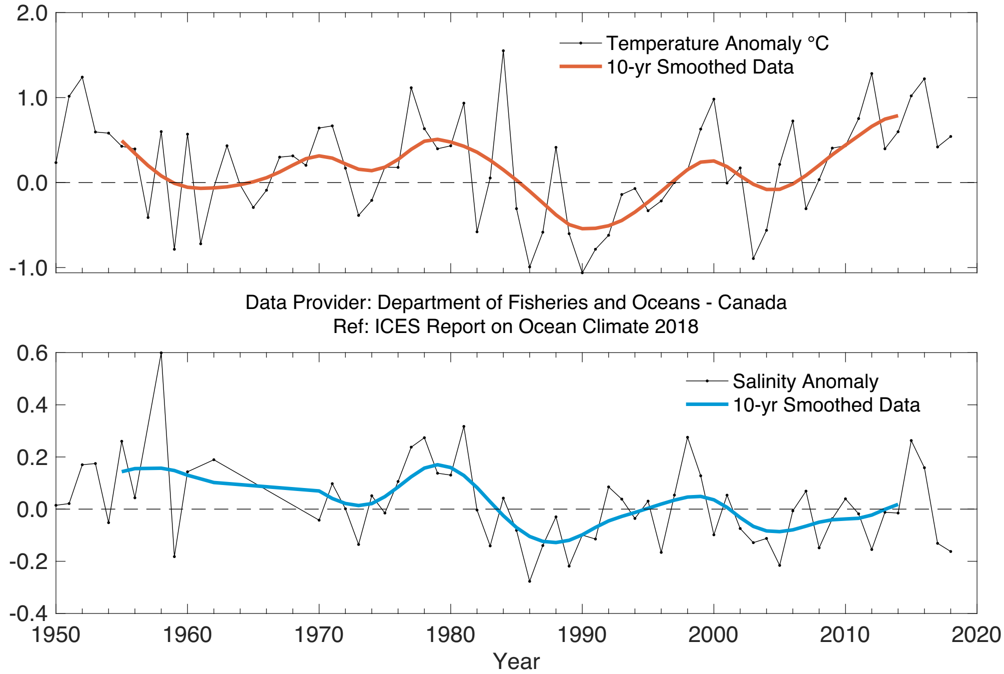

FIGURE 4.15. Northwest Atlantic: Scotian Shelf. Near-bottom temperature (upper panel) and salinity (lower panel) anomalies at Misaine Bank (100 m).

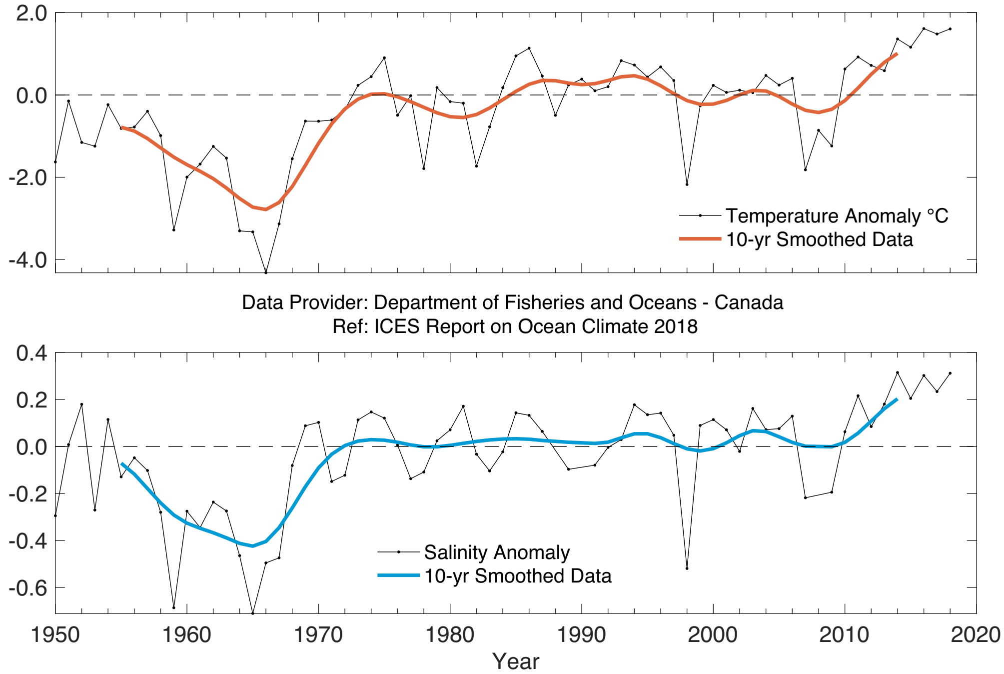

FIGURE 4.16. Northwest Atlantic: Scotian Shelf. Near-bottom temperature (upper panel) and salinity (lower panel) anomalies in the central Scotian Shelf (Emerald Basin, 250 m).

4.5 NORTHEAST US CONTINENTAL SHELF

P. Fratantoni

The Northeast US Continental Shelf extends from the southern tip of Nova Scotia, Canada, southwest through the Gulf of Maine and the Middle Atlantic Bight to Cape Hatteras, North Carolina (Figure 4.17). Contrasting water masses from the Subtropical and Subpolar gyres influence the hydrography in this region. Located at the downstream end of an extensive interconnected coastal boundary current system, the Northeast US Continental Shelf is the direct recipient of cold/fresh Arctic-origin water, accumulated coastal discharge and ice melt that has been advected thousands of kilometres around the boundary of the subpolar North Atlantic. The composition of water masses within this region is also influenced by subtropical water masses advected by the Gulf Stream, slope currents, and associated eddies. The western boundary currents of the Subpolar and Subtropical gyres respond to variations in basin-scale forcing through changes in position, volume transport, and/or water mass composition. It is partly through these changes that basin-scale climate variability is communicated to the local Northeast US Continental Shelf. Shelf-wide hydrographic conditions have been monitored annually in this region since 1977 as part of quarterly ecosystem monitoring and twice-yearly bottom-trawl surveys conducted by the US National Marine Fisheries Service, Northeast Fisheries Science Center.

The majority of the Northeast US Shelf was significantly warmer in 2018 than the mean (1981–2010). Annually, 0–30 m temperatures were 0.5–1.9°C warmer than normal everywhere except in the southern Middle Atlantic Bight (figures 4.18–4.23), with the largest anomalies observed in the Gulf of Maine (figures 4.21 and 4.22). Annual anomalies are consistent with seasonal conditions in most regions, suggesting that no one season dominates the annual mean. Of the seasons sampled, warming was most pronounced during spring in the Gulf of Maine and during summer on Georges Bank (e.g. Figure 4.24), where regional temperature anomalies exceeded 1 s.d.. The exception was the cold conditions observed in the southern Middle Atlantic Bight during 2018, with the annual mean being dominated by cold conditions in September. Similar patterns were observed near the ocean bottom, with warm conditions over most of the region except the southern Middle Atlantic Bight (not shown). During summer, the bottom temperature measured more than 1 s.d. above normal in the northern Middle Atlantic Bight, although similarly large anomalies were observed near the bottom in the western Gulf of Maine year-round. Cold anomalies were observed during autumn near the bottom in the southern Middle Atlantic Bight.

In 2018, waters in the upper 30 m were slightly saltier than normal in the northern Middle Atlantic Bight (Figure 4.20) and eastern Gulf of Maine, and near normal to slightly fresh elsewhere. Seasonally, large positive anomalies (exceeding 1 s.d.) were observed during April/May in the eastern Gulf of Maine (Figure 4.22). Notably fresh conditions were observed in the southern Middle Atlantic Bight during summer/autumn, dominating the annual mean. These large fresh anomalies are linked to anomalous precipitation; 2018 was the 14th warmest and the third wettest year on record for the continental US, with four major storms impacting the US east coast during March and one major hurricane delivering record flooding in the southeast US (NOAA-NCEI, 2019).

Slope waters entering the Gulf of Maine at depth through the Northeast Channel (NEC) represent one of the dominant water mass sources to the Gulf of Maine (Mountain, 2012). These deep waters lying between 150 and 200 m are uninfluenced by seasonal atmospheric forcing. Annually, deep inflow to the Gulf of Maine was very warm and salty in 2018 compared with the long-term mean (Figure 4.25).

Waters on the Northeast US Shelf were warmer than normal, accompanied by notable freshening at several sites.

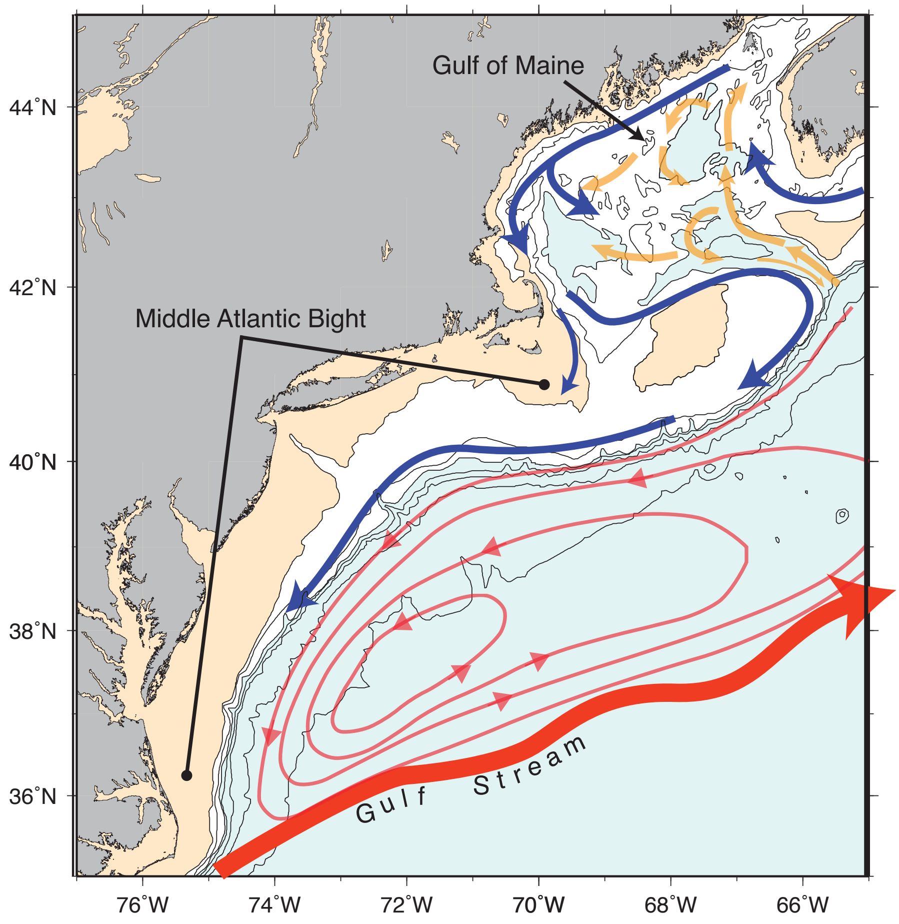

FIGURE 4.17.
Circulation schematic for the Northeast US shelf region. Blue arrows represent shelf water circulation and orange arrows represent deeper slope-water circulation pathways. Water depths deeper than 200 m are shaded blue. Water depths shallower than 50 m are shaded tan.

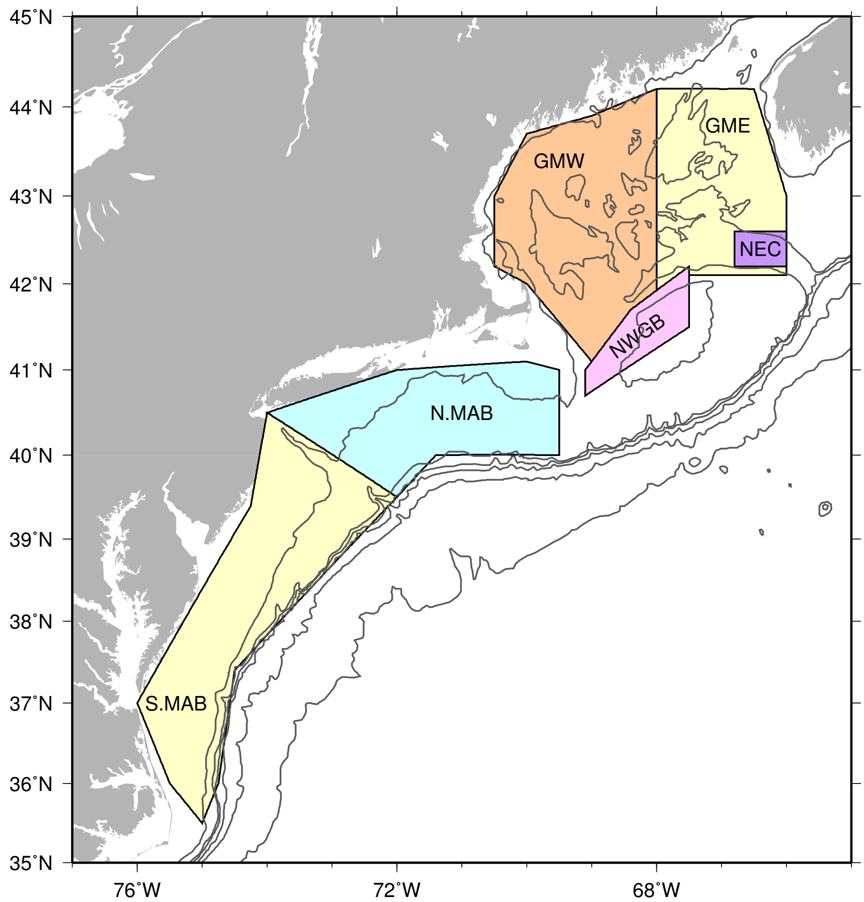

FIGURE 4.18.
Northeast US Continental Shelf. The six regions within which CTD observations are used to compute regional average time-series: eastern and western Gulf of Maine (GME and GMW, respectively); northern and southern Middle Atlantic Bight (N.MAB and S.MAB, respectively); NEC; and Northwest Georges Bank (NWGB). The 50, 200, 500, 1000, 2000, and 3000 m isobaths are also shown.

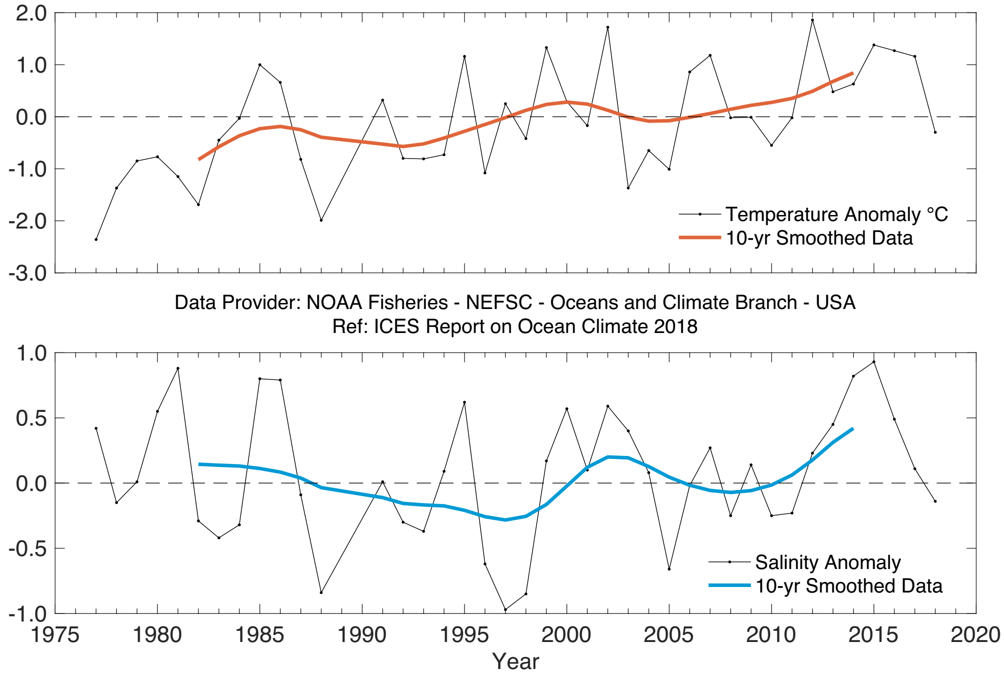

FIGURE 4.19.
Northeast US Continental Shelf. Time-series plots of 0–30 m averaged temperature anomaly (upper panel) and salinity anomaly (lower panel) in the region between Cape Hatteras, North Carolina and Hudson Canyon. Anomalies are calculated relative to the period 1981–2010 using hydrographic data from shelf-wide surveys..

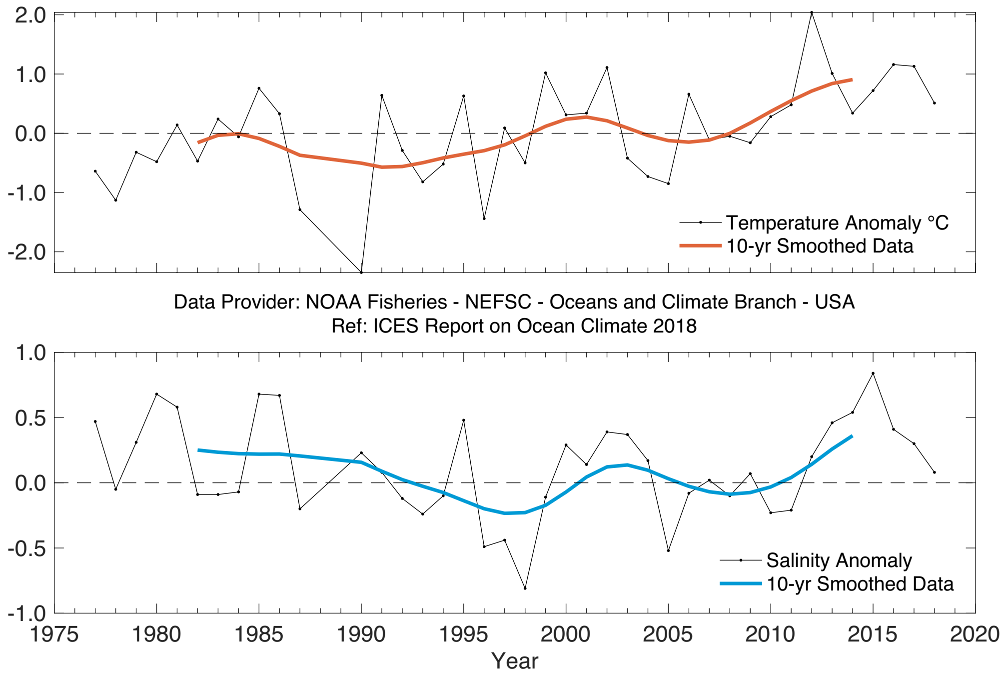

FIGURE 4.20.
Northeast US Continental Shelf. Time-series plots of 0–30 m averaged temperature anomaly (upper panel) and salinity anomaly (lower panel) in the region between Hudson Canyon and Cape Cod, Massachusetts. Anomalies are calculated relative to the period 1981–2010 using hydrographic data from shelf-wide surveys.

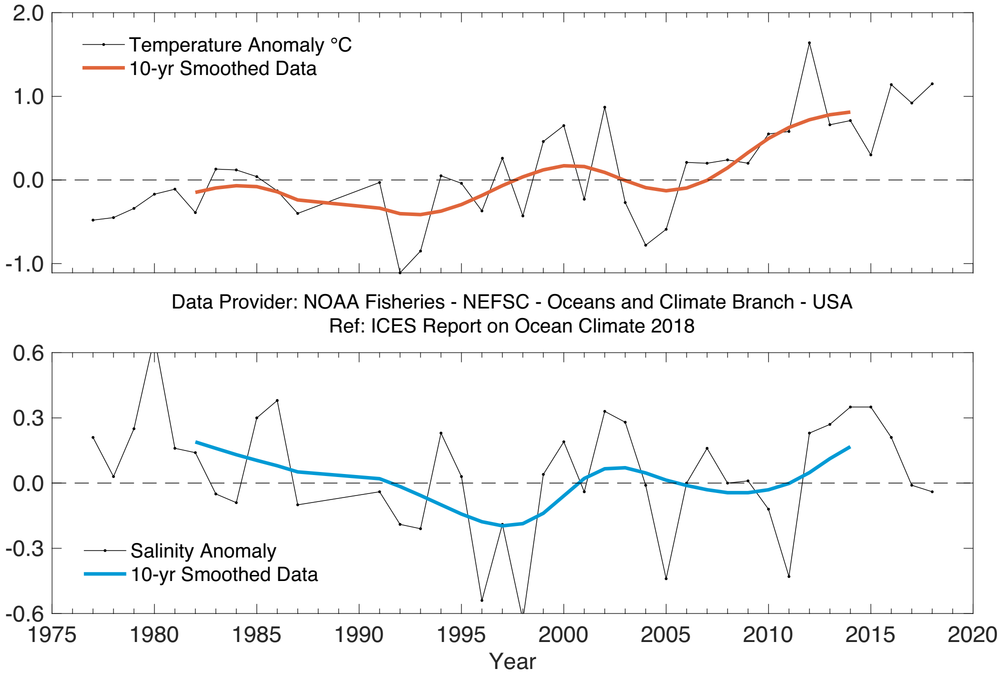

FIGURE 4.21. Northeast US Continental Shelf. Time-series plots of 0–30 m averaged temperature anomaly (upper panel) and salinity anomaly (lower panel) in the western Gulf of Maine. Anomalies are calculated relative to the period 1981–2010 using hydrographic data from shelf-wide surveys.

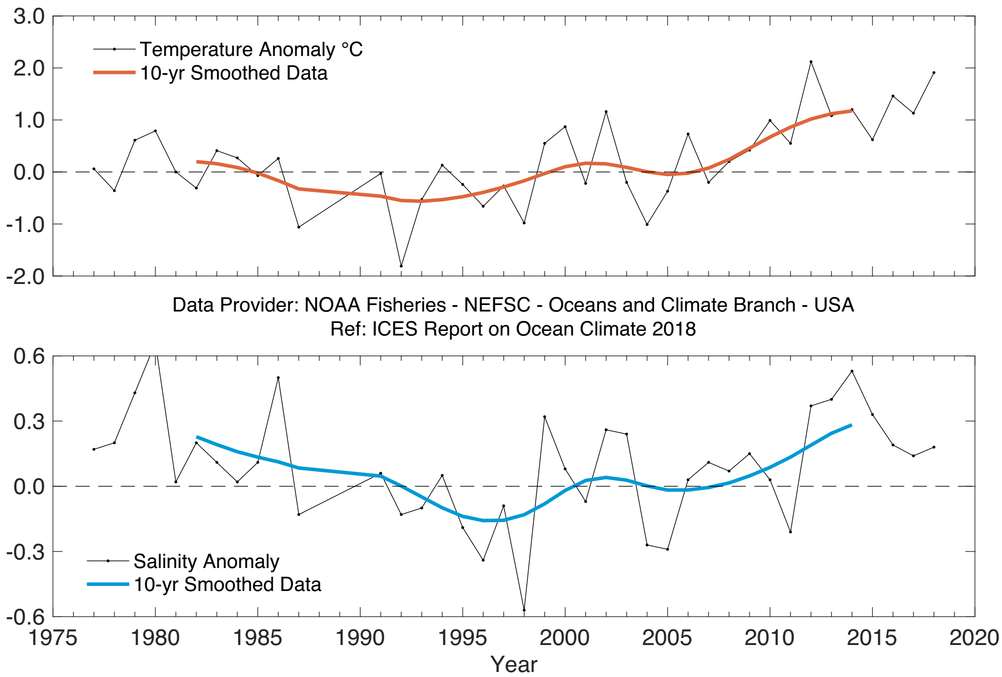

FIGURE 4.22. Northeast US Continental Shelf. Time-series plots of 0–30 m averaged temperature anomaly (upper panel) and salinity anomaly (lower panel) in the eastern Gulf of Maine. Anomalies are calculated relative to the period 1981–2010 using hydrographic data from shelf-wide surveys.

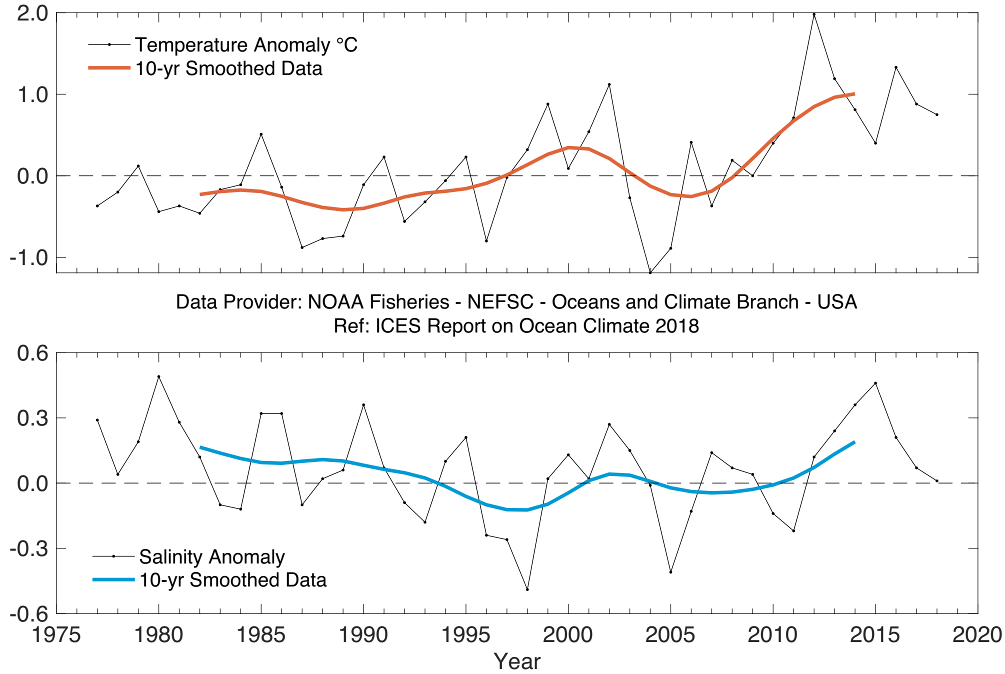

FIGURE 4.23.
Northeast US Continental Shelf. Time-series plots of 0–30 m averaged temperature anomaly (upper panel) and salinity anomaly (lower panel) on George Bank. Anomalies are calculated relative to the period 1981–2010 using hydrographic data from shelf-wide surveys.

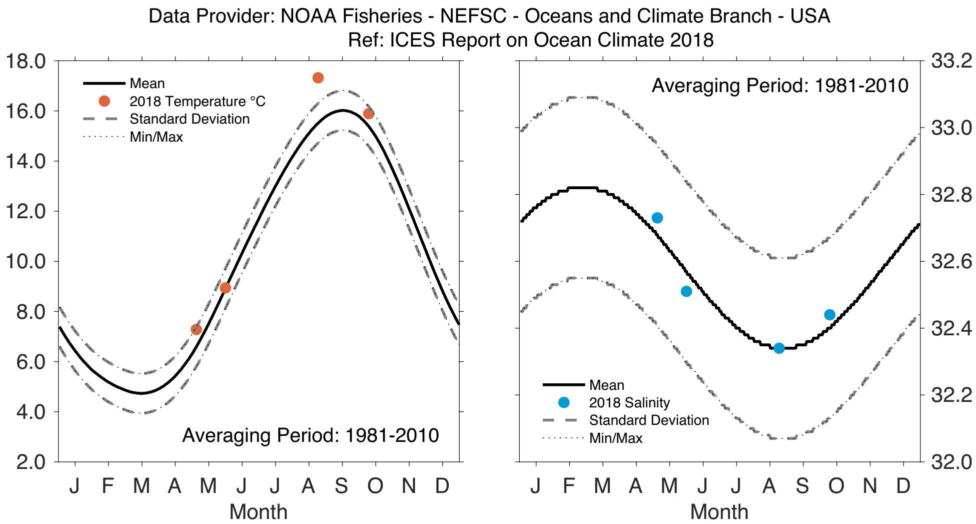

FIGURE 4.24.
Northeast US Continental Shelf. 2018 temperature (left) and salinity (right) averaged over 0–30 m at northwest Georges Bank, relative to the annual cycle calculated 1981–2010. The envelope corresponding to the monthly range and 1 s.d. are shown.

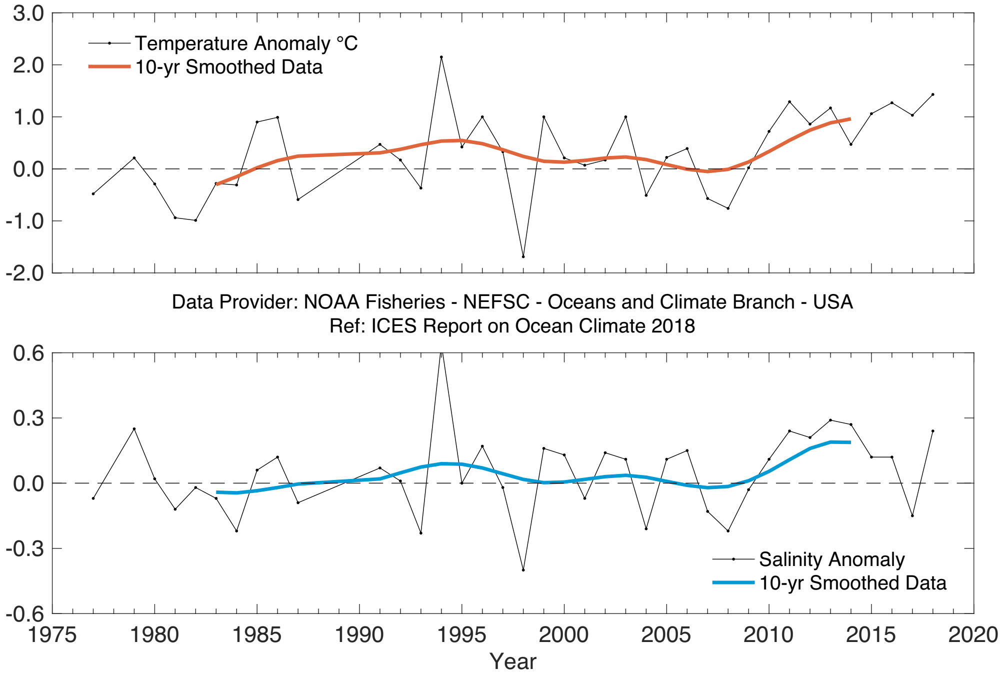

FIGURE 4.25.
Northeast US Continental Shelf. Time-series plots of 150–200 m averaged temperature anomaly (upper panel) and salinity anomaly (lower panel) in the NEC. Anomalies are calculated relative to the period 1981–2010 using hydrographic data from shelf-wide surveys.

Celtic Explorer. Painting by Rosa Velten

4.6 ICELANDIC WATERS

H. Valdimarsson

The Iceland Shelf and seas are identified as a NOAA LME and an ICES ecoregion. Iceland is at the meeting place of warm and cold currents. These converge in an area of submarine ridges (Greenland-Scotland Ridge, Reykjanes Ridge, and Kolbeinsey Ridge) that form natural barriers to the main ocean currents (Figure 4.26). The warm Irminger Current (6–8°C, a branch of the North Atlantic Current) flows from the south, and the cold East Greenland and East Icelandic currents (–1°C to 2°C) flow from the north. Deep bottom currents in the seas around Iceland are principally the overflow of cold water from the Nordic seas and the Arctic Ocean over the submarine ridges into the North Atlantic.

Hydrographic conditions in Icelandic waters are generally closely related to atmospheric or climatic conditions in and over the country and the surrounding seas, mainly through the Icelandic low-pressure and Greenland high-pressure systems. These conditions in the atmosphere and the surrounding seas affect all biological systems including recruitment and abundance of commercially important fish stocks.

Average air temperature for the year was lower in the south (Reykjavik), but continued to be high in the north (Akureyri; Figure 4.27). Temperature in the AW south of Iceland (Figure 4.29) was slightly above average, but salinity was well below average. Temperature north and northeast of Iceland continued to stay above average, but the salinity of surface layers fell to around average (figures 4.27 and 4.30).

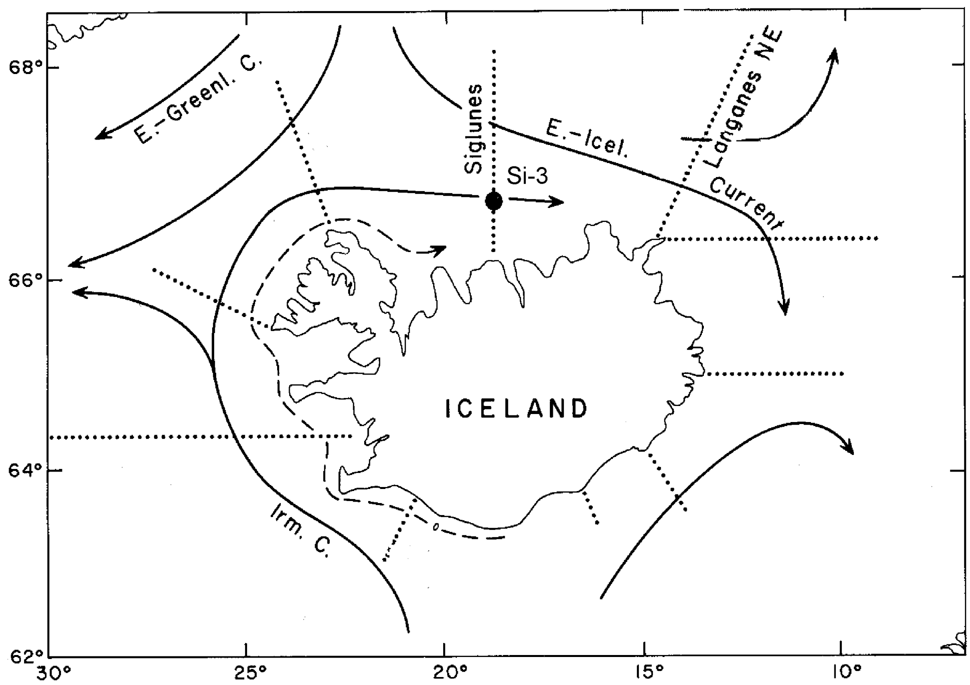

FIGURE 4.26.
Main currents and location of standard sections in Icelandic waters.

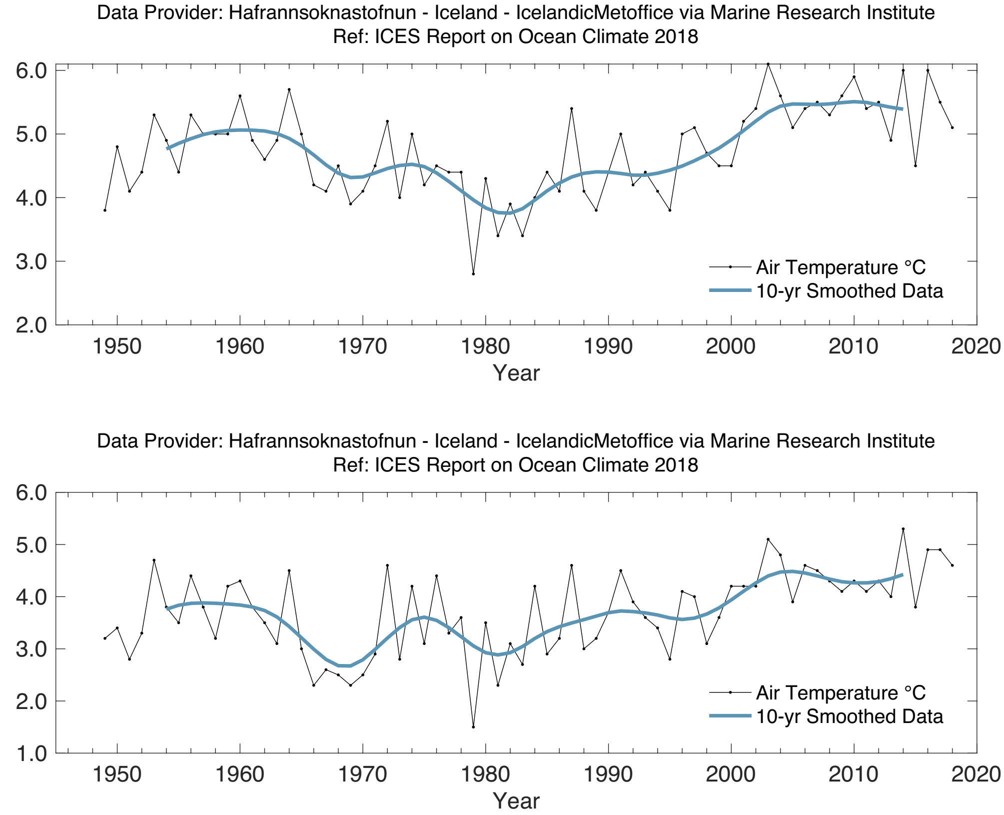

FIGURE 4.27.
Icelandic waters. Mean annual air temperature at Reykjavik (upper panel) and Akureyri (lower panel).

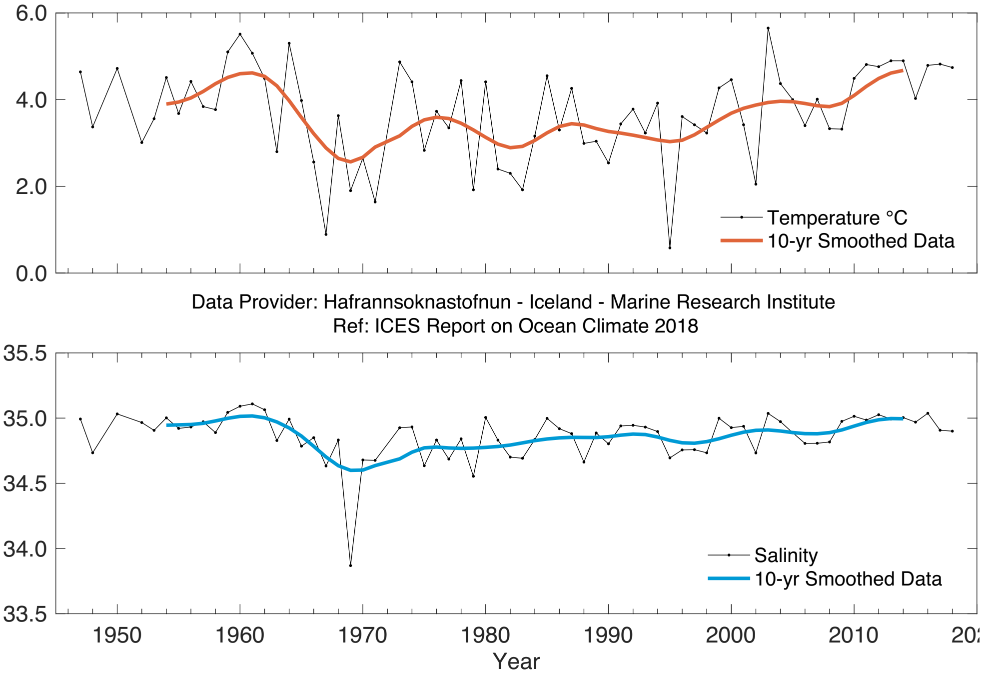

FIGURE 4.28.
Icelandic waters. Temperature (upper panel) and salinity (lower panel) at 50-150 m at Siglunes Stations 2-4 in North Icelandic waters.

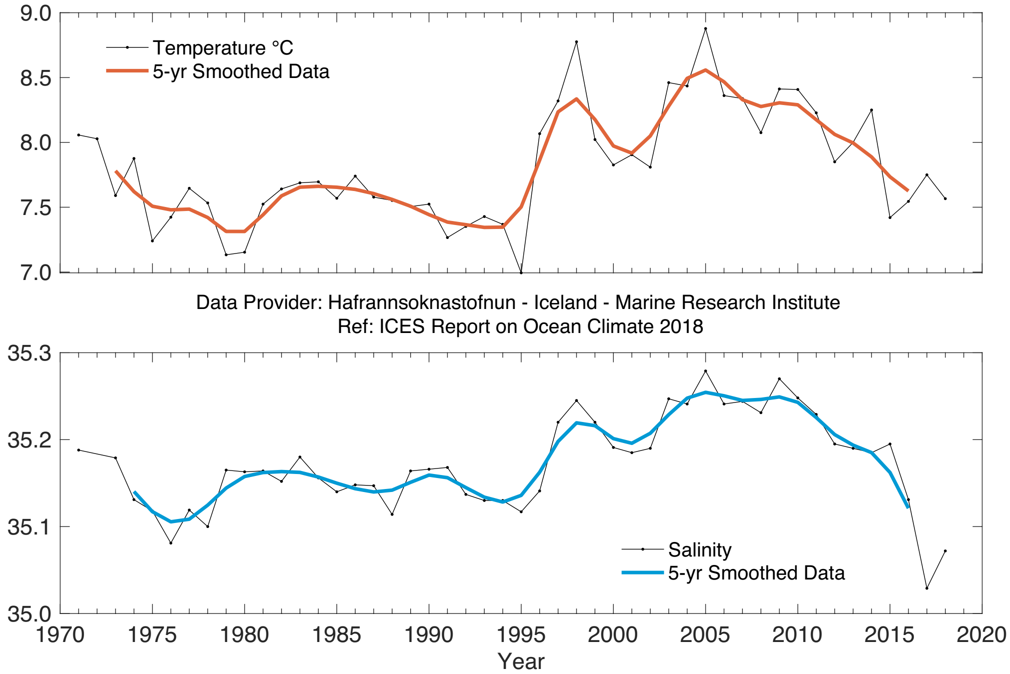

FIGURE 4.29. Icelandic waters. Temperature (upper panel) and salinity (lower panel) at 0–200 m at Selvogsbanki Station 5 in South Icelandic waters.

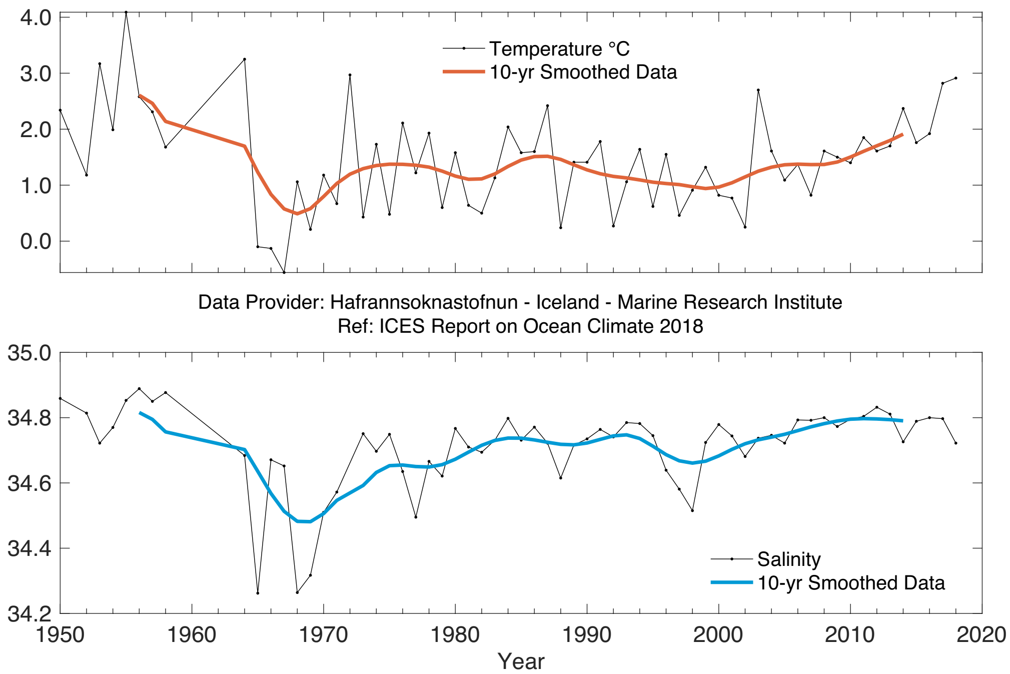

FIGURE 4.30. Icelandic waters. Temperature (upper panel) and salinity (lower panel) at 0–50 m in the East Icelandic Current (Langanes Stations 2–6).

4.7 BAY OF BISCAY AND IBERIAN COAST

A. Fontán, C. González-Pola, and V. Valencia

The western Iberian coast is located at the northeastern edge of the Subtropical Anticyclonic Gyre, sometimes referred to as the intergyre region. It is characterized by weak upper ocean circulation with mean southward flow of few cm s^{-1} (e.g. Paillet and Mercier, 1997). The Bay of Biscay is considered an adjacent sea, with weak anticyclonic circulation (Pingree, 1993; van Aken, 2002). The area also encompasses the northern tip of the northwest African upwelling system. Coastal upwelling events dominate in spring and summer, and a geostrophic balanced poleward flow known as the Iberian Poleward Current develops in autumn and winter (Pingree and Le Cann, 1990). Regional modal waters that comprise the upper permanent thermocline are known as Eastern North Atlantic Central Waters (ENACW). Below this, Mediterranean Water (MW) spreads northwards from the Gulf of Cadiz, mostly as a slope current. Labrador water can be identified at ca. 1800 m, and the deep ocean is occupied by a mixture of cold polar waters known as North Atlantic Deep Water (NADW).

Air conditions in 2018 were warm or very warm in the northern and eastern parts of the Iberian Peninsula and cold or very cold in southern Iberia and the Canaries. Overall, annual temperature anomalies were 0.2–0.5°C warmer relative to 1981–2010 in the southern Bay of Biscay (Figure 4.32). The air temperature seasonal cycle in the southern Bay of Biscay was characterized by the prevalence of very cold conditions in February and very warm conditions in summer. In terms of precipitation, 2018 can be considered wet in the southern Bay of Biscay, resulting from the balance between very wet conditions in winter and spring and normal-to-dry conditions in summer and autumn. The annual continental run-off was more than 1 s.d. above the long-term average (1981–2010), with a seasonal cycle consistent with that of the precipitation.

SST responded to the local atmospheric forcing, with conditions ranging from cold (late winter, early spring, and early autumn) to very warm (summer) in the southern Bay of Biscay. The annual SST anomaly in 2018 was similar to previous years (0.4–0.6°C, +1 s.d. above the long-term average; Figure 4.33).

Cool and fresh subsurface conditions contrast with high summer SST. Progressive freshening continues.

Subsurface waters showed a contrasting trend, with cooler-than-average conditions in the upper 30 m over the shelf at Santander (–0.1°C), effectively reversing recent warm conditions. Salinity from the same series returned to below-average values (Figure 4.34).

Subsurface waters, influenced by the development of winter mixed layers (down to 300 m), were cold and fresh in 2018, being the fifth year in a row with negative anomalies in salinity. The observed ocean conditions are the combination of a cold/deep winter mixed layer caused by a harsh winter–spring period, high precipitation and river run-off, and, likely, the influence of the fresher/colder waters currently spreading across the eastern North Atlantic. The status of deeper waters in the region is described in Section 5.2.6.

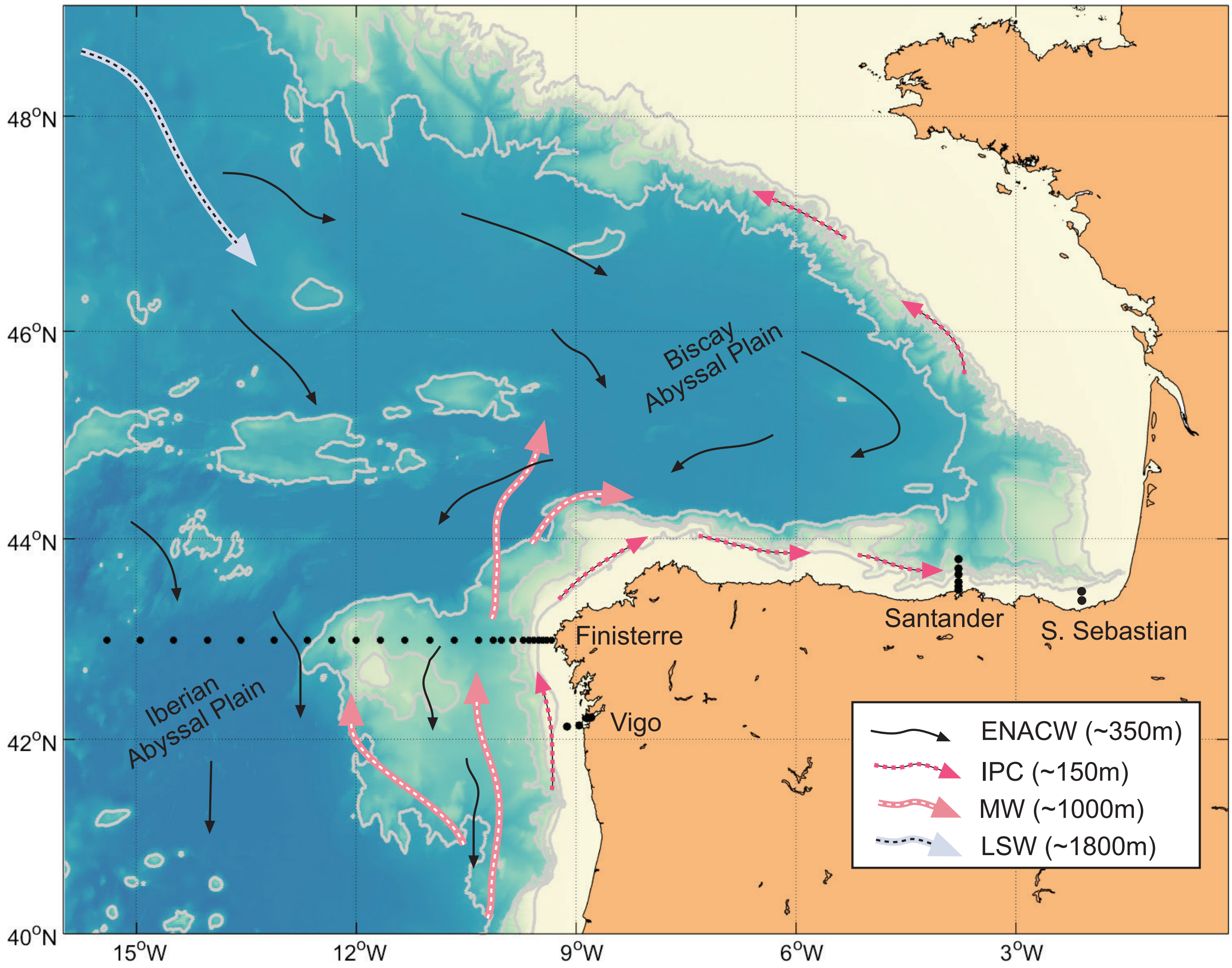

FIGURE 4.31.
Circulation schematic for northwest Iberia and the Bay of Biscay. Thin black arrows show the dominant southward flow in the upper ocean, carrying mainly ENACW. The IPC and the MW pathways are also shown. Black dots show the repeated hydrographic stations, recorded monthly at Vigo, Santander, and San Sebastian, and 1–2 times per year at the Finisterre section.

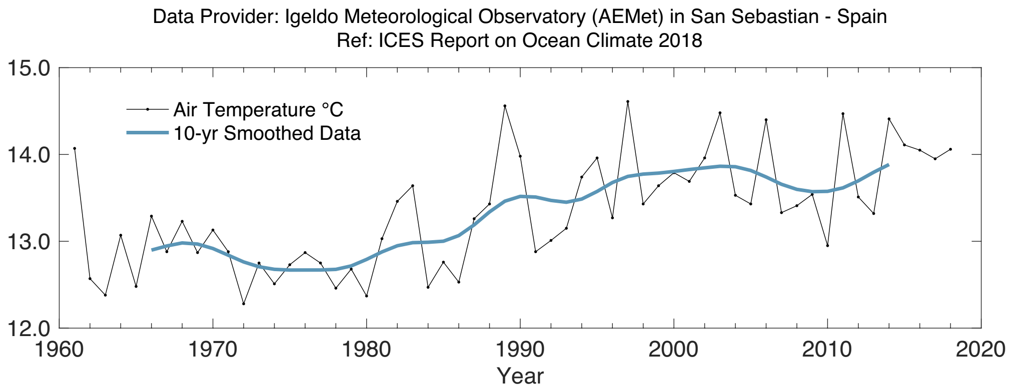

FIGURE 4.32. Bay of Biscay and eastern North Atlantic. Air temperature at San Sebastian (43°18.50´N2°02.37´W).

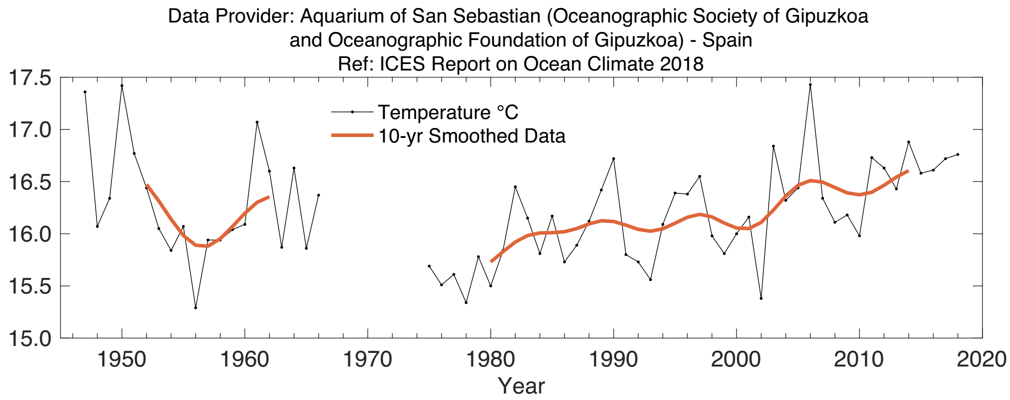

FIGURE 4.33. Bay of Biscay and eastern North Atlantic. SST at San Sebastian (43°18.50´N002°2.37´W). Note previous versions of this record did not present gaps but recent assessments indicated that certain years had few data to provide a reliable annual average.

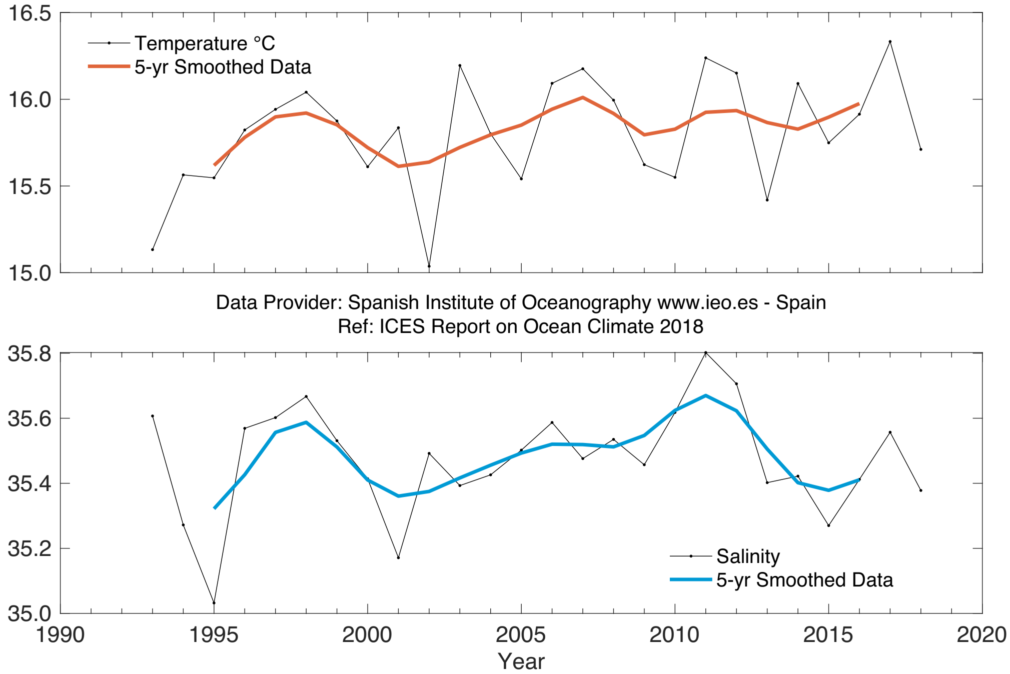

FIGURE 4.34. Bay of Biscay and eastern North Atlantic. Temperature (upper panel) and salinity (lower panel) at Santander Station 6, 0–30 m (43°42.50´N 003°47.00´W).

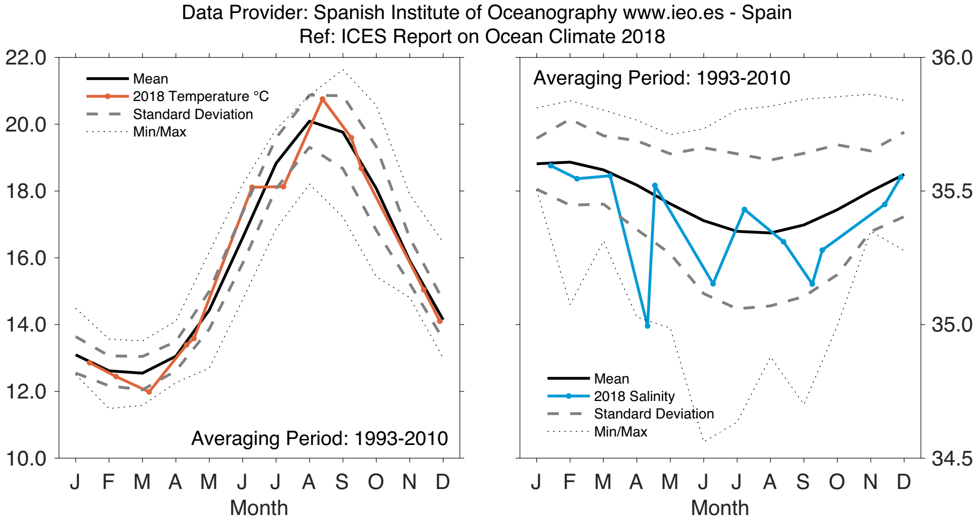

FIGURE 4.35.
Bay of Biscay and eastern North Atlantic. 2018 monthly temperature (left panel) and salinity (right panel) at Santander Station 6, 10 m (43°42.50´N 003°47.00W).

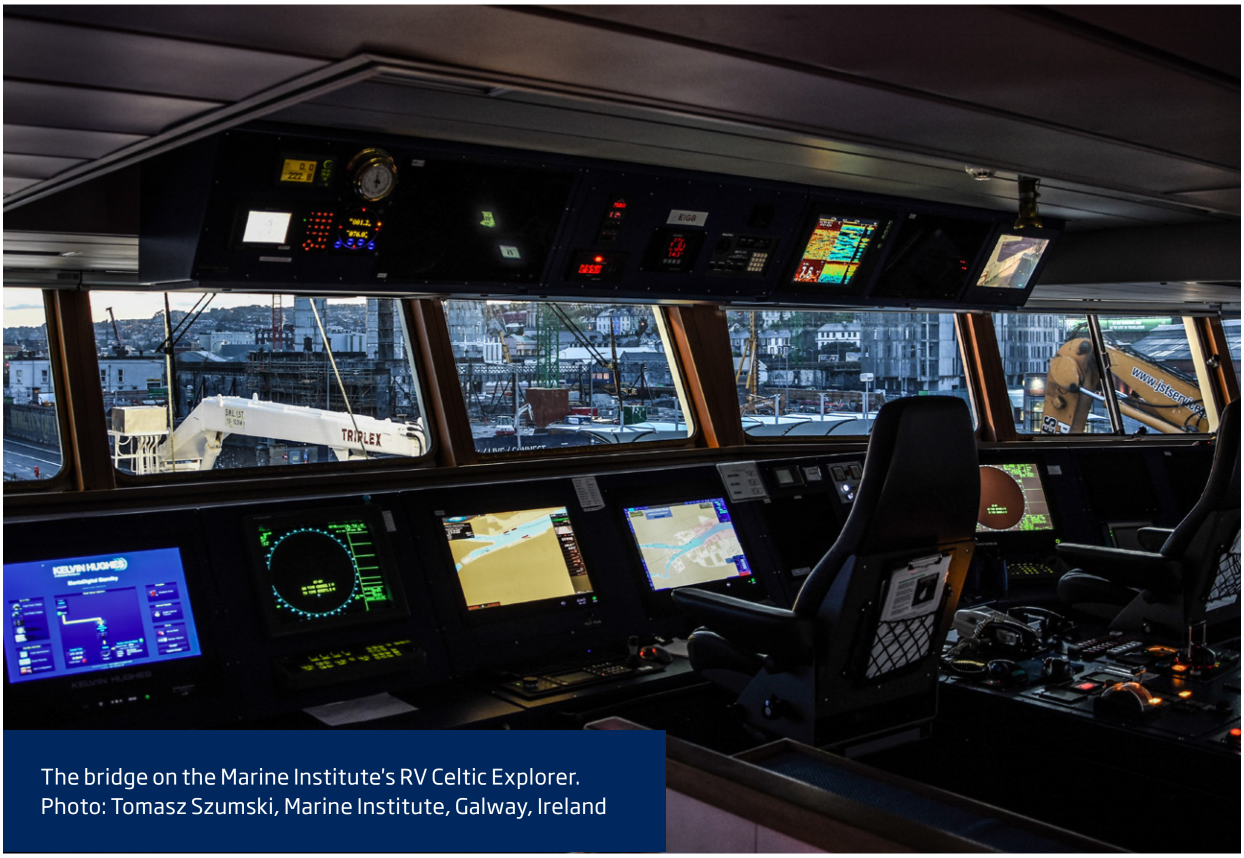

The bridge on the Marine Institute's RV Celtic Explorer.
Photo: Tomasz Szumski, Marine Institute, Galway, Ireland

4.8 GULF OF CADIZ

R. Sánchez-Leal

The Gulf of Cadiz is located off the southwest Iberian Peninsula. The circulation dynamics are largely governed by water exchange through the Strait of Gibraltar, the ocean gateway between the Atlantic Ocean and the Mediterranean Sea. A two-layered inverse estuarine circulation features MW flowing into the Gulf of Cadiz under AW flowing into the Mediterranean Sea. Dominant features include: (i) the baroclinic Gulf of Cadiz Current, that advects relatively fresh and cool waters from the Portuguese Coastal Transition Zone (CTZ) to feed the Atlantic inflow in the Mediterranean basin; (ii) the meridional branch of the Azores Current, a largely barotropic flow that brings warmer more saline AW to supplement the Atlantic inflow into the Mediterranean; (iii) an inshore current system linked with coastal run-off, such as the Guadalquivir River plume; and (iv) the Trafalgar cyclonic cell, an upwelling hotspot generated by tidal stirring over the Trafalgar Banks. The subsurface circulation is given by the MOW, a branched, warm, saline, and dense gravity current, which is attached to the seabed and follows the intricate bottom topography (Figure 4.36).

The instrumental record in the Gulf of Cadiz suggest a statistically significant warming trend (0.24°C per decade) of air and ocean SST over the last two decades. The smoothed time-series indicate interannual variability, with colder-than-average temperatures in 2009, 2013, and 2018, and warmer-than-average temperatures during 2010/2011 and 2016/2017. After a relative maximum at the end of 2016, temperatures dropped from 2017 to 2018, thus making 2018 a cooler-than-average year.

The monthly time-series across the surface layer (0–20 m) shows a seasonal cycle of temperature and salinity (Figure 4.38). The mean and standard deviation are reconstructed from the harmonic fit of all available observations during 2009–2018. The depth-averaged time-series illustrate that this seasonal variability dominates all depth levels of the water column (Figure 4.37). Near-surface temperature and salinity values in 2018 fell within the mean range. Larger deviations from the mean were observed between June and November. Colder conditions occurred from June to August, although late summer and early autumn temperatures were higher than the climatological mean.

Sustained cooling and freshening of upper ENACW from 2009 was briefly interrupted by anomalously strong winter mixing.

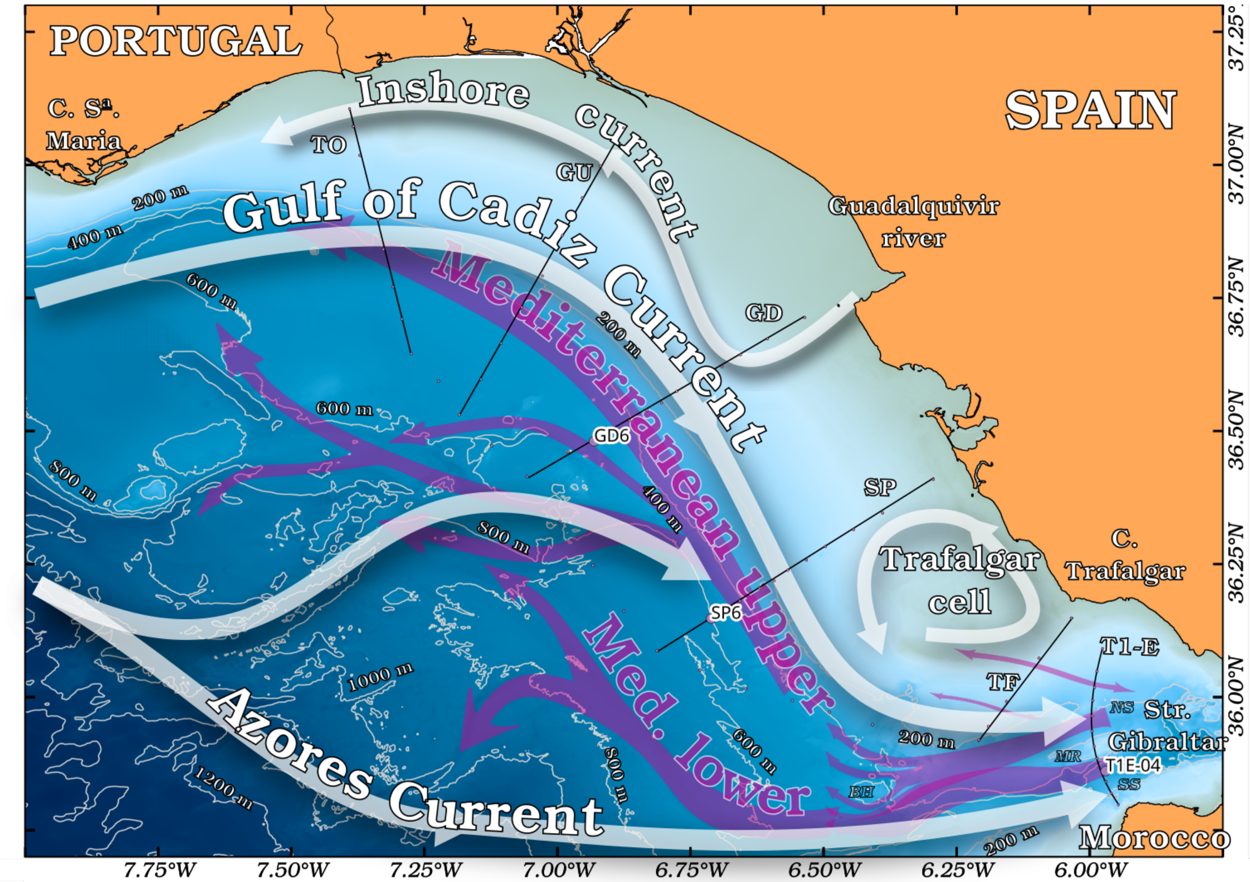

FIGURE 4.36.
Circulation schematic for the Gulf of Cadiz. White arrows show the surface circulation. Cyan arrows show the subsurface circulation. Also included are the STOCA project standard sections (black lines) and fixed oceanographic station under the responsibility of the Spanish Institute of Oceanography, Cadiz, whose data are presented in this report (GD6 and SP6). Puertos del Estado provides data from a weather buoy located at GD6.

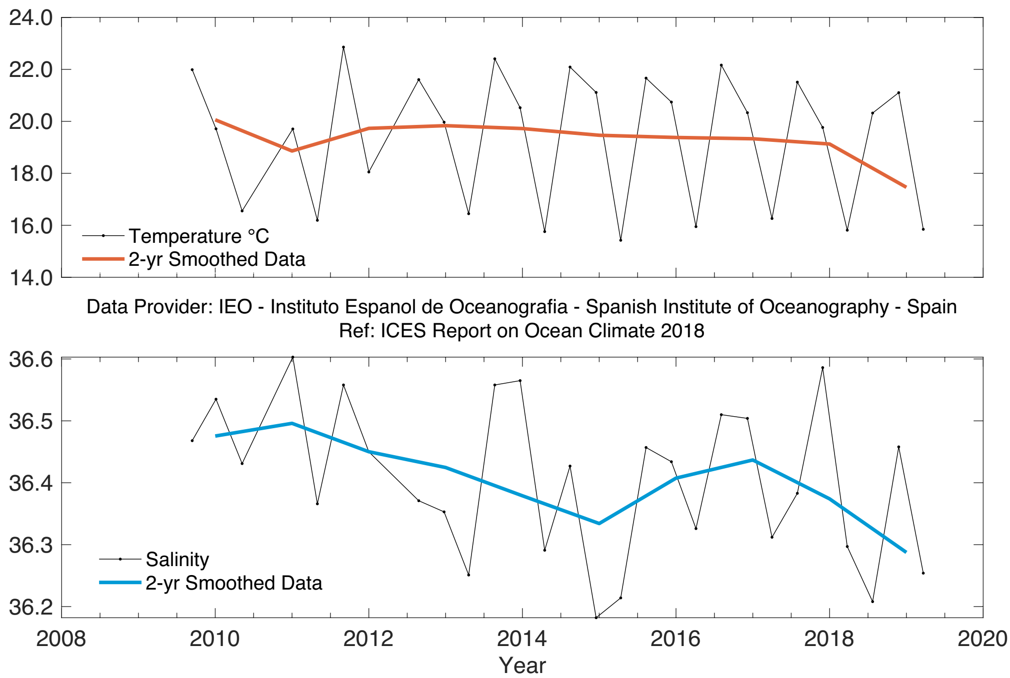

FIGURE 4.37.
Gulf of Cadiz. Potential temperature (upper panel) and salinity (lower panel) for the 0–20 m water column at the station SP6 (36°08.68´N 006°42.76´W) of the STOCA programme.

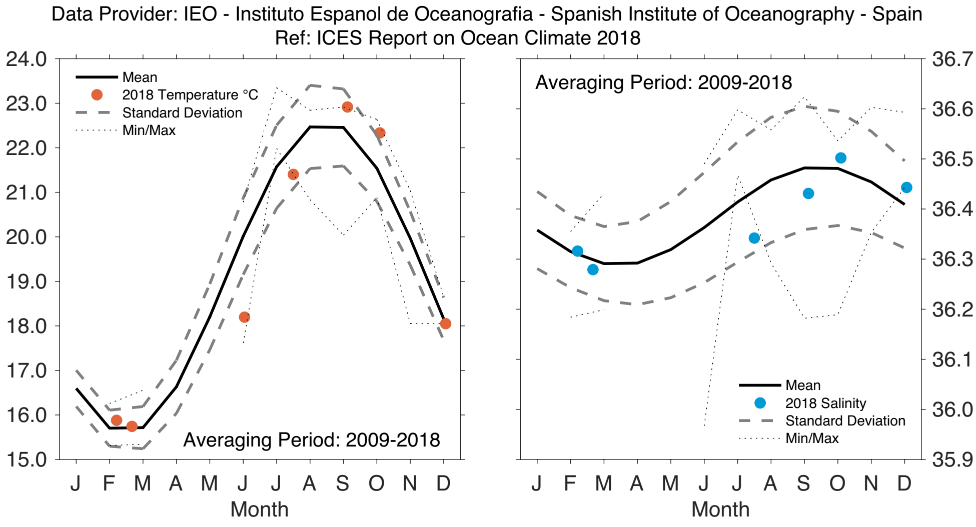

FIGURE 4.38.
Gulf of Cadiz. 2018 monthly temperature (left panel) and salinity (right panel) at STO-CA SP6 station, 10 m (36°08.68´N 006°42.76´W).

4.9 CANARY BASIN

P. Vèlez-Belchí

The Canary Basin sits at the boundary between the oceanic waters of the Subtropical Atlantic Gyre and the upwelling waters from the Canary Current Large Marine Ecosystem (CCLME) off the coast of northwest Africa. Since the early 2000s, the Canary Islands archipelago region has been monitored by the Spanish Institute of Oceanography (Tel *et al.*, 2016). Monitoring has been conducted for the oceanic waters west of Lanzarote (stations 11–23, Figure 4.39) and the CTZ of the CCLME upwelling region (stations 1–10, Figure 4.40).

At the upper levels in the water column, the area is under the influence of the southward flowing Canary Current and the Canary Upwelling Current, associated with the upwelling front (Figure 4.39). At intermediate levels, it is under the influence of the tongue of slowly propagating Mediterranean Waters (MW) and the slope current known as the Canary Intermediate Poleward Current (Hernández-Guerra *et al.*, 2017; Vélez-Belchí *et al.*, 2017).

The waters above the seasonal thermocline are characterized on the θ/S diagram by scattered temperature and salinity values, caused by seasonal heating and evaporation. These waters, considered the surface waters, occupy the upper 300 m in the oceanic region and the upper 100 m in the stations under the effect of the coastal upwelling. Below the seasonal thermocline and to the depth of the permanent thermocline, roughly between 300 and 700 m depth, are the North Atlantic Central Waters (NACW). These waters are characterized on the θ/S diagram by an approximately straight-line relationship between potential temperature (11.4°C < θ < 14.9°C) and salinity (35.6 < S < 36.1). At intermediate levels, roughly between 700 and 1200 m, two distinct water masses are found in the Canary Islands region, the fresher (S < 35.3) and slightly lighter Antarctic Intermediate Waters (AAIW) and the saltier (S > 35.4) and heavier MW. Deeper waters will be discussed in section 5.2.7.

Cooling and freshening continued in 2018 following the decreasing trend since the peak in 2014, when the NACW were at their saltiest and warmest on record. The average values in the 200-800 dbar layer are similar to those found at the beginning of the 2000s.

Between the 1990s and the early 2000s, there was a decrease in temperature and salinity of all upper-layer waters. This was followed in the mid-2000s by a marked increase in both temperature and salinity, which peaked in 2014, the hottest and saltiest year on record. Since 2015, both temperature and salinity have decreased; at the end of 2017, mean temperature and salinity were similar to those observed in the late 1990s (Vélez-Belchí *et al.*, 2015).

In the oceanic surface waters, the overall observed warming (0.19 ± 1.35°C per decade) coincides with satellite SST observations. Although it should be noted that time-series do not properly resolve the seasonal cycle.

In the depth stratum that characterizes the NACW waters (200–800 dbar), there is an overall statistically significant, at the 95% confidence level, warming of 0.082 ± 0.07°C per decade and an increase in salinity of 0.008 ± 0.012°C per decade (Figure 4.40). The overall increase in temperature and salinity almost compensate in density, confirming that the observed trends are caused by deepening of the isoneutral surfaces rather than changes along the isoneutral surfaces. This overall increase in salinity and temperature for the NACW was also observed in the CTZ, although with slightly smaller values resulting from the influence of upwelling. The variability in the CTZ is higher owing to the proximity of the upwelling region and the frequent intrusions of upwelling filaments. For the same reason, uncertainty is higher in the trend estimates.

Surface waters in the CTZ show a non-statistically significant cooling of 0.29 ± 0.49°C per decade and a non-statistically significant decrease in salinity of 0.058 ± 0.069 per decade, both consistent with an increase in the upwelling in the CCLME. 2015 was the coolest and freshest year on record for the upwelling influenced surface waters. Satellite SST observations corroborate these changes in the upwelling regime inferred from the *in situ* observations, with different areas showing increases in upwelling. However, the magnitude of the observed trend for the satellite SST is different, owing to the thin layer of ocean that the satellite observes.

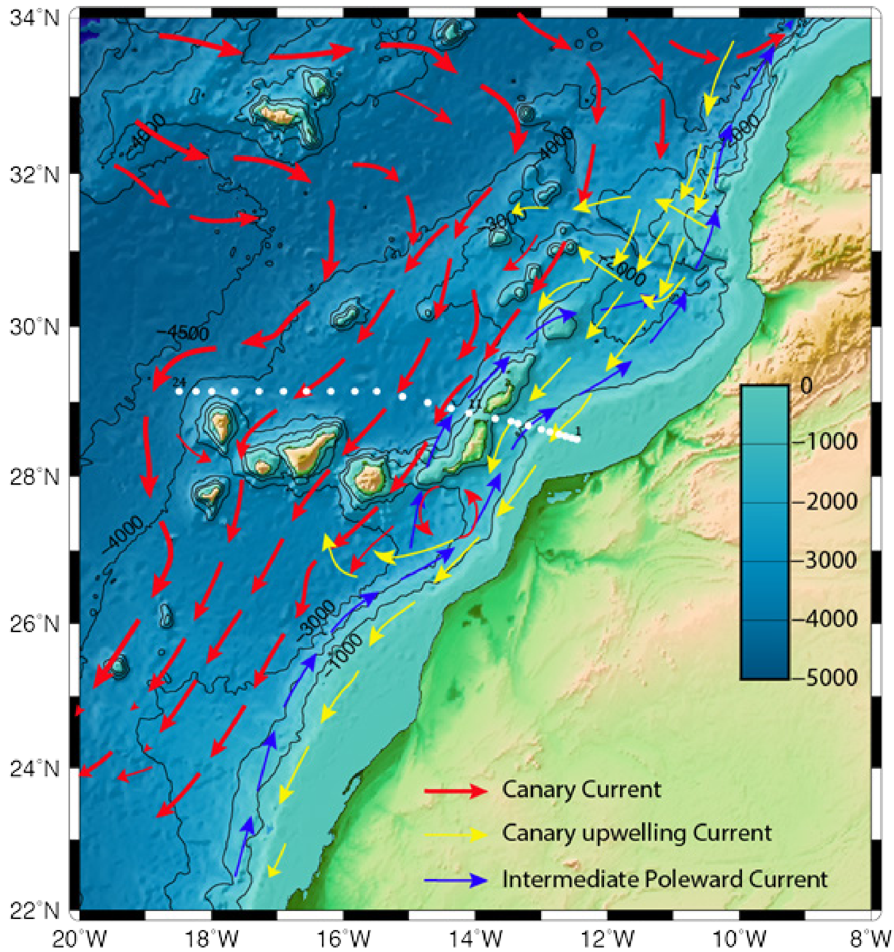

FIGURE 4.39.
Circulation schematic for the Canary Basin. Red arrows show the southward Canary Current carrying mainly NACW and intermediate waters. Yellow arrows show the Canary upwelling Current that flows in the thermocline waters. The white dots represent the distribution of the 24 hydrographic stations sampled in the Canary Islands archipelago region since 1997. Stations 1-10 are used to estimate changes in the CTZ and stations west of Lanzarote (11-24) the oceanic waters.

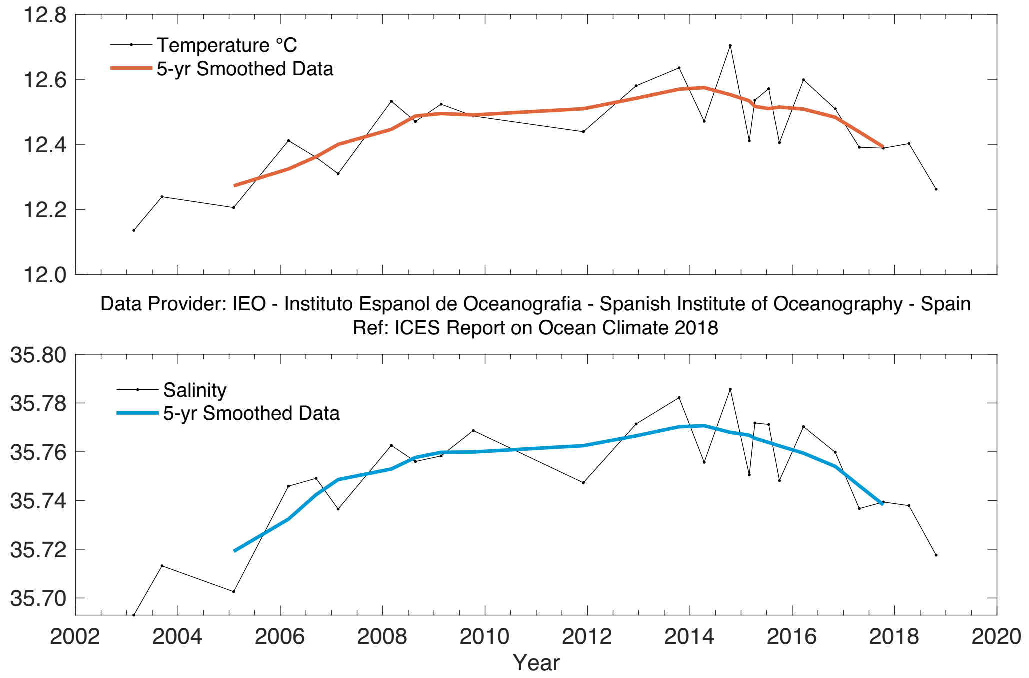

FIGURE 4.40.
Canary Basin. Potential temperature (upper panel) and salinity (lower panel) for the 200–800 m layer in the oceanic waters of the Canary Basin.

4.10 SOUTHWEST APPROACHES

T. Smyth

The datasets presented here are from the western end of the English Channel and the boundary with the Celtic Sea and the Bay of Biscay ecoregions. The area is commonly referred to as the Southwest Approaches, which relates to the passage of shipping through the English Channel. As these data come from a boundary between different ecoregions, this term has also been adopted here, as it relates to the region forming a pathway for AW to enter the southern North Sea.

Station E1 (50.03°N 4.37°W) is situated off the south coast of England in the western English Channel. The water depth is 75 m, and the station is tidally influenced by a 1.1 knot maximum surface stream at mean spring tide. The seabed is mainly sand, resulting in a low bottom stress (1–2 ergs cm^{-2} s^{-1}). The station can be described as oceanic with the development of a seasonal thermocline. Stratification typically starts in early April, persists throughout summer, and is eroded by the end of October. The typical depth of the summer thermocline is ca. 20 m. The station is greatly affected by ambient weather.

Measurements have been taken at this station since the end of the 19th century, with data currently available since 1903 (Figure 4.41). The series is unbroken, apart from gaps for the two world wars and a hiatus in funding between 1985 and 2002. The data take the form of vertical profiles of temperature and salinity. Early measurements were taken with reversing mercury-in-glass thermometers and discrete salinity bottles. More recently, electronic equipment (Seabird CTD) has been utilized. The time-series demonstrates considerable interannual temperature variability.

E1 was sampled on 17 occasions during 2018: approximately fortnightly in summer and monthly in winter. The year was slightly warmer than average until early summer, when exceptional heat and close to record temperatures were observed during June and particularly July (Figure 4.42). The warmth was retained in the water column until the end of the year.

Salinity values were slightly above the long-term mean (ca. 35.2–35.3) during the first half of 2018 (Figure 4.42), followed by a marked drop to lower-than-average salinity values in early summer, which persisted for the rest of the year. A possible source of this freshening may be increased river run-off from the Loire and Gironde, caused by extreme summer precipitation in France.

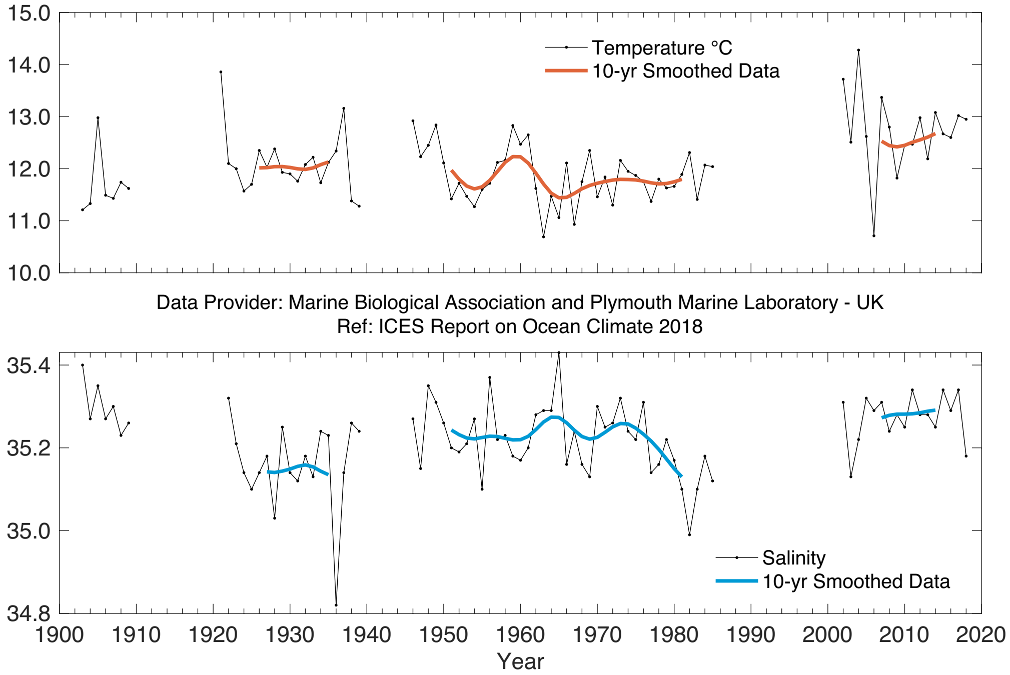

FIGURE 4.41. Southwest Approaches. Temperature (upper panel) and salinity (lower panel) anomalies of surface (0–40 m) water at Station E1 in the western English Channel (50.03°N 4.37°W).

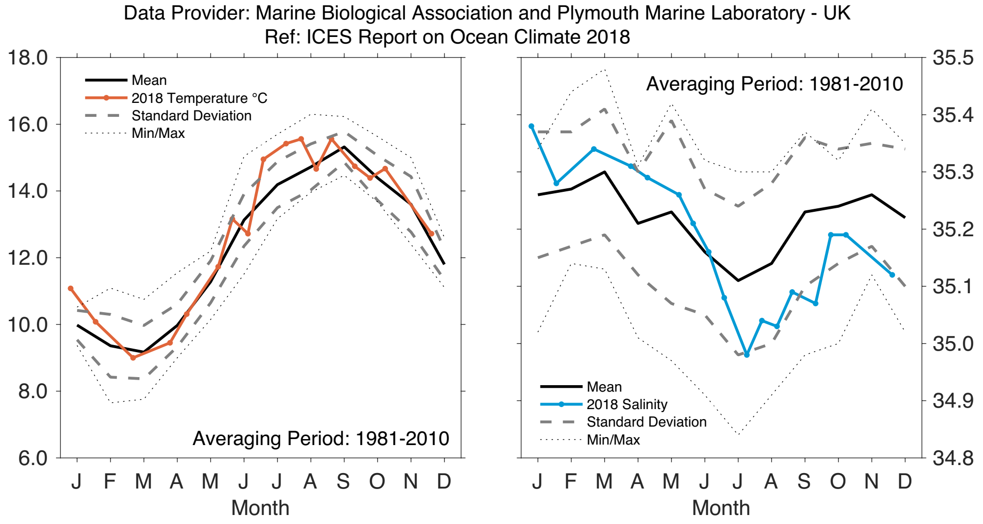

FIGURE 4.42. Southwest Approaches. Monthly average seasonal cycle with 2018 temperature (left panel) and salinity (right panel) observations of surface (0–40m) water at Station E1 in the western English Channel (50.03°N 4.37°W).

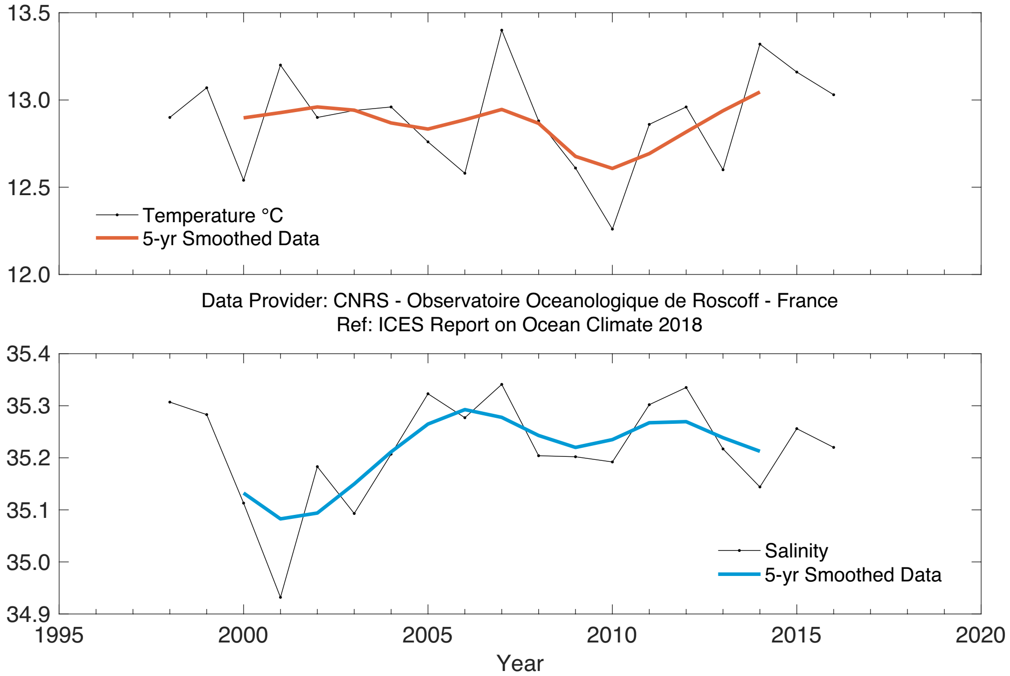

FIGURE 4.43. Southwest Approaches. Temperature (upper panel) and salinity (lower panel) of surface water at the Astan station (48.77°N 3.94°W) base period 1998–2010. Data until 2016.

4.11 CELTIC SEAS

K. Lyons and C. Cusack

The Celtic Seas are defined as an ICES ecoregion, and is included in NOAA LME 24 (Celtic-Biscay Shelf). The Celtic Seas region contains the shelf seas of northwestern Europe and part of the Rockall Trough. The shelf seas are mainly relatively shallow (< 100 m). The structure of the water column on the shelf is primarily driven by (i) vertical mixing caused by tides and wind, and (ii) the seasonal variation of solar heating, leading to seasonal (summer)density-driven currents (e.g. Irish Coastal Current). In addition to the influence of coastal waters on the shelf, the area is strongly influenced by the poleward transport of AW and the continental slope current that brings waters northward from the Biscay region.

Malin Head monthly mean temperatures for 2018 show a colder than average spring (March and April) with all other months at or above the average (Figure 4.44). The mean SST recorded at Malin Head for 2018 was 0.19°C above the 1981–2010 mean (Figure 4.45). For the short M3 buoy SST time-series, the mean in 2018 was slightly below the 2003–2010 mean (Figure 4.44).

Record warm SST at Malin Head station.

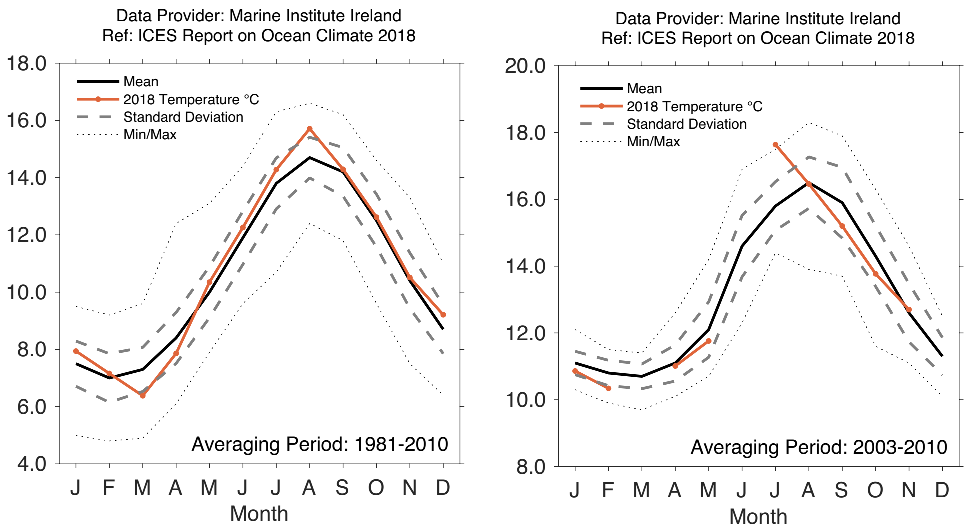

FIGURE 4.44. Celtic Seas. Monthly average seasonal cycle with 2018 monthly temperature at (left) Malin Head and (right) the M3 Weather Buoy southwest of Ireland (51.22°N 10.55°W).

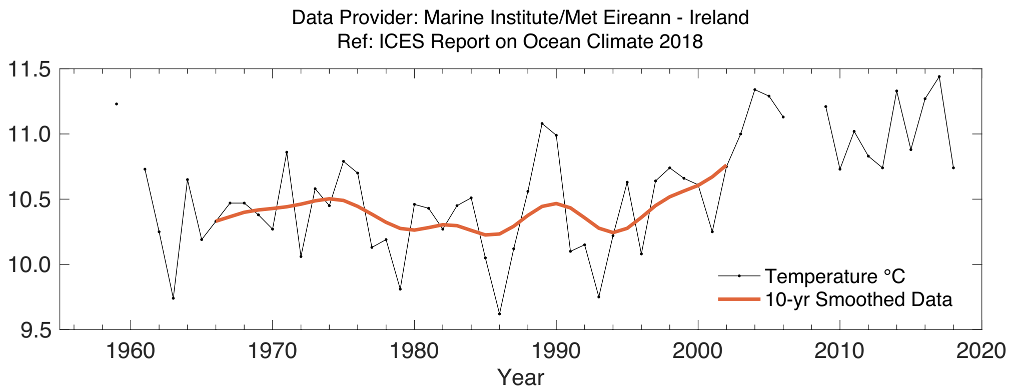

FIGURE 4.45. Celtic Seas: Temperature at the Malin Head coastal station (55.39°N 7.38°W).

4.12 ROCKALL TROUGH

N.P. Holliday and S. Jones

Rockall Trough is a deep ocean basin situated west of Britain and Ireland, within the Celtic Seas and Oceanic Northeast Atlantic ecoregions. It has significantly different oceanographic characteristics than the shallower shelf sea areas. Rockall Trough is separated from the Iceland Basin by Hatton and Rockall banks, and from the Norwegian Sea by the shallow (500 m) Wyville-Thomson Ridge. It is a route for warm North Atlantic upper water to reach the Norwegian Sea, where it is converted into cold, dense overflow water as part of the thermohaline overturning in the North Atlantic. The upper water column is characterized by poleward-moving eastern North Atlantic Water (NAW), which is warmer and more saline than the Iceland Basin waters that also contribute to the Norwegian Sea inflow (Figure 4.46).

The potential temperature of the upper 800 m was close to the 1981–2010 mean in 2018. In general, the upper ocean has been cooling relative to a peak of 9.8°C in 2007, though with a reduced trend since 2016. The salinity of the upper 800 m has been decreasing since the end of the 2000s, with sharp freshening between 2015 and 2016. Upper ocean salinity remained very low in 2018. Between 2016 and 2018, salinity was the lowest observed in the Rockall Trough since 1978 (Figure 4.47).

Fresh and near-average temperature conditions in the Rockall Trough in 2018.

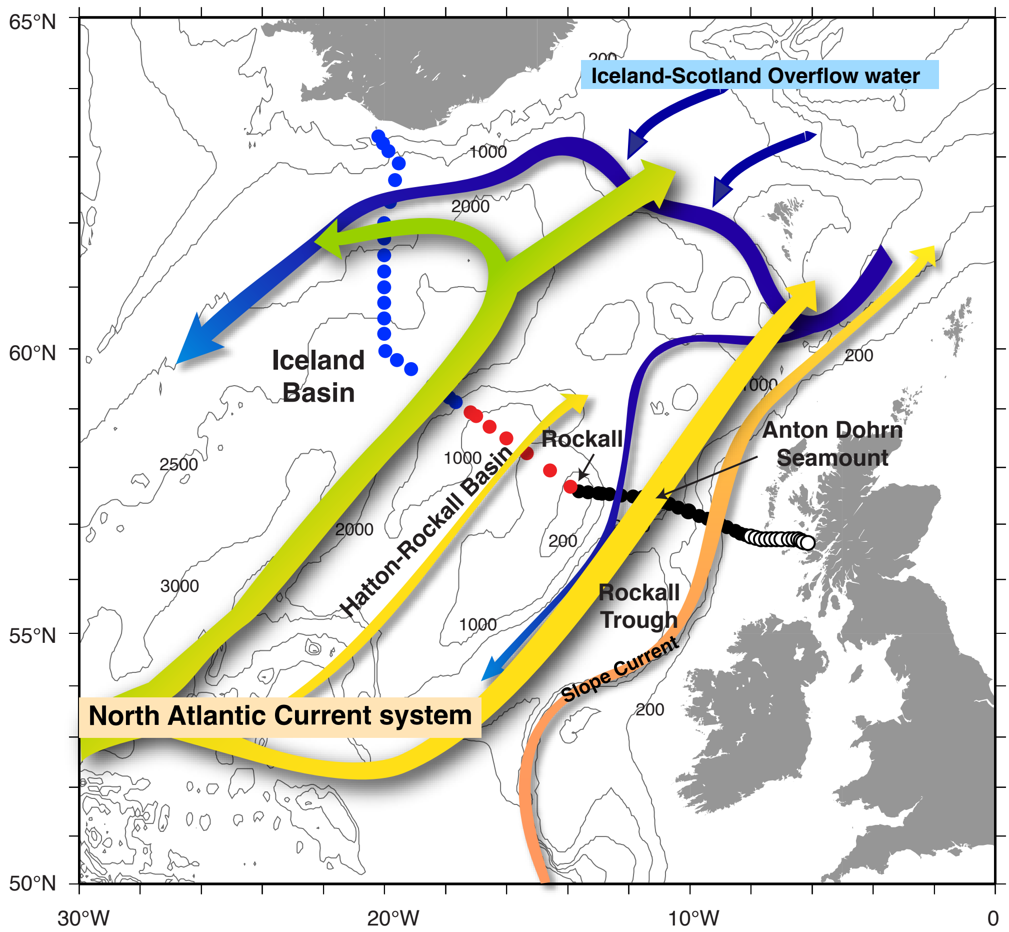

FIGURE 4.46. Circulation schematic for the Rockall Trough, Hatton-Rockall Basin and Iceland Basin. Green, yellow, and orange colours indicate the upper waters of the North Atlantic Current and the slope current. Dark blue arrows show the approximate locations of the main overflow currents.

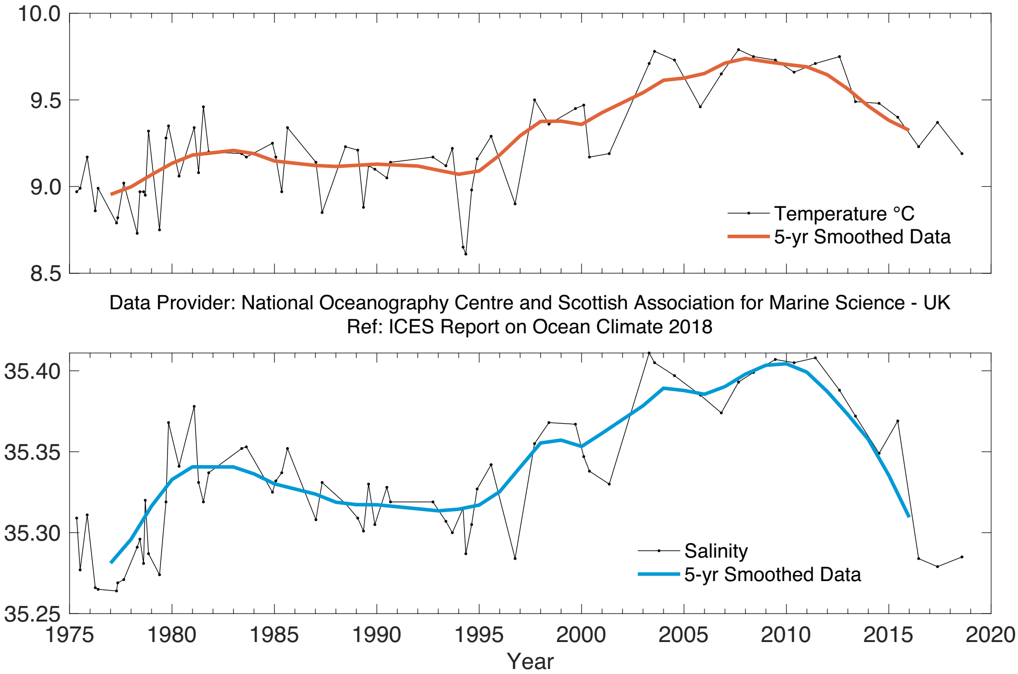

FIGURE 4.47.
Rockall Trough. Temperature (upper panel) and salinity (lower panel) for the upper ocean (potential density 27.2–27.50 kg m^{-3}, representing the top 800 m, but excluding the seasonally warmed surface layer).

The M6 weather buoy.
Photo: Tomasz Szumski, Marine Institute, Galway, Ireland

4.13 HATTON-ROCKALL BASIN

N.P. Holliday and S. Jones

The shallow Hatton-Rockall Basin (1000 m) lies between the Iceland Basin to the west and Rockall Trough to the east and is bounded by the Hatton and Rockall banks. The basin is filled with well-mixed subpolar-mode water moving northward as part of the North Atlantic Current (NAC) complex. Winter mixing reaches 800–1000 m here. Temperature and salinity vary considerably depending on the type of NAC water that enters the basin. The region is in the transition zone between cold, fresh, central Subpolar Water and warm, saline, eastern Subpolar Water.

The range in basin mean temperature and salinity in the upper 800 m is more than 1°C and 0.1 higher, respectively, than the Iceland Basin to the west and Rockall Trough to the east. The lowest values were seen at the start of the time-series in 1996, followed by a steady rise to maximum values in the late 2000s. Since 2010, there has been a decrease in temperature and salinity. In 2018, salinity increased by 0.06 psu, but remained lower than the 1996–2010 average. The temperature has risen since 2016 to a value close to the long-term mean (Figure 4.48).

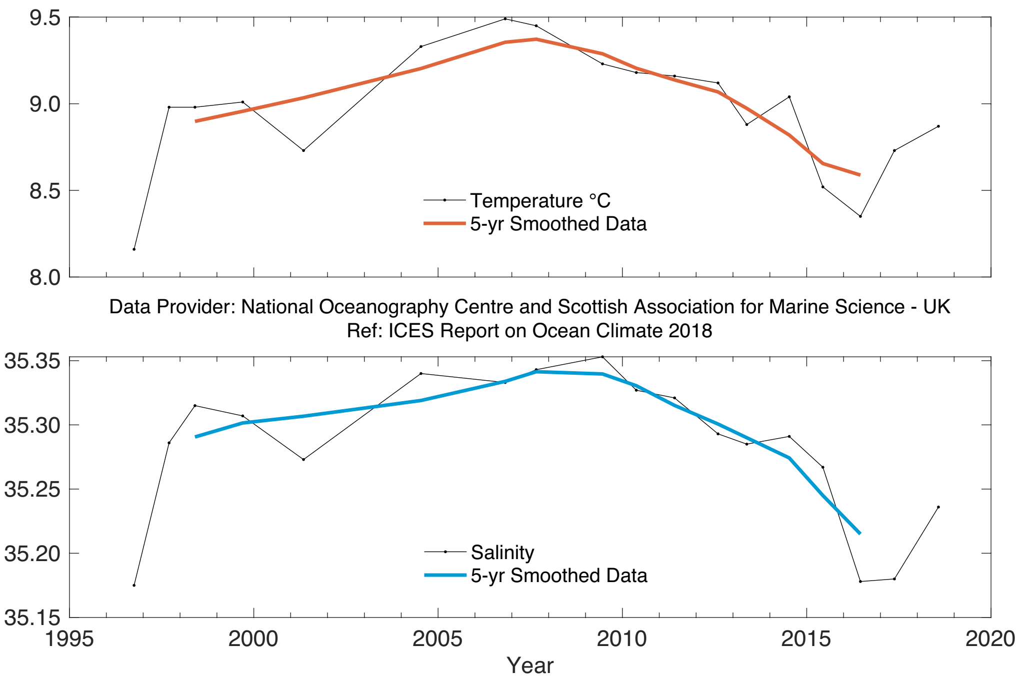

FIGURE 4.48.
Hatton-Rockall Basin: Temperature (upper panel) and salinity (lower panel) for the upper ocean (potential density 27.20–27.50 kg m-3, representing the top 800 m, but excluding the seasonally warmed surface layer).

4.14 ICELAND BASIN

N.P. Holliday and S. Jones

A major part of the NAC flows into the Iceland Basin, adjacent to the shallow Hatton Bank on the southeast side of the basin (Figure 4.46). The NAC typically consists of one or two fronts between warmer, more saline water in the east and colder, fresher water to the north and west. The region is rich in eddy activity, and the water properties are quite variable in time and space. Most of the water entering the Iceland Basin from the south flows through into the Norwegian Sea over the Iceland-Scotland Ridge. A smaller fraction of the NAC water recirculates south of Iceland in the boundary currents of the main anticlockwise circulation of the Subpolar Gyre.

Temperature and salinity of the upper ocean (ca. upper 500–600 m) vary from year-to-year, but also exhibit multiyear changes. Both temperature and salinity increased from 1996 to the late 2000s, but have since been decreasing (Holliday *et al*., 2015; Figure 4.49). The freshening since 2010 implies that the basin is receiving more water originating in the west and central subpolar region and less warm, saline water from the eastern intergyre regions. Superimposed on that multiyear trend is the rapid cooling observed between 2014 and 2015, caused by a high flux of heat from the ocean to the atmosphere (Duchez *et al*., 2016) and the rapid freshening observed in 2015–2017. In 2018, the Ellett Line transect was not occupied; thus, no observations were possible at the regular sample location for this time-series. However, measurements from the adjacent OSNAP line suggest that the recent sharp decline in temperature and salinity may have halted.

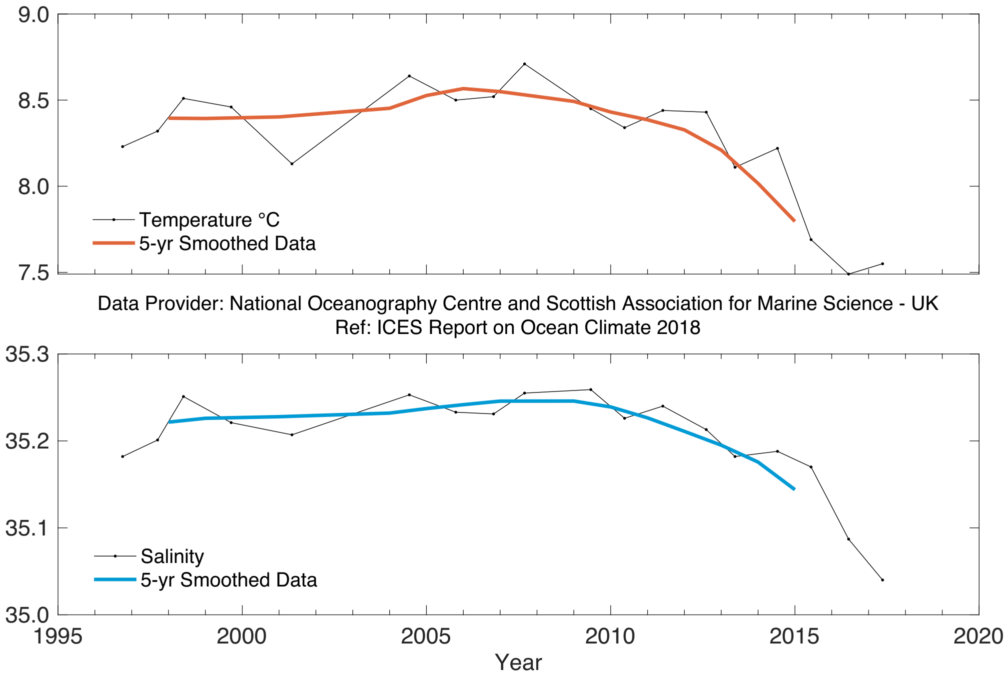

FIGURE 4.49.
Iceland Basin. Temperature (upper panel) and salinity (lower panel) for the upper ocean (potential density 27.20–27.50 kg m^{-3}, representing the top 500 m, but excluding the seasonally warmed surface layer). Data until 2017.

4.15 IRMINGER SEA

M. F. de Jong

The Irminger Sea is the ocean basin between south Greenland, the Reykjanes Ridge, and Iceland. This area forms part of the North Atlantic Subpolar cyclonic Gyre. Due to this gyre, the exchange of water between the Irminger and the Labrador seas proceeds relatively fast. In the bottom layers of the Irminger Sea, cold water originating in the (sub) Arctic seas flows from the Denmark Strait and to the south over the continental slope of Greenland.

The SPMW in the 200–400 dbar pressure interval in the centre of the Irminger Sea showed a minimum in temperature and salinity in 1995/1996 and reached its highest temperature and salinity in 2004 (Figure 4.50). Temperature has shown a decrease since 2004, with some interannual variability superimposed. Salinity remained more stable since 2004, but decreased in 2018, potentially related to the upper ocean freshwater anomaly observed in the Subpolar Gyre. The temperature of the SPMW in the central Irminger Sea was about 0.2°C below the long-term mean, although salinity was –0.002 below the mean. This is the first negative salinity anomaly since 2003. Mixed layers were generally shallow in the Irminger Sea in winter of 2018. Figure 4.51 shows that the pattern of cooling/freshening through convection, and heating/increasing salinity by advection does not only apply to the central Irminger Sea, but also to the northern part of the basin.

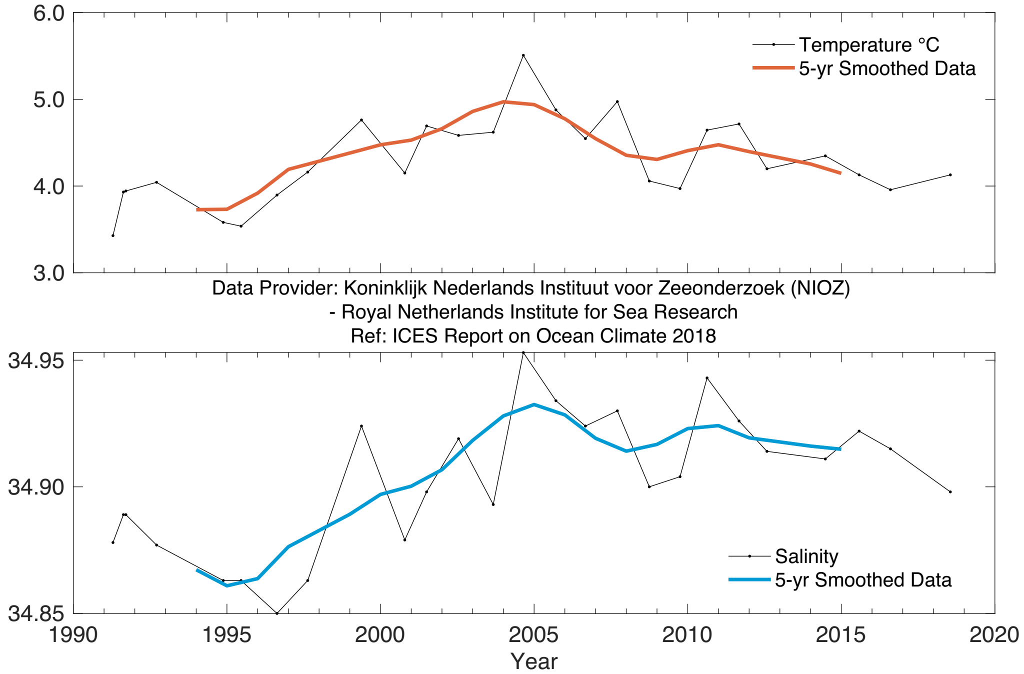

FIGURE 4.50.
Irminger Sea. Temperature (upper panel) and salinity (lower panel) of SPMW in the central Irminger Sea (averaged over 200–400 m).

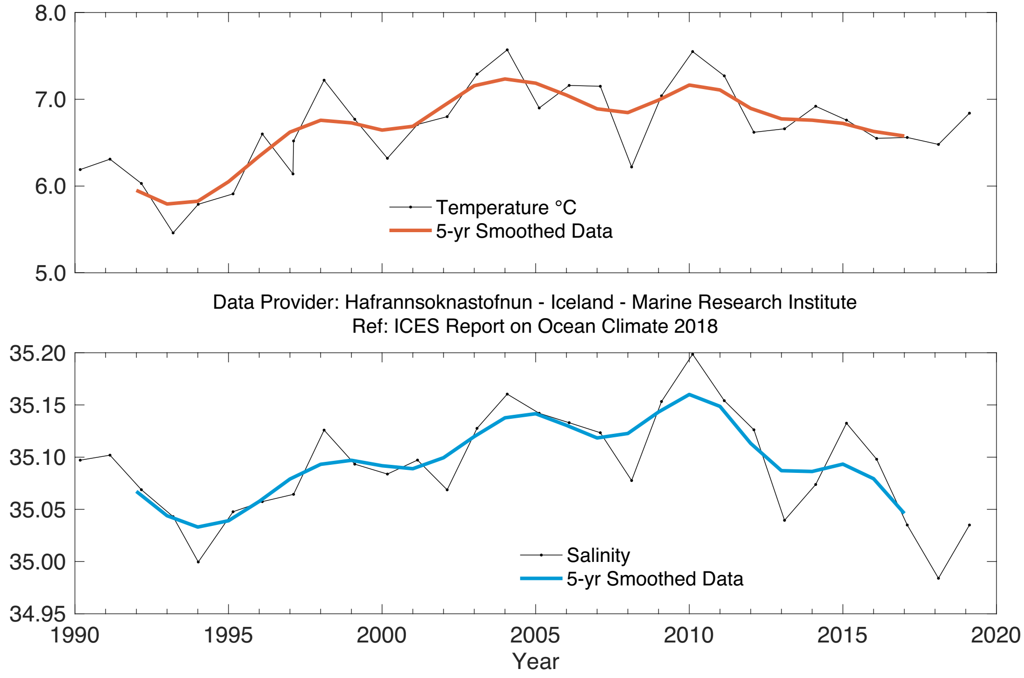

FIGURE 4.51.
Irminger Sea. Temperature (upper panel) and salinity (lower panel) of SPMW in the northern Irminger Sea (Station FX9, 64.33°N 28°W), from winter observations averaged over 200–500 m.

Cobh, Ireland.
Photo: Tomasz Szumski, Marine Institute, Galway, Ireland

4.16 FAROESE WATERS AND THE FAROE-SHETLAND CHANNEL

K. M. H. Larsen, B. Berx, and J. Hindson

Data from the Faroese Waters ecoregion are grouped together here with data from the Faroe-Shetland Channel. This small region sits at the boundary between the Celtic Seas, North Sea, and Norwegian Sea ecoregions and at the boundary between the North Atlantic and Nordic seas. One branch of the NAC crosses the Greenland-Scotland ridge (Figure 4.52), flowing on either side of the Faroes. Its properties are sampled in the Faroe Bank Channel before it crosses the ridge and in the Faroe Current after it crosses the ridge. Some of this water recirculates and is sampled within the Faroe-Shetland channel as modified North Atlantic Water (MNAW). Further to the east, the continental slope current flows along the edge of the Northwest European continental shelf; originating in the southern Rockall Trough, it carries warm, saline AW into the Faroe-Shetland Channel. A proportion of this AW crosses onto the shelf itself and enters the North Sea, where it is diluted with coastal water and eventually leaves in the Norwegian Coastal Current. The remainder of the AW enters the Norwegian Sea and joins the water coming from north of the Faroes to become the Norwegian Atlantic Water.

Generally, both temperature and salinity in all upper-layer waters around the Faroes and the Faroe–Shetland Channel increased markedly during the 1990s and 2000s. Subsequently, both temperature and salinity decreased during the first half of the 2010s.

After the record-high salinities observed in the Faroe Bank Channel (Figure 4.53) and the Faroe Current (Figure 4.54) in November 2009, salinities have decreased at both locations. In the Faroe Bank Channel, salinity decreased from average values in 2015 to record-low values in autumn 2016. This freshening continued throughout 2017 and 2018, although at a slower rate. Record-low values were observed in the Faroe Bank Channel in February 2018, and the 2018 annual average salinity was record-low at both locations. Temperatures in the Faroe Bank Channel and the Faroe Current have been relatively high and stable since the mid-2000s and into the early 2010s. In 2012, they decreased and have been close to the long-term mean in the recent years. However, in 2018, they decreased to values below the long-term mean.

On the Faroe Shelf, the annual average temperature has been relatively high since the early 2000s. However, in 2015, the annual averaged temperature was 0.24°C below the 1991–2010 average and the lowest observed since 2000. In 2017, the temperature increased, but in 2018 was again close to the 2015 value (data not shown). The 2018 monthly mean temperatures were close to mean throughout the year (Figure 4.55; left panel).

The long-term trend in salinity on the Faroe Shelf follows the trend observed in off-shelf waters. Salinities increased from the start of the observations in 1995 to record-high values in 2010, and subsequently have been decreasing. The record-low values observed in the Faroe Bank Channel in autumn 2016 were already evident in the Faroe Shelf salinities in late summer 2016. The off-shelf freshening continued in 2017 and 2018 and, in autumn 2018, record-low values were observed on the shelf. However, the annual mean in 2018 was slightly higher than in 2017 (Figure 4.55; right panel).

The temperature and salinity of the Faroe-Shetland Channel have been decreasing over the past 7 years, in contrast to the previous increasing trend observed since the early 1990s. Salinities of both AW types distinguished in the Channel, NAW, and MNAW, showed significant freshening in 2017 and 2018 (figures 4.56 and 4.57).Temperatures of the AW on both sides of the Faroe-Shetland Channel have decreased significantly since the record-high temperatures of 2010 and are now close to the long-term mean. The salinities of both AW types are now significantly lower than the long-term mean and are the freshest ever observed for MNAW.

Very low salinities were observed in the NAW and MNAW around the Faroes, and steep freshening was observed in the AW in the Slope Current. Temperatures in the whole region were below the long-term mean.

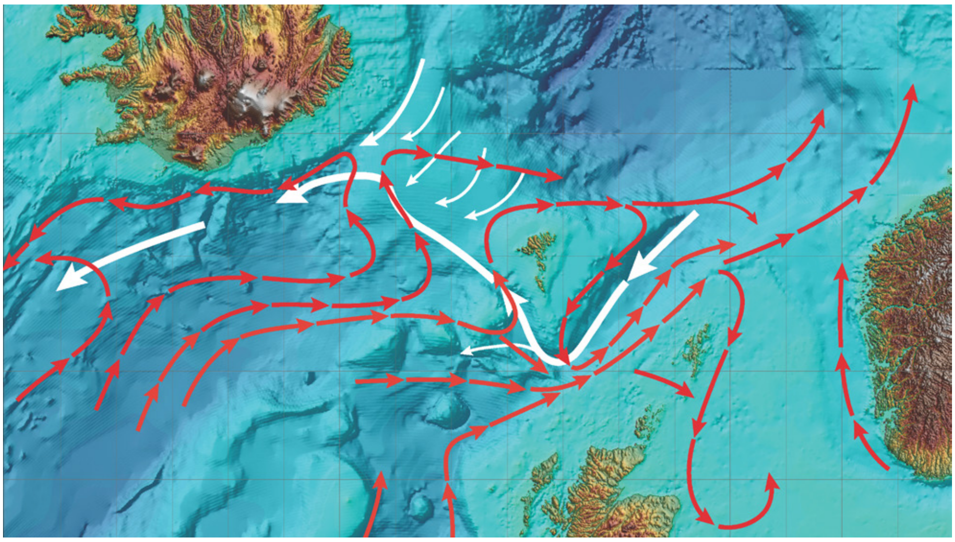

FIGURE 4.52.
Circulation schematic for Faroese Waters and the Faroe-Shetland Channel. Red lines show the poleward movement of AW. Thick white lines show the return circulation (at depth) of waters from the Nordic seas.

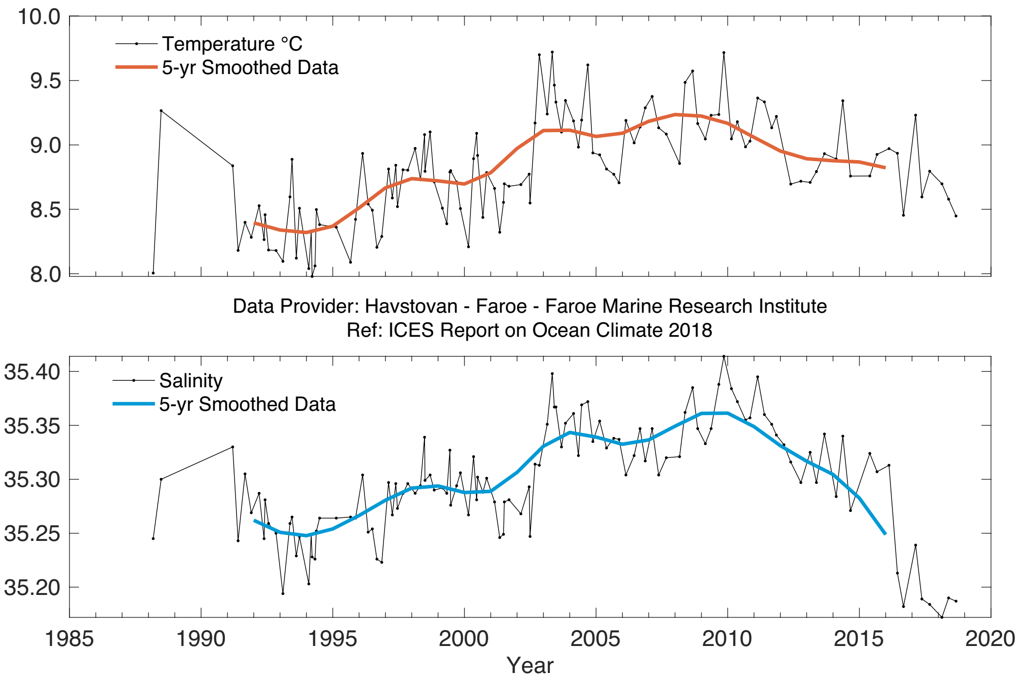

FIGURE 4.53.
Faroese waters. Temperature (upper panel) and salinity (lower panel) in the high salinity core of AW over the Faroe Bank Channel (maximum salinity averaged over a 50 m deep layer).

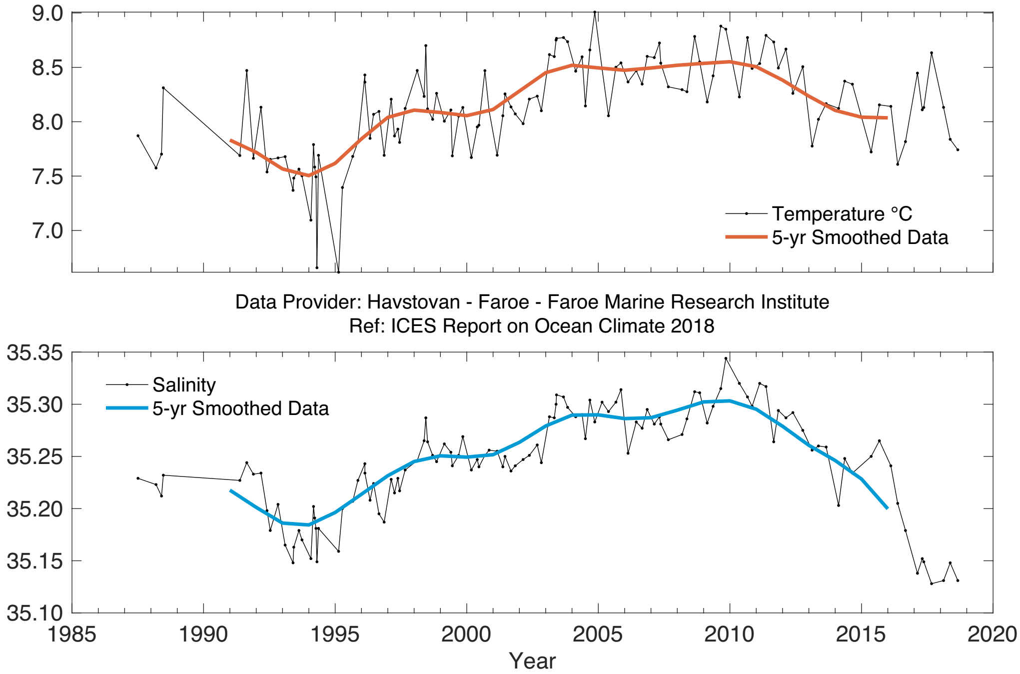

FIGURE 4.54.
Faroese waters. Temperature (upper panel) and salinity (lower panel) in the high salinity core of the Faroe Current north of the Faroes (maximum salinity averaged over a 50 m deep layer).

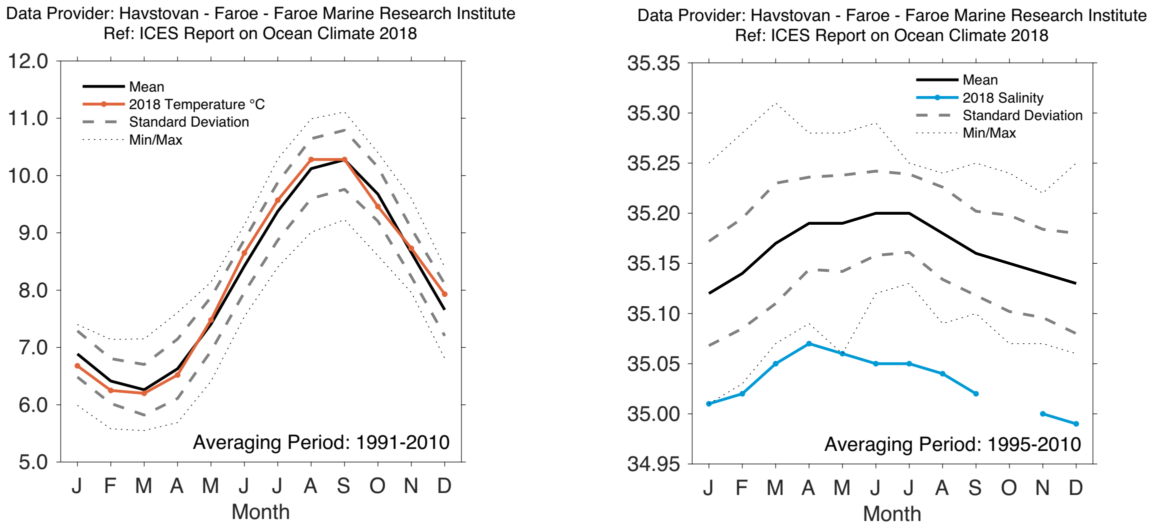

FIGURE 4.55.
Faroese waters. 2018 monthly temperature (left) from the Faroe coastal station at Oyrargjogv (62.12°N 7.17°W) and monthly salinity (right) from the Faroe coastal station at Skopun (61.91°N 6.88°W). Note the different averaging periods.

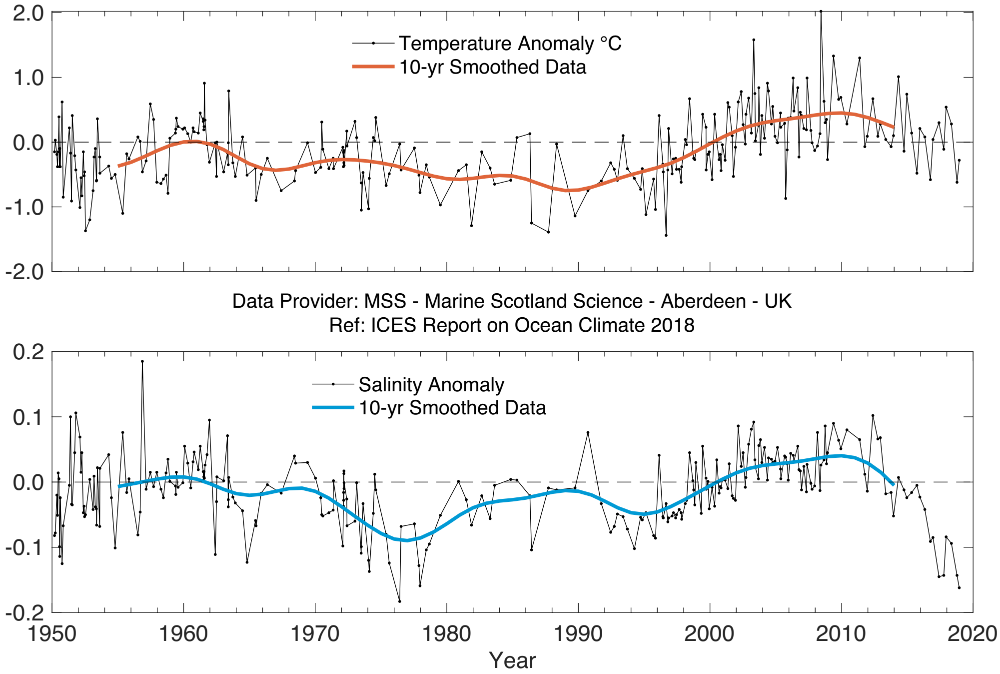

FIGURE 4.56.
Faroe-Shetland Channel. Temperature anomaly (upper panel) and salinity anomaly (lower panel) in the MNAW entering the Faroe-Shetland Channel from the north after circulating around the Faroes.

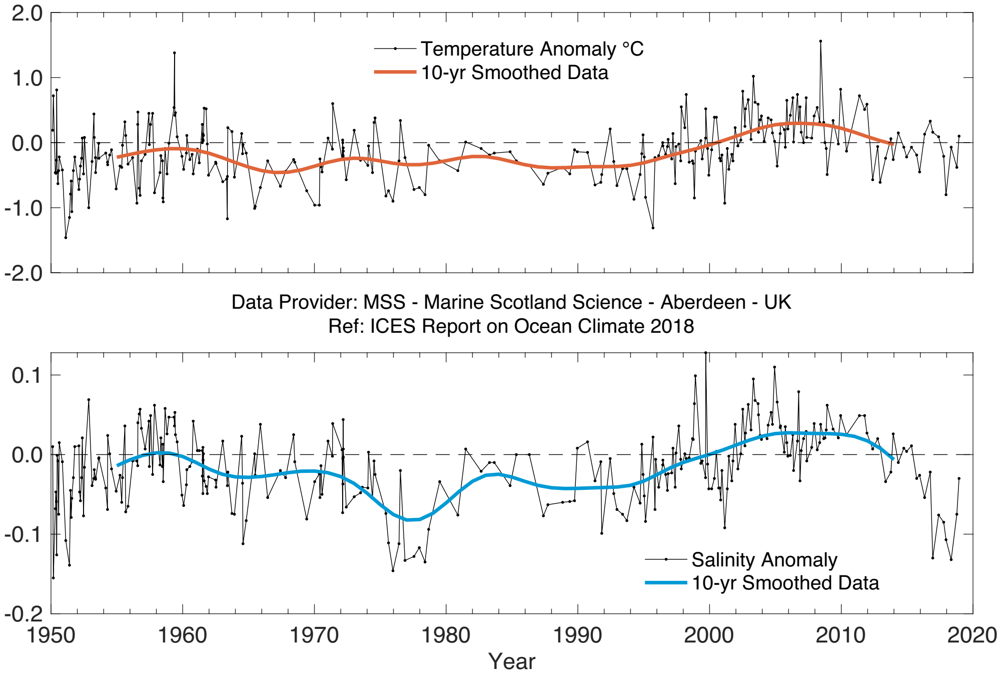

FIGURE 4.57.
Faroe-Shetland Channel. Temperature anomaly (upper panel) and salinity anomaly (lower panel) in the AW in the slope current.

4.17 NORTH SEA

H. Klein, P. Loewe, A. Schulz, and M. Köllner

North Sea oceanographic conditions are determined by the inflow of saline AW (Figure 4.58) and the ocean–atmosphere heat exchange. Inflow through the northern entrances (and, to a lesser degree, through the English Channel) can be strongly influenced by the NAO. Numerical model simulations also demonstrate strong differences in North Sea circulation depending on the state of the NAO. The AW mixes with river run-off and lower-salinity Baltic out flow along the Norwegian coast. A balance of tidal mixing and local heating forces the development of a seasonal stratification from April/May to September in most parts of the North Sea.

The annual area-averaged North Sea SST is still above the climatological mean. High salinity concentrations in the southern German Bight caused by low river run-offs.

In 2018, area-averaged monthly North Sea SSTs started with slightly positive anomalies and dropped to negative anomalies of –1.1 and –0.6°C in March and April, respectively, caused by unusually intensive cooling. This drop was followed by an extremely steep SST rise of 11.4°C from March to July. Such a steep rise has not previously been recorded over the last 50 years of observations (Figure 4.59). The July average of 16.3°C (anomaly +1.6°C) is the second highest July average in the last 50 years and lies only 0.1°C below the July 2014 SST record. The SST average for August was 17.0°C. Autumn anomalies were about 0.5°C above the long-term mean. The same pattern was observed at Helgoland in the southern North Sea, but with a wider range of the seasonal cycle (Figure 4.64).

The annual average SST averaged over the entire North Sea in 2018 was 10.7°C, ca. 0.5°C above the climatological mean (Figure 4.60). The annual average at Helgoland Roads in the southern North Sea was 10.9°C (+0.7°C). Both time-series show the same variability over time, but the extremes at Helgoland Roads are more pronounced on account of the shallow-water depth in the German Bight.

Much of the North Sea SST variability is caused by local ocean–atmosphere heat flux, besides the inflow of warmer AW at the northern boundary and through the English Channel. The annual sea surface salinity (SSS) means at Helgoland Roads (Figure 4.63) have been relatively high in recent years, which corresponds to low river run-offs into the German Bight during the last 5 years.

Compared to the 10-year average (2000–2010), the SST in the southern North Sea showed positive anomalies that reached up to 1.5°C at the southern continental coast. Along the UK coast and off the south coast of Norway, negative anomalies reached 1.5°C. Stronger temperature anomalies were observed in the bottom layer. Positive anomalies reached up to +2.5°C at the coast of the Netherlands and over +1°C in the area of Atlantic inflow between the southern tip of Shetland and Newcastle (Figure 4.62). Negative anomalies occurred at the entrance of Skagerrak (–2°C) and in the central North Sea (–1.5°C). The differences between surface and bottom temperature exceeded 10°C in the central North Sea and over the Norwegian Trench. The area-averaged summer SST (July, August, and September) of 16.1°C is ranked fifth since 1969.

The 54°N section was vertically well mixed in summer, owing to shallow-water depths along the section. The 55°N section was vertically mixed along the shallower eastern part. The sections between 55°N (in its deeper western part) and 60°N showed a massive homogeneous mixed surface layer, with a strong thermocline at about 30 m depth, which weakened along the UK coast on account of strong tidal currents. The temperatures of the upper mixed layer corresponded to values of the 2017 survey, which was about one month early in August, when SSTs had exhibited their highest temperatures. Compared to 2017, the total heat content decreased slightly to 1.650 x 10^{21} J, as a consequence of colder bottom temperatures, but still exceeded the reference mean of 1.631 x 10^{21} J by 0.3 s.d.

During summer, there was a relatively narrow inflow of AW (S > 35 psu) over the east Shetland Shelf and the Fair Isle Channel at 60°N, which was also visible on the 59°N section, but not further south. In the bottom layer, there was a broad inflow over the entire 60°N section reaching southward with a small tip to 56°N. This southern tip is part of an isolated column of AW that extends from bottom to surface. Also the modelled northern inflow between Orkney and Utsira shows a moderate volume transport (Figure 4.61). At the southern connection between the North Sea and the Atlantic, the eastern approach to the Strait of Dover, no AW was detected.

Salinity anomalies over large scales at the surface and at the bottom showed only minor deviations from the 10-year average (2000–2010). Small-scale anomalies of +3 psu were only recorded in the Elbe estuary in the inner German Bight and along the North Frisian coast, caused by low river run-offs and a long-lasting drought starting at the beginning of May. Compared to 2017, the total salt content decreased slightly to 1.102 x 10^{12} t, which is 1.7 s.d. below the 2000–2010 mean. This general decline is also visible in the Fair-Isle Current entering the North Sea from the North Sea (Figure 4.62).

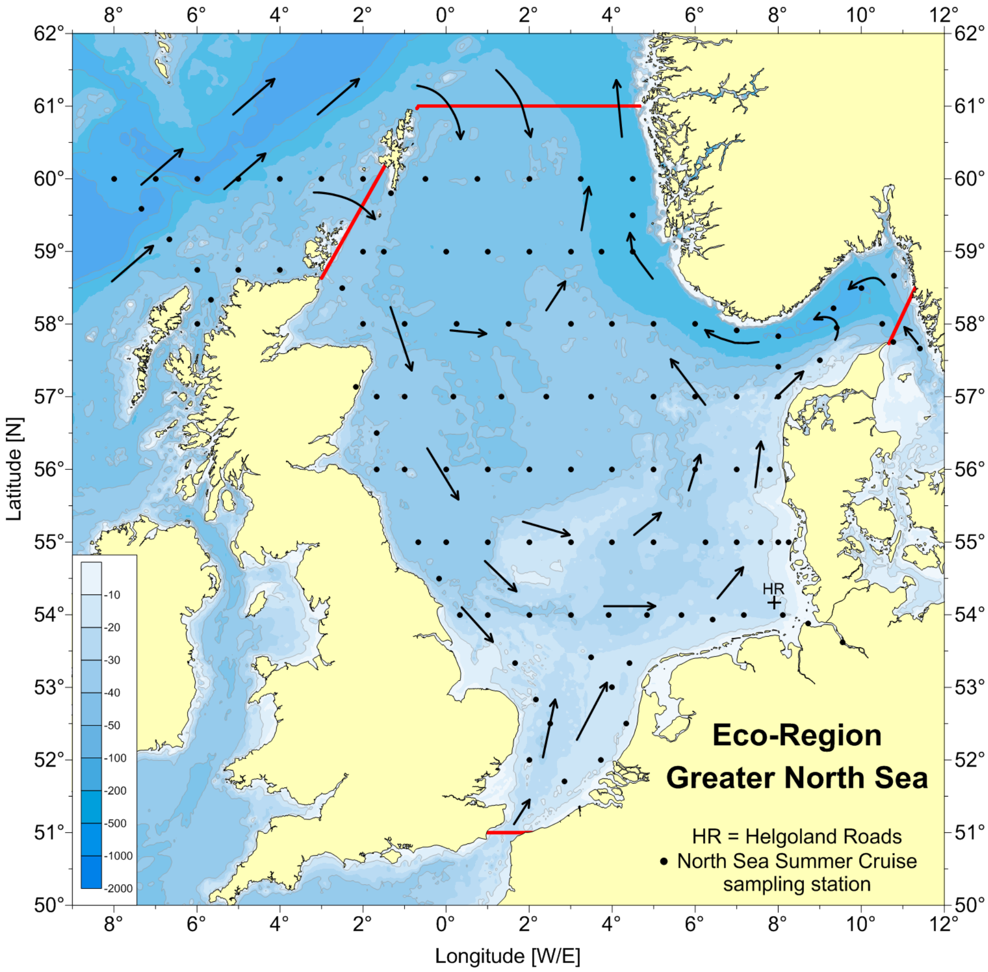

FIGURE 4.58. Circulation schematic for the North Sea. Red lines show extent of the North Sea region. The sampling station at Helgoland Roads is marked with a HR+. Black arrows indicate mean residual circulation patterns. Black dots show the summer sampling undertaken in the North Sea by Bundesamt für Seeschifffahrt und Hydrographie (BSH; German Federal Maritime and Hydrographic Agency).

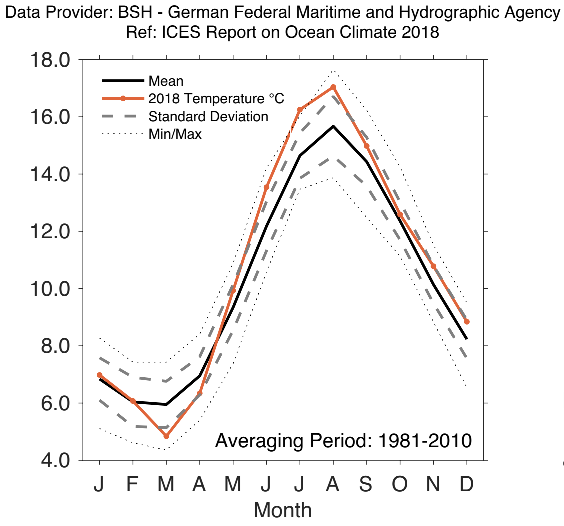

FIGURE 4.59.
Monthly means of area averaged North Sea SST.

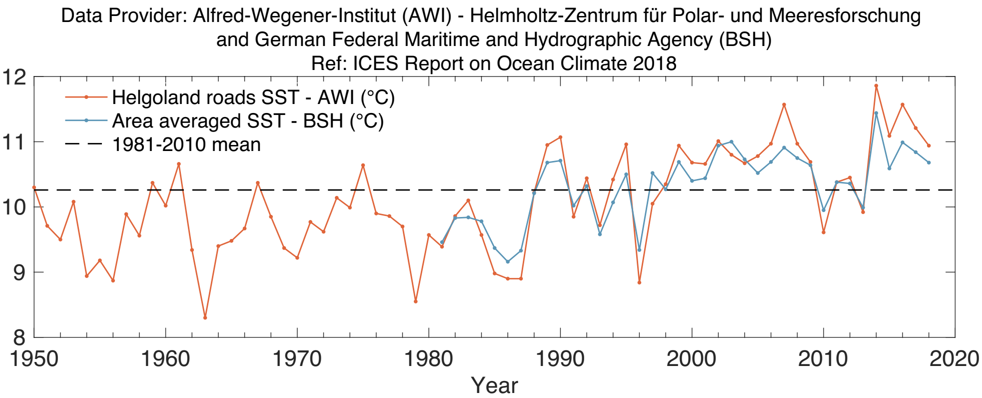

FIGURE 4.60.
Annual average of the area averaged North Sea SSTs

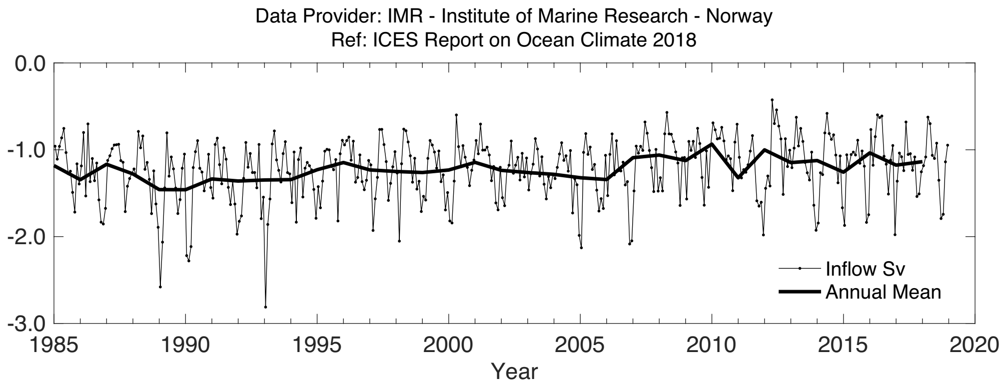

FIGURE 4.61.
Northern North Sea. Modelled annual mean (bold) and monthly mean volume transport of AW into the northern and central North Sea southward between the Orkney Islands and Utsire, Norway.

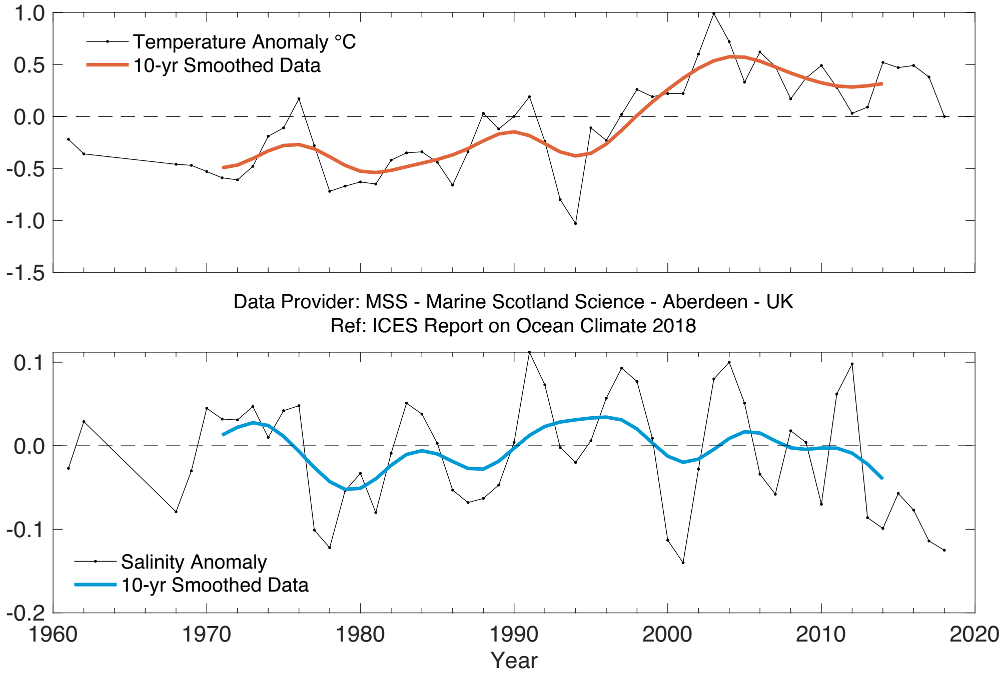

FIGURE 4.62. Northern North Sea. Temperature anomaly (upper panel) and salinity anomaly (lower panel) in the Fair Isle Current entering the North Sea from the North Atlantic.

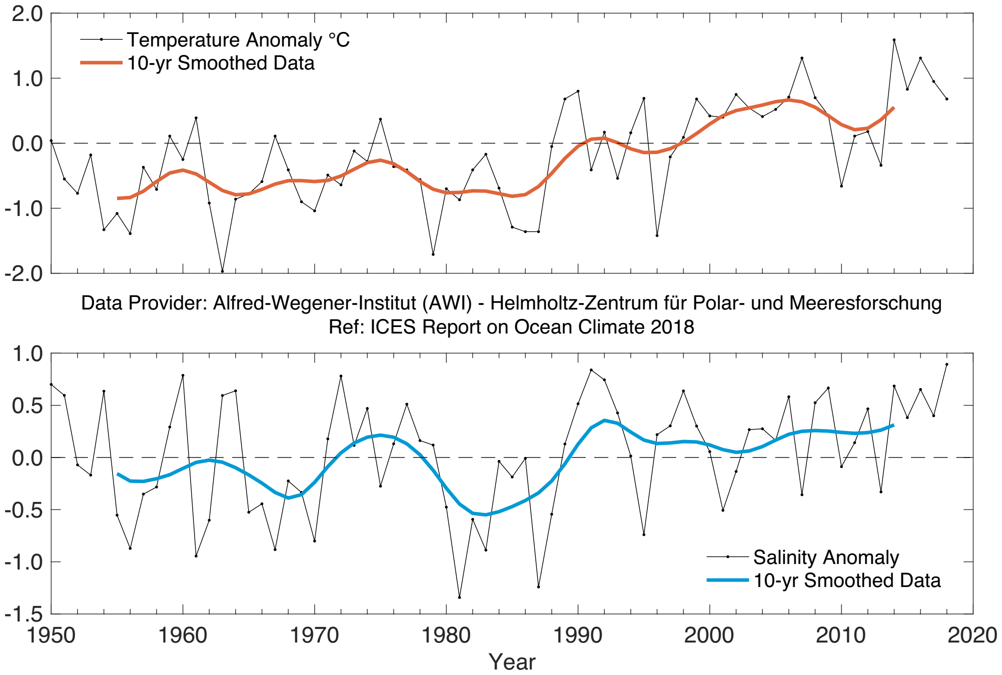

FIGURE 4.63. Southern North Sea. Annual mean surface temperature anomaly (upper panel) and salinity anomaly (lower panel) at Station Helgoland Roads.

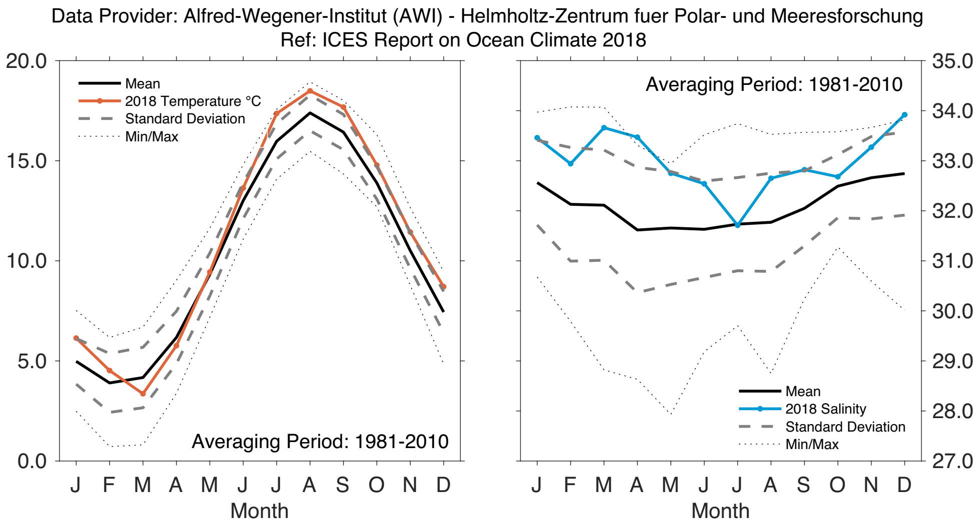

FIGURE 4.64. Southern North Sea. Monthly surface temperature (left panel) and salinity (right panel) at Station Helgoland Roads.

4.18 SKAGERRAK, KATTEGAT, AND THE BALTIC

K. Wesslander and T. Wodzinowski

The Skaggerak, Kattegat, and Baltic Sea are characterized by large salinity variations. In the Skagerrak, water masses from different parts of the North Sea are present. The Kattegat is a transition area between the Baltic and the Skagerrak. The water is strongly stratified with a permanent halocline (sharp change in salinity at depth). The deep water in the Baltic Proper, which enters through the Belts and the Sound, can be stagnant for long periods in the inner basins. In the relatively shallow area in the southern Baltic, smaller inflows pass relatively quickly, and the conditions in the deep water are highly variable. Surface salinity is very low in the Baltic Proper and its gulfs. The Gulf of Bothnia and the Gulf of Finland are covered in ice during winter.

Owing to its central location relative to the Skagerrak, Kattegat, and Baltic, weather in Sweden can be taken as representative for the area. It was very warm and dry in Sweden in 2018. Mean air temperature was above normal throughout the country, with summer in particular being extremely warm. Mean precipitation was lower than normal in almost all parts of Sweden, and the number of sun hours was above normal over all of Sweden.

In the Skagerrak and the Baltic, the year started with SST close to normal (Figure 4.67). However, in spring–summer, extremely warm temperatures were observed near the surface across the Baltic Sea. SSS was below normal in Skagerrak, Kattegat, and the eastern part of the Baltic (Bornholm Basin) in the first half of the year and above normal during the rest of 2018 (Figure 4.67). SSS was above normal year-round in the Baltic Proper.

There was a small inflow of warmer water into the Baltic during summer that caused a rise in near-bottom temperature in the southern Baltic area. No major Baltic inflow was detected in 2018. A major Baltic inflow ventilates deep water along its route into the Baltic Proper, leading to higher oxygen concentrations in deeper waters in the Baltic Proper. The last major Baltic inflow was in winter 2014/2015 and it improved the oxygen condition in the deeper areas of the Baltic Proper. However, in 2018, oxygen concentrations decreased again and the concentration of hydrogen sulphide increased in the eastern and western Gotland Basin. The Bornholm Basin also experienced hydrogen sulphide events. In 2018, around 22% of the seabed regions in the Baltic Proper were anoxic and 32% were hypoxic.

The 2017/2018 ice season started in November and ended in May, which is close to normal. A cold period in March led to ice coverage over most of the Bay of Bothnia, the Quark, and the northern part of the Bothnian Sea. A thin ice cover was also present at that time in the Bay of Finland and the Bay of Riga. The maximum ice extent was already reached on 5 March at 175 000 km2 (Figure 4.70). The ice season ended on 24 May.

An extremely warm year, with continuing low oxygen conditions in the deep waters in the Baltic Proper and extremely high SST.

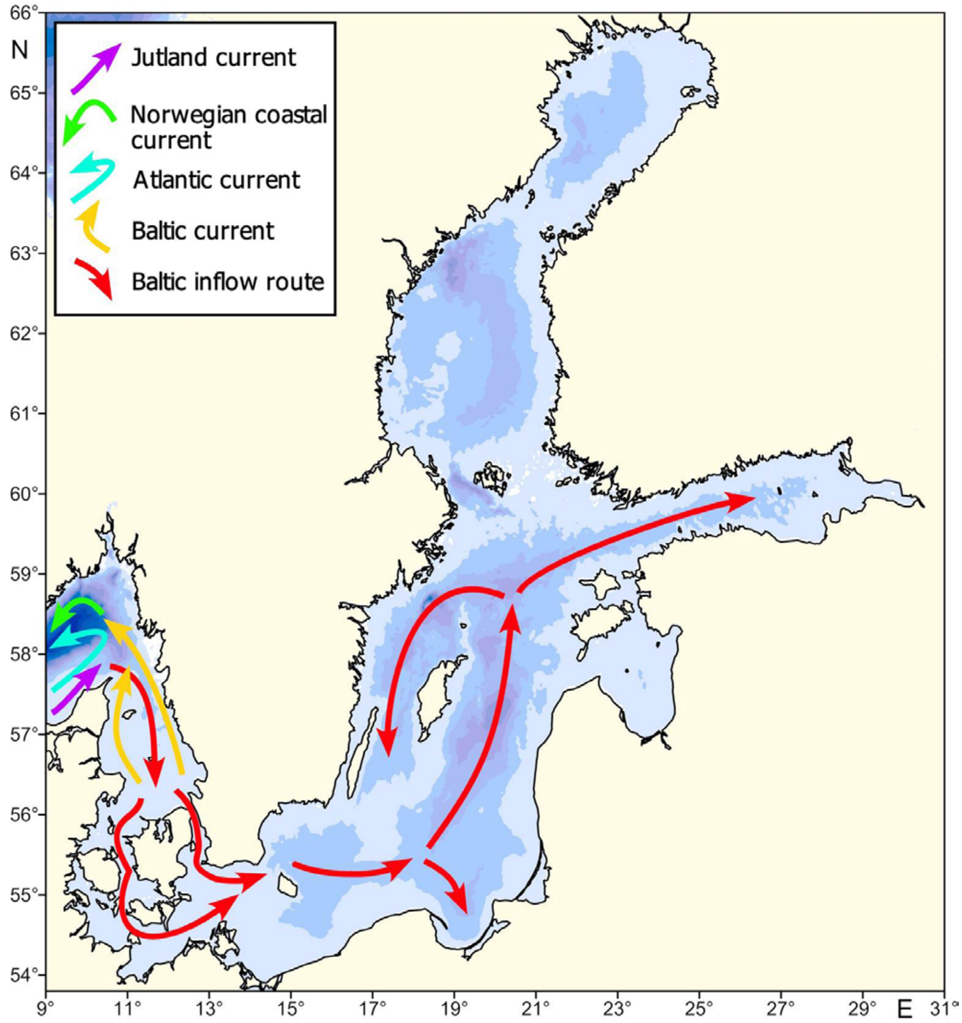

FIGURE 4.65.
Skagerrak, Kattegat, and the Baltic. Circulation map of water masses.

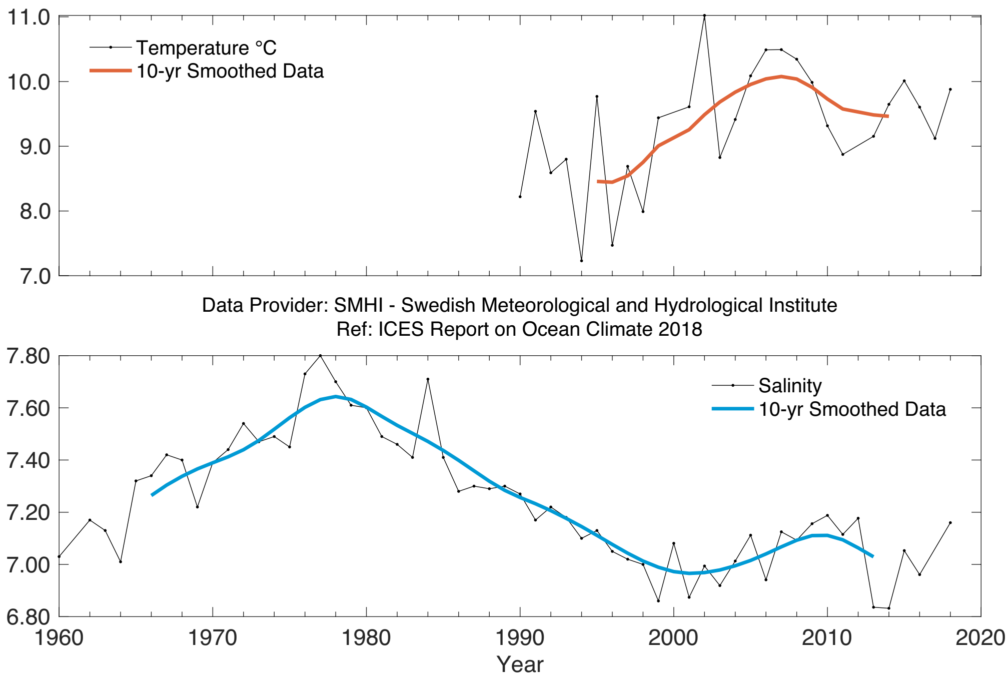

FIGURE 4.66.
Skagerrak, Kattegat, and the Baltic. Surface temperature, yearly mean (upper panel) and surface salinity, yearly mean (lower panel) at Station BY15 (east of Gotland) in the Baltic Proper.

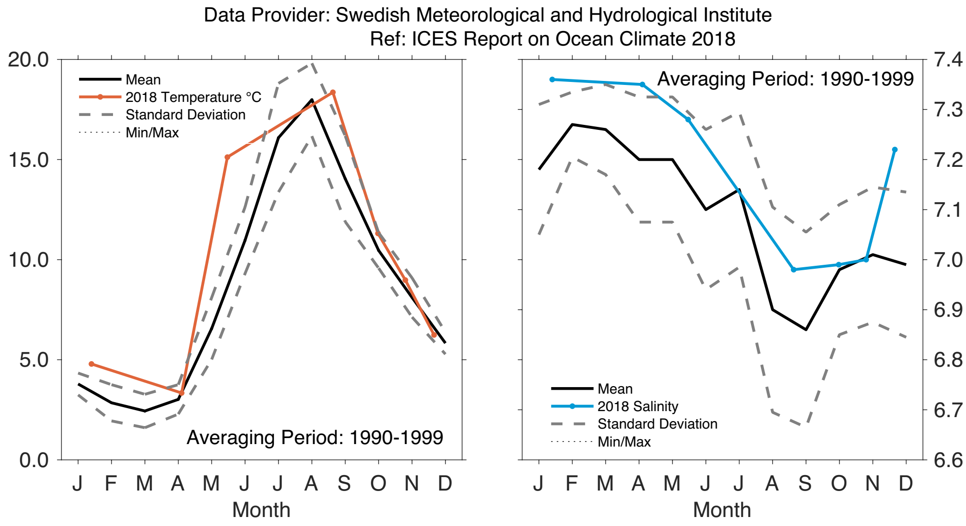

FIGURE 4.67. Skagerrak, Kattegat, and the Baltic. Monthly surface temperature (left panel) and salinity (right panel) at Station BY15 (east of Gotland) in the Baltic Proper.

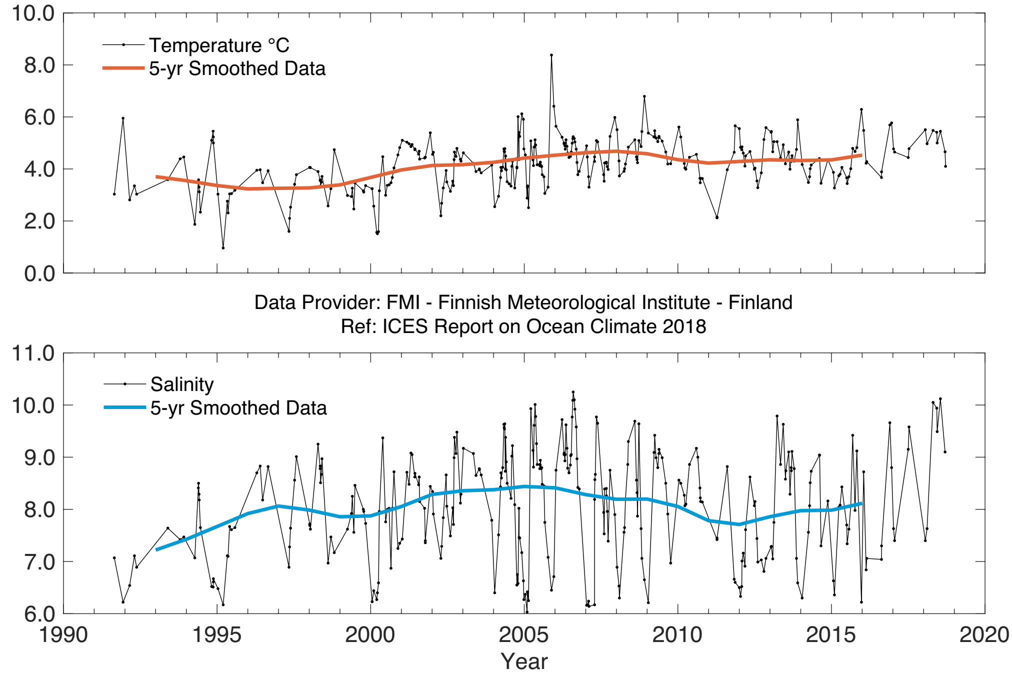

FIGURE 4.68. Skagerrak, Kattegat, and the Baltic. Temperature (upper panel) and salinity (lower panel) at Station LL7 in the Gulf of Finland.

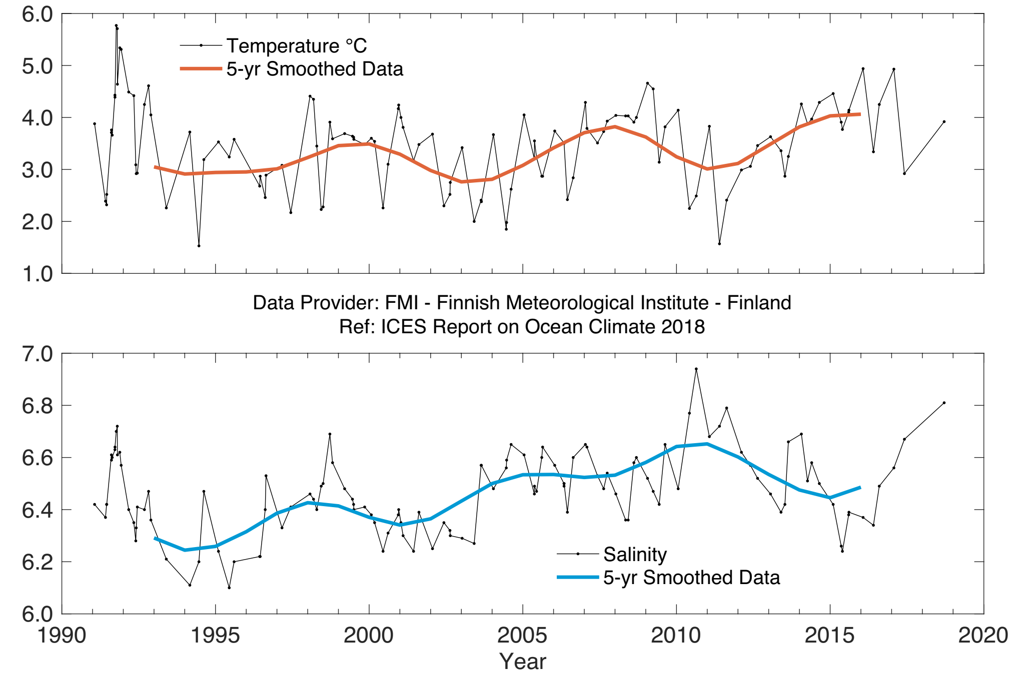

FIGURE 4.69. Skagerrak, Kattegat, and the Baltic. Temperature (upper panel) and salinity (lower panel) at Station SR5 in the Bothnian Sea.

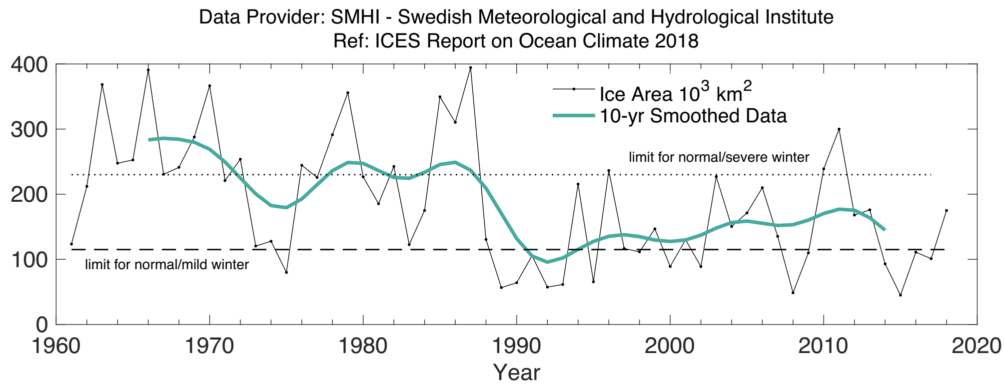

FIGURE 4.70.
Skagerrak, Kattegat, and the Baltic: The maximum ice extent in the Baltic starting from 1960.

.

4.19 NORWEGIAN SEA

K. A. Mork

The Norwegian Sea is characterized by warm AW on the eastern side and cold Arctic water on the western side, separated by the Arctic front (Figure 4.71). AW enters the Norwegian Sea through the Faroe-Shetland Channel and between the Faroes and Iceland via the Faroe Current. A smaller branch, the North Icelandic Irminger Current, enters the Nordic seas on the western side of Iceland. AW flows north as the Norwegian Atlantic Current, which splits when it reaches northern Norway; some enters the Barents Sea, whereas the rest continues north into the Arctic Ocean as the West Spitsbergen Current (WSC).

Three sections, from south to north in the eastern Norwegian Sea, demonstrate the development of temperature and salinity in the core of the AW: Svinøy-NW (Figure 4.72), Gimsøy-NW (Figure 4.74), and Sørkapp-W (Figure 4.75). In general, there has been an increase in temperature in all three sections since the mid-1990s, with the exception of a decline during the most recent years at the Svinøy-NW section. Annual temperature averages in 2018 were 0.1°C below the long-term mean at the Svinøy-NW section and 0.4°C and 0.7°C above their long-term means at the Gimsøy-NW and Sørkapp-W sections, respectively.

Salinity increased until around 2010 and has subsequently decreased in recent years in all three sections. In both the Svinøy-NW and Gimsøy-NW sections, the 2018 annual salinity averages were the lowest since the end of the 1970s. Annual salinity averages in 2018 were 0.1, 0.08, and 0.03 below their long-term means at the Svinøy-NW, Gimsøy-NW, and Sørkapp-W sections, respectively.

Freshening and prolonged high heat content in the Norwegian Sea.

Climate variability in the Norwegian Sea can be described through AW ocean heat and freshwater content using hydrographic data collected during spring since 1951 (Figure 4.76). Heat content in the Norwegian Sea has been above the long-term mean since 2000. It reached a record-high in 2017 and was still relatively high in 2018. Freshwater content has increased since 2010 and was above the long-term mean in 2018.

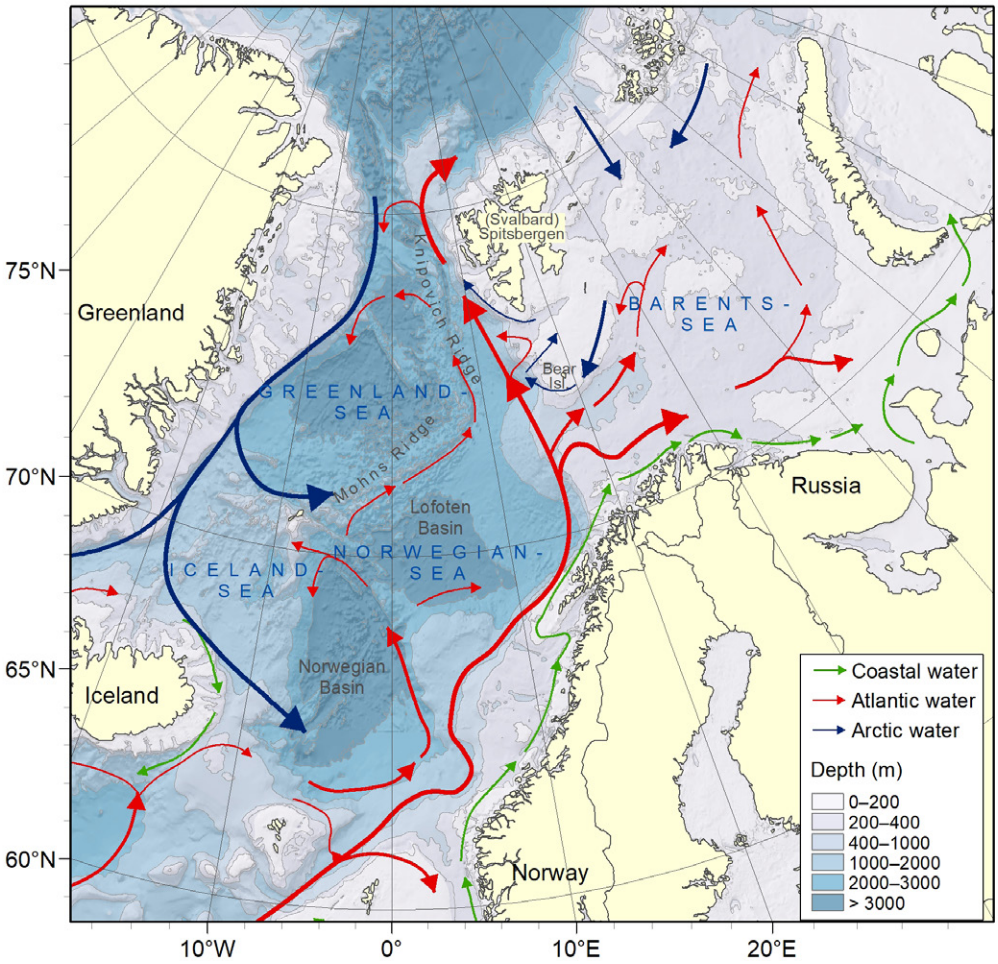

FIGURE 4.71.
Circulation schematic for the Nordic seas and Barents Sea. Red lines show the poleward movement of AW. Blue lines show the circulation of Arctic Water. Green lines show the circulation of coastal waters.

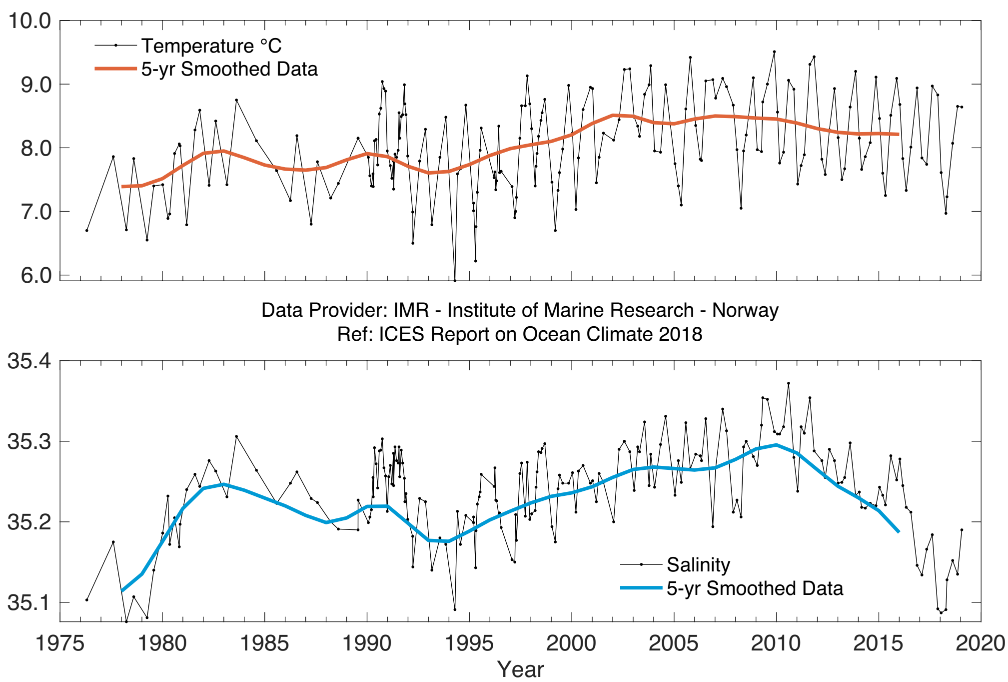

FIGURE 4.72.
Norwegian Sea. Temperature (upper panel) and salinity (lower panel) above the slope at Svinøy Section (63°N).

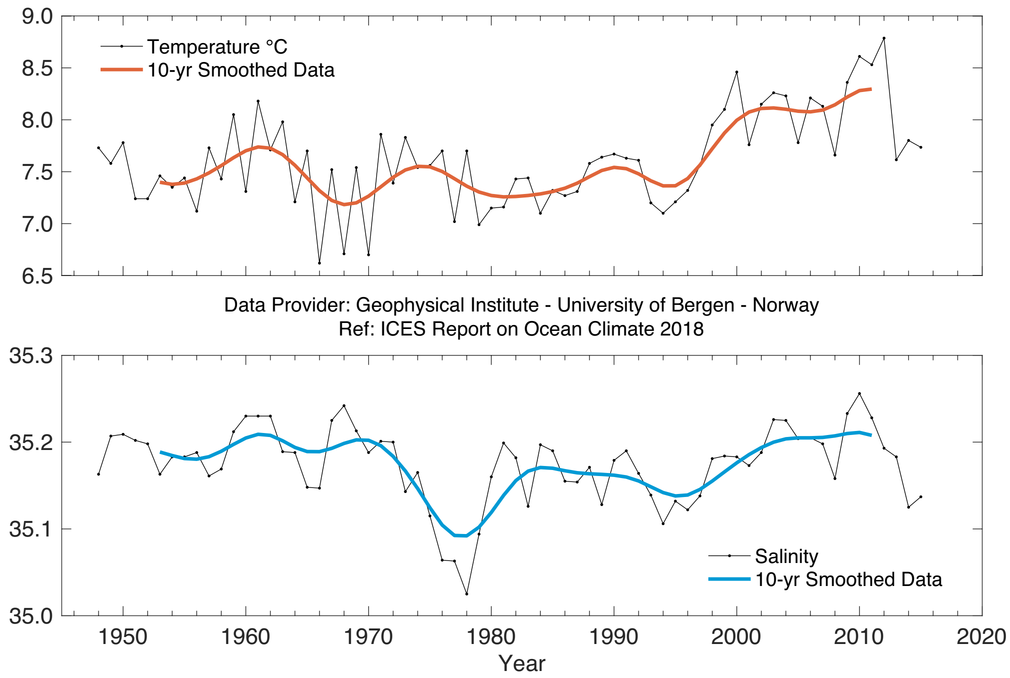

FIGURE 4.73.
Norwegian Sea. Temperature (upper panel) and salinity (lower panel) at 50 m at Ocean Weather Station "M" (66°N 2°E). Data until 2015.

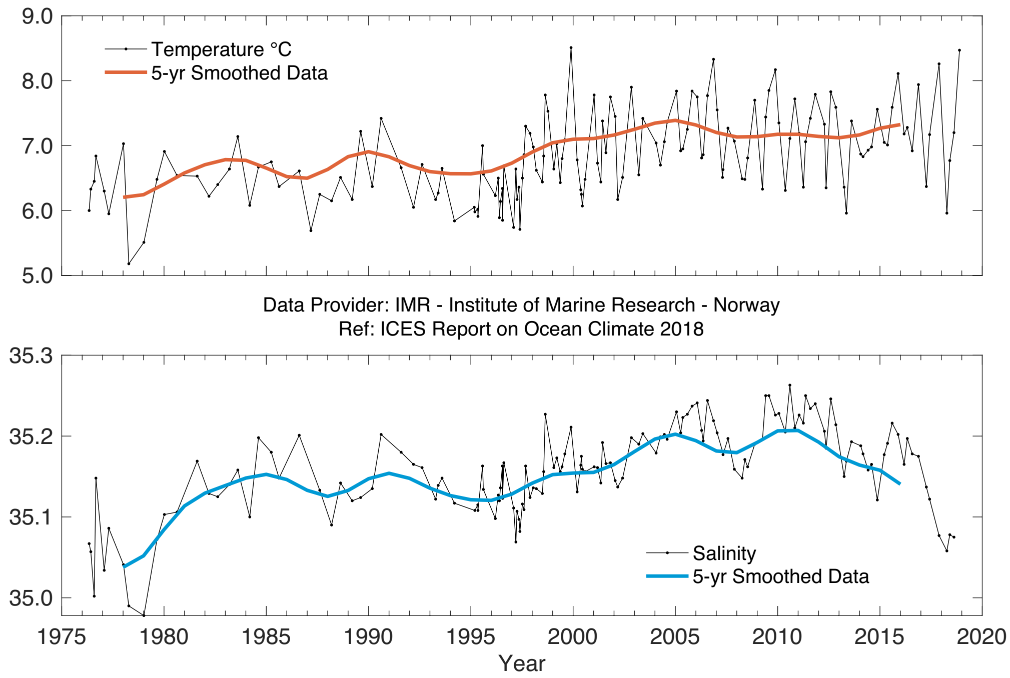

FIGURE 4.74.
Norwegian Sea. Temperature (upper panel) and salinity (lower panel) above the slope at Gimsøy Section (69°N).

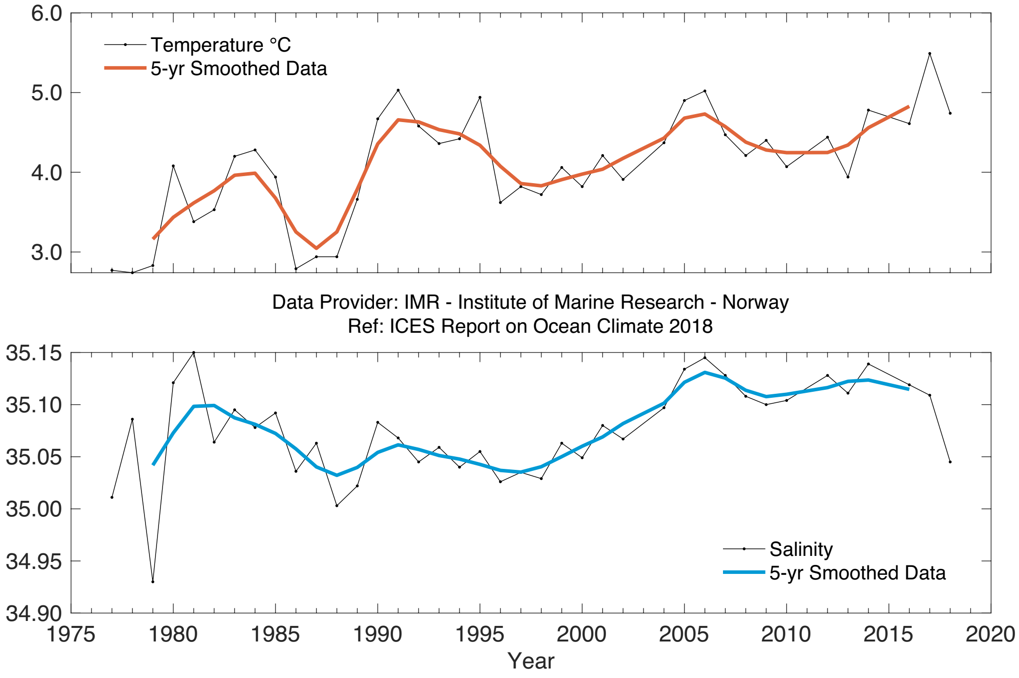

FIGURE 4.75.
Norwegian Sea.
Temperature (upper panel) and salinity (lower panel) above the slope at Sørkapp Section (76°N).

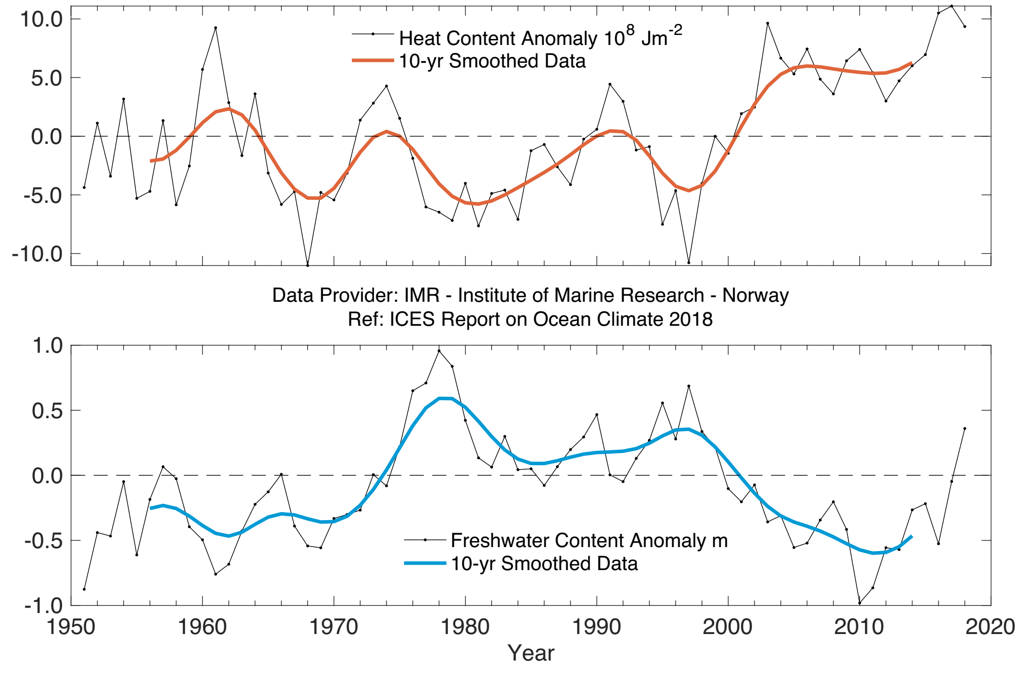

FIGURE 4.76.
Norwegian Sea.
Heat (upper panel) and freshwater (lower panel) contents of Atlantic Water (AW) in the Norwegian Sea.

4.20 BARENTS SEA

A. Trofimov and R. Ingvaldsen

The Barents Sea is a shelf sea that receives an inflow of warm AW from the west (Figure 4.71). The inflow exhibits considerable seasonal and interannual fluctuations in volume and water mass properties, causing high variability in the heat content and ice coverage of the region.

In 1996 and 1997, after a period with high temperatures in the first half of the 1990s, temperatures in the Barents Sea dropped to slightly below the long-term average. From March 1998, temperature in the western Barents Sea increased to just above average, whereas temperature in the eastern part remained below average during 1998. From the beginning of 1999, there was a rapid increase in the western Barents Sea that spread to the eastern part. Since then, temperature has remained above average.

In 2018, water temperatures in the western Barents Sea (the Fugløya-Bear Island section) were still above average (+0.4°C), but substantially lower than in 2017 (Figure 4.77). Salinity was low, with a mean annual salinity anomaly 0.6 below the average and with decreasing anomalies through the year. In the central Barents Sea, air and water temperatures were still well above average and generally close to those in 2017, as is typical for warm and anomalously warm years. From January to August, the observation period along the Kola Section in 2018, coastal and Atlantic waters (0–200 m) were 0.3–1.2°C warmer than average (1981–2010; Figure 4.78). Positive temperature anomalies smoothly decreased from January (+1.0°C) to June (+0.6°C) in coastal waters and from January (+1.1°C) to August (+0.8°C) in AW in the central part of the section (Murman Current). In AW in the outer part of the section (central branch of the North Cape Current), the anomalies initially decreased from +1.2°C in February to +0.3°C in May, but then abruptly increased back up to 1.2°C in August, marking the highest value for this month since 1951.

Throughout the observation period in 2018, coastal waters (inner part of the Kola Section) and AW (central part of the section) were, on average, 0.15 and 0.08 fresher than the long-term mean (1981–2010), respectively, whereas AW salinity in the outer part of the section was close to average. In AW (0–200 m) of the central Kola Section (Figure 4.78), the 2018 annual mean temperature was 0.9°C above average and 0.1°C lower than in 2017, typical of anomalously warm years, whereas the 2018 annual mean salinity was 0.08 below average and the lowest recorded since 1989.

Well above-average temperatures and low ice coverage in the Barents Sea in 2018.

According to data from the Barents Sea Ecosystem Survey in August/September 2018, surface, deeper, and bottom waters in most of the Barents Sea (> 89% of the covered area) were still much warmer than the long-term mean (by an average of 1.0, 0.7, and 0.8°C over the surveyed area, respectively, compared with 1931–2010). Compared to 2017, these waters were warmer in some parts of the sea (33–69% of the surveyed area) and colder in others. The largest positive differences in temperature between 2018 and 2017 were mainly found in the north at all depths and in the south at the surface; the largest negative differences were mostly observed in the west.

Surface waters were saltier (by 0.5 on average) than the long-term mean (1931–2010) in 87% of the surveyed area, with the largest positive anomalies in the north. The anomalies significantly decreased southward to negative values in coastal waters in the southern and southwestern sea. Bottom salinity was close to average in most of the Barents Sea. Positive salinity anomalies of > +0.1 took place only in shallow waters over the Spitsbergen Bank, although significant negative anomalies (–0.1 or more) were mainly found in coastal waters in the southern and southwestern sea, as well as east of the Spitsbergen Archipelago.

In autumn 2018, AW (> 3°C) covered a relatively large area in the Barents Sea, but this area had decreased when compared to 2017. Arctic and cold bottom waters (< 0°C) still covered rather small areas in 2018, though the area of the latter had increased with respect to 2017. The area of mixed waters in 2018 (0 < T < 3°C) was the largest since 1965. In 2018, ice coverage in the Barents Sea was still well below average (1981–2010) and close to that in 2017. There was no ice in the sea from August to October (October had not been ice-free since 1984). In December, ice coverage was the lowest since 1951.

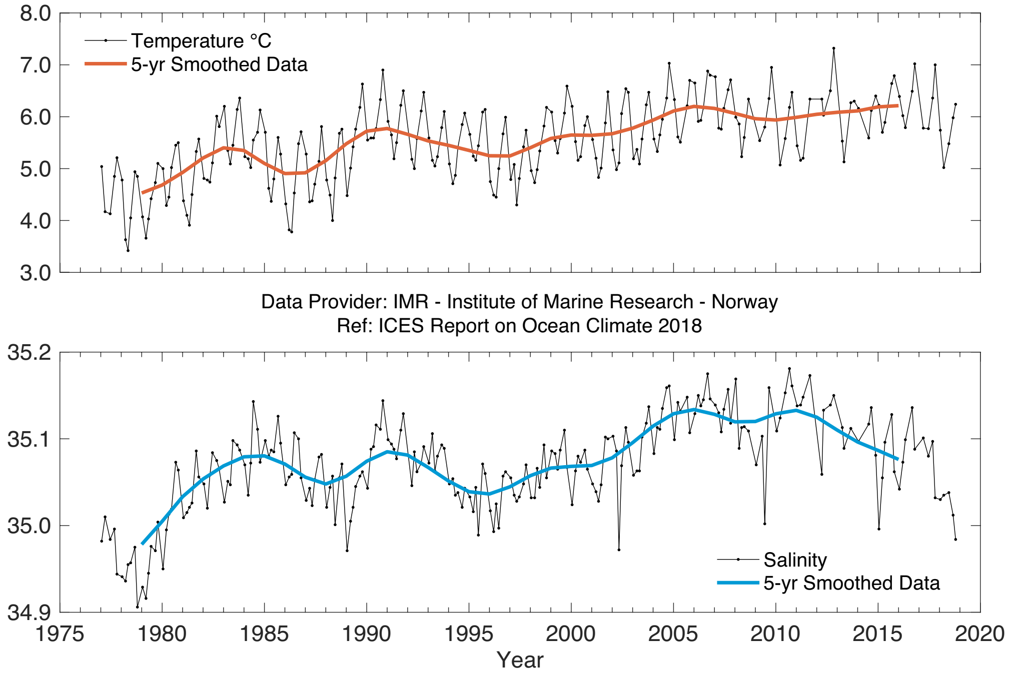

FIGURE 4.77.
Barents Sea. Temperature (upper panel) and salinity (lower panel) in the Fugløya-Bear Island Section.

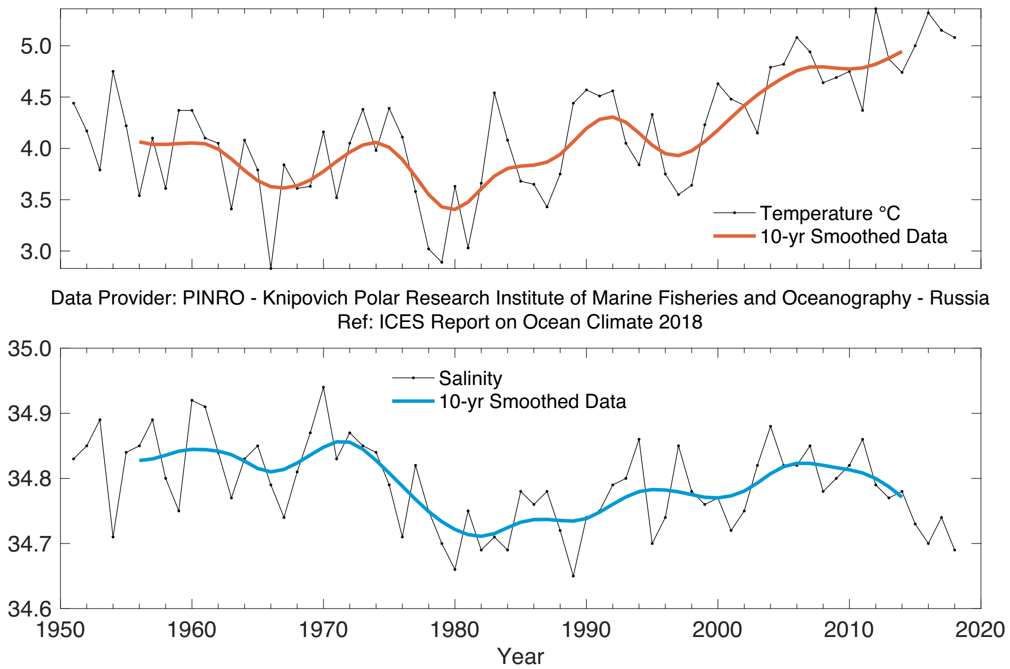

FIGURE 4.78.
Barents Sea. Temperature (upper panel) and salinity (lower panel) in the Kola Section (0–200 m).

4.21 FRAM STRAIT

A. Beszczynska-Möller, W. J. von Appen, and G. Budeus

The Fram Strait (Figure 4.71) is the northern border of the Nordic seas. It is the only deep passage connecting the Arctic to the rest of the world ocean and is one of the main routes whereby AW enters the Arctic (the other is the Barents Sea). The AW flows along the eastern rim of the Greenland Sea and in the Fram Strait is carried north by the WSC. AW temperature, salinity, volume and heat fluxes exhibit strong seasonal and interannual variations. A significant part of the AW also recirculates within and shortly north of Fram Strait and joins the flow to the south as the Return Atlantic Water (RAW). Polar Water from the Arctic Ocean flows south in the East Greenland Current (EGC) and affects water masses in the Nordic seas.

AW temperature at the eastern rim of the Greenland Sea (along the 75°N section between 10° and 13°E, Figure 4.79) was highest in 2005–2007, with a peak in 2006. In 2008–2009, it decreased significantly and remained below its long-term mean until 2012, when it recovered. AW temperature has since remained relatively stable, with small variations (up to 0.5 s.d.) and values exceeding the long-term mean by 0.25–0.55°C. In 2018, AW temperature was 4.78°C, 0.25°C warmer than average and slightly lower than during the three previous years.

Temperature of AW carried poleward along the eastern rim of the Greenland Sea and Fram Strait remained high with small changes in the last five years, although a strong drop was observed in 2018 in salinity.

In 2005–2006, a significant increase in AW salinity in the East Greenland Sea (Figure 4.79) was observed, with a maximum of 35.16 in 2006 (exceeding the long-term average by 0.07). This peak was followed by a sharp decrease in 2007 and a further slow descent until 2009, when AW salinity returned to its long-term average. In 2010, salinity started to rise again and reached its second peak in 2012 (0.06 above its long-term mean). It remained relatively steady until 2014 (with a slight decrease found in 2013). Since 2015, a notable decrease in salinity has been observed. In 2018, it reached the lowest value in the last 15 years (35.073), marking the first time in 14 years that AW salinity has been below its long-term average (0.02 or 0.5 s.d. below its long-term average).

The west and central parts of the Greenland Sea section at 75°N have not been measured since 2010. RAW temperature at the western rim of the Greenland Sea reached its maximum in 2006 (2.9°C) and then slowly decreased until the end of the observation period, reaching values slightly below the long-term average during 2008–2010. The RAW temperature maximum in 2006 was accompanied by a very strong peak in salinity (0.13 above the long-term mean, more than threefold larger than the standard deviation). In 2007, RAW salinity dropped, remained slightly higher than its long-term average until 2008, and then decreased further to close to the long-term average in 2009–2010. Temperature and salinity in the upper layer of the central Greenland Basin, within the Greenland Gyre, are modified by the advection of AW and winter convection.

In the southern Fram Strait at the standard section along 76.50°N (at the level of 200 dbar, spatially averaged between 9° and 12°E, Figure 4.80), a record-high summer temperature for AW was observed in 2006 (maximum of 4.5°C, 1.3°C above the long-term average), accompanied by the highest AW salinity in the observation period (35.13, 0.07 above the long-term mean). Subsequently, temperature and salinity decreased rapidly during 2007–2008 before increasing again in summers 2009–2012. During 2011–2015, AW temperature in the southern Fram Strait remained relatively constant (3.7–3.8°C, ca. 0.6°C above average), with the exception of summer 2013, when it dropped to 3.22°C and levelled out at the long-term mean. A moderate AW temperature increase has been observed since 2015 and reached a decadal maximum of 4.1°C in 2017, the second largest value in the observation period. Generally, in 2016–2018, AW temperature has remained nearly constant with a slight decrease to 4.05°C in 2018. AW salinity matched the 2006 maximum in 2011, 2012, and 2014. In 2015, AW salinity dropped and remained constant during 2016–2017 at about 1 s.d., i.e. 0.04, above its long-term mean of

35.06. In 2018, it decreased notably to a minimum of 35.07, the lowest value observed in the last 14 years.

In the northern Fram Strait at the standard section along 78.83°N, three characteristic areas can be distinguished in relation to the main flows: the WSC between the shelf edge and 5°E, the RAC between 3°W and 5°E, and the Polar Water in the EGC between 3°W and the Greenland Shelf (Figure 4.81).

The spatially averaged mean temperature of the upper 500 m layer in the WSC reached its peak in 2006 at 4.54°C and subsequently decreased, varying during 2007–2011 ± 0.4°C with respect to the long-term average. In 2012–2013, temperature in the WSC dropped further to 0.7–0.8°C below the long-term mean. Since 2014, it has been rising again and reached the second highest value for the observation period (4.24°C, 1.13°C above the long-term mean) in 2015. In 2016–2018, temperature in the WSC dropped slightly, but remained ca. 1 s.d. above its long-term average. In 2018, AW temperature in the WSC was 3.56°C, 0.5°C warmer than average. The highest salinity in the upper 500 m in the WSC was observed in 2006 (35.11), followed by a decrease to the long-term average in 2007–2008. Since 2009, the WSC salinity increased again, reaching 0.06 above the long-term mean in 2011. AW salinity reached new maximums in 2014 (35.09) and in 2017 (35.07, 0.05 above the long-term average), following slight decreases in 2012/2013 and 2015/2016, respectively. In 2018, the WSC salinity dropped significantly, reaching the value slightly below the long-term average.

In 2018, AW at the standard section along 78.83°N occupied the core of the WSC down to a similar depth as in 2017 (not shown). In 2017 and 2018, the isotherm of 2°C in the WSC core, located over the upper shelf slope, reached down to about 700–800 m, whereas in 2016, it was found slightly shallower at the depth of about 500–600 m. The offshore branch of the WSC located over the lower shelf slope was less pronounced in 2018 than in 2017, and the AW layer was slightly shallower (with the isotherm of 2°C found at the depth of about 400 m). The low salinity surface layer, which covered the upper 20–30 m over the WSC core in 2017, was absent in 2018.

The RAC and EGC domains were not measured in 2017 and 2018 (Figure 4.81). RAC temperature in 2016 remained close to that in the previous year, and the temperature difference between AW flowing to the north in the WSC, and AW recirculating in the RAC (a proxy for the recirculation strength) was, at 0.7°C, only half of the 2015 value of 1.5°C. The highest temperatures in the RAC were observed in 2005 (3°C) and in 2009–2010 (slightly above 2.9°C), whereas the temperature remained close to the long-term average of 2.2°C during 2011-2013. In recent years, the RAC temperature has increased slowly and reached 2.8°C in 2016. Maximum salinity in the RAC was observed in 2010 and in 2011, 2012, and 2014 it exceeded its long-term mean by about 0.05. In 2015, it levelled out before increasing again in 2016.

In the EGC domain, temperature reached its peak in 2007 (1.9°C), decreased significantly to 0.3°C in 2008, and since then has remained relatively stable (within ± 0.3°C of the long-term mean, with a slight decrease to 0.3°C in 2014 and a return to 1.0°C in 2015). In 2016, the EGC temperature was slightly higher than in the previous year. The EGC salinity was highest in 2007 (34.90) and subsequently dropped below its long-term average, except for an intermediate peak (34.72) in 2011. In 2008 and 2014, EGC salinity reached the lowest values during the last decade (34.50; the record-low was observed in 2000 and 2002 at 34.45). Since 2014, salinity has steadily increased and was slightly above its long-term mean in 2016.

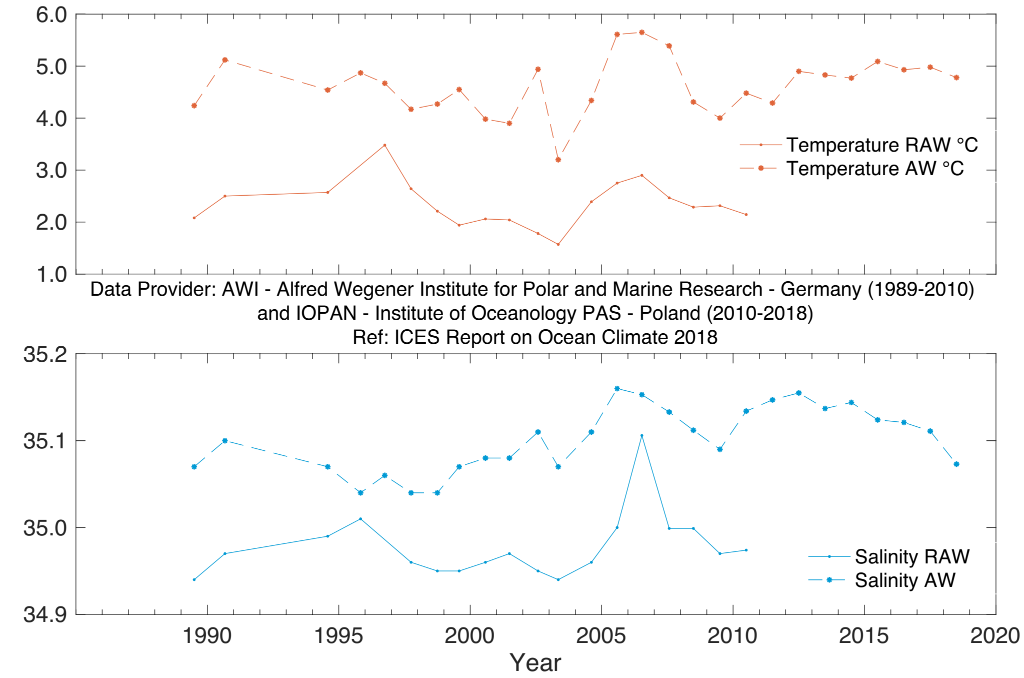

FIGURE 4.79.
Greenland Sea and Fram Strait. Temperature (upper panel) and salinity (lower panel) of AW and RAW in the Greenland Sea Section at 75°N. AW properties are 50-150m averages at 10-13°E. The RAW is characterized by temperature and salinity maxima below 50 m averaged over three stations west of 11.5°W (not updated since 2010).

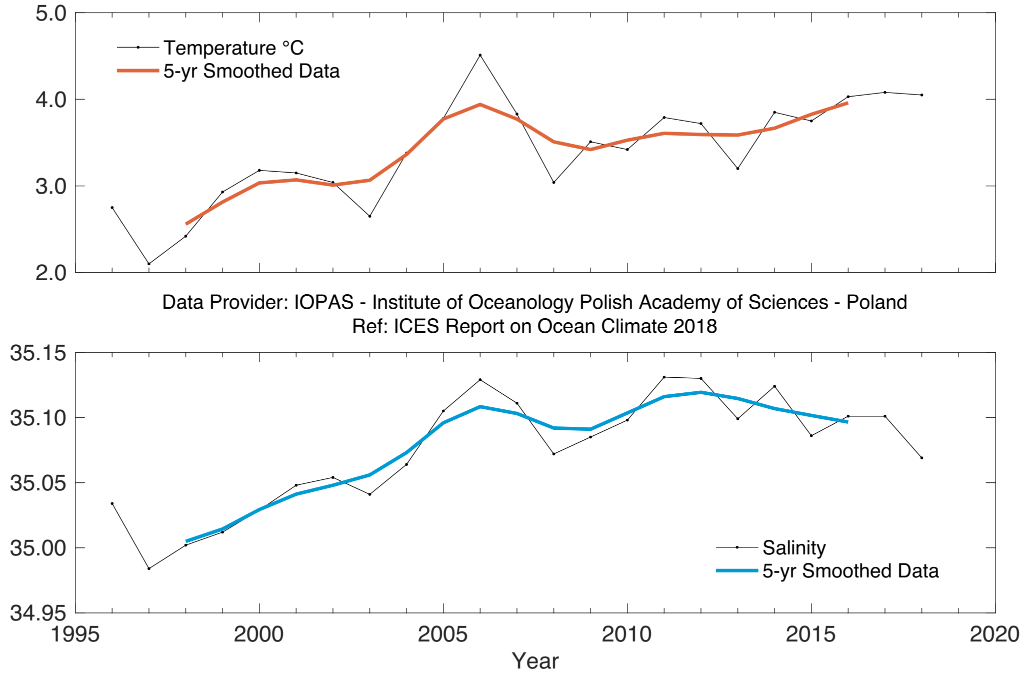

FIGURE 4.80.
Greenland Sea and Fram Strait. Temperature (upper panel) and salinity (lower panel) at 200 dbar in the southern Spitsbergen Section (76.50°N).

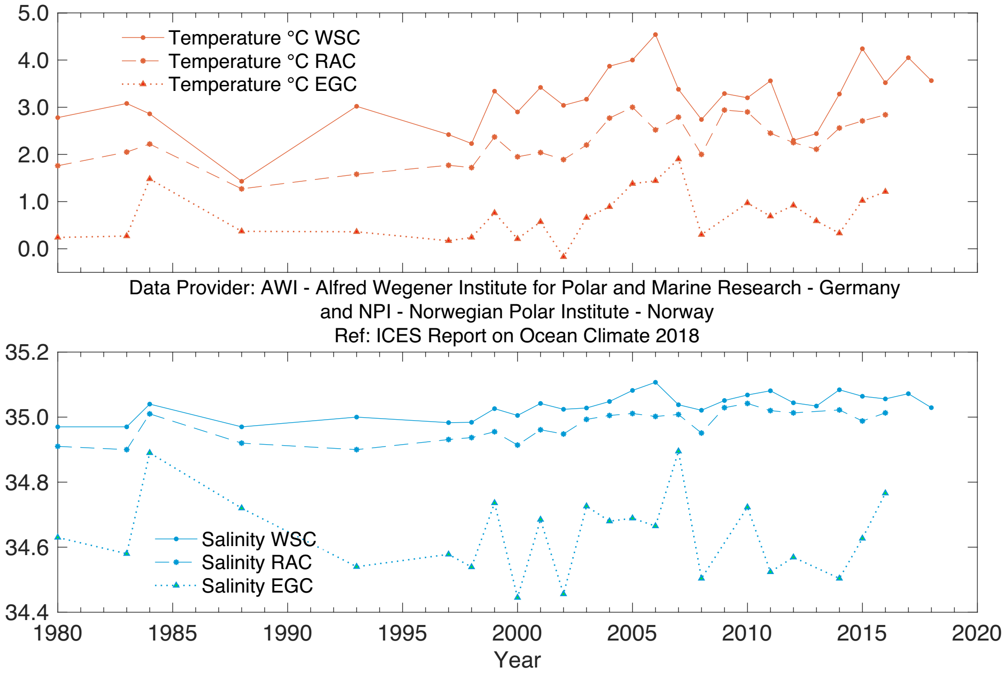

FIGURE 4.81.
Greenland Sea and Fram Strait. Temperature (upper panel) and salinity (lower panel) in Fram Strait (78.83°N) at 50–500m: in the AW in the WSC (between the shelf edge and 5°E), in the Return Atlantic Current (RAC; between 3°W and 5°E), and in the Polar Water in the EGC (between 3°W and the Greenland Shelf).

Port of Cork, Ireland.
Photo: Tomasz Szumski, Marine Institute, Galway, Ireland

5. DETAILED AREA DESCRIPTIONS, PART II: THE INTERMEDIATE AND DEEP OCEAN

INTRODUCTION

In this section, we focus on the deeper waters of the Nordic seas and the North Atlantic, typically below 1000 m. The general circulation scheme and dominant water masses are given in Figure 5.1.

At the northern boundary of the region of interest, the cold and dense outflow from the Arctic Ocean enters Fram Strait along its western side and reaches the Greenland Sea. The outflow is a mixture of Eurasian Basin and Canadian Basin deep waters and Upper Polar Deep Water (UPDW). The Eurasian Deep Water feeds the densest water of all the Nordic seas, the Greenland Sea Bottom Water. The Canadian Basin Deep Water and UPDW supply the Arctic Intermediate Waters (AIW) in the Greenland Sea, and the UPDW also includes products of the winter convection.

The deep southward outflow from the North Atlantic in the deep western boundary current is fed by the cold and dense overflow waters. The deepest and densest is the Denmark Strait Overflow Water (DSOW). This water mass originates in the AIW produced in the Greenland and Iceland seas by winter convection and mixing with surrounding water masses. The DSOW sinks to the bottom as it passes over the Denmark Strait sill, vigorously entraining ambient water. Downstream, it is overlain by LSW, an intermediate water mass formed by deep winter convection in the Labrador Sea. The middle layer of the deep, cold-water export in the deep western boundary current is supplied by the Iceland–Scotland Overflow Water (ISOW) that originates in water masses formed in the Norwegian Sea (AIW and Norwegian Sea Deep Water). Passing through the Iceland Basin, ISOW also entrains upper ocean water and LSW. The deep Antarctic Bottom Water enters the North Atlantic on the western side, but its signature is also present in eastern Atlantic abyssal basins. At intermediate levels, MW originates from vigorous mixing of Atlantic central waters and MOW at the Gulf of Cadiz. This water mass spreads at about 1000 m depth in all directions, with a main vein progressing northward along the European margin. Around the Canaries, MW encounters the northern limit of AAIW.

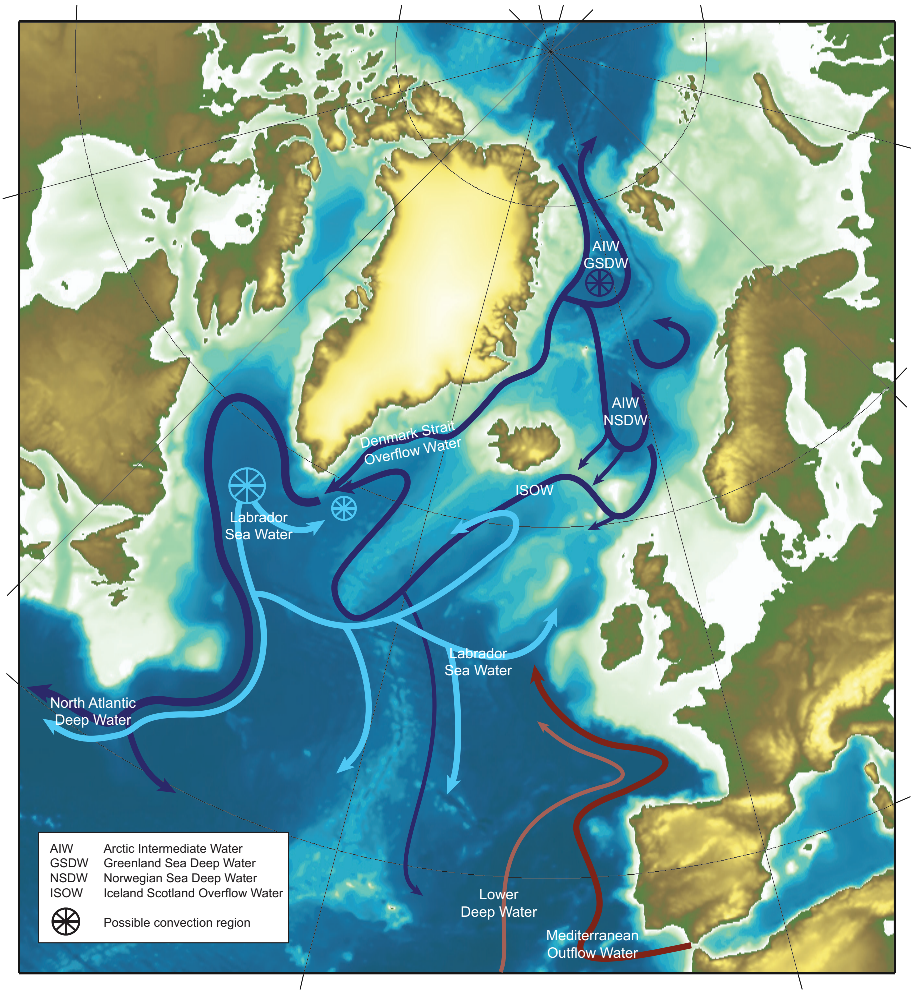

FIGURE 5.1. Schematic circulation of the intermediate to deep waters in the Nordic seas and North Atlantic.

5.1 NORDIC SEAS

The deep waters of the Greenland, Iceland, and Norwegian seas are all warming. The source of the warming is the deep outflow from the Arctic Ocean, a southward flowing current of the Eurasian and Canadian Basin Deep Waters, and UPDW found on the western side of Fram Strait at ca. 2000 m depth. The Greenland Sea Deep Water (GSDW) is warming fastest owing to its direct contact with this Arctic outflow, whereas the Iceland and Norwegian seas are warming more slowly because they are products of the mixing of their own ambient waters with GSDW and Arctic outflow water.

5.1.1 Greenland Sea

A. Beszczynska-Möller and G. Budeus

Continuous warming has been recorded since observations began in 1993 in the Greenland Sea deep layer at 3000 m, both in the Greenland Sea Gyre (not measured since 2011) and in the eastern part of the deep basin (at 5°E, measured since 2001; Figure 5.2.). The GSDW temperature is similar at both locations and has relatively steadily increased in temperature from −1.18°C to 0.88°C between 1993 and 2018. The strongest temperature increase of 0.03°C occurred between 2010 and 2011. During the most recent period, year-to-year temperature changes have been lower (0–0.02°C). Between 2017 and 2018, the deep water in the eastern Greenland Sea warmed by 0.003°C. For the entire observing period (1993–2018), the average warming rate in the deep Greenland Sea can be estimated at 0.11°C per decade.

The warming of deep waters in the Greenland Sea is accompanied by an increase in salinity (Figure 5.2), albeit with differing interannual variability between the central Greenland Sea Gyre (observed during 1993–2010) and the eastern Greenland Sea (measured since 2001). A relatively steady increase in salinity from 34.901 in 1993 to 34.916 in 2010 was observed in the Greenland Sea Gyre. In the eastern part of the deep Greenland Sea, the year-to-year changes are much stronger than in the central gyre, but the overall trend during 2001–2018 is positive and similar to that in the central basin. The salinity increase is of the order of 0.01 per decade. The maximum salinity of

34.919 was recorded in the eastern Greenland Sea in 2015 and 2017, with a slight drop to 34.916 in 2018. During the entire last decade, salinity in the deep layers of the eastern Greenland Sea has remained above its long-term average.

After a cessation of deep convection, the doming structure in the Greenland Sea Gyre is being replaced by a two-layered water mass arrangement. During the measurement period 1993–2010, the winter convection depth varied between 700 and 1600 m and was only significantly deeper in small-scale convective eddies. In winter 2007/2008, the maximum convection depth was estimated to be 1700 m, deeper than the previous year (1200 m) and similar to the maxima observed during 2001/2002 and 2002/2003. The import of warm saline AW to the Greenland Sea is currently not balanced by an import of cool fresh Polar Water from the north. The AW dominates changes in the upper ocean and tends to prevent ice formation and to vertically homogenize waters ventilated by convective processes. The GSDW formerly included a small admixture of surface freshwater through the convective process and, therefore, had a lower salinity than the Arctic outflow waters. The observed increase in GSDW salinity may be the result of an adjustment to the Arctic outflow in the continued absence of deep convection and an increased presence of AW in the upper layer.

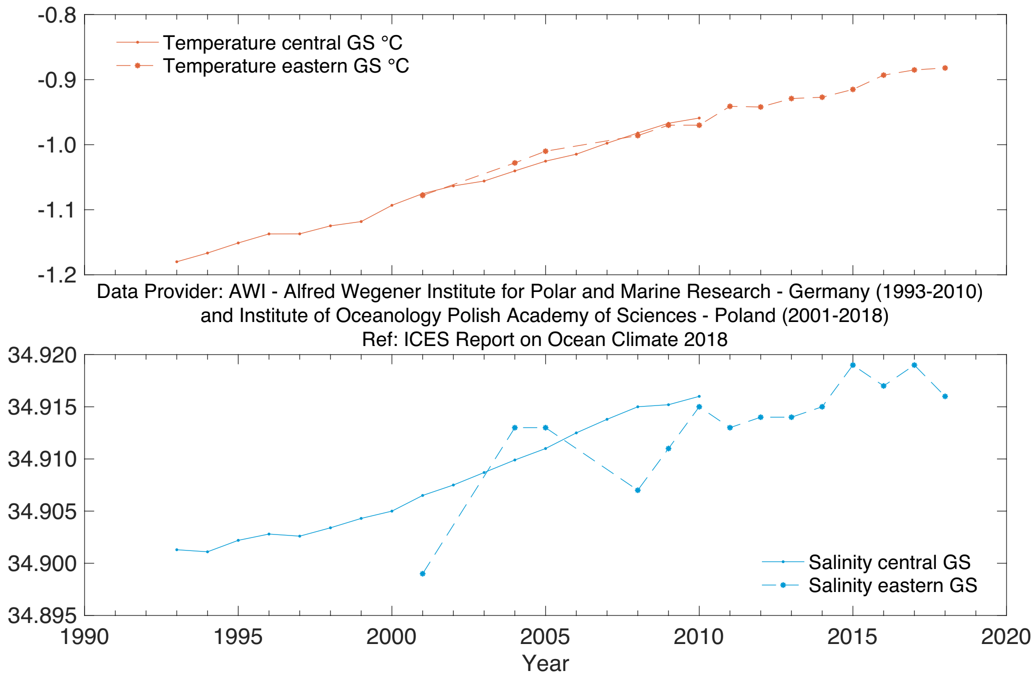

FIGURE 5.2.
Greenland Sea and Fram Strait. Temperature (upper panel) and salinity (lower panel) at 3000 m in the Greenland Sea Section at 75°N (solid line in the central Greenland Sea Gyre, dashed line in the eastern Greenland Sea at 5°E)

5.1.2 Norwegian Sea

S. Østerhus

The longest time-series in the Nordic seas is from Ocean Weather Station M (OWS-M) in the Norwegian Sea. This station was served by weatherships from 1948 until 2009. Since 2010, OWS-M has been visited by research vessels four to six times per year. In addition, instrumented moorings (Sea-Bird MicroCATs and Aanderaa RCMs) have been deployed intermittently since 2009. Between 1948 and 2009, temperature was recorded by means of reversing mercury thermometers. Salinity samples were stored in glass bottles and brought onshore for laboratory analyses. After 2009, temperature and salinity have been obtained using well-calibrated CTDs. The temperature at 2000 m reveals steady warming from the mid-1980s until 2018. Between 2010 and 2014, temperature varied more than in the preceding period, but this may be the result of changes in the observation method and fewer observations. The warming of the Norwegian Sea Deep Water is the consequence of the reduced formation of deep water in the Greenland Sea and an increase in the fraction of warmer deep water received from the Arctic Ocean. Salinity at 2000 m exhibits relatively large year-to-year variations and no significant trend over the last few decades (Figure 5.3).

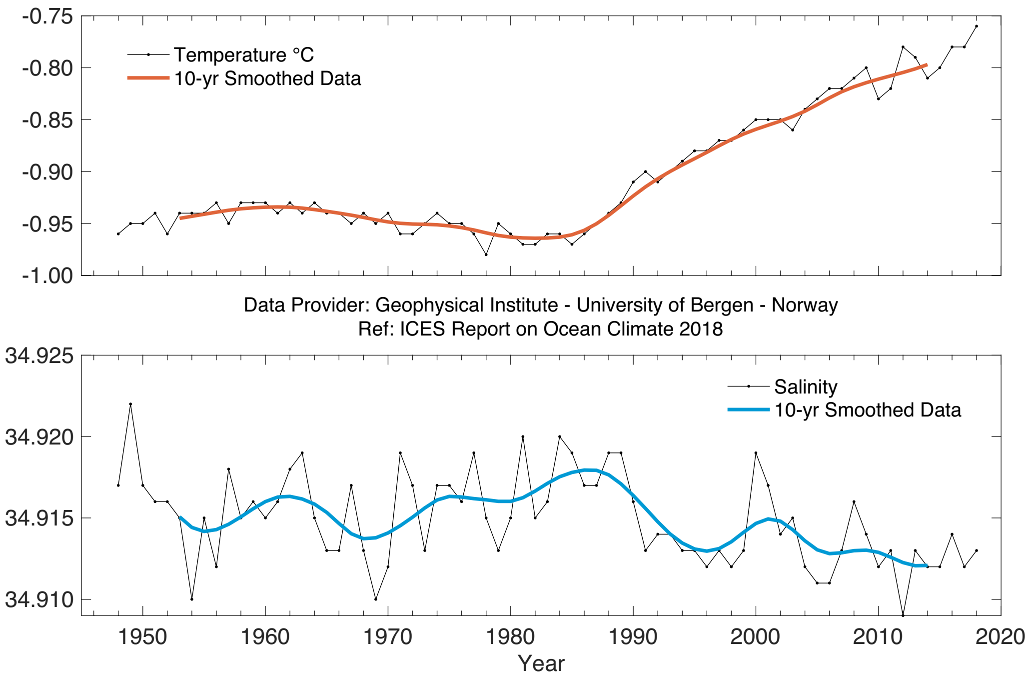

FIGURE 5.3. Norwegian Sea. Temperature (upper panel) and salinity (lower panel) at 2000 m at OWS-M (66°N 2°E).

5.1.3 Iceland Sea

H. Valdimarsson

In the Iceland Sea, an increase in temperature in the depth range 1500–1800 m has been observed almost continuously since the beginning of the time-series in the early 1990s. Temperature continued to rise slowly until the end of 2018 (Figure 5.4). Deep water in the eastern part of the Iceland Sea has warmed 0.2°C in 28 years.

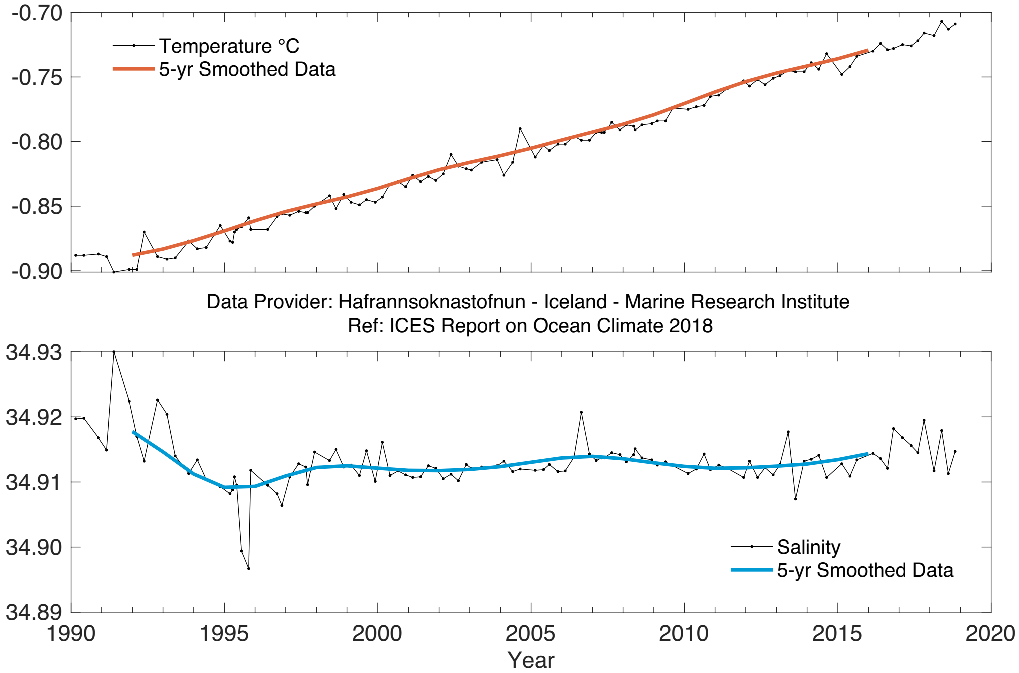

FIGURE 5.4.
Icelandic waters. Temperature (upper panel) and salinity (lower panel) at 1500–1800 m in the Iceland Sea (68.00°N 12.67°W).

Mooring deployment on Scotian Shelf. Photo: David Herbert, Fisheries and Oceans Canada, Dartmouth, Nova Scotia.

5.2 NORTH ATLANTIC

5.2.1 Iceland-Scotland Ridge overflow waters

B. Berx and J. Hindson

In the deep layers of the Faroe–Shetland Channel, the properties at 800 m are the same as those of Norwegian Sea Deep Water as it passes through the Channel back into the North Atlantic.

A relatively strong variability can be observed for temperature at this depth, but an overall decreasing temperature trend took place from 1950s to the 1990s (Figure 5.5). Following a subsequent period of some fluctuations, with both increasing and decreasing temperatures, there has been an increasing temperature trend since about 2000 and up to 2018. Temperatures observed in 2018 were close to the highest observed in the early 1980s. The relatively stable salinity in the first period of measurements (1950 to mid-1970s) was followed by a slow decline. The lowest annual mean salinity values were observed in 1997, after which there has been a slow but gradual increase (Figure 5.5).

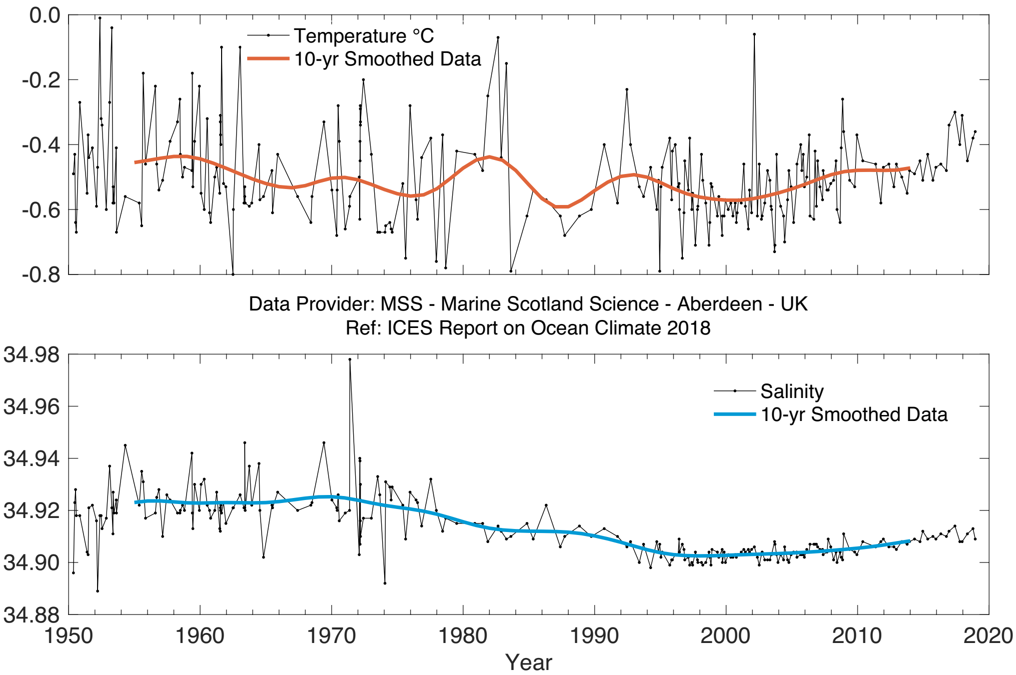

FIGURE 5.5.
Faroe-Shetland Channel. Temperature (upper panel) and salinity (lower panel) at 800 m.

5.2.2 Iceland Basin

N. P. Holliday and S. Jones

In the Iceland Basin, LSW is the dominant water mass below ca. 1000 m, evident as a large recirculating body of relatively fresh, low-stratified water with a core lying between 1700 and 2000 m (Holliday et al., 2015). After the Norwegian Sea Deep Water flows through the Faroe–Shetland Channel and Faroe Bank Channel and into the Iceland Basin, it becomes known as ISOW (Figure 4.46). The dense water, supplemented by a small amount of additional flow over the sill between Iceland and the Faroes, mixes rapidly with the upper ocean and intermediate water of the Iceland Basin, entraining the lighter water and increasing the volume of the overflow plume. Properties of the ISOW (Figure 5.7), measured at 20°W in the Iceland Basin, become, therefore, a product of the properties of the dense water at the sill and the entrained ambient water.

ISOW temperature and salinity (Figure 5.7) vary closely with the LSW (Figure 5.6) and upper ocean water in the Iceland Basin. Since 1996, the water has warmed and increased in salinity, although there has been a slight decrease in both since 2011. In 2018, the Ellett Line transect was not occupied and thus no observations were possible at the regular sample location for this time-series. However, measurements from the adjacent OSNAP line suggest that the freshening trend in intermediate and deep waters has not halted, in contrast to observations from the upper ocean.

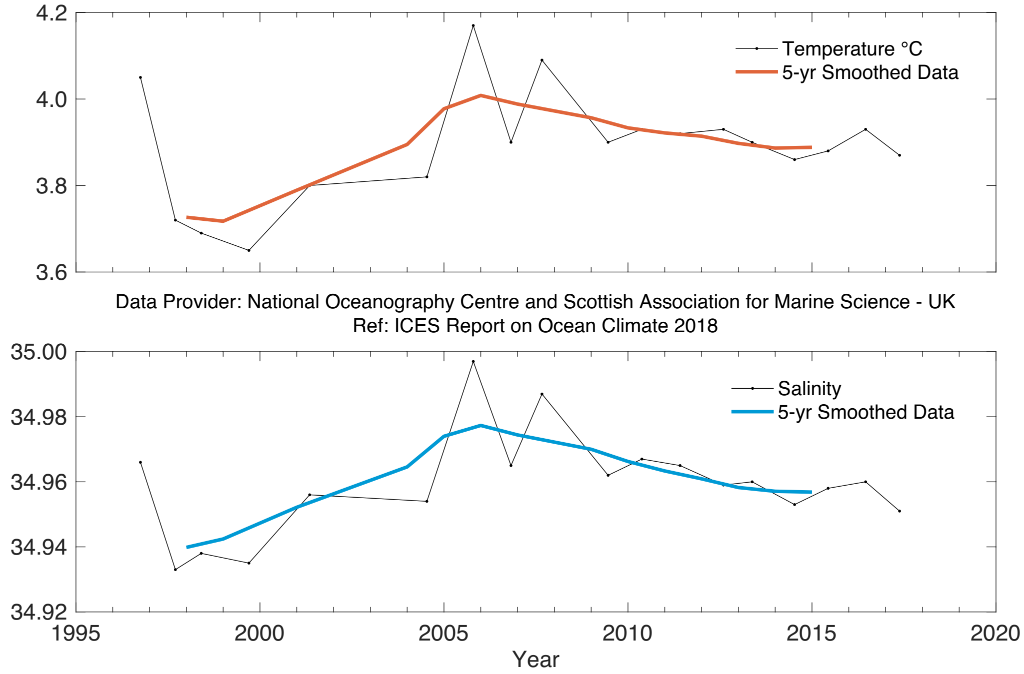

FIGURE 5.6.
Iceland Basin. Temperature (upper panel) and salinity (lower panel) of LSW ($27.70 \leq \sigma_\theta \leq 27.85$ kg m^{-3}, ca. 1200–2000 m). Data until 2017.

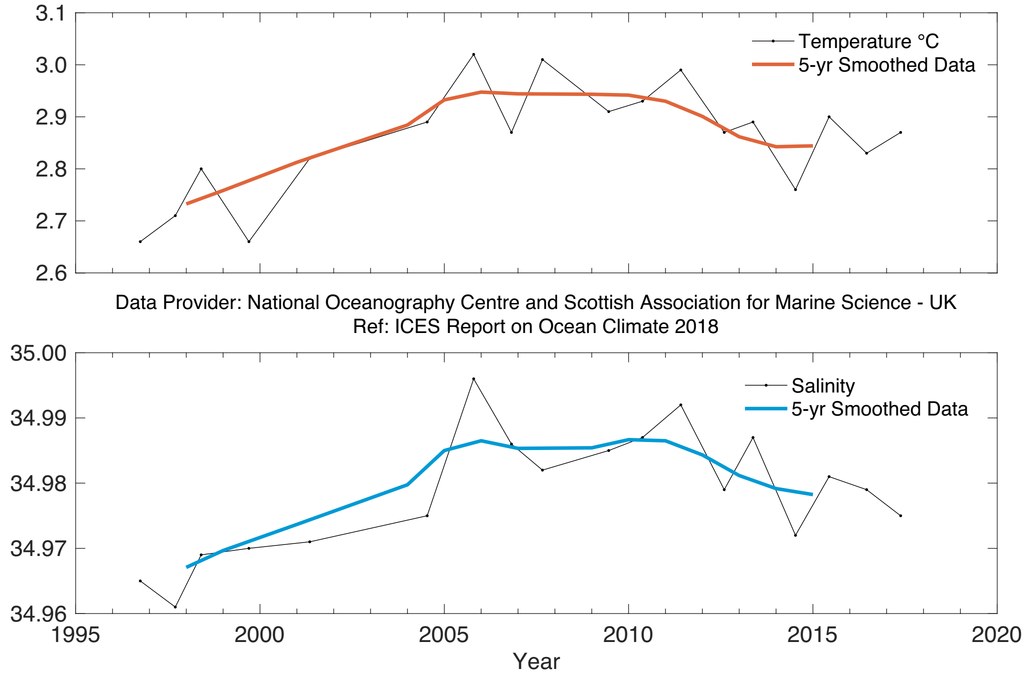

FIGURE 5.7.
Iceland Basin. Temperature (upper panel) and salinity (lower panel) of ISOW ($\sigma_\theta > 27.85$ kg m^{-3}, ca. 2000–2600 m). Data until 2017.

5.2.3 Rockall Trough

N. P. Holliday and S. Jones

In Rockall Trough, LSW is the dominant water mass below ca. 1500 m and usually has its maximum concentration between 1700 and 2000 m. East of the Anton Dohrn seamount, this peak tends to be characterized by a minimum in salinity and potential vorticity. However, its patchy temporal distribution (possibly caused by aliasing of mesoscale eddies) results in a noisy year-on-year signal.

Over the time-series, there is no significant trend. From 1975 to the mid-1990s, there was a cooling and freshening trend, which was followed by gradual warming and increasing salinity. In 2018, the LSW potential temperature and salinity were close to the long-term means (Figure 5.8).

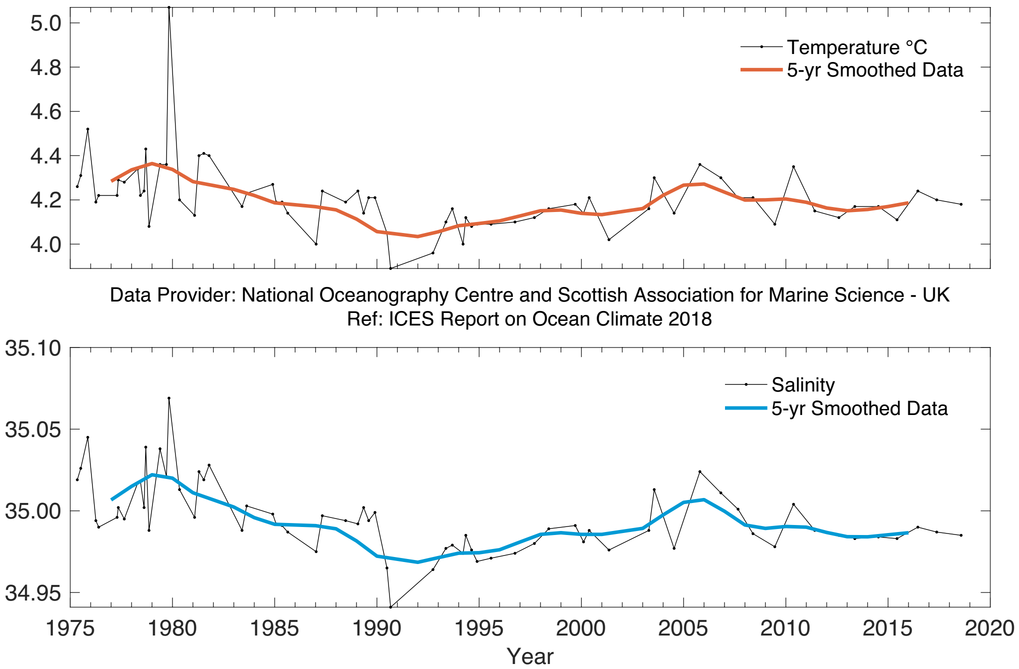

FIGURE 5.8.
Rockall Trough. Temperature (upper panel) and salinity (lower panel) LSW (27.70 ≤ σ_θ ≤ 27.85 kg m^{-3}, ca. 1500–2000 m).

5.2.4 Irminger Basin

M. F. de Jong

A cold and low-salinity core was observed between 1600 and 2000 m in the central Irminger Sea during the early 1990s. This was the result of the presence of deep LSW formed in the Labrador Sea during1988–1995, combined with local deep convection. Since summer 1996, this LSW core has generally been increasing in temperature and salinity as it mixes with surrounding water masses. Within the overall trend of increasing temperature, there are slight drops in temperature after winters with deep convection in the Irminger Sea. This occurred in winters 2008/2009, 2011/2012, and 2014/2015, but the Irminger Sea convection does not generally reach deep enough to influence waters below 1600 m. The temperature recorded in 2018 is the highest on record, nearly 0.33°C above the long-term mean, although still close to the value of 2016. Salinity reached a maximum in 2014 after which it levelled off. It is now at 0.043 above the long-term mean (Figure 5.9).

Salinity and potential temperature of the DSOW near Cape Farewell showed correlated interannual variations between 1991 and 2007 (correlation = 0.75). However, since 2007, variations in DSOW temperature and salinity have been more weakly correlated. This continued to be the case in 2018. More strikingly, the range in variability in annual temperature and salinity seems to have been decreasing since 1995. The density of the DSOW hardly changes over long time-scales. In 2018, DSOW temperature was 0.056°C above the long-term mean and salinity was 0.015 above the mean (Figure 5.10).

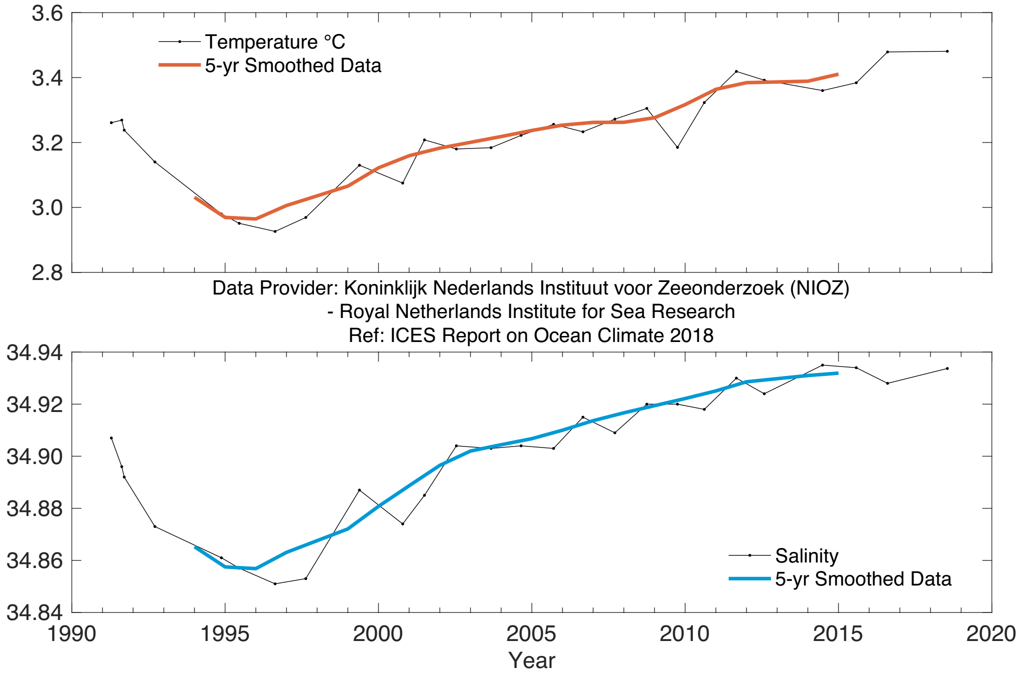

FIGURE 5.9.
Irminger Sea. Temperature (upper panel) and salinity (lower panel) of LSW (averaged over 1600–2000 m).

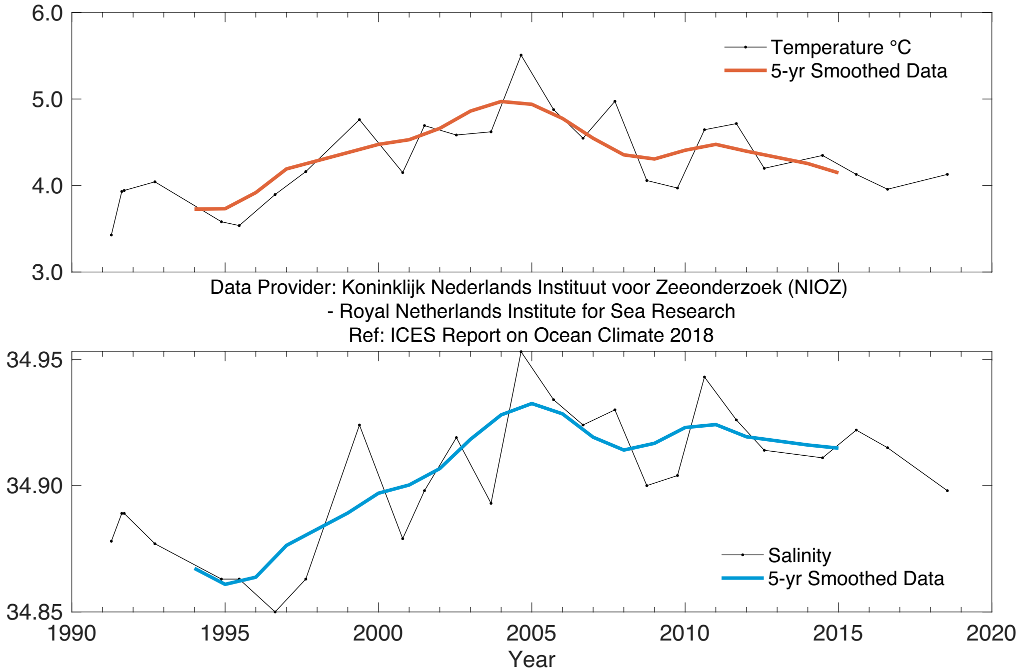

FIGURE 5.10.
Irminger Sea. Temperature (upper panel) and salinity (lower panel) in DSOW on the East Greenland Slope.

5.2.5 Labrador Basin

I. Yashayaev and B. Cisewski

In the Labrador Sea, the 1000–1800 m depth average temperature and salinity decreased between the beginning of the 1970s and the early 1990s by about 0.9°C and 0.09, respectively. In 2011, in less than two decades after reaching its record minimum, temperature was as high as in 1970 when its previous maximum was observed, whereas salinity was also highest since 1971. These trends were interrupted in winter 2011/2012 by strong convection. Temperature of the deep intermediate layer (1000–1800 m) continued to decrease during the subsequent years, 2013–2018. However, breaking a freshening trend observed in the intermediate waters at the time of recent cooling, the last two years, 2017 and 2018, showed a steady increase in the salinity of the intermediate layer (Figure 5.11).

The properties of the NADW in the deep boundary current west of Greenland are monitored at 2000 m depth at Cape Desolation Station 3. The temperature and salinity of this water mass underwent strong interannual variability during the 1980s. Since the beginning of the 1990s, both temperature and salinity decreased and reached minimum values in 1998 and 1997, respectively. Subsequently, NADW temperature exhibited a positive trend until 2014, whereas salinity stagnated between 2007 and 2014. In 2018, the Cape Desolation Section was not occupied owing to mechanical problems with the survey vessel (Figure 5.12).

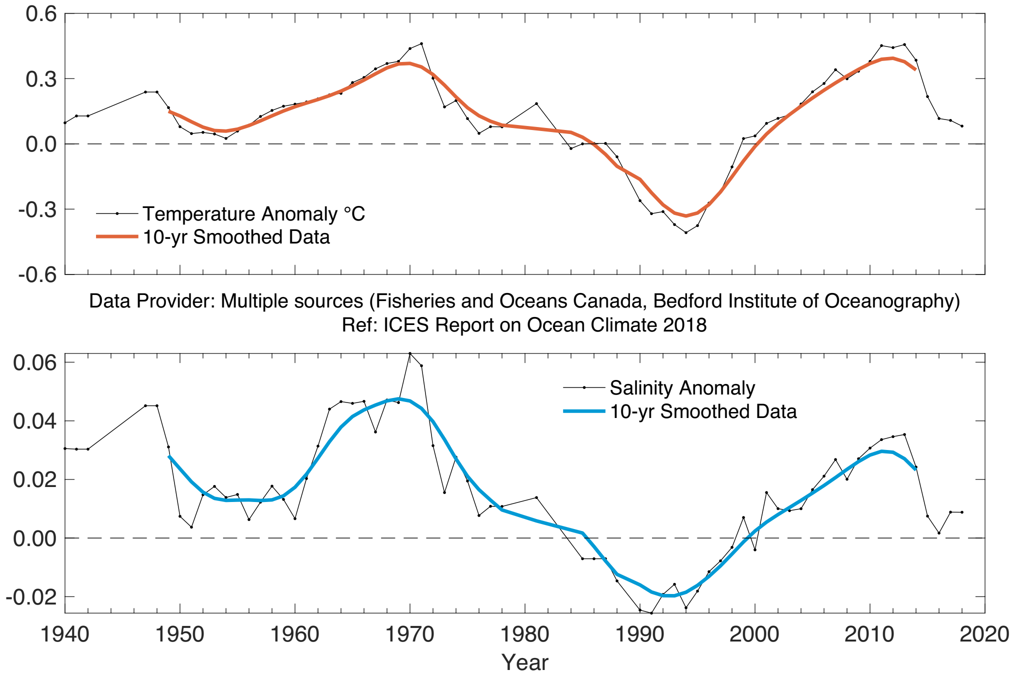

FIGURE 5.11.
Labrador Sea. Temperature (upper panel) and salinity (lower panel) anomalies in the deep intermediate layer of the Labrador Sea. Vertical profile data to 2018 were averaged over 1000–1800 m, then over calendar years.

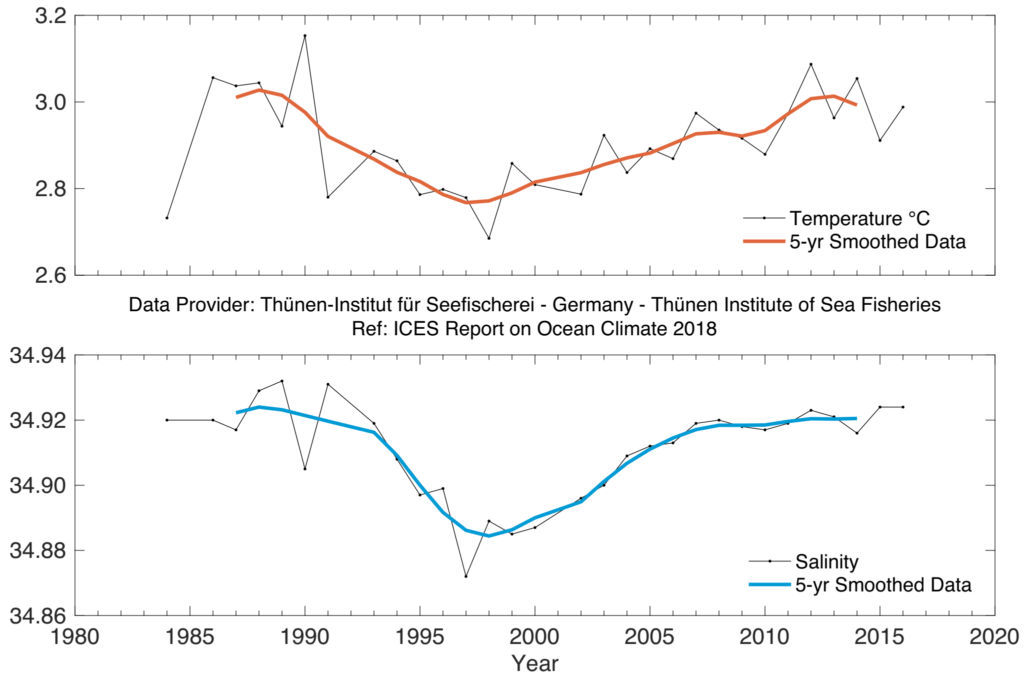

FIGURE 5.12.
West Greenland. Temperature (upper panel) and salinity (lower panel) at 2000 m water depth at Cape Desolation Station 3 (60.47°N 50°W). Data until 2016.

5.2.6 Western Iberian Margin

C. González-Pola

In the outer slope stations in Santander (Figure 4.31), the whole water column has been sampled down to 1000 m (core of MW) on a monthly basis since the early 1990s (González-Pola *et al.*, 2005). Overall, warming during the past 20 years is evident at most layers corresponding to the East North Atlantic Central Water (ENACW, 300–600; Figure 5.13) and upper MW (600–1000; Figure 5.14).

The evolution of the water masses has been strongly influenced by a significant shift in salinity at lower ENACW (ca. 400 m) in 2005 after the occurrence of very strong winter mixing (Somavilla *et al.*, 2009). In 2014, upper central waters showed freshening and cooling for the first time in about a decade. Salinity values in 2015 fell continuously, ending the year about 0.05 units lower than were observed in mid-2014. During 2016 and 2017, salinity stalled at about the same level as in late 2015, i.e. fresher and colder than in recent years. Finally, 2018 showed a further drop in salinity and lower temperature. Deeper, at the level of the MW, water masses have stayed relatively stable since the mid-2000s, but have been getting progressively fresher at the MW core following the salinity maximum reached around 2007–2009 (figures 5.13 and 5.14).

Since 2003, waters deeper than 1000 m have been monitored in the region, and the full water column has been monitored at the Western Iberian Margin (> 5500 m) by a programme designed to supplement the monthly monitoring of the upper ocean in the area (Prieto *et al.*, 2015). Cruises were carried out semi-annually during 2003–2010 and annually after that. The Finisterre section, measuring roughly 400km in length, starts west of the Iberian Peninsula (43.0°N 9.3°W) and reaches the centre of the Iberian Abyssal Plain (43.0°N 15.5°W).

The Finisterre section provides information about upper, intermediate, and deep waters. The core of LSW and the base of the permanent thermocline are typically centred ear 2000 m depth, which is, therefore, considered the limit of intermediate waters. From the core of MW to the core of LSW, there is a strong gradient and some coherence in variability, indicating the influence of large-scale atmospheric patterns. The main highlight of the time-series is the occurrence of a cold fresh anomaly between 2008 and 2010 centred at the core of LSW. Overall, for the last decade at these levels there has been 3–5 years swings over a cooling/freshening background trend. 2018 show a slight rebound with respect to 2017 values.

The abyssal waters in this basin are NADW (composed of a mixture of all Arctic water masses) and Lower Deep Waters, which reflect a signature of Antarctic origin waters. Interannual variability of these abyssal waters within the monitored period has been weak, with interannual swings below 0.1°C and 0.01 in salinity and no observed trends. In 2018, potential temperature and salinity are near long-term averages (Figure 5.16).

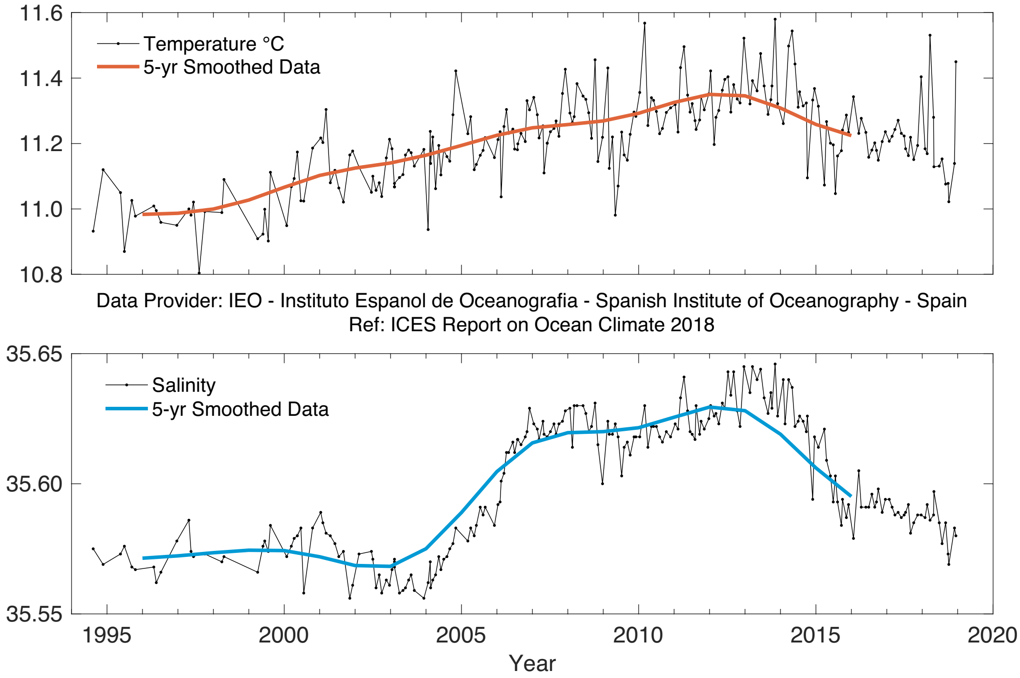

FIGURE 5.13.
Bay of Biscay. Potential temperature (upper panel) and salinity (lower panel) for the 300–600 m layer at Santander station 7.

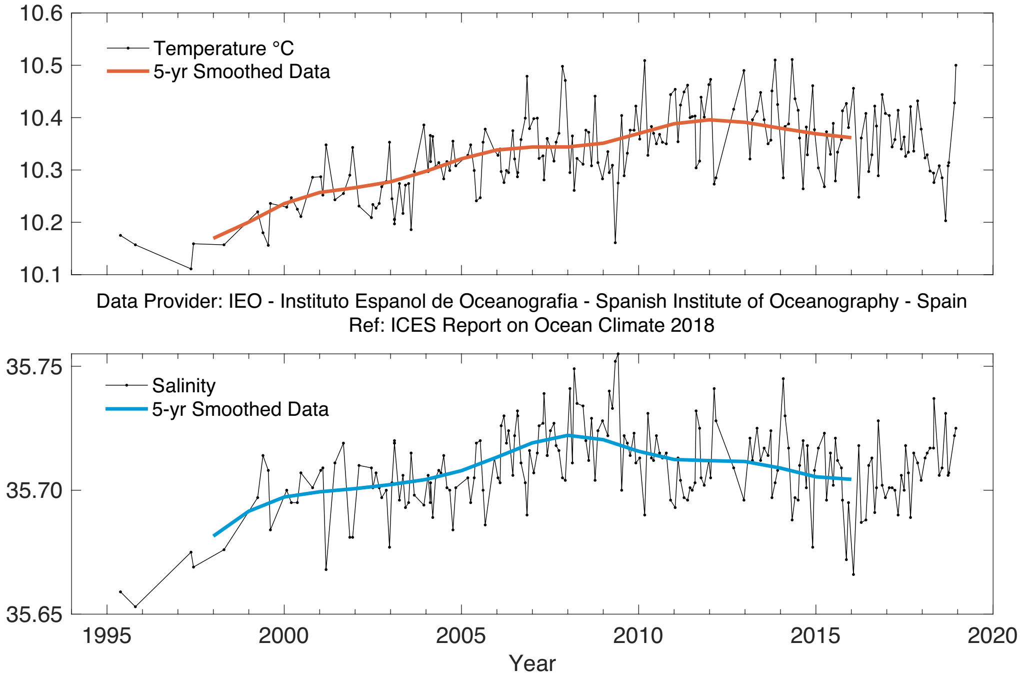

FIGURE 5.14.
Bay of Biscay. Potential temperature (upper panel) and salinity (lower panel) for the 600–1000 m layer at Santander station 7.

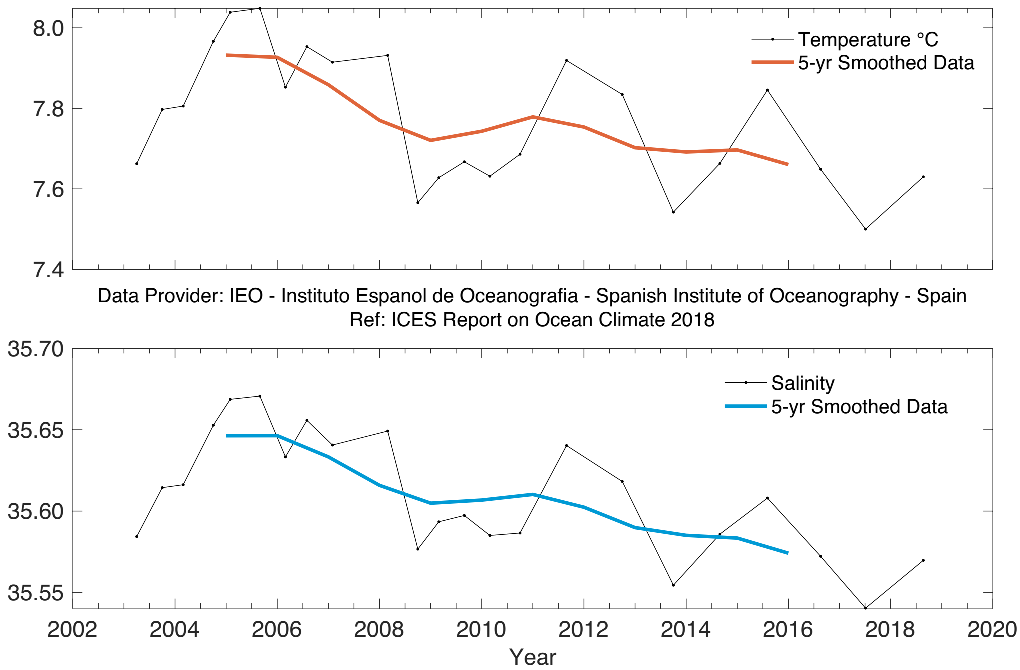

FIGURE 5.15.
Western Iberian Margin. Potential temperature (upper panel) and salinity (lower panel) for the 800–2000 m layer averaged across the Finisterre section.

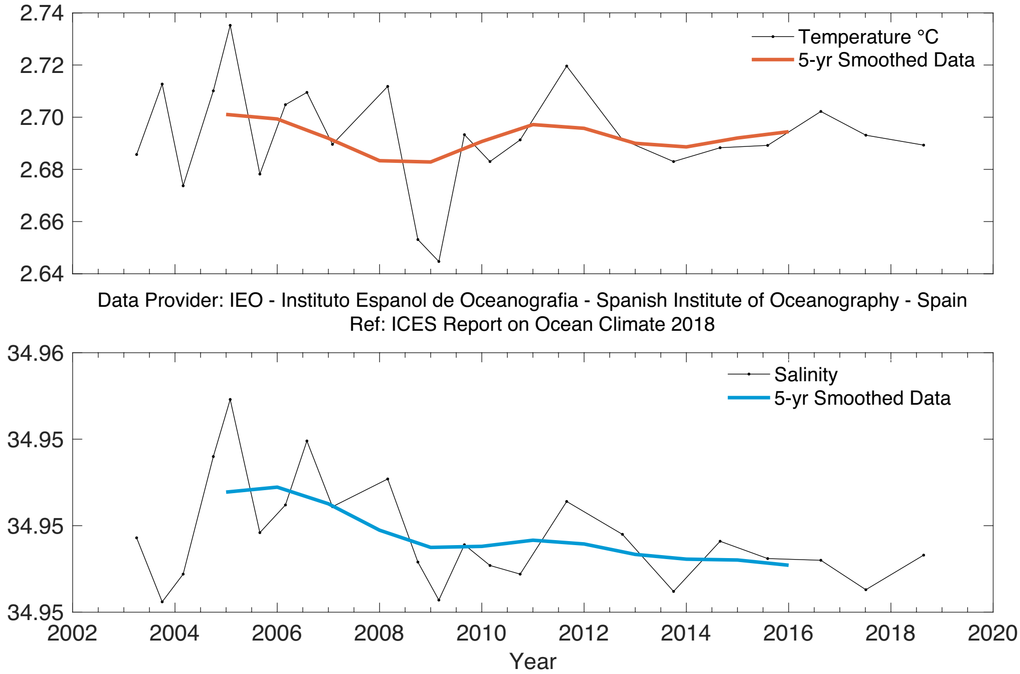

FIGURE 5.16.
Western Iberian Margin. Potential temperature (upper panel) and salinity (lower panel) for the 2000–5500 m layer averaged across the Finisterre section.

5.2.7 Canary Basin

P. Vélez-Belchí

In the stratum corresponding to intermediate waters (800–1400 m), weak cooling and decreasing salinity has been observed since the 1990s (Figure 5.17), although the changes are not statistically different from zero in the oceanic region or in the CTZ. Both time-series show high variability, reflective of the two very different intermediate water masses present in the region, i.e. the MW and AAIW.

In the layer corresponding to the upper NADW (1700–2600 m), there has been a weak increase in temperature and in salinity, neither of which is statistically significantly different from zero. However, in strata corresponding to the NADW (2600–3600 m; Figure 5.18), a marginally statistically significant, at the 95% confidence level, freshening (–0.002 ± 0.002 per decade) can be observed, although no trend could be confirmed for temperature (–0.005 ± 0.01°C per decade).

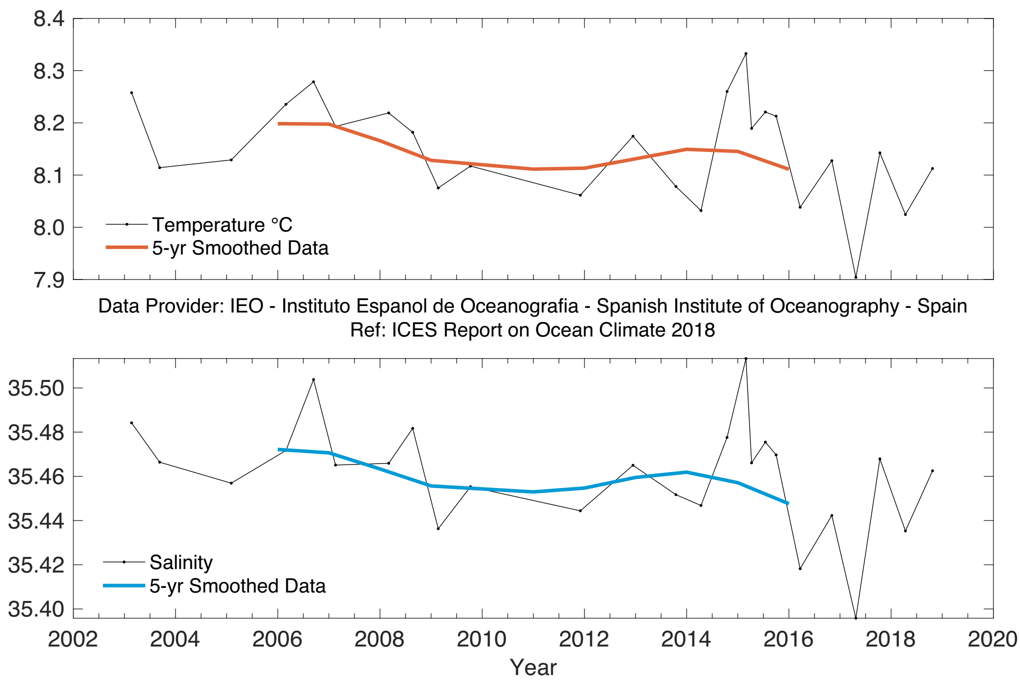

FIGURE 5.17.
Canary Basin. Potential temperature (upper panel) and salinity (lower panel) for the 800-1400 m layer.

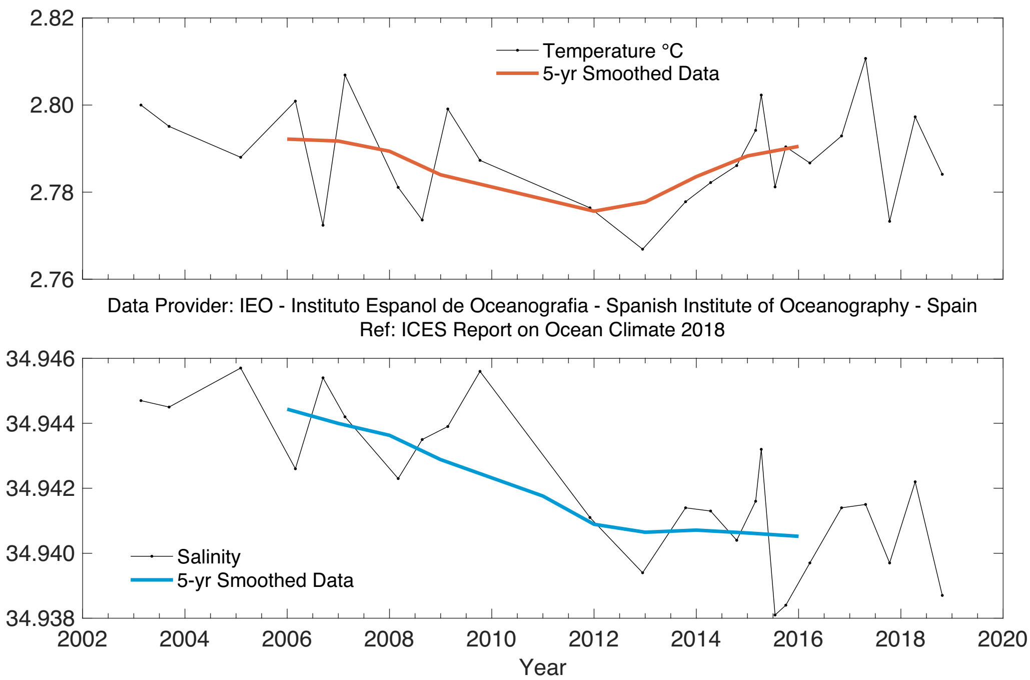

FIGURE 5.18.
Canary Basin. Potential temperature (upper panel) and salinity (lower panel) for the 2600-3600 m layer averaged across the Canaries section.

North of Faroes.
Photo: Karin M. H. Larsen, Faroe Marine Research Institute, Tórshavn, Faroe Islands.

6 REFERENCES

Berx, B., and Payne, M. R. 2017. The Sub-Polar Gyre Index - a community data set for application in fisheries and environment research. Earth System Science Data, 9: 259–266. https://doi.org/10.5194/essd-9-259-2017

Buckley, M. W., and Marshall, J. 2016. Observations, inferences, and mechanisms of the Atlantic Meridional Overturning Circulation: A review. Reviews of Geophysics, 54: 5–63. https://doi.org/10.1002/2015RG000493

Cappelen, J. 2019. Greenland-DMI historical climate data collection 1784–2018, DMI Technical Report 19–04.

de Boyer Montégut, C., Madec, G., Fischer, A. S., Lazar, A., and Iudicone, D. 2004. Mixed layer depth over the global ocean: An examination of profile data and a profile-based climatology. Journal of Geophysical Research: Oceans, 109 (C12). https://doi.org/10.1029/2004JC002378

Delworth, T. L., Zeng, F., Vecchi, G. A., Yang, X., Zhang, L., and Zhang R. 2016. The North Atlantic Oscillation as a driver of rapid climate change in the Northern Hemisphere. Nature Geoscience, 9: 509–512. https://doi.org/10.1038/ngeo2738

Duchez, A., Frajka-Williams, E., Josey, S. A., Evans, D. G., Grist, J. P., Marsh, R., McCarthy, G. D., *et al.* 2016. Drivers of exceptionally cold North Atlantic Ocean temperatures and their link to the 2015 European heat wave. Environmental Research Letters. 11 (7): 074004. https://doi.org/10.1088/1748-9326/11/7/074004

Dunstone, N., Smith, D., Scaife, A., Hermanson, L., Eade, R., Robinson, N., Andrews, M., *et al.* 2016. Skilful predictions of the winter North Atlantic Oscillation one year ahead. Nature Geoscience, 9 (11): 809–814. https://doi.org/10.1038/ngeo2824

Gaillard, F., Reynaud, T., Thierry, V., Kolodziejczyk, N., and von Schuckmann, K. 2016. *In situ*–based reanalysis of the global ocean temperature and salinity with ISAS: variability of the heat content and steric height. Journal of Climate. 29 (4): 1305–1323. https://doi.org/10.1175/jcli-d-15-0028.1

González-Pola, C., Lavín, A., and Vargas-Yáñez, M. 2005. Intense warming and salinity modification of intermediate water masses in the southeastern corner of the Bay of Biscay for the period 1992–2003. Journal of Geophysical Research. 110: C05020. https://doi.org/10.1029/2004JC002367

González-Pola, C., Fratantoni, P., Larsen, K. M. H., Holliday, N.P., Dye, S., Mork,K.A., Beszczynska-Möller, A., *et al.* The ICES Working Group on Oceanic Hydrography: A bridge from in-situ sampling to the remote autonomous observation era. Frontiers in Marine Science, 6:103, 2019. https://doi.org/10.3389/fmars.2019.00103

Häkkinen, S., and Rhines, P. B. 2004. Decline of subpolar North Atlantic circulation during the 1990s. Science, 304 (5670): 555–559. https://doi.org/10.1126/science.1094917

Hátún, H., Azetsu-Scott, K., Somavilla, R., Rey, F., Johnson, C., Mathis, M. Mikolajewicz, U., *et al.* 2017. The subpolar gyre regulates silicate concentrations in the North Atlantic. Scientific Reports, 7: 14576. https://doi.org/10.1038/s41598-017-14837-4

Hátún, H. and Chafik L. 2018. On the recent ambiguity of the North Atlantic subpolar tyre index. Journal of Geophysical Research, 123(8): 5072–5076.https://doi.org/10.1029/2018JC014101

Hátún, H., Lohmann, K., Matei, D., Jungclaus, J. H., Pacariz, S., Bersch, M. Gislason, A., *et al.* 2016. An inflated subpolar gyre blows life toward the northeastern Atlantic. Progress in Oceanography, 147: 49–66. https://doi.org/10.1016/j.pocean.2016.07.009

Hátún, H., Payne, M., Beaugrand, G., Reid, P., Sandø, A., Drange, H., Hansen, B., *et al.* 2009. Large bio-geographical shifts in the north-eastern Atlantic Ocean: From the subpolar gyre, via plankton, to blue whiting and pilot whales. Progress in Oceanography, 80 (3): 149–162. https://doi.org/10.1016/j.pocean.2009.03.001

Hátún, H., Sandø, A. B., Drange, H., Hansen, B., and Valdimarsson H. 2005. Influence of the Atlantic Subpolar Gyre on the Thermohaline Circulation. Science, 309 (5742): 1841–1844. https://doi.org/10.1126/science.1114777

Hernández-Guerra, A., Espino-Falcón, E., Vélez-Belchí, P., Pérez-Hernández, M. D., Martínez- Marrero, A., and Cana, L. 2017. Recirculation of the Canary Current in fall 2014. Journal of Marine Systems, 174: 25–39. https://doi.org/10.1016/j.jmarsys.2017.04.002

Holliday, N. P., Cunningham, S. A., Johnson, C., Gary, S. F., Griffiths, C., Read, J. F., and Sherwin, T. 2015. Multidecadal variability of potential temperature, salinity, and transport in the eastern subpolar North Atlantic. Journal of Geophysical Research: Oceans, 120: 5945–5967. https://doi.org/10.1002/2015jc010762

Hurrell, J. W., and Deser, C. 2010. North Atlantic climate variability: the role of the North Atlantic Oscillation. Journal of Marine Systems, 79: 231–244. https://doi.org/10.1016/j.jmarsys.2009.11.002

Hurrell, J. W., Kushnir, Y., Ottersen, G., and Visbeck M. 2003. An overview of the North Atlantic oscillation. In The North Atlantic Oscillation: Climatic Significance and Environmental Impact Ed. by J. W. Hurrell, Y. Kushnir, G. Ottersen, and M. Visbeck. Wiley Online Library. https://doi.org/10.1029/134GM01

Hurrell, J., and National Center for Atmospheric Research Staff (Eds). 2017. Climate Data Guide: Hurrell North Atlantic Oscillation (NAO) Index (station-based). https://climatedataguide.ucar.edu/climate-data/hurrell-north-atlantic-oscillation-nao-index-station-based, accessed 25 September 2017.

Hurrell, J., and National Center for Atmospheric Research Staff (Eds). 2018. Climate Data Guide: Hurrell North Atlantic Oscillation (NAO) Index (station-based). https://climatedataguide.ucar.edu/climate-data/hurrell-north-atlantic-oscillation-nao-index-station-based. Last modified 04 Aug 2018.

Kalnay, E., Kanamitsu, M., Kistler, R., Collins, W., Deaven, D., Gandin, L., Iredell, M., *et al.* 1996. The NCEP/NCAR 40-Year Reanalysis Project. Bulletin of the American Meteorological Society, 77: 437–471. https://doi.org/10.1175/1520-0477(1996)077<0437:TNYRP>2.0.CO;2

Kolodziejczyk, N., Prigent-Mazella, A., and Gaillard, F. 2017. ISAS-15 temperature and salinity gridded fields. SEANOE. https://doi.org/10.17882/52367

Moffa-Sánchez, P., and Hall, I. R. 2017. North Atlantic variability and its links to European climate over the last 3000 years. Nature Communications, 8: 1726. https://doi.org/10.1038/s41467-017-01884-8

Mountain, D. 2012. Labrador slope water entering the Gulf of Maine–response to the North Atlantic Oscillation. Continental Shelf Research, 47: 150–155. https://doi.org/10.1016/j.csr.2012.07.008

NOAA National Centre for Environmental Information, State of Climate: Annual National Climate Report for 2018. https://www.ncdc.noaa.gov/sotc/national/201813. Accessed 30 April 2019.

Paillet, J., and Mercier, H. 1997. An inverse model of the eastern North Atlantic general circulation and thermocline ventilation, Deep Sea Research Part I: Oceanographic Research Papers, 44 (8): 1293–1328. https://doi.org/10.1016/s0967-0637(97)00019-8

Pingree, R. D. 1993. Flow of surface waters to the west of the British Isles and in the Bay of Biscay. Deep Sea Research Part II: Topical Studies in Oceanography, 40 (1–2): 369–388. https://doi.org/10.1016/0967-0645(93)90022-f

Pingree, R. D., and Le Cann, B. 1990. Structure, strength and seasonality of the slope currents in the Bay of Biscay region. Journal of the Marine Biological Association of the UK, 70 (4): 857–885. https://doi.10.1017/S0025315400059117

Prieto, E., González-Pola, C., Lavín, A., and Holliday, N. P. 2015. Interannual variability of the northwestern Iberia deep ocean: Response to large-scale North Atlantic forcing. Journal of Geophysical Research: Oceans, 120: 832–847. https://doi.org/10.1002/2014jc010436

Pujol, M. I., Faugère, Y., Taburet, G., Dupuy, S., Pelloquin, C., Ablain, M., and Picot, N. 2016. DUACS DT2014: the new multi-mission altimeter data set reprocessed over 20 years. Ocean Science, 12: 1067–1090. https://doi.org/10.5194/os-12-1067-2016

Scaife, A. A., Arribas, A., Blockley, E., Brookshaw, A., Clark, R. T., Dunstone, N. Eade, R., *et al.* 2014. Skillful long-range prediction of European and North American winters. Geophysical Research Letters, 41: 2514–2519. https://doi.org/10.1002/2014gl059637

Scaife, A. A., Karpechko, A. Y., Baldwin, M. P., Brookshaw, A., Butler, A. H., Eade, R., Gordon, M., *et al.* 2015. Seasonal winter forecasts and the stratosphere. Atmospheric Science Letters, 17: 51–56. https://doi.org/10.1002/asl.598

Somavilla, R., Gonzalez-Pola, C., Rodriguez, C., Josey, S. A., Sanchez, R. F., and Lavin, A. 2009. Large changes in the hydrographic structure of the Bay of Biscay after the extreme mixing of winter 2005. Journal of Geophysical Research: Oceans, 114 (C1). https://doi.org/10.1029/2008jc004974

Tel, E., Balbin, R., Cabanas, J-M., Garcia, M-J., Garcia-Martinez, M. C., Gonzalez-Pola, C., Lavin, A., *et al.* 2016. IEOOS: the Spanish Institute of Oceanography Observing System. Ocean Science, 12 (2): 345–353, https://doi.org/10.5194/os-12-345-2016.

van Aken, H. M. 2002. Surface currents in the Bay of Biscay as observed with drifters between 1995 and 1999. Deep Sea Research Part I: Oceanographic Research Papers, 49 (6): 1071–1086. https://doi.org/10.1016/s0967-0637(02)00017-1

Vélez-Belchí, P., González-Carballo, M., Pérez-Hernández, M. D., and Hernández-Guerra, A. 2015. Open ocean temperature and salinity trends in the Canary Current Large Marine Ecosystem. In Oceanographic and biological features in the Canary Current Large Marine Ecosystem, pp. 201–213. Ed. by L. Valdés and I. Déniz-González. IOC Technical Series No. 115. IOC-UNESCO, Paris. 383 pp.

Vélez-Belchí, P., Pérez-Hernández, M. D., Casanova-Masjoan, M., Cana, L., and Hernández-Guerra, A. 2017. On the seasonal variability of the Canary Current and the Atlantic Meridional Overturning Circulation. Journal of Geophysical Research: Oceans, 122 (6): 4518–4538. https://doi.org/10.1002/2017jc012774

Yashayaev, I. 2007. Hydrographic changes in the Labrador Sea, 1960–2005. Progress in Oceanography, 73(3-4): 242– 276.

Yashayaev, I., and Loder, J. W. 2009. Enhanced production of Labrador Sea Water in 2008. Geophysical Research Letters, 36: L01606. https://doi.org/10.1029/2008GL036162

Yashayaev, I., and Loder, J. W. 2016. Recurrent replenishment of Labrador Sea Water and associated decadal-scale variability. Journal of Geophysical Research: Oceans, 121, https://doi.10.1002/2016JC012046

Yashayaev, I., and Loder, J. W. 2017. Further intensification of deep convection in the Labrador Sea in 2016. Geophysical Research Letters, 44 (3): 1429–1438. https://doi.org/10.1002/2016gl071668

7 ABBREVIATIONS AND ACRONYMS

AAIW	Antartic Intermediate Waters
AIW	Arctic Intermediate Waters
Argo	Not an acronym, but the name of a type of instrument used to collect data. The name ARGO is a reference to Greek mythology.
AR7W	Atlantic Repeat 7 West
AW	Atlantic Water
AZOMP	Atlantic Zone Off-Shelf Monitoring Program
BSH	Bundesamt für Seeschifffahrt und Hydrographie (German Federal Maritime and Hydrographic Agency)
CCLME	Canary Current Large Marine Ecosystem
CIL	Cold Intermediate Layer
CIRES	Cooperative Institute for Research in Environmental Sciences (USA)
CTD	Conductivity Temperature Depth
CTZ	Coastal Transition Zone
DJF(M)	December/January/February(March)
DSOW	Denmark Strait Overflow Water
EGC	East Greenland Current
GME	Gulf Of Maine East
GMW	Gulf Of Maine West
GSDW	Greenland Sea Deep Water
GTS	Global Telecommunication System
ENACW	Eastern North Atlantic Central Waters
IFREMER	Institut Français de Recherche pour l'Exploitation de la MER (French Institute For Ocean Research)
IPC	Iberian Poleward Current
IROC	ICES Report on Ocean Climate
ISAS	*In Situ* Analysis System
ISOW	Iceland–Scotland Overflow Water
LME	Large Marine Ecosystem
LSW	Labrador Sea Water
MNAW	modified North Atlantic Water
MOW	Mediterranean Overflow Water
MLD	Mixed-Layer Depths
MW	Mediterranean Waters
NAO	North Atlantic Oscillation
NAW	North Atlantic Water
NACW	North Atlantic Central Waters
NADW	North Atlantic Deep Water
NEC	Northeast Channel
N.MAB	Northeast Middle Atlantic Blight
NOAA	National Oceanic and Atmospheric Administration (USA)
NWGB	Northwest Georges Bank
OISST.v2	Optimum Interpolation SST dataset version 2
RAW	Return Atlantic Water
SLP	sea level pressure
S.MAB	Southeast Middle Atlantic Blight
SPMW	Subpolar Mode Water
SST	sea surface temperature
SSS	sea surface salinity
SSW	Sudden Stratospheric Warming
STOCA	Series Temporales de Datos Oceanograficos de Cadiz (Time-series of Cadiz Oceaongraphic Data)
TSG	Thermosalinograph
UPDW	Upper Polar Deep Water
WGC	West Greenland Current
WGOH	Working Group Oceanic Hydrography
WGWIDE	Working Group on Widely Distributed Stocks
WOA05	World Ocean Atlas 05
WSC	West Spitsbergen Current

8 AUTHORS BY SECTION

All sections for which no authors are specified were written jointly by all WGOH authors

SECTION	AREA/TOPIC	AUTHORS	E-MAIL	AFFILIATION
2. Summary of upper ocean conditions in 2018				
2.3	Argo gridded temperature and salinity fields	Nicolas Kolodziejczyk	Nicolas.Kolodziejczyk@univ-brest.fr	University of Brest (UBO), CNRS, IRD, Ifremer, Laboratoire d'Océanographie Physiqueet Spatiale (LOPS, Laboratory for Ocean Physics and Satellite remote sensing), Brest, France
		Damien Desbruyères	Damien.Desbruyeres@ifremer.fr	Ifremer, University of Brest (UBO), CNRS, IRD, Laboratoire d'Océanographie Physique et Spatiale (LOPS, Laboratory for Ocean Physics and Satellite remote sensing), Brest, France
		Gilles Reverdin	gilles.reverdin@locean-ipsl.upmc.fr	Laboratoire d'Océanographie et du Climat: Expérimentations et Approches Numériques (LOCEAN, Laboratory for Oceanography and Climate: Experiments and Numerical Approaches), Paris, France
2.4	Surface sampling along AX01 and AX02 (North Atlantic sub-polar gyre)	Nicolas Kolodziejczyk	Nicolas.Kolodziejczyk@univ-brest.fr	Ifremer, University of Brest (UBO), CNRS, IRD, Laboratoired'Océanographie Physique et Spatiale (LOPS, Laboratory for Ocean Physics and Satellite remote sensing), Brest, France.
		Gilles Reverdin	gilles.reverdin@locean-ipsl.upmc.fr	Laboratoire d'Océanographie et du Climat: Expérimentations et Approches Numériques (LOCEAN, Laboratory for Oceanography and Climate: Experiments and Numerical Approaches), Paris, France
2.5	Subpolar Gyre Index	León Chafik	leon.chafik@misu.su.se	Department of Meteorology (MISU), Stockholm University
		Hjálmar Hátún	hjalmarh@hav.fo	Faroe Marine Research Institute (FAMRI), Tórshavn, Faroe Islands
		Barbara Berx	B.Berx@MARLAB.ac.uk	Marine Scotland Science (MSS), Aberdeen, UK
3. The North Atlantic atmosphere				
All		Stephen Dye	stephen.dye@cefas.co.uk	Centre for Environment, Fisher-ies and Aquaculture Science (CEFAS), Lowestoft, UK
4. Detailed Area Descriptions, part I: The upper ocean				
4.1	West Greenland	Boris Cisewski	boris.cisewski@thuenen.de	Thünen-Institut für Seefischerei (TI-SF, Thünen Institute of Sea Fisheries), Bremerhaven, Germany
		John Mortensen	jomo@natur.gl	Greenland Institute of Natural Resources (GINR), Nuuk, Greenland
4.2	Labrador Sea	Igor Yashayaev	Igor.Yashayaev@dfo-mpo.gc.ca	Fisheries and Oceans Canada (DFO), Dartmouth, Nova Scotia
4.3	Newfoundland-Labrador Shelf	Frédéric Cyr	Frederic.Cyr@dfo-mpo.gc.ca	Fisheries and Oceans Canada (DFO), St.John's, Newfoundland, Canada
		Eugene Colbourne	Eugene.Colbourne@dfo-mpo.gc.ca	
4.4	Scotian Shelf	David Hebert	David.Hebert@dfo-mpo.gc.ca	Fisheries and Oceans Canada (DFO), Dartmouth, Nova Scotia
		Roger Pettipas	Roger.Pettipas@dfo-mpo.gc.ca	Ocean Monitoring and Observation Section, Oceans and Ecosystem Division, Bedford Institute of Oceanography, Fisheries and Oceans (BIO), Dartmouth, Nova Scotia
4.5	Northeast US Continental Shelf	Paula Fratantoni	paula.fratantoni@noaa.gov	NOAA Fisheries, NEFSC, Oceans and Climate Branch, Woods Hole, MA, USA
4.6	Icelandic Waters	Héðinn Valdimarsson	hedinn.valdimarsson@hafogvatn.is	Hafrannsóknastofnun (Marine and Freshwater Research Institute, MFRI), Reykjavík, Iceland
4.7	Bay of Biscay and Iberian Coast	Almudena Fontán	afontan@azti.es	AZTI. Aquarium of San Sebastian (SOG) and Idalgo Meteorological Observatory (AEMet), San Sebastian, Spain
		Victor Valencia	vvalencia@azti.es	
		Cesar González-Pola	cesar.pola@ieo.es	Instituto Español de Oceanografía (IEO, Spanish Institute of Oceanography), Gijón Oceanographic Centre, Gijón, Spain
4.8	Gulf of Cadiz	Ricardo Sánchez-Leal	rleal@ieo.es	Instituto Español de Oceanografía (IEO, Spanish Institute of Oceanography), Cádiz Oceanographic Centre, Cádiz, Spain
4.9	Canary Basin	Pedro Vélez-Belchí	pedro.velez@ieo.es	Instituto Español de Oceanografía (IEO, Spanish Institute of Oceanography), Canary Islands Oceanographic Centre, Tenerife, Spain
4.10	Southwest Approaches	TimJ. Smyth	TJSM@pml.ac.uk	Marine Biological Association and Plymouth Marine Laboratory (PML), Plymouth, UK

4.11	Celtic Seas	Kieran Lyons	Kieran.lyons@Marine.ie	Marine Institute, Galway, Ireland
		Caroline Cusack	caroline.cusack@ Marine.ie	
4.12	Rockall Trough	N. Penny Holliday	penny.holliday@ noc.ac.uk	National Oceanography Centre (NOC), Southampton UK
		Sam Jones	Sam.Jones@sams.ac.uk	Scottish Association for Marine Science (SAMS), Oban, UK
4.13	Hatton-Rockall Basin	N. Penny Holliday	penny.holliday@ noc.ac.uk	National Oceanography Centre (NOC), Southampton UK
		Sam Jones	Sam.Jones@sams.ac.uk	Scottish Association for Marine Science (SAMS), Oban, UK
4.14	Iceland Basin	N. Penny Holliday	penny.holliday@ noc.ac.uk	National Oceanography Centre (NOC), Southampton UK
		Sam Jones	Sam.Jones@sams.ac.uk	Scottish Association for Marine Science (SAMS), Oban, UK
4.15	Irminger Sea	M. Fremke de Jong	Femke.de.Jong@nioz.nl	Koninklijk Nederlands, Instituut voor Zeeonderzoek (NIOZ, Royal Netherlands Institute for Sea Research), Texel, Netherlands
4.16	Faroese Waters and the Faroe-Shetland Channel	Karin Magretha H. Larsen	karinl@hav.fo	Havstovan (Faroe Marine Research Institute, FAMRI), Tórshavn, Faroe Islands
		Barbara Berx	B.Berx@MARLAB.AC.UK	Marine Scotland Science (MSS), Aberdeen, UK
		Jenny Hindson	J.Hindson@ MARLAB.AC.UK	Marine Scotland Science (MSS), Aberdeen, UK
4.17	North Sea	Holger Klein	Holger.Klein@bsh.de	Bundesamt für Seeschifffahrt und Hydrographie (BSH, Federal Maritime and Hydrographic Agency, Hamburg, Germany
		Peter Loewe	peter.loewe@bsh.de	
		Achim Schulz		
		Manuela Köllner	manuela.koellner@ bsh.de	
4.18	Skaggerak, Kattegat and the Baltic Sea	Karin Wesslander	karin.wesslander@ smhi.se	Swedish Meteorological and Hydrological Institute (SMHI), Göteborg, Sweden
		Tycjan Wodzinowski	tycjan@mir.gdynia.pl	National Marine Fisheries Research Institute (MIR-PIB), Gdynia, Poland
4.19	Norwegian Sea	Kjell-Arne Mork	kjell.arne.mork@hi.no	Institute of Marine Research (IMR), Bergen, Norway
4.20	Barents Sea	Alexander Trofimov	trofimov@pinro.ru	Knipovich Polar Research Institute of Marine Fisheries and Oceanography (PINRO),Murmansk, Russian Federation
		Randi Ingvaldsen	randi.ingvaldsen@ imr.no	Institute of Marine Research (IMR), Bergen, Norway
4.21	Fram Strait	Agnieska Beszczynska-Möller	abesz@iopan.gda.pl	Institute of Oceanology, Polish Academy of Sciences (IOPAN), Sopot, Poland
		Wilken-Jon von Appen	Wilken-Jon.von. Appen@awi.de	Alfred Wegner Institute, Hermholtz Centre for Polar and marine Research (AWI), Bremehaven, Germany
		Gereon Budeus	gereon.budeus@awi.de	
5. Detailed Area Descriptions, part II: The intermediate and deep ocean				
5.1.1	Greenland Sea	Agnieska Beszczynska-Möller	abesz@iopan.gda.pl	Institute of Oceanology, Polish academy of sciences (IOPAN), Sopot, Poland
		Gereon Budeus	gereon.budeus@awi.de	Alfred Wegner Institute, Hermholtz Centre for Polar and marine Research (AWI), Bremehaven, Germany
5.1.2	Norwegian Sea	Svein Østerhus	svos@norceresearch.no	Norwegian Research Institute (NORCE), Bergen
5.1.3	Iceland Sea	Héðinn Valdimarsson	heddin.valdimarsson@ hafogvatn.is	Hafrannsóknastofnun (Marine and Freshwater Research Institute (MFRI)), Reykjavik, Iceland
5.2.1	Greenland-Scotland Ridge overflow waters	Barbara Berx	B.Berx@MARLAB.ac.uk	Marine Scotland Science (MSS), Aberdeen, UK
		Jenny Hindson	J.Hindson@ MARLAB.AC.UK	Marine Scotland Science (MSS), Aberdeen, UK

5.2.2	Iceland Basin	N. Penny Holliday	penny.holliday@noc.ac.uk	National Oceanography Centre (NOC), Southampton UK
		Sam Jones	Sam.Jones@sams.ac.uk	Scottish Association for Marine Science (SAMS), Oban, UK
5.2.3	Rockall Trough	N. Penny Holliday	penny.holliday@noc.ac.uk	National Oceanography Centre (NOC), Southampton UK
		Sam Jones	Sam.Jones@sams.ac.uk	Scottish Association for Marine Science (SAMS), Oban, UK
5.2.4	Irminger Basin	M. Fremke de Jong	Femke.de.Jong@nioz.nl	Koninklijk Nederlands, Instituut voor Zeeonderzoek (NIOZ, Royal Netherlands Institute for Sea Research), Texel, Netherlands
5.2.5	Labrador Basin	Igor Yashayaev	Igor.Yashayaev@dfo-mpo.gc.ca	Ocean Monitoring and Observation Section, Oceans and Ecosystem Division, Bedford Institute of Oceanography, Fisheries and Oceans (BIO), Bedford, Canada
		Boris Cisewski	boris.cisewski@thuenen.de	Thünen-Institut für Seefischerei (TI-SF, Thünen Institute of Sea Fisheries), Bremehaven, Germany
5.2.6	Western Iberian Basin	Cesar González-Pola	cesar.pola@ieo.es	Instituto Español de Oceanografia (IEO, Spanish Institute of Oceanography), Gijón Oceanographic Centre, Gijón, Spain
5.2.7	Canary Basin	Pedro Vélez-Belchí	pedro.velez@ieo.es	Instituto Español de Oceanografia (IEO, Spanish Institute of Oceanography), Canary Islands Oceanographic Centre, Tenerife, Spain

9 CONTACT INFORMATION: DATASET PROVIDERS

AREA	SECTION	FIGURES	TIME-SERIES	CONTACT	INSTITUTE
West Greenland	4.1	4.4	Nuuk air temperature	Boris Cisewski boris.cisewski@thuenen.de	Danish Meteorological Institute, Copenhagen, Denmark
West Greenland	4.1 5.2.5	4.5 4.6 5.10	Fylla and Cape Desolation section	Boris Cisewski boris.cisewski@thuenen.de	Thünen-Institut für Seefischerei (Thünen Institute of Sea Fisheries), Bremehaven, Germany
Northwest Atlantic	4.4	4.13 4.14 4.15 4.16	Sable Island air temperature, Cabot Strait sea ice, Misaine Bank, Emerald Bank	David Hebert David.Hebert@dfo-mpo.gc.ca Roger Pettipas Roger. Pettipas@dfo-mpo.gc.ca	Ocean Monitoring and Observation Section, Oceans and Ecosystem Division, Bedford Institute of Oceanography, Fisheries and Oceans Canada (DFO), Dartmouth, Nova Scotia.
Northwest Atlantic	4.3	4.9 4.10 4.11 4.12	Newfoundland and Labrador sea ice, Cartwright air temperature, Station 27 CIL	Frederic Cyr frederic.cyr@dfo-mpo.gc.ca	Northwest Atlantic Fisheries Centre, St. Johns, Newfoundland, Canada
Labrador Sea	4.2 5.25	4.8, 5.11	Section AR7W	Igor Yashayaev Igor.Yashayaev@dfo-mpo.gc.ca	Ocean Monitoring and Observation Section, Oceans and Ecosystem Division, Bedford Institute of Oceanography, Fisheries and Oceans Canada (DFO), Dartmouth, Nova Scotia.
Northeast US continental shelf	4.5	4.19 4.20 4.21 4.22 4.23 4.24 4.25	MAB, Gulf of Maine, Georges Bank, Northeast Channel	PaulaFratantoni paula.fratantoni@noaa.gov	NOAA Fisheries, NEFSC, Oceans and Climate Branch, Woods Hole, MA, USA
Icelandic waters	4.6 5.13	4.27 4.28 4.29 4.30 5.4	Reykjavik and Akureyri air temperature, Siglunes stations 2-4, Selvogsbanki Station 5, Langanes stations 2-6, Faxafloi Station 9, Icelandic deep water (1800 m)	Hedinn Valdimarsson hedinn.valdimarsson@ hafogvatn.is	Hafrannsóknastofnun (Marine and Freshwater Research Institute), Reykjavik, Iceland
Bay of Biscay	4.7	4.32 4.33	San Sebastian air and water temperature	Almudena Fontán afontan@azti.es	AZTI, Aquarium of San Sebastian (SOG) and Igeldo Meteorological Observatory (AEMet), San Sebastian, Spain
Bay of Biscay and western Iberian margin	4.7. 5.2.6	4.32 4.33 5.13 5.14 5.15 5.16	Santander and Finisterre sections	César González-Pola cesar.pola@ieo.es	Instituto Español de Oceanografía (IEO, Spanish Institute of Oceanography), Gijón Oceanographic Centre, Gijón, Spain
Gulf of Cadiz	4.8	4.37	STOCA Station SP6 - Gulf of Cadiz time-series	Ricardo F. Sánchez-Leal rleal@ieo.es	Instituto Español de Oceanografía (IEO, Spanish Institute of Oceanography), Cadiz Oceanographic Centre, Cadiz, Spain
Canary Basin	4.9 5.27	4.40 5.17 5.18	Canary Basin Oceanic Waters Section	Pedro Vélez-Belchí pedro.velez@ieo.es	Instituto Español de Oceanografía (IEO, Spanish Institute of Oceanography), Canary Islands Oceanographic Centre, Tenerife, Spain
NW European continental shelf	4.10	4.43	Astan Section, Point 33	Pascal Morin pmorin@sb-roscoff.fr	CNRS-UPMC, Observatoire Oceanologique de Roscoff, Roscoff, France
NW European continental shelf	4.10	4.41 4.42	Western Channel Observatory, Station E1	Tim J. Smyth tjsm@pml.ac.uk	Marine Biological Association and Plymouth Marine Laboratory, Plymouth, UK
NW European continental shelf	4.11	4.44 4.45	Malin Head Weather Station, M3 Weather Buoy	Caroline Cusack Caroline.Cusack@Marine.ie	Marine Institute, Galway, Ireland
Rockall Trough and Iceland Basin	4.12 4.13 4.14 5.2.2 5.2.3	4.47 4.48 4.49 5.6 5.7 5.8	Ellett Line	N. Penny Holliday penny.holliday@noc.ac.uk	National Oceanography Centre, Southampton and Scottish Association for Marine Science, Southampton, UK
Irminger Sea	4.15	4.51	Station FX9 (64.33°N 28°W)	Hedinn Valdimarsson hedinn.valdimarsson@ hafogvatn.is	Hafrannsóknastofnun (Marine and Freshwater Research Institute), Reykjavik, Iceland
Irminger Sea	4.15 5.2.4	4.50 5.9 5.10	Central Irminger Sea, East Greenland slope	Laura de Steur Laura.de.Steur@nioz.nl M. Femke de Jong Femke.de.Jong@nioz.nl	Koninklijk Nederlands, Instituut voor Zeeonderzoek (NIOZ, Royal Netherlands Institute for Sea Research), Texel, Netherlands
Faroe Bank Channel	4.16	4.53 4.54 4.55	Faroe Bank Channel-West Faroe Islands, Faroe Current - North Faroe Islands, Faroe Shelf	Karin Margretha H. Larsen KarinL@hav.fo	Havstovan (Faroe Marine Research Institute, FAMRI), Faroe Islands
Faroe-Shetland Channel	4.16 5.2.1	4.56 4.57 5.55	Faroe-Shetland Channel, Faroe Shelf and Shetland Shelf deep waters (800 m)	Barbara Berx B.Berx@marlab.ac.uk	Marine Scotland Science (MSS), Aberdeen, UK

North Sea	4.17	4.61	North Sea Utsira, modelled North Sea inflow	Jon Albretsen jon.albretsen@imr.no Solfrid Hjollo solfrids@imr.no	Institute of Marine Research (IMR), Bergen, Norway
North Sea	4.17	4.62	Fair Isle Current water	Barbara Berx B.Berx@marlab.ac.uk	Marine Scotland Science (MSS, Aberdeen), UK
North Sea	4.17	4.63 4.64	Helgoland Roads coastal waters, German Bight, North Sea	Karen Wiltshire Karen.Wiltshire@awi.de	Alfred Wegener Institute for Polar and Marine Research (AWI)/Biologische Anstalt Helgoland (BAH), Germany
Baltic Sea	4.18	4.66 4.67 4.68	Station BY15, Baltic Proper, east of Gotland, and observed ice extent	Johanna Linders johanna.linders@smhi.se	Swedish Meteorological and Hydrological Institute (SMHI), Norrköping, Sweden
Baltic Sea	4.18	4.69 4.70	Stations LL7 and SR5	Pekka Alenius pekka.alenius@fimr.fi	Finnish Institute of Marine Research (FIMR), Helsinki, Finland
Norwegian Sea	4.19	4.72 4.74 4.75	Svinøy, Gimsøy, and Sørkapp sections	Kjell Arne Mork kjell.arne.mork@imr.no	Institute of Marine Research (IMR), Bergen, Norway
Norwegian Sea	4.19 5.1.2	4.73 5.3	Ocean Weather Station Mike (50 and 2000 m)	Svein Østerhus svos@norceresearch.no	NORCE Norwegian Research Centre, Institute of Marine Research (IMR) and University of Bergen (UiB), Norway
Barents Sea	4.20	4.77	Fugløya–Bear Island section, Western Barents Sea	Randi Ingvaldsen randi.ingvaldsen@imr.no	Institute of Marine Research (IMR), Bergen, Norway
Barents Sea	4.20	4.78	Kola section, Eastern Barents Sea	Oleg V. Titov titov@pinro.ru	Knipovich Polar Research Institute of Marine Fisheries and Oceanography (PINRO), Russian Federation
Greenland Sea and Fram Strait	4.21 5.1.1	4.79 5.2	Greenland Sea section N, west of Spitsbergen (76.5°N)	Agnieszka Beszczynska-Möller abesz@iopan.gda.pl	Institute of Oceanology, Polish Academy of Sciences (IOPAN), Sopot, Poland
Greenland Sea and Fram Strait	4.21 5.1.1	4.79 5.2	Greenland Sea section 75°N, Greenland Sea deep waters	Gereon Budeus Gereon. Budeus@awi.de	Alfred Wegener Institute, Helmholtz Centre for Polar and Marine Research (AWI), Bremerhaven, Germany
Greenland Sea and Fram Strait	4.21	4.80	Fram Strait (78.83°N), West Spitsbergen Current and East Greenland Current	Wilken-Jon von Appen Wilken-Jon.von.Appen@awi.de	Alfred Wegener Institute, Helmholtz Centre for Polar and Marine Research (AWI), Bremehaven, Germany